

Nanoscale Characterization of Melatonin and Amyloid Beta in Model Membranes- in Relation to Alzheimer's Disease

by

Youngjik Choi

A thesis
presented to the University of Waterloo
in fulfillment of the
thesis requirement for the degree of
Doctor of Philosophy
in
Biology

Waterloo, Ontario, Canada, 2014

©Youngjik Choi 2014

Author's Declaration

This thesis consists of material all of which I authored or co-authored: see Statement of Contributions included in the thesis. This is a true copy of the thesis, including any required final revisions, as accepted by my examiners.

I understand that my thesis may be made electronically available to the public.

Statement of Contributions

Section 2.3 (p. 52) contains work from collaboration. As the first author of the published data included in this section, I have designed and conducted most of the experiments, collected and interpreted the data, and produced the final draft of the manuscript. Data analysis and figure production were done with the help of Dr. S. Attwood, and E. Drolle contributed with data collection for the pure cholesterol and DPPC isotherms. This section is based on parts of a manuscript and all authors (Y. Choi, S. Attwood, M. Hoopes, E. Drolle, M. Karttunen, and Z. Leonenko) contributed to its editing and finalizing. The publication is titled, "Melatonin directly interacts with cholesterol and alleviates cholesterol effects in dipalmitoylphosphatidylcholine monolayers". *Soft Matter*, vol. 10, no. 1, p. 206-13, 2014, DOI: 10.1039/c3sm52064a. Figures from the publication are presented with written permission.

Section 2.5 (p.80) contains work from collaboration. Dr. S. Attwood, Dr. Z. Leonenko, and I have designed the experiments. I have collected, analyzed, and interpreted the data and received figure production help from Dr. S. Attwood. Dr. Z. Leonenko provided inputs on the design of the experiment, provided supervision, and access to facilities.

Section 3.2.4 (p. 124) contains work that has culminated in a second author publication titled "Preparation of DOPC and DPPC Supported Planar Lipid Bilayers for Atomic Force Microscopy and Atomic Force Spectroscopy" (S. Attwood, Y. Choi, and Z. Leonenko) *Int. J. Mol. Sci.*, vol. 14, no. 2, pp. 3514–39, 2013. DOI: 10.3390/ijms14023514. All authors contributed to the design, planning, analysis, and presentation of the experiment. Dr. S. Attwood spearheaded the experiments and drafted the manuscript, and I have planned and performed the experiments alongside the main author (Dr. S. Attwood). I also performed and assisted in data analysis as well as in the manuscript preparation. Dr. Z. Leonenko provided the equipment facilities, chemicals, project supervision, and final editing and submission of the manuscript. The section has been written based on the manuscript, and figures from the publication are also presented with written permission.

Section 4.2 (p.169) The experiments were designed by Dr. M. Campbell, Dr. Z. Leonenko, L.Emptage and myself. Retina samples were provided by The Eye Bank of Ontario to Dr. M. Campbell's lab (University of Waterloo) and the sample preparation and staining procedures were planned in collaboration with Dr. M. Campbell and L. Emptage but ultimately prepared by L. Emptage. The imaging was done on a damp sample mounted on a glass microscope slide. Specific

contributions made by the author include setting up the fluorescence microscope to be used in conjunction with the AFM. Fluorophore selection, inverted microscope modification, filter cube selection, developing procedures for obtaining fluorescence microscopy (FM) images with a color camera, setup procedures and test FM image capturing using an EMCCD (electron multiplying charge coupled device) camera, and developing procedures and producing technical manuals for conducting FM-AFM combined imaging were also contributed by the author. Technical assistance was provided throughout, including sample preparation methods and data production preparation for various written works (scientific articles, poster presentations, conference papers, and abstracts). The contributions made obtaining the initial results possible, which provided the underlying proof of concept for the project. Data analysis was provided by L. Emptage and Dr. M. Campbell. Further data collected by L. Emptage using the developed protocols are currently being prepared for journal submission.

Section 4.3 (p. 173) was performed in collaboration with Dr. M. Beazely and his student L. Liu at the University of Waterloo. Contributions made in this section include using the AFM to assess A β aggregates incubated in cell culture media and providing sample preparation guidelines. L. Liu provided amyloid incubation samples in cell culture media. Dr. M. Beazely provided facilities and supplies needed to produce the samples. Dr. Z. Leonenko provided access and training for the AFM and discussion of the results.

Section 4.4 (p. 175) was conducted in collaboration with H. Broom and Dr. E. Meiering at the University of Waterloo. Dr. E. Meiering granted permission to access and use the equipment, H. Broom provided equipment training and helped with results interpretation through providing a guide manual. Experimental data collection and final data analysis were performed by the author.

Section 4.5 (p. 177) includes results from molecular dynamics (MD) simulations. MD simulation data in this section were contributed by Dr. M. Karttunen and Dr. M. Hoopes and were previously published in "Melatonin directly interacts with cholesterol and alleviates cholesterol effects in dipalmitoylphosphatidylcholine monolayers" (Y. Choi, S. Attwood, M. Hoopes, E. Drolle, M. Karttunen and Z. Leonenko) *Soft Matter*, vol. 10, no. 1, p. 206-13, 2014, DOI: 10.1039/c3sm52064a. The experimental concept and the parameters used were contributed by the author, and Dr. M. Karttunen and Dr. M. Hoopes (University of Waterloo) conducted the simulations. Dr. Z. Leonenko has planned, initiated, and coordinated the collaboration with Dr. M. Karttunen and Dr. M. Hoopes. The MD simulation results were compared with the results found in section 2.3, which were mostly

produced by the author with the help of E. Drolle, and Dr. S. Attwood, under the supervision of Dr. Z. Leonenko. Contributions for the monolayer results are described in detail in the Statement of Contributions for section 2.3. All results are presented with written permission.

Appendix B (p.241) Cell viability assays using A β and melatonin were performed on several different cell lines, including mouse hippocampal culture, RGC-5 cell line (retinal ganglion cells) and also SH-SY5Y (human derived neuroblastoma cell line). Dr. M. Beazely's group members, L. Liu and M. Vasefi have gathered and provided the final data and analysis presented here. Dr. M. Beazely designed the experiments, provided the facilities for the experiments including all necessary supplies and cell lines. He also provided guidance and supervision throughout the project. The author's contributions included providing material support, conducting literature reviews, assisting in cell treatments, and participating in conducting MAP2 (neuronal cell viability) assay.

Abstract

Increasing evidence suggests that cell membranes play an important role in the pathophysiology of Alzheimer's disease (AD). Direct interaction of small molecules, such as cholesterol and melatonin, with cellular membrane can alter the physical structure of the membrane lipid bilayer, which can affect the interaction of membrane with amyloid- β ($A\beta$) peptides that are implicated as one of the main culprits of the disease. The hormone melatonin has been shown to decrease the toxic effects of $A\beta$ peptides. Evidence suggests that melatonin may interact with lipid membranes non-specifically in exerting its protective effects. The goal of the project was to measure the non-specific membrane interaction of melatonin (and contrast it to cholesterol) and also to characterize how the membrane's action affects $A\beta$ peptide's interaction with and accumulation on the membrane.

First, Langmuir monolayers were used to study the effects of melatonin. The results show that melatonin acts on the monolayer membrane model in ways that reduce or counter the effects of cholesterol. Contrary to condensing and thickening effect of cholesterol, melatonin showed thinning and fluidizing effects. It was also discovered that melatonin's precursor molecules, which have also been shown to have protective effects in AD, also exert similar effects in the membrane as melatonin.

The action on the membrane of melatonin and its effects on $A\beta$ binding to the membrane were studied using atomic force microscopy and breakthrough force spectroscopy on supported bilayer membrane models. Protocols and methods for producing good quality supported bilayers, obtaining control breakthrough force spectroscopy data, and imaging of

A β binding to the membrane were successfully developed and performed. However, conclusively showing the effects melatonin's membrane action and on binding and accumulation of A β on the membrane using AFM will require further investigation.

In conclusion, the work confirmed and characterized the membrane action of melatonin and its related molecules, however, it was not possible to show how it affected the A β peptide accumulation in the membrane. The results indicated that the direct membrane interaction of molecules may have significant effects on the biophysical properties of the membrane, but verifying the impact of the effects will require further work. The results of this work added new important discoveries in the field of membrane biophysics, and the techniques, methods, and protocols developed throughout the work further contributed to the field by fostering future work.

Acknowledgements

I would like to thank my supervisor, Prof. Zoya Leonenko, for all the support and direction she has given me throughout the project. I would also like to thank Dr. Simon Attwood for his support and advice as well as direct experimental guidance and leadership. I also thank Dr. Helen Russell for her invaluable support for making this thesis possible. I would like to also thank Ms. Krista Parsons for her kindness and support throughout, and Drs. R. Hill and W. Power for overseeing and helping with the thesis revision process.

I'd like to thank members of my thesis committee, Dr. Michael Beazely, Dr. David Spafford, and Dr. Melanie Campbell for their unrelenting support in providing guidance, collaborative projects and reference letters. I would also like to thank many other collaborators, including Dr. Mikko Karttunen, Dr. Matthew Hoopes, Dr. Elizabeth Meiering, Emrah Ozel, Laura Emptage, Hui (Lucy) Liu, Maryam Vasefi, Liz Drolle, and Helen Broom. To all those whom I have worked with, thank you for graciously providing me with the opportunity to learn from you and to also obtain exciting and impactful data.

I would also like to thank my other colleagues and members of the lab, Dr. Francis Hane, Robbie Henderson and countless others for support and helpful discussions. For technical support, I thank Dr. Song Xu (Agilent technologies), Dr. Marc Richter (JPK Instruments), Greg Willis (BiolinScientific, Inc.) and Husain Mehkri (GTL Ltd.)

I also acknowledge financial support from CIHR scholarship, WIN Fellowship and OGS scholarship. Last but not least, I thank my family and friends, mom, dad, Ruth, Matt, Michael and Abiy for their immeasurable love and support throughout.

Table of Contents

Author's Declaration	ii
Statement of Contributions	iii
Abstract	vi
Acknowledgements	viii
Table of Contents	ix
List of Figures	xi
List of Tables	xiv
Chapter 1 Introduction	1
1.1 Alzheimer's Disease and Amyloid Hypothesis	1
1.2 Cell Membrane Connection	5
1.3 Membrane Biophysics	8
1.4 Melatonin and Related Molecules	10
1.5 Project Overview	13
Chapter 2 Langmuir-Blodgett Monolayer	17
2.1 Introduction	17
2.2 Method Development	27
2.3 Melatonin Directly Interacts with Cholesterol and Alleviates Cholesterol Effects in Dipalmitoylphosphatidylcholine Monolayers	52
2.3.1 Introduction	52
2.3.2 Materials and Methods	54
2.3.3 Results	56
2.3.4 Discussion	65
2.3.5 Conclusion	69
2.4 Testing A β Binding in Langmuir Monolayers	71
2.4.1 Materials and methods	74
2.4.2 Results and Discussion	75
2.4.3 Conclusion	79
2.5 Determining the Effects of Molecules that are Precursors to Melatonin in DPPC Monolayers	80
2.5.1 Introduction	80
2.5.2 Materials and Methods	85
2.5.3 Results and Discussion	87

2.5.4 Conclusions.....	100
Chapter 3 Atomic Force Microscopy Study of Supported Bilayers	102
3.1 Introduction.....	102
3.1.1 Atomic Force Microscopy (AFM).....	102
3.1.2 AFM Force Spectroscopy	107
3.1.3 Vesicle Fusion	109
3.2 AFM Experiments to Assess Bilayers	110
3.2.1 Bilayer Imaging	110
3.2.2 Force Spectroscopy Experiment 1	114
3.2.3 Force Spectroscopy Experiment 2	118
3.2.4 Bilayer Protocol Redevelopment.....	124
3.2.5 Force Spectroscopy Experiment 3 - Force Spectroscopy on Supported DOPC Bilayers..	139
3.2.6 Summary of Force Spectroscopy Results	144
3.2.7 Concluding Remarks for AFM Force Experiments.....	146
3.3 Imaging Amyloid- β (A β) Accumulation on Bilayers.....	147
3.3.1 Materials and Methods	149
3.3.2 Results and Discussion	152
3.3.3 Summary and Conclusion.....	167
Chapter 4.....	168
Collaborative Works	168
4.1 Introduction.....	168
4.2 Investigating A β Deposits on Human Retina	169
4.3 Cell Viability Testing with A β and Melatonin	173
4.4 Dynamic Light Scattering (DLS).....	175
4.5 Other Contributions- Molecular Dynamics Simulations	177
Chapter 5 Summary and Conclusions.....	178
5.1 Summary	178
5.2 Conclusion	180
Copyright Permissions.....	182
Bibliography	219
Appendix A Tip Modification	239
Appendix B Cell Viability Study.....	241

List of Figures

Figure 1- Alzheimer's schematic	4
Figure 2- A β production mainly occurs in membrane lipid rafts	6
Figure 3- Molecular illustration of three different membrane phase states.....	7
Figure 4- Illustrations of different molecules in the membrane	9
Figure 5- A photograph of a modern Langmuir monolayer trough.....	18
Figure 6- Depicting a Wilhelmy plate	20
Figure 7- Schematic of a monolayer isotherm.....	23
Figure 8- DPPC monolayer isotherms from literature.....	29
Figure 9- Raw initial DPPC monolayer isotherms	31
Figure 10- Raw DPPC isotherms.....	32
Figure 11- Data from figure 10 converted.....	33
Figure 12- Isotherms gathered from the lab machine	35
Figure 13- Area versus time data for the two troughs	37
Figure 14- Comparing the differences in the loss rate.....	39
Figure 15- Increasing the speed of compression for isotherms	41
Figure 16- Averaged DPPC control isotherm with the standard error of the mean (SEM).....	44
Figure 17- Variability in the control isotherms from differing aliquots	47
Figure 18- DPPC and DPPC/Cholesterol mixed isotherms.....	49
Figure 19- DPPC/Cholesterol isotherms	51
Figure 20- Melatonin in DPPC monolayers	56
Figure 21- DPPC isotherms with melatonin.....	61
Figure 22- Compression isotherms for lipid/ cholesterol mixtures with melatonin	64
Figure 23- Relative change in the area per molecule	65
Figure 24- Schematics illustrating packing of DPPC molecules in a monolayer.....	68
Figure 25- Schematic of a pressure hold experiment	72
Figure 26- Illustration showing an ideal area versus time data for a pressure hold experiment	73
Figure 27- Results of pressure hold experiment with control DPPC monolayers	76
Figure 28- Pressure-hold experiments	79
Figure 29- Molecular structures of tryptophan, serotonin, N-Acetylserotonin (NAS) and melatonin ..	83
Figure 30- DPPC Langmuir monolayer isotherms	89

Figure 31- Compressibility modulus C_s^{-1} (mN/m) versus pressure Π (mN/m)	96
Figure 32- Cartoon of an AFM cantilever/tip and the sample	103
Figure 33- Force versus tip-sample distance graph	106
Figure 34- Force spectroscopy vertical deflection (force) versus height (displacement) graph.....	108
Figure 35- Schematic diagram of vesicle fusion process	109
Figure 36- DPPC bilayers with and without melatonin.....	111
Figure 37- Force spectroscopy data of DPPC bilayer	116
Figure 38- AFM image of the DOPC and DPPC mixed (70:30) bilayer.....	121
Figure 39- Images showing how DPPC and DOPC molecules intermix and form domains	126
Figure 40 -AFM images of DOPC bilayer patches	128
Figure 41- Time series of DOPC bilayer formation	132
Figure 42- Illustration of the dewetting test used to confirm bilayer coverage.....	133
Figure 43- Effect of cooling rate on DPPC bilayers in water.....	135
Figure 44- Effect of mica temperature during deposition	136
Figure 45- DPPC bilayer with the best compromise	138
Figure 46- Example BT-force and the values estimated from the curves	141
Figure 47- Force versus time graphs of breakthrough.....	142
Figure 48- A β preparation thawed and deposited on mica.....	151
Figure 49- A β (1-42) on brain extract bilayers in 3 different concentrations.....	152
Figure 50- Sequential images of 10 μ M A β on brain extract bilayer taken from the same area	154
Figure 51- Even at the highest concentration of A β tested (18 μ M) incubated for 48 hours	154
Figure 52- 5 μ M A β added to brain extract bilayer in 2.0 mM melatonin solution	155
Figure 53- Control brain extract bilayer at 1 hr (left) and after 24 hours (right).....	156
Figure 54- Image of a control DPPC bilayer with extended intact bilayer areas	158
Figure 55- DPPC bilayers with A β at 12 μ M	161
Figure 56- DPPC with A β incubated for 2 hours	162
Figure 57- Control DPPC bilayers with A β	164
Figure 58- DPPC bilayer with A β incubated for 2 hours with 2.0 mM melatonin.....	165
Figure 59- Three different trials of 1 hour incubation without melatonin (.....	166
Figure 60- Testing the combined FM and AFM imaging of A β aggregates	171
Figure 61- Images of post-mortem human retinas.....	172
Figure 62- Representative images of three different A β aggregate samples	174

Figure 63- DLS measurements of DPPC vesicle solutions 176

List of Tables

Table 1- Reported literature values for DPPC and DOPC bilayer thickness	112
Table 2- BT-force data on the DOPC regions of the samples using various parameters	122
Table 3- Summary Comparison of Force Spectroscopy Data Set Results	145

Chapter 1

Introduction

1.1 Alzheimer's Disease and Amyloid Hypothesis

Alzheimer's disease (AD) is the most common age related neurodegenerative disease[1]. Also as the most prevalent form of dementia[1], the clinical symptoms of the disease include progressive memory loss[2], and aberrant night time behavior, which includes sleep disturbance and nightly mood swings[3]. It is one of the most serious diseases as currently there is no effective treatment or cure available that can stop the progression of the disease[4], [5].

Historically, Dr. Alois Alzheimer first discovered the disease back in 1907[5], [6]. During post-mortem examination he found and described three pathological alterations in the brain of a female patient who has succumbed to the disease[6]. The three hallmark features of the disease, as described by Alzheimer, included "peculiar substance" occurring as extracellular deposits in some brain regions, which are now known as "amyloid plaques"[6]. The second feature identified were neurofibrillary tangles (NFTs), which are intracellular legions of phosphorylated proteins. Third, he described the presence of "adipose inclusions" or "lipoid granules", hinting that abnormal lipid metabolism may be involved[6]. Since then, on-going research has revealed that there are many other structural and functional alterations that are present, such as signs of inflammatory responses and oxidative stress[5]. The combined result of all the pathological changes observed are believed to be responsible for the severe neuronal synaptic dysfunction and loss observed in the patients[5]. The disease's effects on the brain tissue can be quite dramatic, as the brain of an AD patient at the time of death may weight about one third less compared to an age-matched healthy individual[5].

Of the aforementioned pathological hallmarks of AD, the most attention has been given to studying the amyloid plaque formations, as they are the distinguishing pathological feature in the diseased brain[7]. Although the jury is still out on the extent and significance of the different pathophysiological changes observed in the brain, current consensus is that amyloid pathophysiology plays a central role and that it is also involved as a co-factor in many of the other pathophysiological changes in AD[8]. Thus much focus was given in studying the amyloid plaques, and by the mid 1980s, researchers characterized them as containing a particular form of peptide, now named amyloid- β ($A\beta$) peptide. Culminating research has now established the hypothesis that overproduction and accumulation of $A\beta$ peptide is likely a causal factor in AD[8].

Although it is widely agreed that the over accumulation of $A\beta$ is fundamental to the disease[9], it is still not exactly clear why it occurs, and also how the presence of the peptide results in neuronal death[10],[11]. In order to better understand the disease processes, attention has been given to studying a portion of AD patients who suffers from a genetically linked form of AD called 'familial AD'. Familial AD is passed down through generations in an autosomal dominant fashion[8], however, the familial form of AD represented less than 1% of all cases; the vast majority suffer from what is classified as the "sporadic" form of AD with unknown exact causes[12]. Although not the majority, examining the genetic form of AD to study and understand $A\beta$ related processes proved to be advantageous for several reasons. Symptom presentation in the genetic form of AD is highly predictable, thus it was possible to develop various animal models of AD that can reliably reproduce the pathophysiological and clinical features of AD. The sporadic form has no traceable known cause[13], but the pathological

features are similar in both the genetic and sporadic forms of AD. In the genetic model of AD, various mutations are found in a genes that codes for amyloid related components, such as the amyloid precursor protein (APP), the presenilins[14], and secretases[15] that together produce A β . However, attempts at targeting these protein products in order to decrease the production of A β have yielded limited success[8]. Because decreasing the precursors of A β proved to be less than successful, instead the focus was then shifted toward trying to increase or accelerate the clearance of A β . Many different compounds and approaches (vaccination being a major one) have been tried and tested to inhibit the production of A β as well as increase or facilitate the clearance of A β (basically decrease the amount of A β in the brain). However, to date the interventions that utilize this strategy has all failed in Phase III clinical trials or earlier [8], [16]. Thus currently, any form of treatment for AD is limited to managing the symptoms by increasing the activities of cholinergic neurons through acetylcholinesterase inhibitors (Sp3 inhibitors), and/or by targeting glutamatergic neurons with NMDA antagonists such as Memantine[10]. However, treatment offers little to no effect on the long term progress of the disease[4].

There is one other strategy that is being tested. Apart from reducing the amount (production, accumulation) of A β in the brain or compensating for the neuronal deficit, targeting the cell damaging mechanism of A β may be a meaningful (capable of disease modification) therapeutic strategy. However, the cytotoxic mechanisms of A β are highly complex[17], [18]. A β , along with other amyloidogenic peptides, are known to cause a host of different diseases, which are grouped together as "amyloidosis". There are many different amyloid peptides with different primary sequences that are involved in the various different amyloid-related diseases[19], but it has been postulated that these peptides may employ a common cytotoxic mechanism.

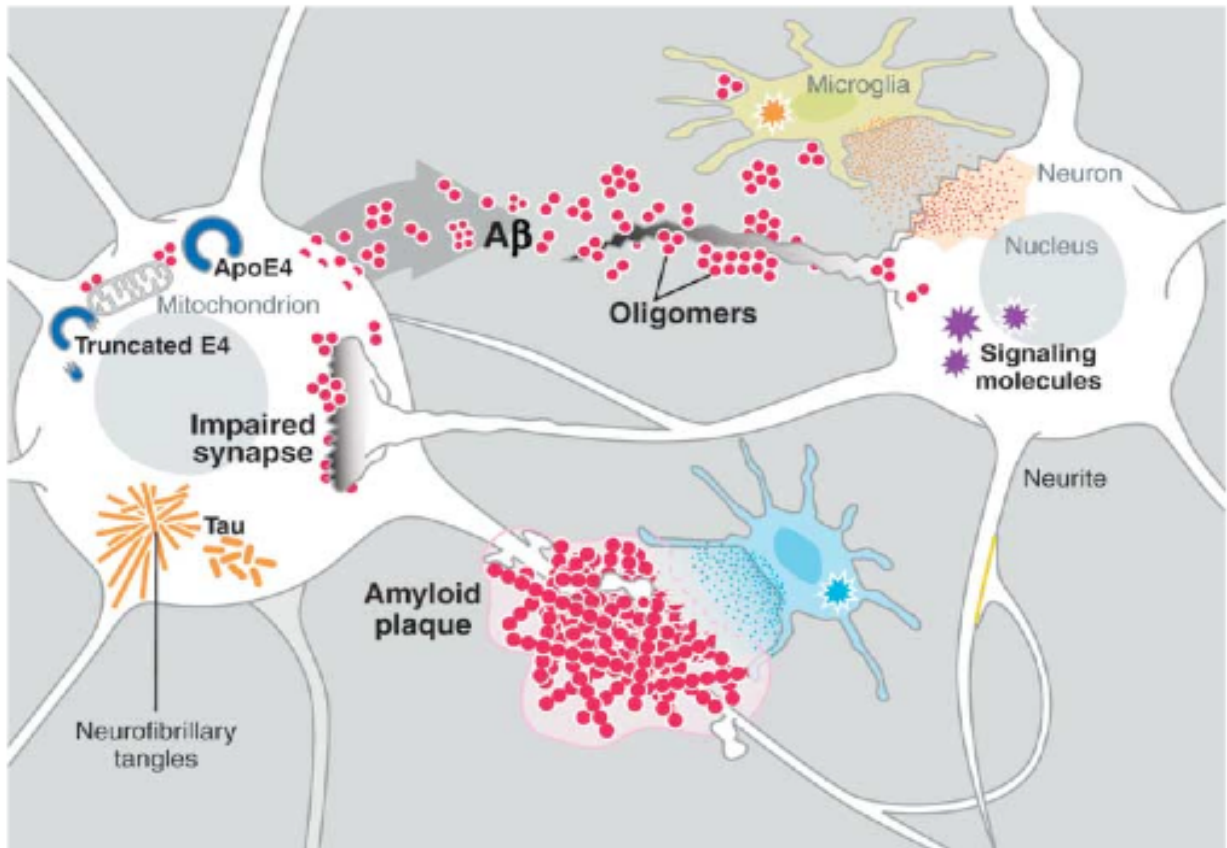


Figure 1- Alzheimer's schematic. A β oligomers and plaques (shows as red dots) are involved in AD pathophysiology through inducing synaptic/ dendritic impairment, and plaque formation, modified from E. D. Roberson and L. Mucke, "100 years and counting: prospects for defeating Alzheimer's disease" *Science*, vol. 314, no. 5800, pp. 781–4, Nov. 2006. Reprinted with written permission from AAAS [7].

All amyloid peptides are known to form various different self-aggregates that are toxic to cells. They are capable of spontaneously forming twisted strands of fibrillar aggregations that are rich in β - sheet formations, consisting of hundreds and thousands of individual peptides. They can also form smaller more amorphous aggregates consisting of a lower number of peptides than the fibrillar aggregates [20]. The smaller aggregates are called "oligomers", and they have been shown to be more toxic than the larger fibrillar aggregates. However, it is still unclear what exact

oligomeric aggregate is the most toxic form[21]. Characterizing the toxicity of oligomers is highly challenging due to their varying sizes and transient nature (spontaneously aggregates and changes over time). The structure specific toxicity of A β oligomers is unclear, and it is currently widely being investigated[22]. It should be noted that many receptor types and groups have been implicated as targets of these oligomers, including prion protein C (PrP^C)[23], G-protein coupled receptors[24], as well as AMPA and NMDA receptors[25].

Increasing evidence suggests that rather than focusing on the exact species of oligomers, understanding the cellular condition that provokes and fosters the process of A β aggregation may be of greater importance[21]. The primary site of A β production, aggregation and toxic effects, is the cell plasma membrane. Therefore, the membrane environment is receiving increased attention as a potential target for AD therapeutic approaches[26]–[29]. Specifically, regions within a membrane that are rich in cholesterol have been implicated in the disease[6], [30], [31]. Cholesterol containing membrane areas are known to have increased density of the A β precursor components, such as the APP (which is known to directly bind to cholesterol) and also the β and γ secretases[6], [30]. By increasing the interaction of the A β producing components, cholesterol in the lipid membrane has been shown to be associated with increased A β production[6], [32], aggregation, and toxic effects[30], [31], [33].

1.2 Cell Membrane Connection

A β originates from the cell plasma membrane and is cleaved from the membrane-spanning amyloid precursor protein (APP)[34]. Also the harmful effects of A β are primarily linked with destabilizing the structure and function of the lipid membranes[6]. Furthermore, the amount of membrane bound A β directly correlates to AD symptoms in humans[35]. Therefore,

understanding the effects of A β on the lipid membrane is thought to be crucial in understanding the overall disease mechanism and pathophysiology.

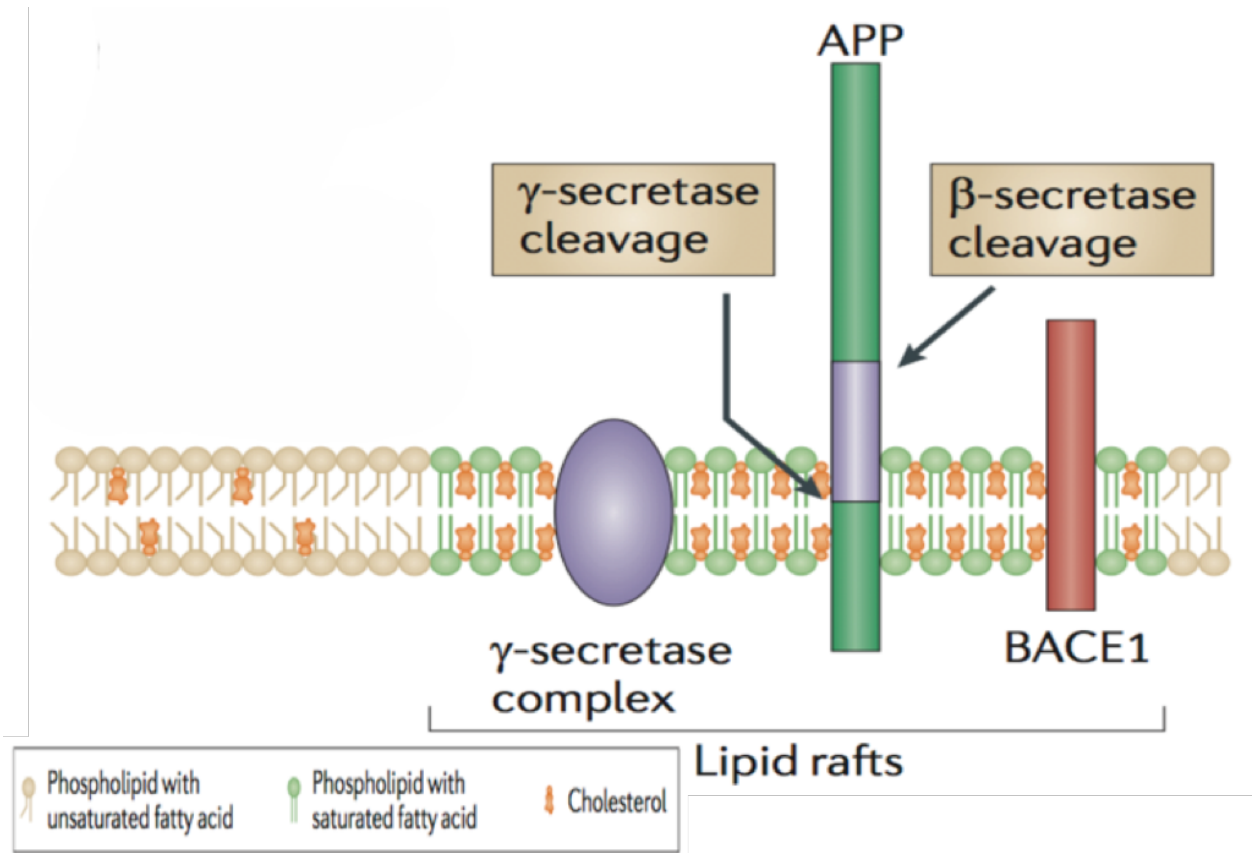


Figure 2- A β production mainly occurs in membrane lipid rafts. Amyloid precursor protein (APP) as well as the enzymes required for A β (depicted as purple section within APP, shown in green) production prefer to locate in lipid rafts, favoring amyloidogenic proteolytic processing of APP, adapted by written permission from Macmillan Publishers Ltd: Nat Rev Neurosci DOI: 10.1038/nrn3012, copyright 2011 [6].

It is known that membrane raft domains, enriched in cholesterol and sphingolipids facilitate amyloid clustering, aggregation, as well as production[30]. It was found that cholesterol levels directly influence the enzymatic activity and local density of the A β producing constituents

(APP, Beta-site APP Cleavage Enzyme1 or BACE1, and γ -secretase)[6]. When these components are present in non-raft regions, the amount of interactions are relatively low and are qualitatively different such that $A\beta$ becomes a minor product. However, the components are more frequently found in lipid raft regions where their interaction highly favors amyloidogenic processing of APP [32], [33]. Thus it is evident that lipid rafts play a major role in $A\beta$ pathophysiology, and targeting them could become an effective treatment strategy[6].

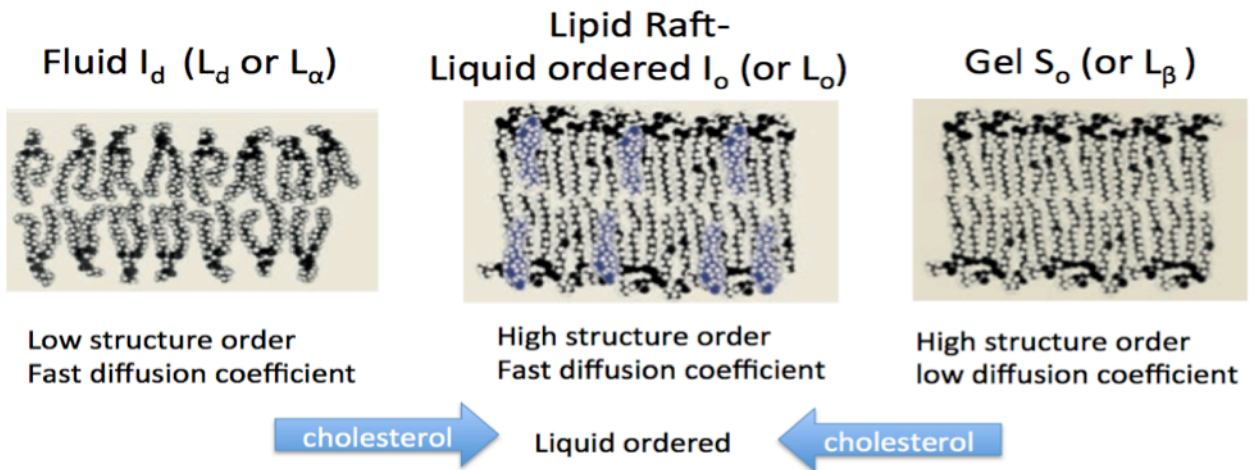


Figure 3- Molecular illustration of three different membrane phase states. (Left) Normal cellular membrane bilayers are in a 'fluid' or L_d state where the lipid molecules are highly mobile. (Middle) Addition of cholesterol reduces the structural freedom of the membrane lipid molecules to form a 'lipid raft' or liquid ordered (L_o) state. (Right) Gel phase membranes consist of lipids with saturated fatty acid chains that are inherently stable in terms of molecular motional and diffusional freedom. Blue arrows at the bottom show how adding cholesterol can change the membrane phases into the liquid ordered state. Adapted by written permission from Macmillan Publishers Ltd: Nat Rev Mol Cell Biol, DOI:10.1038/nrm2330, copyright 2008 [36].

1.3 Membrane Biophysics

Membrane lipids have traditionally been considered to be passive bystanders in cellular processes. However, as illustrated in the A β related processes in AD, they are now considered to be an important factor involved in many cellular processes including stabilizing membrane bound protein motifs and affecting protein channel gating/ conductance properties[37], [38]. The most widely known membrane lipid effect on proteins is called the 'hydrophobic mismatch', where there is a discrepancy between the thickness of the hydrophobic region of a protein and the surrounding hydrophobic bilayer environment[38]. This mismatch can affect protein function through influencing its structural conformation. Many pharmacologically active compounds (drugs including antibiotics and anesthetics) are believed to alter such protein-lipid boundary conditions, at least in part by non-specifically interacting with the membrane lipids and changing the biophysical properties of the membrane bilayer[39], [40]. Small biologically active compounds such as anesthetics[41], [42] and other drug/ pharmacological agents including non-steroidal anti-inflammatory drugs[43] have been shown to exert part of their effects through altering the properties of the lipid bilayer[44].

The potency of these pharmacological agents correlates well with the molecules' hydrophobicity, and hydrophobicity, in turn, corresponds with their ability to incorporate into lipid membranes[45]. The relationship between anesthetic potency of molecules and their measured water-oil partition coefficients display a positive correlation, which is dubbed as the Meyer-Overton rule. New evidence suggests that the potency correlation becomes even stronger and more reliable if the effects were measured in the bilayer instead of the water-oil phase[46]. However, some of the molecules do not follow this simple potency versus lipid-water (or

membrane) partition coefficient relationship. The effect of solutes on the bilayer properties that alter protein conformational equilibria may depend not only on their concentration in the membrane (as determined by their hydrophobicity), but also on the structure dependent interaction of the solute[45]. Thus, a more structure based understanding of the membrane interaction of small molecules is needed to further improve the understanding of the functional mechanisms of these biomolecules that involve non-specific interactions with lipid membranes[47].

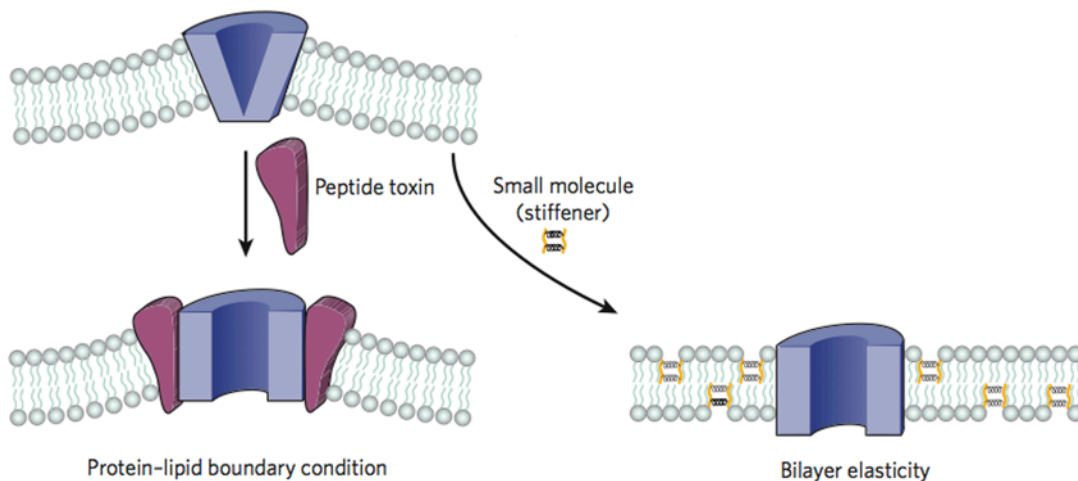


Figure 4- Illustrations of how different molecules in the membrane bilayer (peptide toxin shown as red, or other small molecules, shown as yellow) can alter membrane channel protein (blue) structure configuration and function by affecting the protein-lipid boundary conditions. (Bottom right) Small molecules can affect membrane proteins by changing the physical property (elasticity) of the bilayer, adapted by written permission from Macmillan Publishers Ltd: Nature, DOI: 10.1038/nature08147, copyright 2009 [38].

1.4 Melatonin and Related Molecules

Melatonin (N-[2-(5-methoxy-1H-indol-3-yl)ethyl] acetamide) is a hormone known to reduce the effects of A β toxicity[48]. It is a neuro-hormone secreted mainly in the pineal body in the brain, and it is best known for its involvement in the circadian rhythm[49]. Melatonin is also a hormone associated with aging, since its synthesis and rhythmical secretions decline with age[50]. In the pineal body, melatonin is converted from serotonin via two enzymes, serotonin-N-acetyltransferase (SNAT) and hydroxyindole-O-methyl transferase (HIOMT). The circadian rhythm of SNAT is controlled by the hypothalamic suprachiasmatic nuclei (SCN), which in turn produces melatonin's rhythmic production[51]. Due to relatively short (~30min) half life of melatonin in systemic circulation[52], melatonin levels fluctuate closely to its production. Interestingly, melatonin has also been shown to play a protective role in age related diseases such as in Parkinson's disease as well as in AD[53].

Early links between melatonin and AD came from sleep studies where many AD patients reported having abnormal sleep/wake cycles. It was discovered that they also had impaired melatonin secretion at night[54]. Melatonin levels in the cerebrospinal fluid/ brain of AD patients were significantly lower compare to aged matched control[55], and AD patients with ApoE- ϵ 4/4 alleles (know AD genetic risk factor) showed even lower melatonin levels and more severe symptoms than the patients without the genetic risk factor[54]. A recent report showed that sleep disturbances correlated with increased A β levels in the brain, so optimization of sleep, perhaps through enhancing melatonin's function, may help to reduce the levels of A β in slowing the progression of AD[56].

In vitro cell studies also confirmed that melatonin provided protection against most of the currently identified cytotoxic processes associated with A β , including intracellular calcium accumulation, reactive oxygen species production, inflammatory autoimmune responses, nitric oxide production, decreased membrane fluidity, and alteration of cytoskeleton [57]–[64]. Furthermore, melatonin was able to decrease the A β self-aggregation process[65]. This effect (decrease amyloid fibrillization and neurotoxicity) was even more prominent in the presence of APOE (apolipoprotein E), which is the gene product of an AD risk factor gene ApoE- ϵ 4[66]. The result corresponds with another related report that showed patients with the ApoE- ϵ 4/4 alleles had lower melatonin levels and more severe symptoms, compared to patients without the gene[54]. In transgenic mouse models of AD *in vivo*, melatonin reduced the amyloid load in the brain, and it also increased the longevity of the animals when treatment starting from an early age[67], [68]. Much of its positive effects have been attributed to its anti-oxidative effects, however, melatonin has been shown to be more potent than its related analogues (with very similar anti-oxidative properties) or compared to other well-known anti-oxidants such as vitamins C and E. This may indicate that there are other additional mechanisms involved in melatonin's protective effects[69].

Melatonin's protective mechanism may also involve direct interactions with the cell membrane. Many studies have shown evidence that melatonin is able to interact with lipid membranes, however, the exact manner of interaction and the effects it has on the membrane is not yet clarified[70], [71]. It may be worth pursuing, as *in vitro* experiments showed that melatonin is able to increase cell survival by maintaining cell membrane lipid fluidity and blocking increased membrane ion conductance induced by A β [57], [60], [72], [73]. Also, in

primary rat hippocampal co-cultures, melatonin prevented calcium permeation through the mitochondrial membranes[74]; mitochondrial/ cell membrane depolarization via calcium ion influx is one of the well-known aspects of A β toxicity.

Interestingly, there may be a relationship between melatonin and cholesterol. Melatonin has been shown to reduce the A β induced membrane ion conductance (uncontrolled permeability), but the presence of cholesterol has been shown to increase it[31]. Melatonin has been shown to lower serum cholesterol level in humans and animals, and it may also be directly competing with cholesterol in binding to membrane lipids[75]. It is possible that melatonin may have opposing or competing effects compared to cholesterol on the physical properties of the membrane. However, this has not been directly investigated as yet.

In summary, it is possible that melatonin may be involved in protecting the membrane by directly interfering with the A β induced membrane effects, and also by having counteractive effects to cholesterol in the membrane. The hypothesis of the project is that melatonin is able to produce protective effects against A β by influencing the physical structure of the membrane. Through such effects then, it may be able to reduce the binding and accumulation of A β on the membrane. Although it may be true that receptor activation is not needed to provide cell protection[76] the concentrations of melatonin required to provide cell protective effects against A β are sufficient high (>10 μ M concentrations needed versus nM to pM affinity for melatonin receptors[77]) to involve and invoke receptor activation. Thus, it is reasonable to assume that non-specific membrane effects of melatonin also promote and coincide with receptor activation and that the two phenomena are not mutually exclusive.

In addition to activating its own membrane receptors, membrane actions of melatonin may also indirectly influence the function of many other membrane proteins by altering the lipid membrane properties. Considering that A β also binds to large number of different types of membrane receptors[24], it is possible that melatonin may be involved in slowing down or altering the activities of these receptors through affecting the membrane environment. It is also possible that, in line with the hypothesis of this project, melatonin may be able to decrease the amount of A β available in the membrane that are able to bind and activate these receptors. Although the primary focus of this project is to study the membrane effects of melatonin and other relevant molecules, establishing the connection between membrane protein function and membrane actions of the molecules might be essential to fully understand their role in AD as well as in cell biology in general.

1.5 Project Overview

The overall objective of the project is to clarify the effects of melatonin on the biophysical properties of membranes that occur through receptor independent non-specific interactions. It is also to show that the effects are involved in and responsible for its protective effects against A β . The consequence of melatonin's effects on membranes will be determined by assessing A β accumulation on model membranes.

There are several points to be considered in this project of studying melatonin's membrane effects. In addition to its non-specific interactions, melatonin has two other receptor independent effects that are probably involved in its protective effects. One of the effects is its ability to reduce A β aggregation in solution through directly interacting with A β [65], [78]. Second is its ability to reduce oxidative stress induced by A β through its anti-oxidative properties[69], [70].

The significance of these properties will need to be verified against its membrane effects, in order to clearly distinguish the extent and the significance of its non-specific membrane action in A β toxicity. For example, suppose melatonin is found to reduce the amount of A β aggregates present in the membrane. Knowing how much of its anti-aggregation properties contributed toward the results will be important in distinguishing the significance of the membrane effects.

Another factor to be considered is that measuring the reduction of A β aggregates present on membranes surfaces due to melatonin may only infer a possible reduction of the toxic effects of A β . It is difficult to ascertain the exact correlation between A β membrane accumulation and A β toxicity, as the relationship between the amount of A β in the membrane and the toxic effects are not yet clearly understood[28]. It is probable that if reduction of A β is observed with melatonin, then additional studies may be required to verify that toxicity reduction also occurs under the same condition, in order to strongly suggests a correlation between membrane action and toxicity.

There were two main techniques utilized for the project: Langmuir monolayer technique and Atomic Force Microscopy (AFM). In consideration of the capabilities of the techniques utilized, the overall objective of the project has been distilled down to two specific goals. First goal was to characterize and measure the membrane effects of the hormone melatonin (and other related molecules) on model lipid membrane assemblies' physical structure. Once the membrane actions of the molecules in altering the physical properties were assessed, the second goal was to determine to what extent the measured membrane actions of the molecules affect the membrane association of A β . Experiments have been designed and conducted accordingly, and the details

of the experiments as well as the results are presented in the main body of the thesis, which is divided into three chapters (chapters two, three and four).

In chapter two, development and experimental results using the Langmuir-Blodgett monolayer technique are shown. In this chapter, steps involved in developing the technique in order to improve the precision of the measurements are explained, followed by the results of assessing the effects of small molecules, such as melatonin and other tryptophan derived molecules as well as cholesterol, on the lipid monolayer assembly. Finally, results from A β binding and incorporation studies using the technique are included.

In the third chapter, results from AFM imaging and AFM force spectroscopy are presented. Detailed steps taken in developing the necessary protocols for producing supported bilayers, as well as measuring bilayer membrane properties through using breakthrough force measurements are also presented. Results from assessing A β binding and assimilation on model bilayer membrane is also presented in this chapter.

In chapter four, collaborative work was conducted to obtain complementary data to support and verify the membrane experiments, and also to extend the scope and relevance of the project in higher order biological systems, such as cells and tissues. Works including characterizing A β deposits in the human retina, as well as testing melatonin's effects in cell cultures are presented. Other collaborative works featuring other techniques are also presented, and the featured techniques include molecular dynamics simulations, and dynamic light scattering. The collaborative studies were conducted and utilized to obtain supportive and complementary data for the results in the main part of the study presented in the previous two main chapters.

The last, fifth chapter contains a summary of all of the experiments. Concluding remarks with perspectives on merits and achievements of the project are also included in this chapter.

Chapter 2

Langmuir-Blodgett Monolayer

2.1 Introduction

There are various techniques that study phospholipid assemblies as model systems for the plasma lipid bilayer membrane. One of the techniques, called the Langmuir-Blodgett (L-B) monolayer technique, is widely used to study compression isotherms of films at the air water interface and for deposition of films on solid supports[79]. The technique focuses on studying a single layer of phospholipid molecules (or any amphiphilic molecule) by studying them at the air-water interface. It utilizes the air-water interface as a surface on which amphiphilic phospholipid molecules can be spread very thin (single molecule layer thick) spontaneously. Historically, an American statesman, Benjamin Franklin, has first reported this property to the British Royal Society back in 1774:

"At length at Clapman where there is, on the common, a large pond, which I observed to be one day very rough with the wind, I fetched out a cruet of oil, and dropped a little of it on the water. I saw it spread itself with surprising swiftness upon the surface. The oil, though not more than a teaspoonful, produced an instant calm over a space several yards square, which spread amazingly and extended itself gradually until it reached the leeseide, making all that quarter of the pond, perhaps half an acre, as smooth as a looking glass." [79]

This observation makes the first reported demonstration of how amphiphilic molecules form a self-organized structure or film at the interface between water and air. It is now known that amphiphilic surfactant molecules undergo self-orientation at the water-air interface by having their hydrophobic portions face toward the air and the hydrophilic portions orient toward water,

in forming a single molecule thick film. Irving Langmuir first systematically studied the floating monolayer films in the late 1910's and early 20's[80].

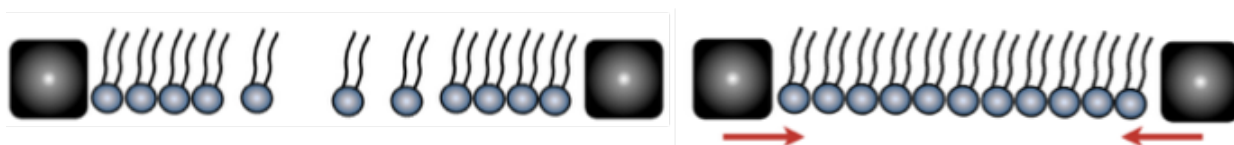
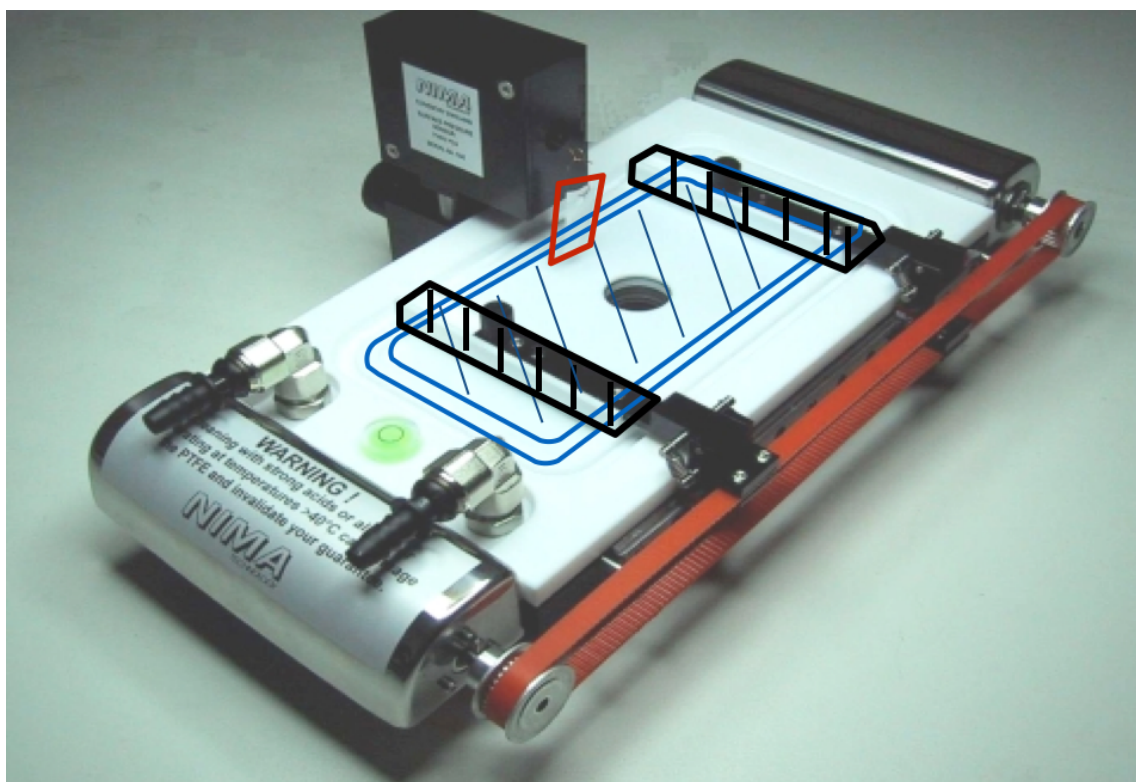


Figure 5- A photograph of a modern Langmuir monolayer trough with movable barriers used in the experiments. The movable barriers are highlighted with black lines, and the trough area where water is held is highlighted in blue. The paper pressure plate used to measure the monolayer film pressure is marked by a red box. Below the photograph is a set of illustrations showing how the monolayer sample becomes compressed using the barriers.

L-B monolayer studies have been extensively used for studying lung surfactants[81]. Lung surfactants are in majority phospholipids[82], [83]. The surfactants are naturally arranged in a monolayer formation at the air exchange surfaces along the lining of the alveoli, which are the air sacs in the lungs. They help to facilitate the expansion and contraction of the alveoli by reducing the surface tension at the liquid-air interface to near zero[83]. Langmuir monolayer simply reconstitutes the components of the lung surfactant onto a bath of water that is enclosed with movable walls or barriers. By bringing the barriers closer to or further from each other, one can replicate the expansion and contraction of the surfactant material and study its physical properties. Some of the measurable physical properties using the technique include area per molecule, lateral pressure per given area, compressibility, and surface tension. Also by incorporating various other molecules into the monolayer, thermodynamics of molecular interactions can be determined, such as binding kinetics and molecular mixing[84], [85].

Moving beyond studying lung surfactants, lipid monolayers can be used to mimic and study the two-dimensional behavior that would occur in a membrane bilayer[86]. It is not technically possible as yet to measure directly the parameters in a bilayer, such as its lateral expansion and contraction as well as lateral pressure profiles[87]. A half of a bilayer (monolayer) spread at the air-water interface can be used to estimate such effects using the bilayer correspondence theory[40]. Further usefulness of the monolayer technique is that when studying incorporation of small molecules into the membrane lipid assembly, the effects such as the area per lipid and time of incorporation can be readily measured.

In this work, the technique will be used to study monolayer isotherms, the most common and simple structural measure for floating monolayers. In an "isotherm", the surface pressure change

upon compressing the monolayer is measured against the area occupied by the film. The temperature is held constant during an isotherm, hence the name. During an isotherm experiment, the area of the trough (the monolayer film area) is reduced by moving the barriers closer to each other, and the surface pressure exerted by the film will increase as the result. Surface pressure (Π) is defined as a difference in the surface tension of water (γ) and water with the surfactant present (γ_0) [80].

$$\Pi = \gamma - \gamma_0 \quad (1)$$

Changes in the surface pressure are measured using the Wilhelmy plate method. A thin plate made from a choice of materials (very thin plate of platinum, quartz, mica, glass or filter paper) is suspended at the water surface partially immersed. The forces acting on the plate include gravity and surface tension pulling the plate down towards the water, and buoyancy pushing up on the plate from displacement of water. For a rectangular Wilhelmy plate with dimensions l_p , w_p and t_p , of material ρ_p , immersed to a depth h_1 into the subphase containing liquid with a density of ρ_l , the equation for the net downward force is given by the following equation:

$$F = \rho_p \times g \times l_p \times w_p \times t_p + 2\gamma(t_p \times w_p)(\cos\theta) - \rho_l \times g \times t_l \times w_l \times h_l \quad (2)$$

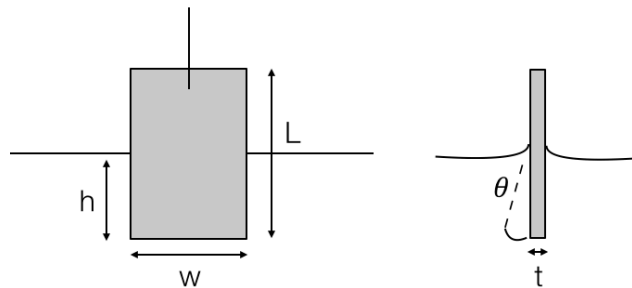


Figure 6- Depicting a Wilhelmy plate suspended at the air-water interface. Figure redrawn with written permission [79].

$$F = \rho_p \times g \times l_p \times w_p \times t_p + 2\gamma(t_p \times w_p)(\cos\theta) - \rho_l \times g \times t_l \times w_l \times h_l \quad (2)$$

The first term of the equation (2), represents contributions from gravity (g) acting on the plate. The last term of equation (2) represents the upward force due to buoyancy. When measuring the change in surface tension or Π , only the γ is assumed to be changing and contributions from either the gravity or buoyancy are ignored, as they do not change. The middle part of the equation represents contribution from surface tension related to the contact angle of the plate ($\cos\theta$) in respect to the surface of the water. Assuming that the plate is completely wetted, this angle should be 0° , thus the $\cos\theta = \cos 0 = 1$. Also the plate thickness is minimized to increase sensitivity, where $t_p \lll W_p$. Then, for $\Delta\gamma$, the equation becomes

$$\Delta F = (\text{gravity contribution ignored}) + 2\Delta\gamma(t_p \times w_p)(1) - (\text{buoyancy contribution ignored}) \quad (3)$$

$$\Delta F = 2\Delta\gamma(t_p \times w_p), \text{ but } t_p \lll w_p \quad (4)$$

$$\Delta F = 2\Delta\gamma(w_p) \quad (5)$$

$$\Delta\gamma = \Delta F/(2w_p) \quad (6)$$

Since Π (surface pressure) is the difference between the initial and final surface tension,

$$\Pi = -\Delta\gamma = -\Delta F/(2w_p) \quad (7)$$

The change in force in equation (7) is measured by measuring the changes in mass of the Wilhelmy plate. Thus the plate is directly attached to a sensitive electrobalance to continuously and accurately measures the force, which is then used to calculate the surface pressure change[80].

Measuring the surface pressure change as a function of the area occupied by the molecules is an important indicator of monolayer properties. This pressure (Π) vs area (cm^2 or $\text{\AA}^2/\text{molecule}$) measure, or the isotherm, contains several features that are unique to the amphiphilic material being tested. There are several discontinuities present in the isotherm and these regions are called phases[88]. At the beginning of an isotherm, the area is large and the monolayer molecules are far apart to have minimum intermolecular interaction. This phase is denoted as a gaseous state (G). As the area is compressed constantly during the isotherm, the molecules in the gaseous phase are compressed further and reach a liquid expanded (LE) phase. With continuing decrease in the area, some of the molecules in the LE phase undergo a shift in their molecular orientation to a more compact form. This is called liquid condensed arrangement or LC phase. The molecules in the LE/LC phases can co-exist (shown as a plateau area in the isotherm) and the decrease in area is being compensated by shifting the molecular orientation and packing rather than by increasing the pressure. Decreasing the area further converts all of the molecules into the LC configuration. Further compression of the LC phase molecules will reach their minimum possible molecular area until the 2-dimensional monolayer can no longer be sustained. This final phase of the isotherm is dubbed as the solid (S) phase. Similar to crumpling a flat sheet of paper, compression beyond the solid phase will induce buckling of the monolayer (monolayer collapse into 3 dimensionally folded structure) due to the area being too small to sustain a 2-dimensional monolayer film[89].

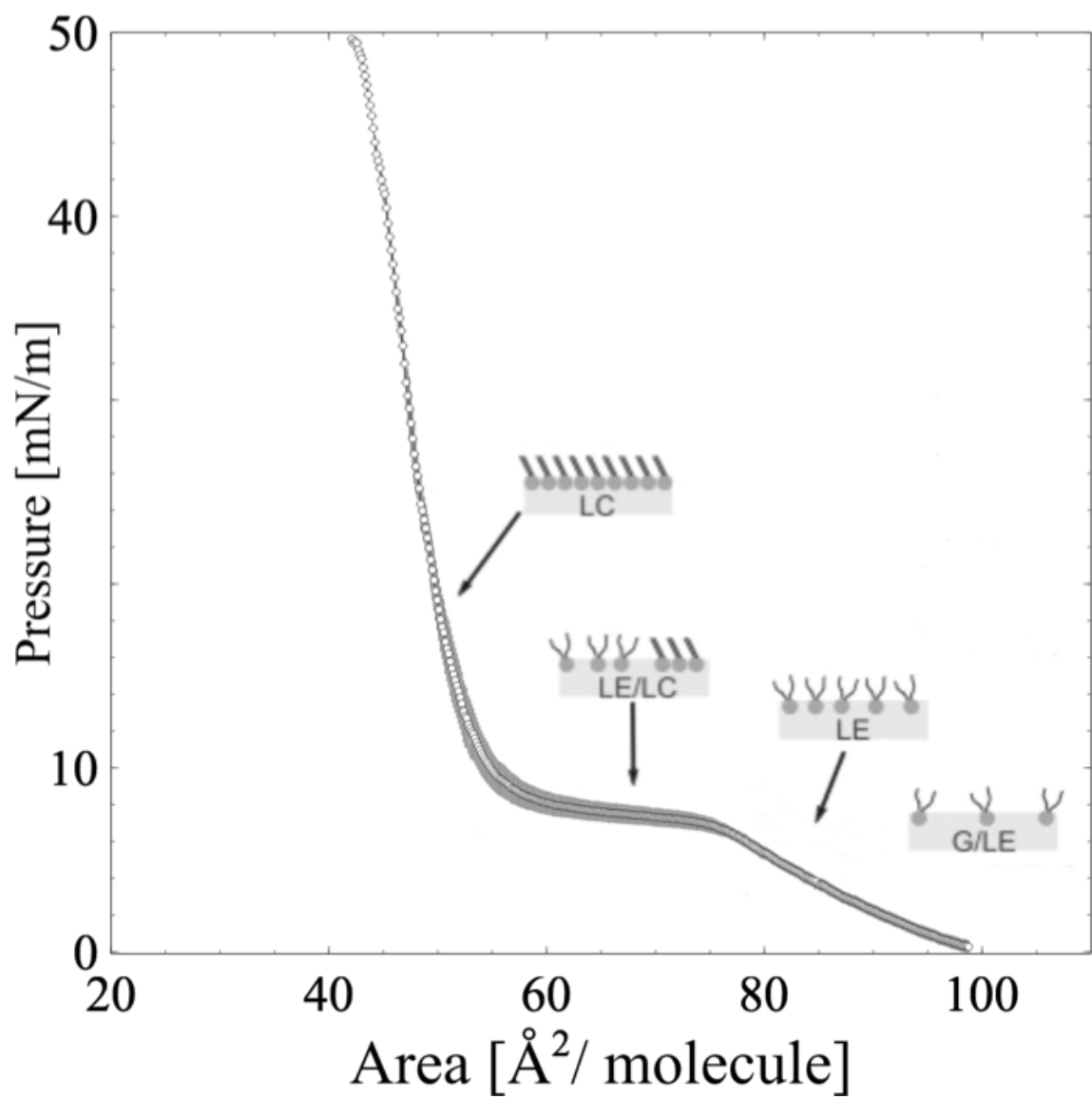


Figure 7- Schematic of a monolayer isotherm, displaying the various different phases during a monolayer compression.

The Langmuir monolayer technique often serves as a platform for characterizing and comparing the mode of molecular interaction of the group of biologically relevant molecules to the membrane lipids. The advantages of this technique, which utilizes a simple membrane model to obtain a pressure versus area isotherm, are that it is possible to quantitatively analyze the mechanochemical and thermodynamic properties of the solutes[90]. The data can also be related to the bilayer using the lipid monolayer-bilayer correspondence theory[86], [91], [92]. In the past, the technique has been mostly utilized to study the mixing behavior of lipids and other hydrophobic compounds[84], [93] as well as to study the incorporation of proteins in lipids[85]. For such reasons, it was decided to use this technique to accomplish two different purposes. The first was to study the incorporation of melatonin into the membrane lipid monolayer assembly. The second purpose was to characterize A β incorporation into the monolayer.

For the first part of the study, Langmuir monolayer isotherms (area versus pressure measurement) were utilized. Monolayer isotherm measurements are used to study molecular ordering in two dimensions. The water surface serves as a flat substrate on which amphiphilic phospholipid molecules can be arranged and manipulated mechanically to form various differently arranged configurations (different phases). Such direct mechanical control of surface pressure using the movable barriers is unique to this method. The advantage of this lateral pressure manipulation is that it can be used to estimate the 3-dimensional compression that occurs in a biological bilayer membrane, considering that a bilayer may be thought of simply as two coupled monolayers on top of each other. The 3-dimensional compression or expansion of a bilayer can be analogously analyzed through examining the 2-dimensional pressure of a monolayer at constant temperature, and this measure is called the 'pressure versus area isotherm'.

The isotherm measure is especially useful since lateral pressure components in a bilayer are extremely difficult to measure experimentally[86], [87].

The most frequently used phospholipid in monolayers as a membrane model has traditionally been DPPC. DPPC has many advantages as a staple compound used for monolayer experiments. It has saturated acyl chains (palmitate, 16:0), which are stable in air from degradation by reacting with oxygen in the atmosphere. Phospholipids with unsaturated acyl chains, or tails, can undergo oxidative damage within minutes when exposed to oxygen while being spread across the water-air interface such as in a Langmuir trough environment[94]. Monolayer studies designed to utilize unsaturated lipids require extra care, such as having a gas-tight enclosure, to ensure the damage is minimized. A further advantage of using DPPC is the abundance of published data, which makes it possible to directly compare and verify the findings with respect to the previously published studies. Newly establishing a standard with a less commonly utilized phospholipid molecule would have been time consuming and unnecessary.

Monolayer isotherms, especially DPPC monolayer isotherms can be used to study mixing behavior of multiple component monolayers. Studying how cholesterol and its closely related analogues behave in DPPC monolayers has been the most numerous published in the field. DPPC is also suitable in that the phosphocholine headgroup (PC) is the most abundant phospholipid headgroup type found in biological membranes[36]. PC molecules amount to nearly 50% of all membrane lipids. Particularly, it makes up a very high proportion of the outer leaflet of the plasma membrane[36]. It is also the principal phospholipid in lung surfactant as well as in the blood plasma. It is also an integral component of lipoproteins, which are cholesterol binding and carrying molecules. Accordingly, studies examining cholesterol and

membrane lipid interaction often use DPPC as the model PC. It is also the top choice for studies investigating lipid rafts, which are determined as membrane fractions that are not dissolved by detergent extraction[95]. Lipid rafts are hypothesized as cholesterol rich domains (domain refers to a specific area or patch within a membrane). The lipid rafts, or the cholesterol condensed domain (liquid ordered) regions are resistant to detergent extraction (figure 3). This is due to the fact that the high cholesterol raft fractions are highly enriched in saturated acyl chains relative to the average for whole cell phospholipids. This finding converged with studies of cholesterol interactions with saturated chain PCs, particularly DPPC, to suggest that the lipids of rafts, as defined by detergent insolubility, were in a liquid-ordered (Lo) phase. This phase was first defined in theoretical work based on five different experimentally determined phase diagrams for DPPC and cholesterol[95]. Since then, the DPPC and cholesterol system have been most widely used for both experimental and theoretical work, especially in Langmuir monolayer and molecular dynamics studies. Cholesterol has mainly a laterally condensing effect on both the monolayer and the bilayer, and this type of behavior can be best measured using the monolayer technique and/or *in silico*, and it is very difficult to measure directly in a bilayer.

It is also possible to study how different molecules interact with lipid monolayers from the water subphase using the technique. Many compounds including water soluble drugs as well as a variety of different peptides have been studied with the technique[96]–[103]. Such studies involve monolayer isotherms as well as binding assays. Monolayer binding assays involve compressing a monolayer to a set pressure and then set it to hold the pressure, add the molecule of interest into the subphase, and observe any changes in the molecular area. Any increase in the area per molecule indicates that the added compound is capable of inserting into the monolayer.

The kinetics of the incorporation can be determined also by monitoring the time of interaction until no more changes are observed (reaches equilibrium).

2.2 Method Development

In order to characterize changes brought on by molecules in the monolayer, precise measurement of control monolayers needed to be made. However, protocols for the method vary widely among many groups, and there is no rigorously established technical standard in Langmuir monolayer studies, even though DPPC monolayers have been extensively studied and work on them has been published in the literature. The protocols used in the literature were examined thoroughly to determine optimal practice to maximize the precision of monolayer measurements. The following list generally describes the steps used in the method development.

Step 1. Gather preliminary data

Step 2. Compare the results with literature

Step 3. Assess areas of improvement

Step 4. Test and improve each criterion

Step 5. Establish the best possible protocol for obtaining control measures

Step 6. Proceed to conduct experiments with the molecules of interest

First, control isotherms of DPPC were collected. Having control values that agree with previously published data is essential for validating our data. The first initial isotherm data from the experiments are shown in figure 8. Previously published data is also shown in the same figure. The vast majority of monolayer papers only feature isotherms from a single trial of

compression without any error bars. Most of the papers only mention in the methods section that the data shown in the paper are representative sample of multiple trials[72], [93], [103]–[109]. The published experimental isotherms shown as green lines in the figure are highly varied. Some contributing factors in creating the variability seen in the published isotherms may include differences in compression rate, geometry of experimental apparatus, experimental artifacts (leakage, impurities, etc.), as well as experimental parameters (pH, ionic strength of subphase and spreading solvent)[103]. However, they vary within a range. The consensus in the published isotherms is that the area spans from about $110 \text{ \AA}^2/\text{molecule}$ to no less than $40 \text{ \AA}^2/\text{molecule}$ for all of them (the pressure ranges from 0 mN/m to 55 mN/m). It is reasonable to assume that the true reference value for DPPC lies somewhere within this range since the range encompasses the molecular areas measured or calculated for DPPC using other techniques[110], [111].

The preliminary isotherms collected by myself and a colleague (red and blue lines) did not fall within the published range, aside from one of the later isotherms (purple line, figure 8). The collected isotherms show a much lower area per molecule than expected. A dark black line is drawn at the $40 \text{ \AA}^2/\text{molecule}$ mark to indicate the lowest area reached by the published isotherms, and our experimental isotherms clearly are shifted further to the left of this line. The line at $40 \text{ \AA}^2/\text{molecule}$ is also drawn in figures 9, 10, and 11 for the purpose of indicating where the published isotherms usually end. However, researchers need to be aware that the published isotherm data varies widely.

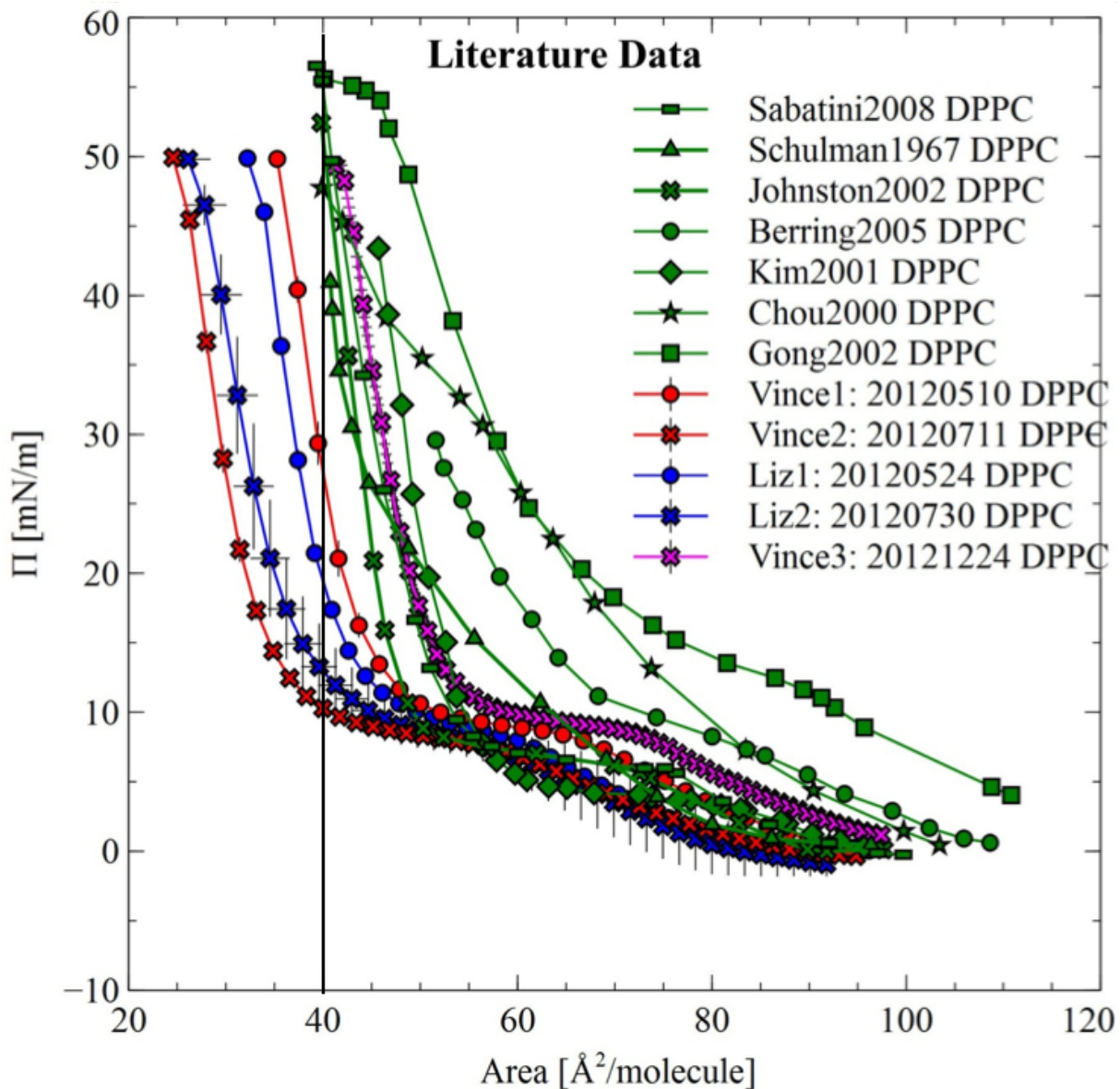


Figure 8- DPPC monolayer isotherms from literature compared to our own preliminary data from the lab. Green lines denote previously published monolayer isotherms, blue, red and purple lines denote our own data. The purple line represents an isotherm that agrees with the literature, which starts at about 100 \AA^2 per molecule and ends at about 40 \AA^2 per molecule. The black line at 40 \AA^2 /molecule is included for clarity (Figure credit Dr. Attwood, modified and presented with written permission).

Precision of the isotherms was measured by repeating the trials. The variability (standard deviation) of the data is shown in figure 9. Overall, each of the three groups of ten isotherms varied in area by $>10 \text{ \AA}^2/\text{molecule}$. The changes produced by adding melatonin in the subphase were evident (figures 10, 11), and at 11.5 mN/m, the difference between control and either of the two melatonin samples were significant ($p < 0.05$). However the difference between the two melatonin groups was not significant. The observed precision (degree of variability as shown by the standard deviation) suggests that a representative (average) isotherm should be accompanied by error bars. Although melatonin's effects were discernable compared to control, the range of the isotherms (compared to the literature values) was still not initially within the previously reported values (figure 9). The shift in the isotherms away from the literature values is lower in figures 10 and 11, due to making various protocol adjustments as explained in this section below.

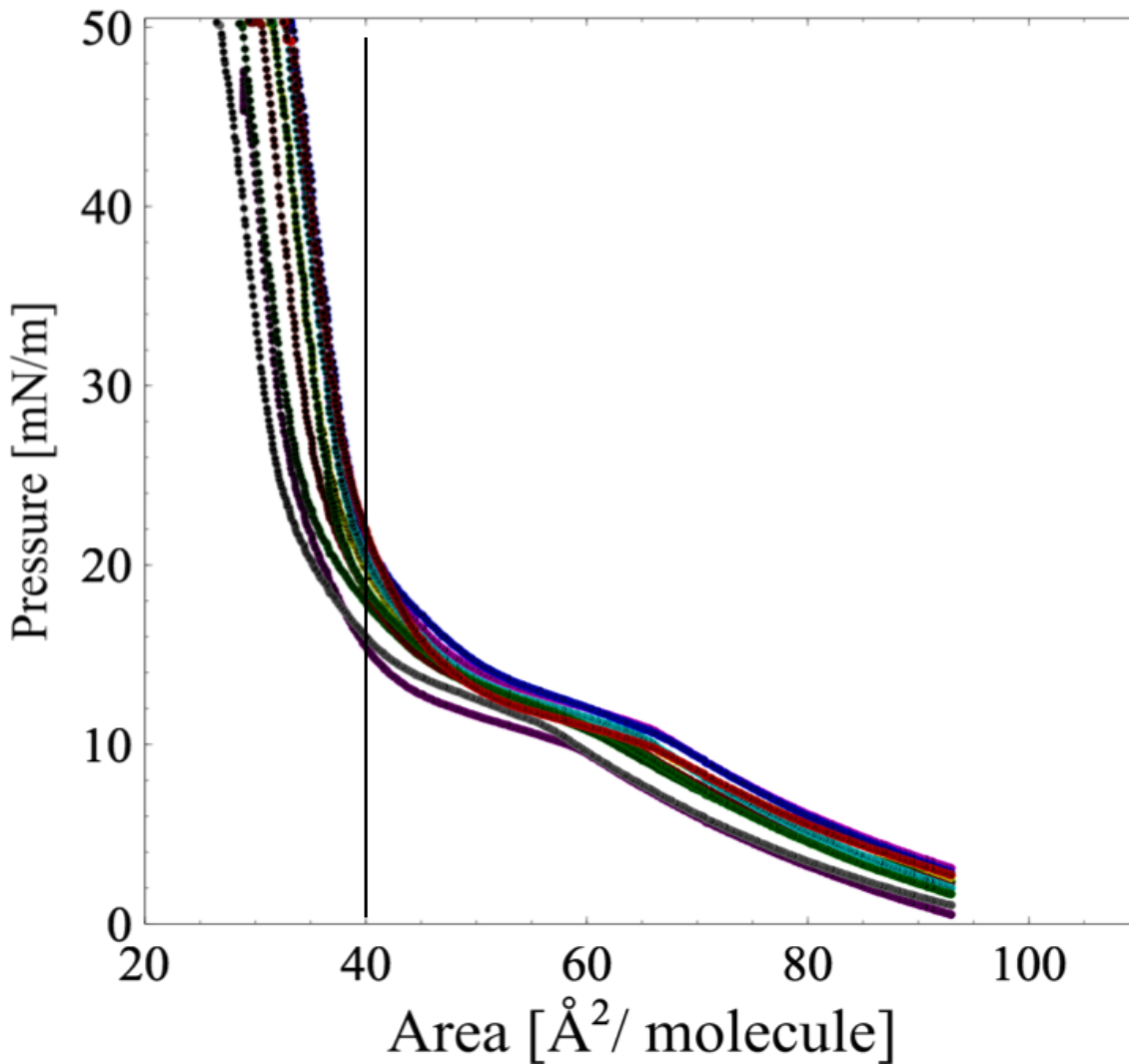


Figure 9- Raw initial DPPC monolayer isotherms. Each line represents an independent trial. Black line at area per molecule 40 \AA^2 is included to clearly indicate the shift toward area values lower than that found in the literature observed in the data. DPPC was used at room temperature, spreading solvent was chloroform, micropipette was used, and lipid solution concentration was 1 mg/ml with deposition volume of 10.0 \mu l . The starting points of all the isotherms are consistent due to the machine area capacity being at the maximum area possible. Varying amounts of lipids were deposited onto the trough at the beginning of the experiment due to variability in the procedures, and having different amounts of lipids resulted in the vertical shifts of the starting points, due primarily to having excess amount of lipids.

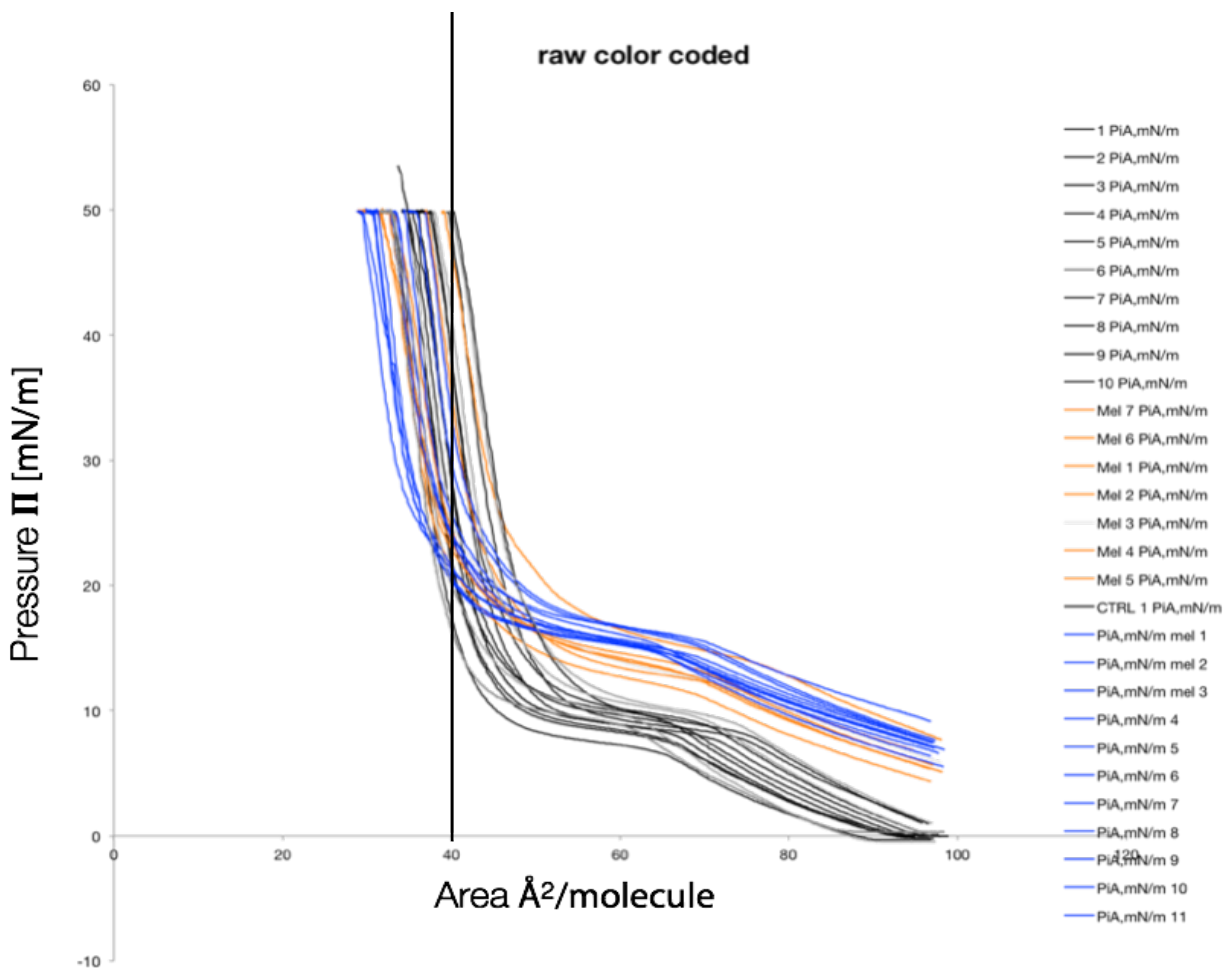


Figure 10- Raw DPPC isotherms. Control DPPC (black), DPPC with 1.0 mM melatonin (orange), and DPPC with 2.0 mM melatonin (purple) in the subphase are shown. DPPC was used with melatonin in the subphase (water) at room temperature, spreading solvent was chloroform, micropipette was used, and lipid solution concentration was 1mg/ml with deposition volume of 10.0 μ l. The starting points of the isotherms are higher compared to figure 9, but they are in agreement with figure 8, purple line. A different maximum area was used in these trials than in figure 9, causing higher values at the start of the isotherms.

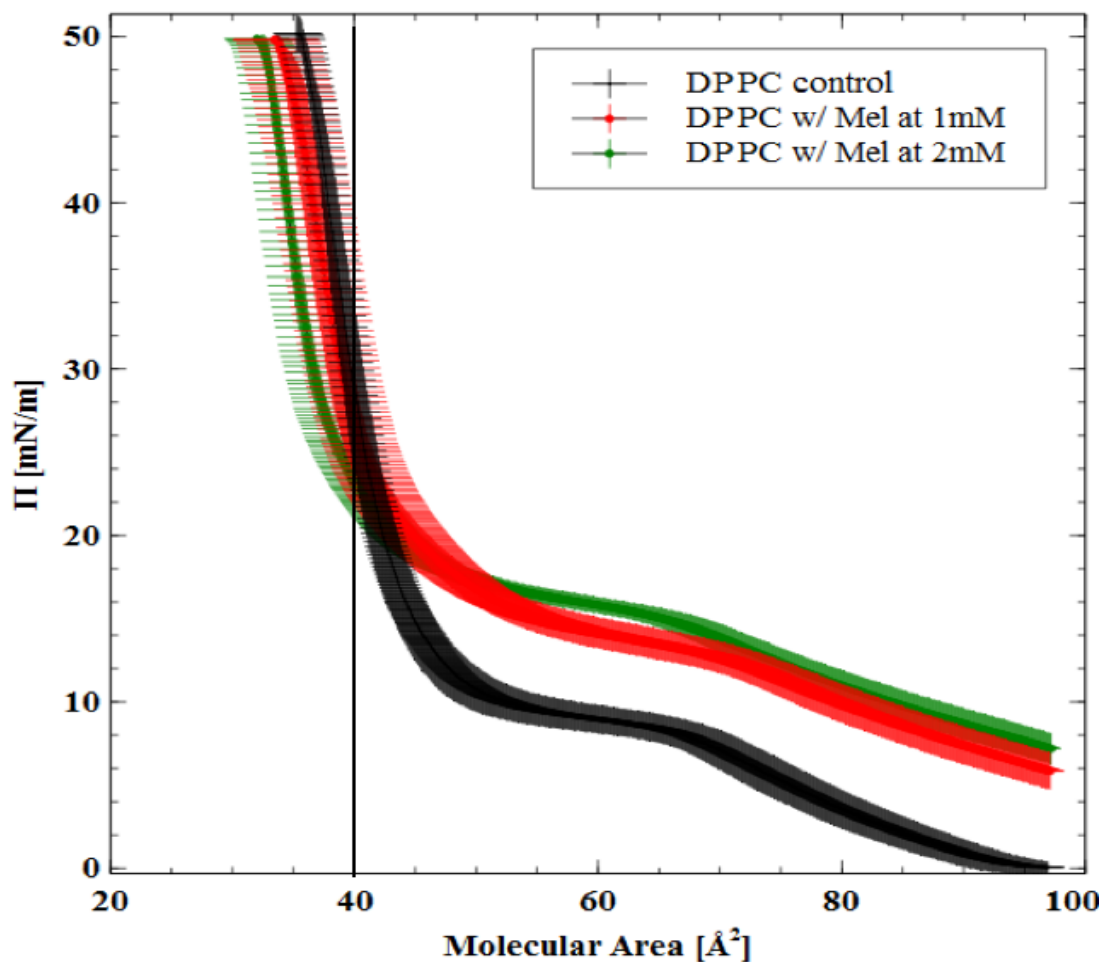


Figure 11- Data from figure 10 is converted to show averaged isotherms with standard error of the mean (SEM). Averaged control DPPC is shown in black, averaged isotherm with 1.0 mM melatonin is shown in red, and 2.0 mM melatonin is shown in green. Black line at area 40\AA^2 denotes the minimum area most often observed for published isotherms in the literature (figure 8). The curves are tested with Student's t-test at critical points to confirm differences. The number of curves averaged for control (black curve) was 11, for melatonin 1.0 mM (red), $n=7$ and for 2.0mM melatonin (green), $n=11$ (Figure credit Dr. Attwood, modified and presented with written permission).

In an attempt to further improve the precision of our isotherms, a detailed comparison of experimental parameters was performed to screen anomalies in the protocol used for the initial data. Factors such as the pH of subphase, experimental temperature, compression rate, source and purity of the compounds, concentration, experimental apparatus, spreading solvent, subphase, evaporation time after deposition, as well as solution volume were considered. Other than the apparatus used (all groups used different machines), the approaches used for the initial data were overall in agreement with the parameters used by other groups.

Testing the apparatus involved comparing two different Langmuir monolayer troughs using an identical protocol. WATLab, University of Waterloo, provided access to a second monolayer trough. Isotherms as well as pressure hold measures were conducted using the two machines. The results are shown in figure 12. For the isotherms, our machine showed lower molecular area measures (isotherms were shifted to the left of the ideal range), whereas the WATLab machine had isotherms shifted to higher area per molecule values. The results were consistent even after multiple rounds of checking calibrations for both of the machines. The pressure hold experiments revealed that over time, both machines showed decreased area while keeping a constant compression pressure. The result indicates that DPPC molecules kept inside the trough between the barriers is decreasing and are being lost during compression, either through barrier leakage or through solubilization into the subphase. Even though both machines showed inadequacies in the isotherms as well as in pressure hold experiments, it was decided to improve our own existing trough by replacing its barriers.

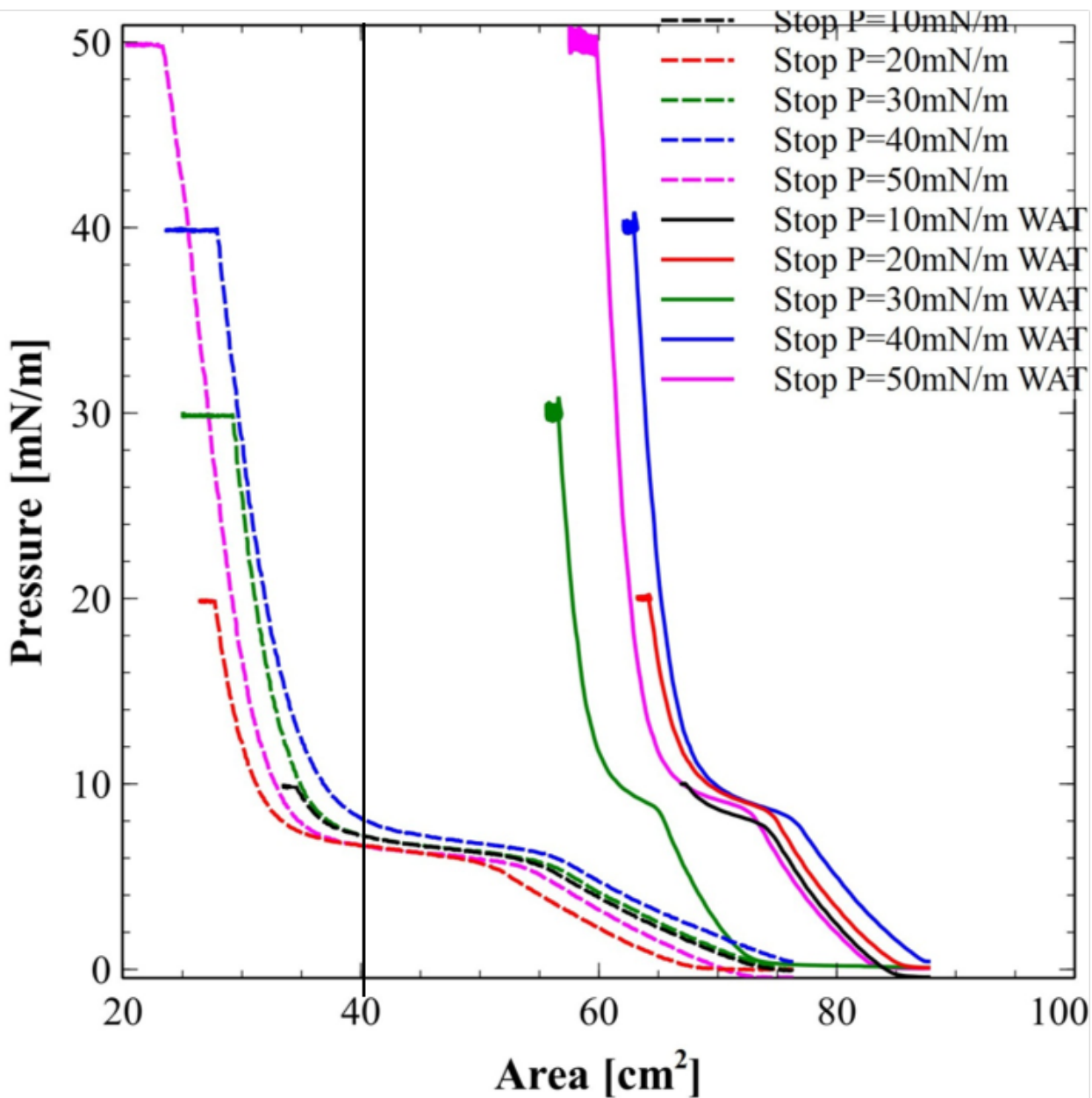


Figure 12- Isotherms gathered from the lab machine (dotted lines) and also from another machine at WATLab (solid lines) with increasing pressure. The shift of curves with pressure is similar for the two machines but those shifts are not a consistent function of pressure. However the WATLab machine (solid lines) showed an irreconcilable software bug that incorrectly skewed the results toward higher areas. The lab machine (dotted lines) has an opposite problem where the isotherms were shifted left or drawn out and skewed toward lower areas (Figure credit Dr. Attwood, modified and presented with written permission).

To test for leakage, pressure hold experiments were conducted on both of the two machines. Pressure hold experiment involved compressing the isotherm to a set pressure, and setting the trough machines to hold that pressure for an extended amount of time. A full range of pressures was manually selected for testing to determine the pressure dependency on leakage rate. The selected pressures were 10, 20, 30, 40, and 50 mN/m. The data is represented in an area versus time graph. An ideal case for a pressure hold experiment should yield a flat horizontal line in the area versus time graph starting from the point at which the target area is reached (the area value is determined by the corresponding compression pressure, which is manually selected for the trial. The higher the pressure values are, the lower the area is). At all five pressures tested, both machines showed evidence of leakage. The area values decreased at various rates over time, rather than remaining constant. The area decrease indicates that in order to maintain the set lateral pressures, the barriers had to continuously move in and shrink the compressible area, implying that the material was constantly being lost through leakage.

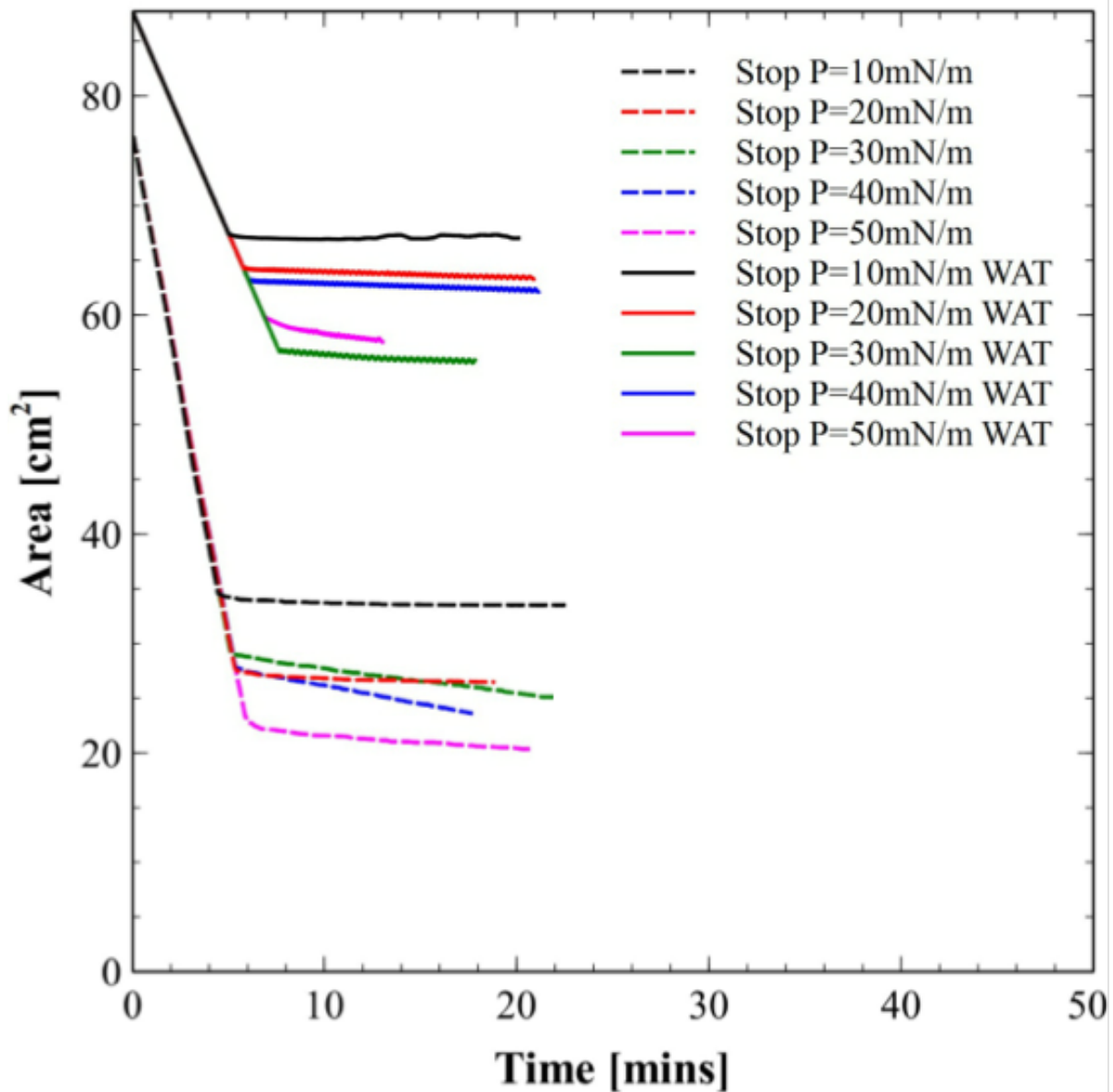


Figure 13- Area versus time data for the two troughs. Own machine data is represented in dotted lines, WATLab data is shown in solid lines. The initial downward slope represents the initial compression to the set pressure point, and then the area should remain unchanged in an ideal case. However, some trials show a decreasing trend (negative slopes) in the area over time. The decrease was immediate from the beginning of the pressure hold, and the pressure decrease is a problem for conducting pressure-hold experiments with A β , which may require up to 300 minutes of sustained monolayer pressure (Figure credit Dr. Attwood, modified and presented with written permission).

Strategies to mitigate the problem involved purchasing new barriers. The new barriers were made of Delrin, which is a hydrophilic plastic specifically chosen for the monolayer application. Traditionally, monolayer trough machines utilized barriers made of Teflon, which is a hydrophobic polymer. Delrin barriers were chosen as the leakage of the material during a pressure hold experiment should be much lower compared to Teflon barriers[112]. Unfortunately, even with two sets of Delrin barriers, the trough leakage persisted, with the new second set of barriers providing a slight improvement over the old pair. One of the issues discovered was that the manufacturer recommended cleaning procedures for the barriers were obsolete and incorrect. The Delrin barriers were being cleaned using chloroform, which is only recommended for cleaning Teflon barriers due to their hydrophobicity. It was since corrected to only use ethanol and water for cleaning. A comparison of the leakage rates for the old and the new sets of barriers are shown in figure 14. There was a measurable decrease in leakage with the new barriers but the difference was not remarkable.

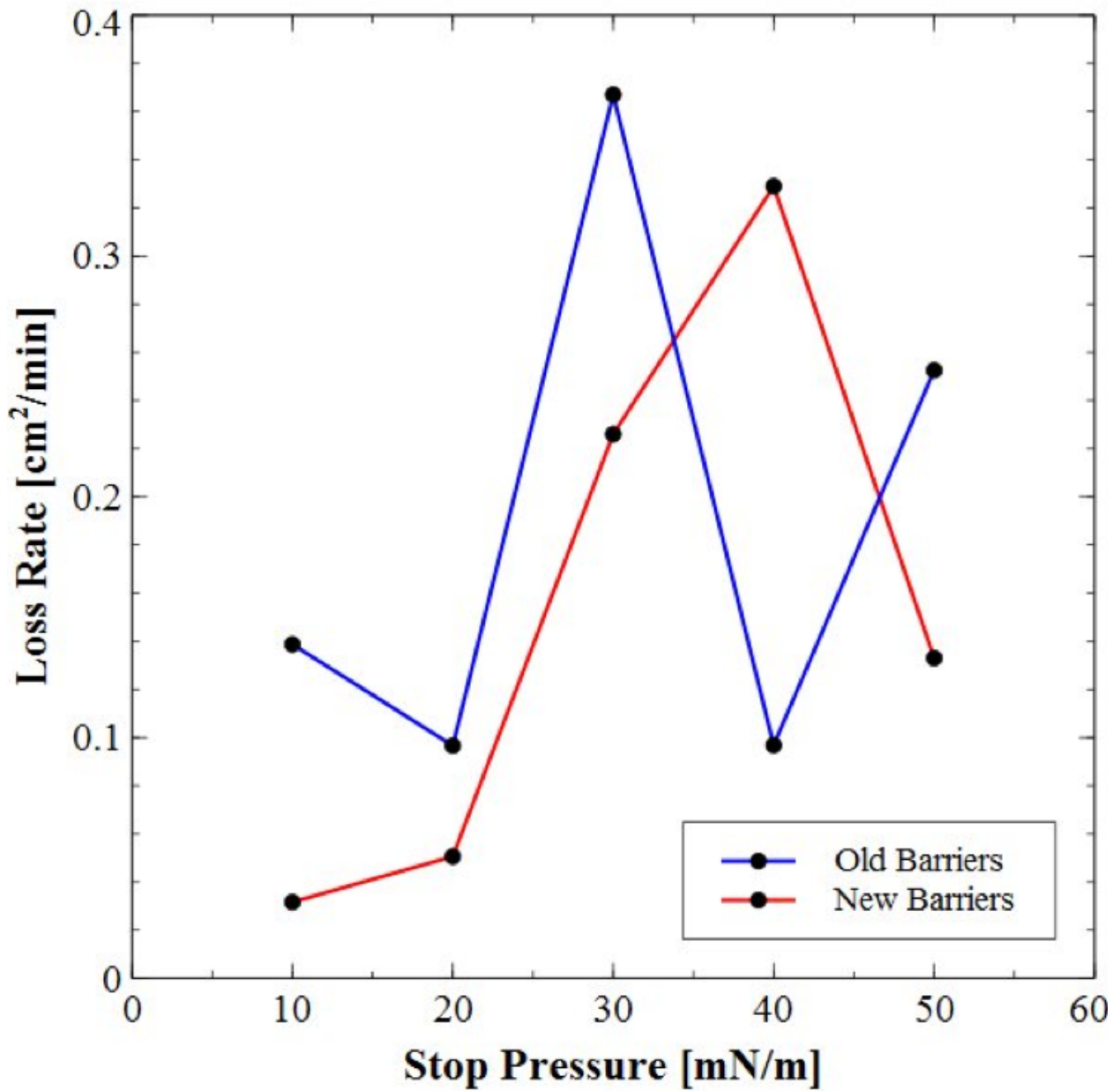


Figure 14- Comparing the differences in the loss rate (leakage) of two different sets of Delrin barriers at given pressures. The old barriers (blue) have been cleaned using chloroform, and new barriers were cleaned using ethanol only. A light reduction in the loss rate is observed with the new barriers (Figure credit Dr. Attwood, modified and presented with written permission).

A second strategy was to increase the compression speed while collecting isotherms. Since leakage occurs over time, it was reasonable to assume that minimizing the compression time in completing the isotherm may reduce or minimize the overall amount of leakage. The strategy worked to improve the compression isotherms by bringing the values closer toward the expected published values and also resulted in increased precision (repeatability). However, the speed at which the results showed most improvement surpassed the valued used in all other previously published reports. This is potentially a concern if speed is a factor in changing the shape of the isotherms. Fortunately, it has been reported that speed should not be a major factor in determining the characteristics of monolayer isotherms[103]. The single best speed value that gave the most consistent results was chosen and the same setting was kept for all subsequent isotherms for consistency.

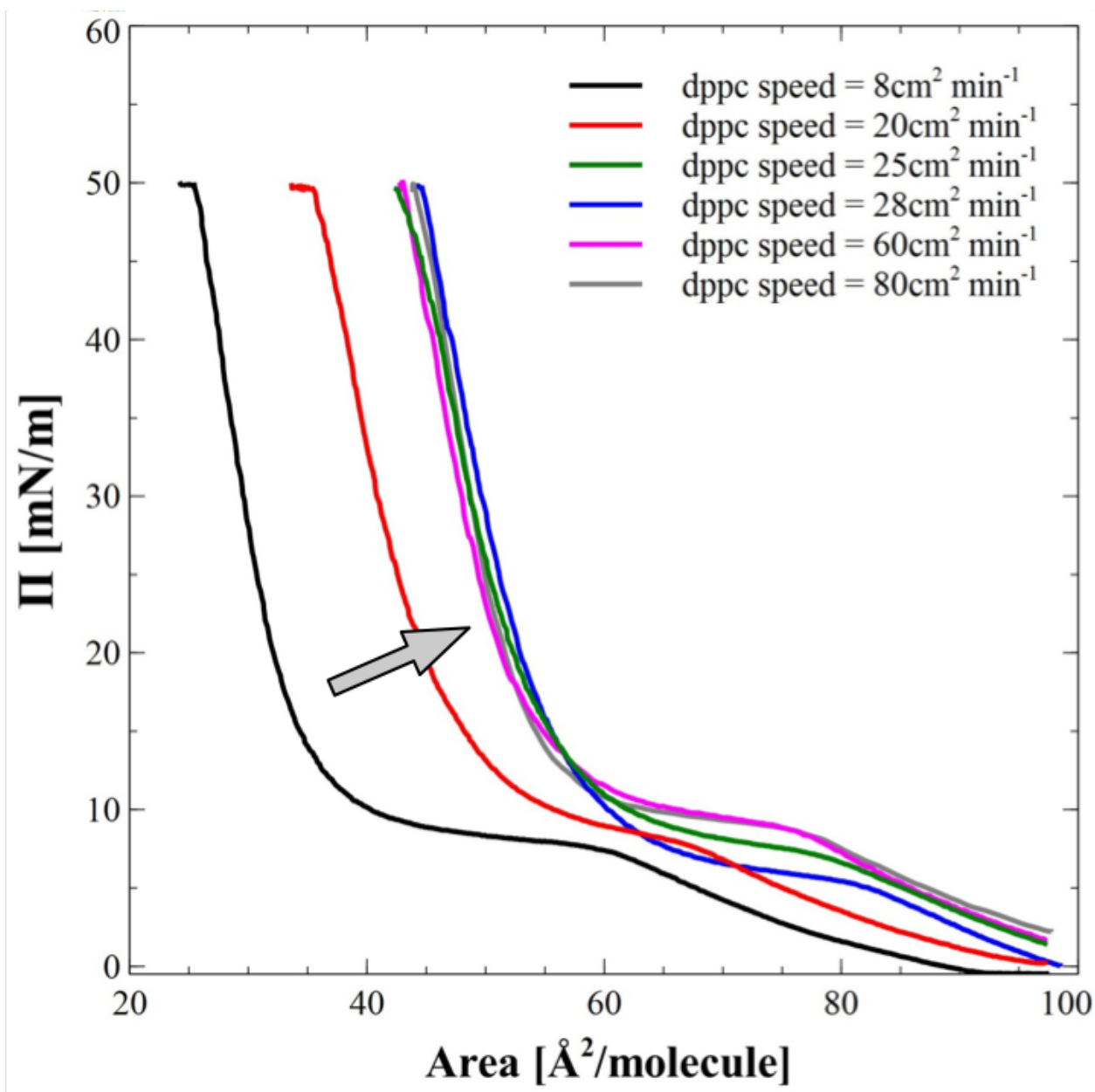


Figure 15- Increasing the speed of compression for isotherms shifted them toward previously published values (grey arrow), presumably by decreasing the compression time, which meant that there was less time overall for phospholipid leakage to occur. Increased speed also resulted in closer grouping of the isotherms as the variability in the isotherms was reduced. DPPC was deposited at room temperature using a micropipette and chloroform was used as the spreading solvent.

Following the aforementioned steps in improving the control isotherms, obtaining reproducible (precise) and consistent (with the literature values) isotherms for DPPC at a given pressure was possible (figure 16). There were numerous other procedural changes that were made also that contributed to the overall improvement of the isotherms. First, the trough area, barriers, and the paper Wilhelmy plates were thoroughly cleaned after each trial. The spreading solvent, chloroform, was also changed to include a fraction of methanol (chloroform: methanol, 4:1 ratio) to reduce evaporation, which results in increased solute concentration. Chloroform evaporates very quickly at room temperature, thus glass vials with the smallest openings (2 ml volume) were utilized. The vials were also always kept cold at -20°C and the solution was used right out of the freezer with minimum waiting time spent at room temperature (temperature equilibration occurred during evaporation time). Various evaporation times, after deposition, were also tested (as low as 1 minute up to an hour), and it was determined that 5 minutes was optimal. Deposition time is also not a major factor in changing the isotherms. Use of plastic pipette tips to measure the $10.0\ \mu\text{l}$ of the depositing solution was also abandoned. The piston micropipettes available in the lab require buffer gas to be consistently present in the chamber in order to accurately pipette the correct amount of the volatile solution. Also, the pipettes require a specific calibration in order to correctly compensate for the density difference between the volatile spreading solvents and water. The majority of published papers as well as trough manufacturers recommend using glass syringes for depositing volatile solutions. Some considerations for using glass syringes are as follows. Since they are not disposable, they must be cleaned for use but also stored correctly according to the manufacturer instructions. Using the syringes with the vials can be tricky as there will be a constant presence of air within the needle space when the solution is drawn up in to the syringe without inverting the syringe. Inverting the

syringe to push the air bubble out of the chamber cannot be performed without causing extra solution to be left on the surface of the needle, which will increase the number of molecules being deposited on the surface of the trough. Consistently drawing the exact amount of solution every time without the aid of special syringe attachments (syringe reproducibility adaptor) will take a great amount of effort and practice. With care, it was possible to achieve highly consistent results manually without using the adaptor.

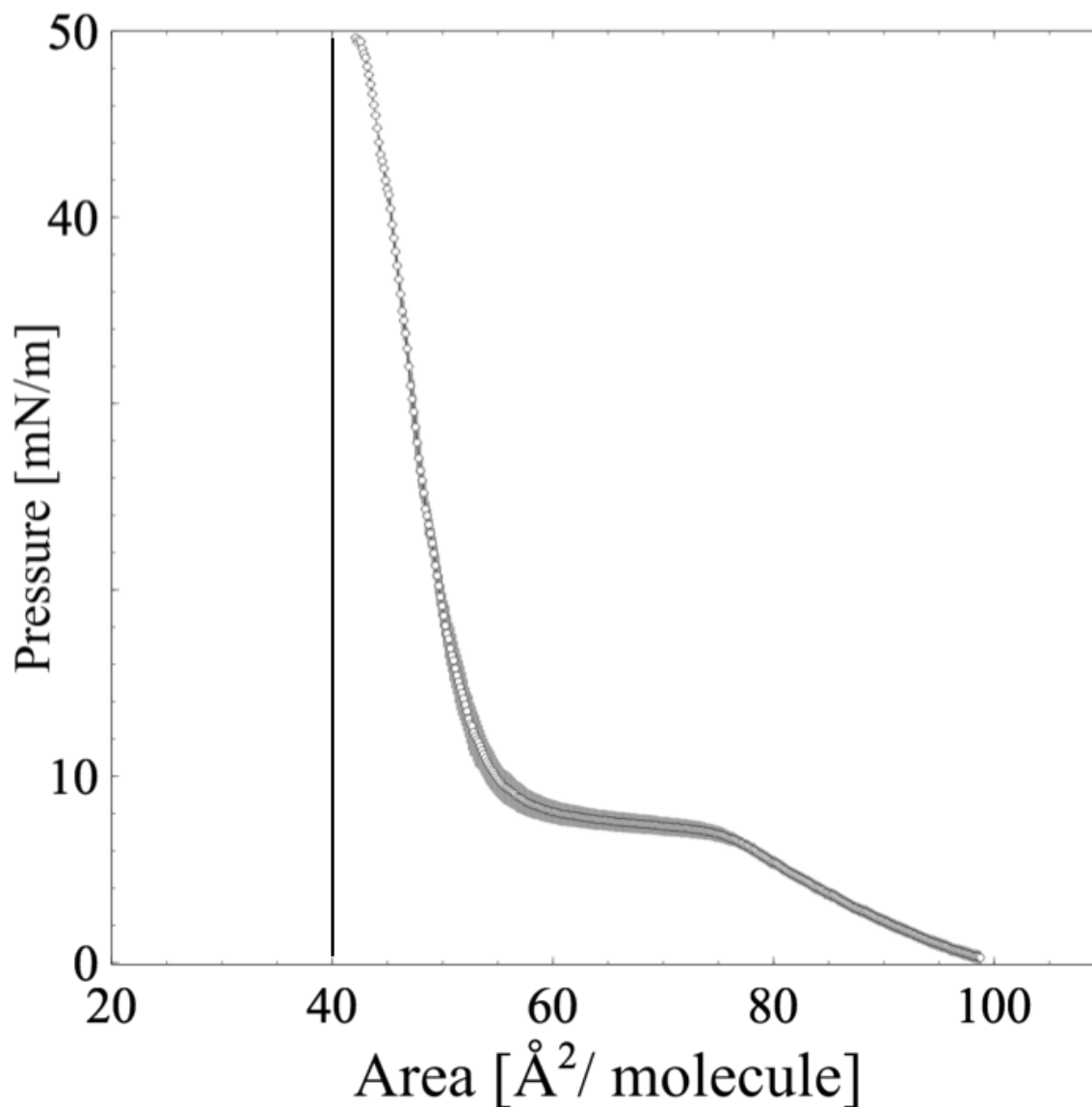


Figure 16- Averaged DPPC control isotherm with the standard error of the mean (SEM) calculated from three independent trials after procedure adjustments and improvements were made. The quality of the isotherm well matches and/or surpasses that of DPPC isotherms that were previously reported in the literature. DPPC was compressed at room temperature using chloroform:methanol 4:1 as the spreading solvent and glass syringe was used to deposit the monolayer onto the trough. Compression speed was 82 cm²/min.

The results of the steps taken to improve the isotherms produced highly precise control DPPC isotherms that had low variability with values that agreed with the previous publications (figure 16). However, there are still variations in control isotherms that stem from technical limitations. From one set of experiments to another, the averaged control isotherms show a variation (figure 17). This is due to several reasons.

In order to eliminate as much of the variability seen in the isotherms as possible, the aliquots must be precisely prepared to achieve the final concentration of 1mg/ml DPPC in the spreading solvent (chloroform:methanol, 4:1). Making the solution requires using micropipettes with plastic tips to measure the volatile solutions. Also a very precise amount of DPPC in powder form (as received from the manufacturer) must be measured, yet DPPC as a phospholipid may be hygroscopic and increase in weight while being measured in a scale with the chamber full of ambient air. Despite best efforts, each batch of aliquots will contain slightly different concentrations of DPPC. Once the solution aliquots are made, solvent evaporation occurs from accessing the solution (opening and closing the bottle to use the solution) and the concentration of the solution changes over time. Also it is important to note that clean glassware has a capacity to decrease the solution concentration as the solutes may end up coating the inside wall of the vials. It was technically impossible to precisely produce the exact same concentration of solutions in different aliquots.

The isotherms produced from two different aliquots are shown in figure 17. The differences observed are minimal, as the difference between the isotherms fell within one standard deviation of each other (figure 17 B). This small difference is also evident when the data is derived from them to produce compressibility modulus plot (figure 17 C). For experiments, each aliquot was

treated as a separate batch, and only data produced from a single aliquot on the same day (one batch) was used when directly comparing the effects of different molecules on the isotherms.

The probable sources of experimental uncertainty and variability included inconsistencies in solution aliquoting, monolayer deposition, and environmental conditions. Aliquoting steps involved unavoidable lipid loss to the glass vial walls during liquid transfer while making dilutions of the stock solutions. Pipetting error and uncontrolled evaporative loss of the volatile solvent (chloroform and methanol) also occurred during the process. During monolayer deposition, having different amounts of extra lipids left on the syringe needle surface from being dipped in the solution may also have contributed to the uncertainty. In addition, variations in the distance between the needle tip and the trough water surface during deposition and the speed at which the lipid solution was being dispensed could not be precisely controlled. Lastly, variable environmental conditions included vibrations, room temperature, ambient atmospheric pressure and chamber area saturation.

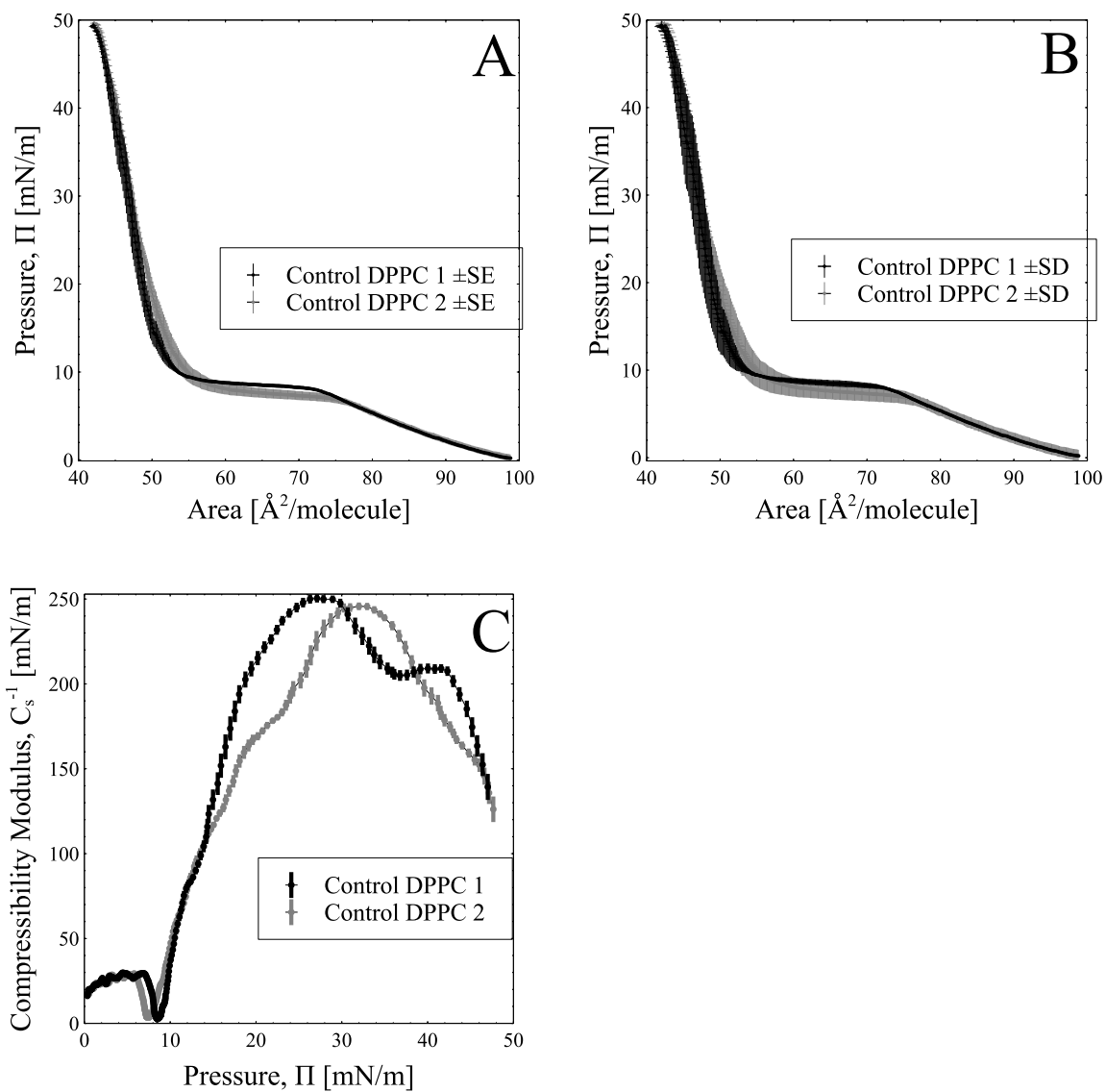


Figure 17- Variability in the control isotherms from differing aliquots. Two averaged control isotherms obtained from separate experiments on different days are presented (A) with standard error of the mean, (B) standard deviation (SD), and (C) the compressibility modulus. The differences in the averaged controls from different trials indicate existence of uncertainty, even after the procedures were optimized for the technique. This causes a larger % uncertainty in the compressibility results. However, results from the second aliquot are within 1 SD of the first.

Once the methods of collecting control data had been optimized, mixed monolayer isotherms were collected for the purpose of comparing cholesterol effects on the monolayer. DPPC and cholesterol isotherms have been extensively studied and published by many groups before, as it served as a model system for the lipid rafts[95], which are highly relevant to many biological and disease processes. Studying melatonin effects on DPPC as well as DPPC and cholesterol mixed monolayers was part of this project's plan as well, so it was important that we obtain DPPC/cholesterol monolayer data that matches or agrees with the published norm.

Initial averaged isotherms with cholesterol are shown in figure 18. It is usual to include various different concentrations of cholesterol (in our case 5%, 20% and 33%, by weight) when studying the mixed monolayers. The initial results were anomalous compared to the previously published data[108], [113] using ratios of molecules. Cholesterol and DPPC mixed monolayers typically show a trend in decreasing area at all pressures with increasing fractions of cholesterol, and in theory, cholesterol is also expected to decrease the area with increasing amounts proportional to the DPPC. Cholesterol has been found to strongly remain in the monolayer and not readily solubilize into the subphase (water solubility of cholesterol is 2.6×10^{-8} g/ml[114]). However, in our data, the lowest fraction of cholesterol (5%) showed the highest decrease in the area per molecule. Secondly, the 20% and the 33% cholesterol isotherms did not show a decrease in area when compared to control at pressure above 15 mN/m. Overlapping or crossing isotherms as a function of cholesterol concentrations are not a feature of published isotherms[115].

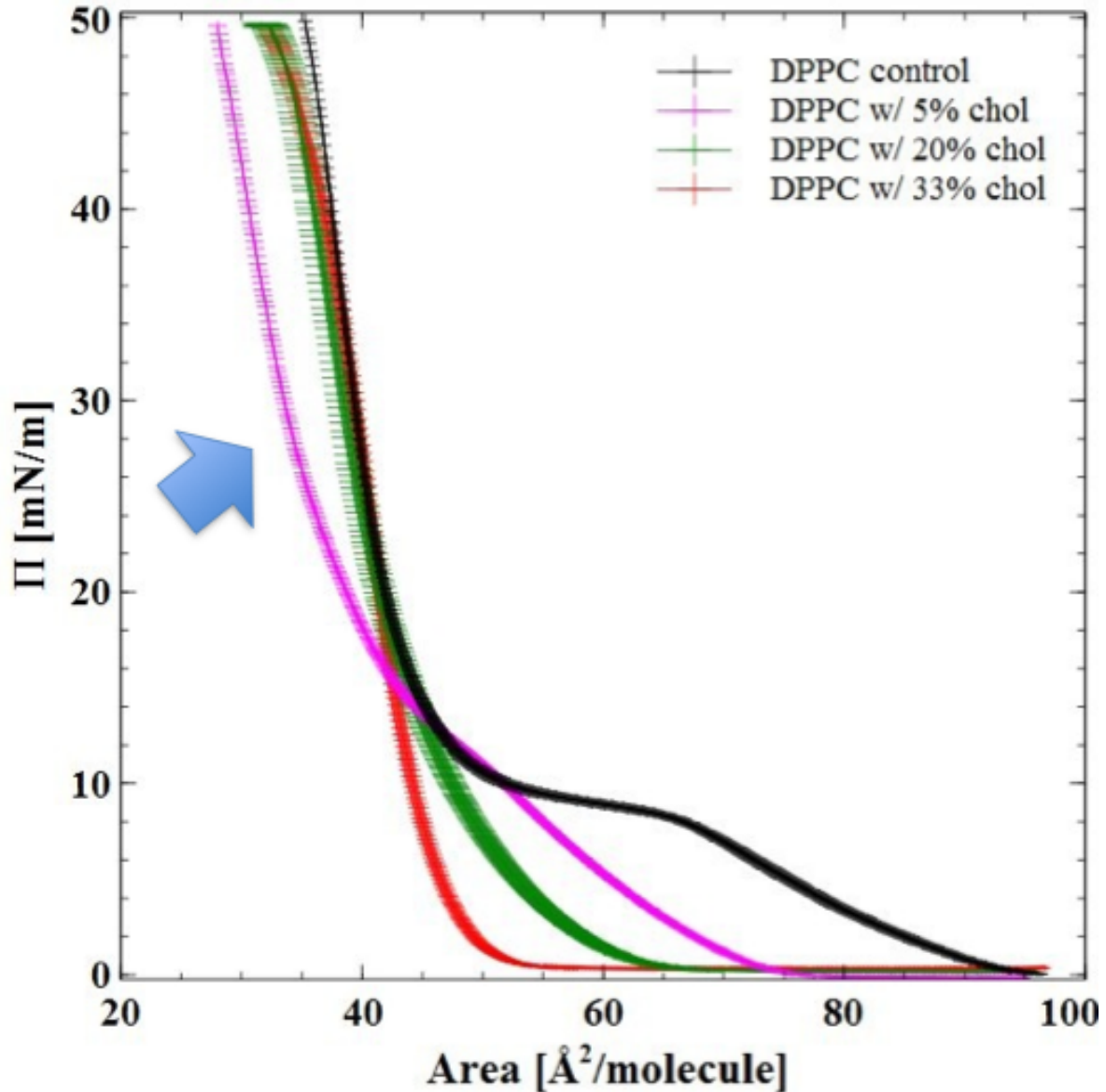


Figure 18- DPPC and DPPC/Cholesterol mixed isotherms. Black line is the averaged control DPPC isotherm, pink is 5% cholesterol, green is 20% cholesterol and red is 33% cholesterol. The blue arrow indicates an anomalous crossover of the 5% cholesterol/DPPC monolayer isotherm resulting in a decreased area per molecule value. The overall decrease in the area per molecule is as expected, however, it is unexpected to have a lower fraction cholesterol (5%, pink line) show a greater decrease in the area per molecule compared to isotherms that contain higher fractions of cholesterol (green and red lines corresponding to 20% and 30% cholesterol, respectively). Figure credit Dr. Attwood, modified and presented with written permission.

Initially, we were using a weight % of cholesterol, as many lung surfactant papers appeared to [83] but later decided to switch to using molar ratio to precisely control the ratio between the number of DPPC and cholesterol molecules. As a simple illustration, having 10 molecules of DPPC with 2 molecules of cholesterol in a monolayer (20% molecular ratio) will yield a different result, compared to having a 0.20 fraction of cholesterol to DPPC monolayer (in this case, there are 10 total number molecules, 2 of which is cholesterol). The final DPPC/cholesterol isotherms showed minimal overlapping or crossover between the different concentration (molar fraction) isotherms, and also the values for the isotherms closely matched those in the literature using pure DPPC systems with cholesterol[84], [107], [116], [117].

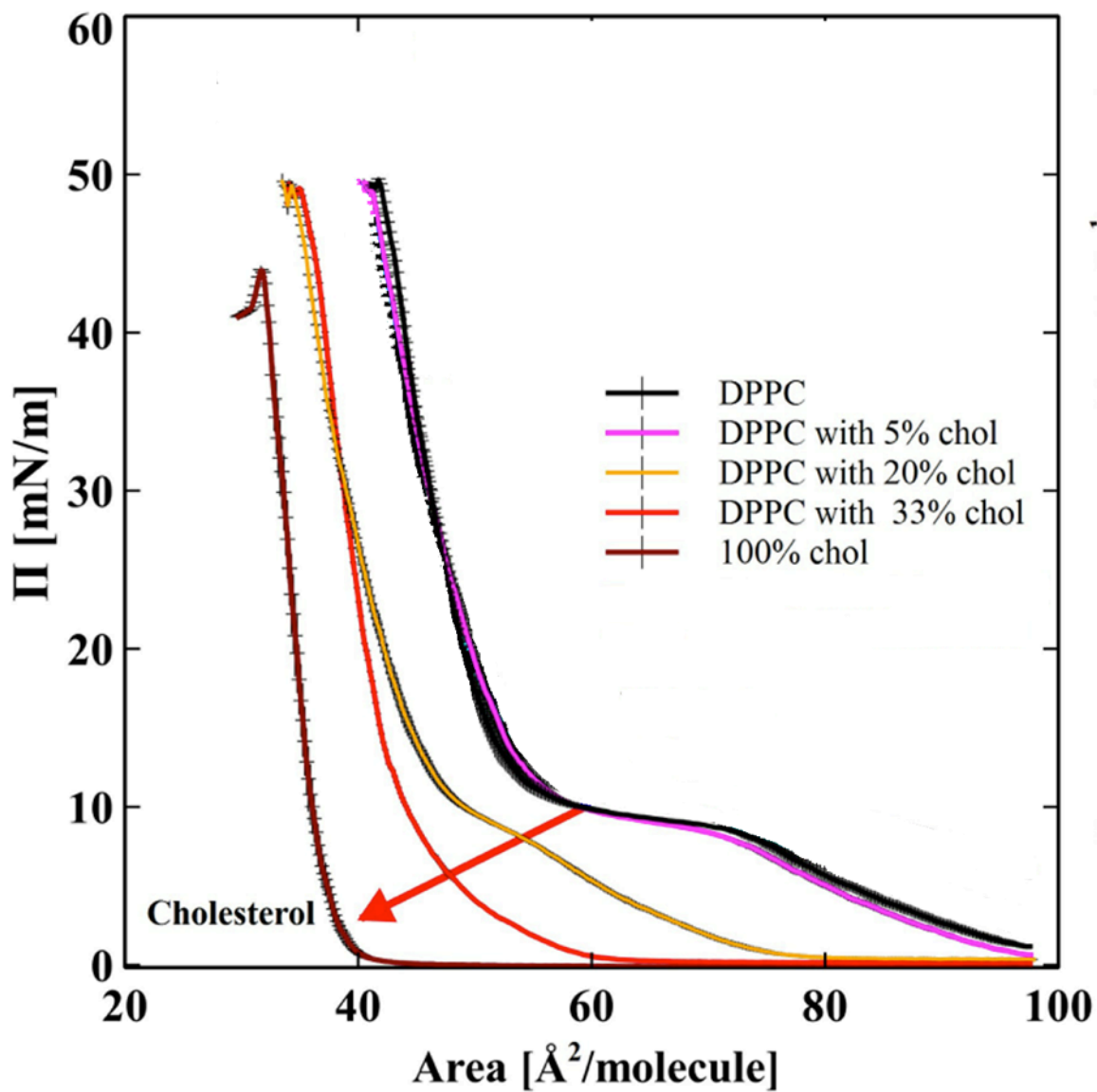


Figure 19- DPPC/Cholesterol isotherms. Increasing the molar fraction of cholesterol leads to decreasing area per molecule (indicated by the red arrow). DPPC and cholesterol was dissolved in chloroform and spread using a micropipette. Compression speed was 82 cm²/min (From [118], modified and presented with written permission).

2.3 Melatonin Directly Interacts with Cholesterol and Alleviates Cholesterol Effects in Dipalmitoylphosphatidylcholine Monolayers

2.3.1 Introduction

The first experiment involved assessing the effects of the hormone melatonin on DPPC monolayers, and also on DPPC/cholesterol mixed monolayers. Cholesterol has received a lot of attention as a molecule of interest in many diseases such as cardiovascular disease, cancers, as well as Alzheimer's disease[119]. Melatonin has also received attention as showing protective effects in these cholesterol-implicated diseases[120], [121]. There may be a countering relationship between cholesterol and melatonin in that melatonin may be able to decrease the overall amount of cholesterol in the body. Melatonin has been shown to negatively correlate with serum total cholesterol and LDL cholesterol levels in pre and post-menopausal women[121]. Several in vitro studies of atherosclerosis development, in relation to cardiovascular diseases, have reported that melatonin reduced plasma levels of total cholesterol, very low-density lipoprotein (VLDL)-cholesterol and low-density lipoprotein (LDL) cholesterol in hypercholesterolemic rats[120]. The exact mechanism of how melatonin is linked to the reduction of cholesterol levels is not known, however it is hypothesized that melatonin may be able to augment the existing endogenous cholesterol clearance pathways[120].

Cholesterol is used and stored in the body mostly in lipid membranes in general as a ubiquitous constituent. Its function in the membranes is still being studied, however, its involvement in the formation of lipid raft regions is considered to be of utmost significance[6]. Membrane lipid raft regions are considered as the site for many important cellular processes, including the pathophysiology of many cholesterol related diseases, particularly in Alzheimer's disease. The possible involvement of cholesterol rich membranes as the site of A β production

and toxicity is of particular interest[30]. One of the hypotheses of this project is that the membrane cholesterol may be key in establishing a connection between cholesterol and the protective role of melatonin. The idea is that the seemingly counteractive and contrasting effects of cholesterol and melatonin seen in these diseases could be partly due to their competition in the membrane. Melatonin's protective effects seen in various diseases may be due to its ability to directly interact and change the physical properties of the membrane. In addition, its effects in reducing the effects of cholesterol in the membrane may also be indirectly contributing to its protective effects.

Melatonin has been shown to have protective effects against cholesterol related diseases[120], [121], and also it has been shown to interact with the membrane and affect its properties[71]. Further, melatonin has been shown to compete with cholesterol in binding to phospholipids in lecithin reverse micelles [74]. Bongiorno et al.,[75] further suggested that when present in high concentrations, melatonin should be able to displace some cholesterol from the membrane. However, there was no evidence of direct interaction and displacement of cholesterol by melatonin.

It was decided that melatonin and cholesterol interaction should be measured and investigated using the monolayer technique. The goal of the experiment was two fold. First, melatonin's effect on the DPPC monolayer was to be assessed to confirm and characterize its standalone effect in the phospholipid assembly. Melatonin's effects in both lipid monolayer and bilayers have been reported before, however, monolayer isotherm measurements have never been previously reported. Cholesterol effects on DPPC monolayers have been widely available before. The second goal was to assess how melatonin interacts with cholesterol in the monolayer and to

characterize the competing interactions. Cholesterol is capable of forming a monolayer on its own, but melatonin is not and only stays dissolved in the aqueous subphase. Thus the effects of two different concentrations of melatonin in the subphase were assessed on pure cholesterol monolayers as well as for mixtures of cholesterol and DPPC monolayers.

2.3.2 Materials and Methods

Standard monolayer isotherm methods, as developed in the previous method development section (section 2.2) have been utilized. Melatonin, cholesterol, and DPPC were all purchased from Sigma-Aldrich in powder form and were used without further purification. Melatonin was directly dissolved in Millipore water (resistivity > 18.2 M Ω ·cm) by gentle agitation to yield the final solutions used in the monolayer subphase[122].

Lyophilized, powdered DPPC was dissolved in chloroform (1.0 mg/ml). 10 ml of the DPPC solution was deposited using a micropipette on to a Langmuir–Blodgett micro-trough (NIMA, UK) with a subphase volume of approximately 50 ml. Melatonin solutions in water were used as the subphase at 0.2 mM, and 1.0 mM concentrations, to allow melatonin partitioning from water subphase into the lipid monolayer. Such high pharmacological concentrations of melatonin have been used in previous melatonin and membrane studies [122]–[124]. Such concentrations were chosen in order to observe its effects most clearly. Cholesterol enriched monolayer samples were prepared by dissolving cholesterol and DPPC in chloroform and spreading the chloroform solution onto the trough. Cholesterol to lipid percentages were: 5%, 20%, 33% and 100% by mol%. 10 μ l of the sample solution was deposited for each isotherm experiment. The compression rate for the isotherms was 80 cm²/min or 9.8 A²/(molecule \times min). The subphase

was kept at room temperature at 24°C. The isotherms were repeated in at least triplicate in order to obtain an accurate average for each concentration and averaged isotherms are shown in the results. Each pressure versus area isotherm represents an average of three separate experiments, with the error bars calculated as standard error of the mean.

The elastic compressibility was calculated from the pressure versus area isotherm using equation (1). C_s^{-1} is the compression modulus, A is the area in the trough, and π is the pressure.

$$C_s^{-1} = A(d\pi/dA) \quad (1)$$

In general, a lower C_s^{-1} value means an increase in the monolayer compressibility[125].

2.3.3 Results

DPPC monolayer compression isotherms with 0.2 mM and 1.0 mM melatonin are shown in figure 20.

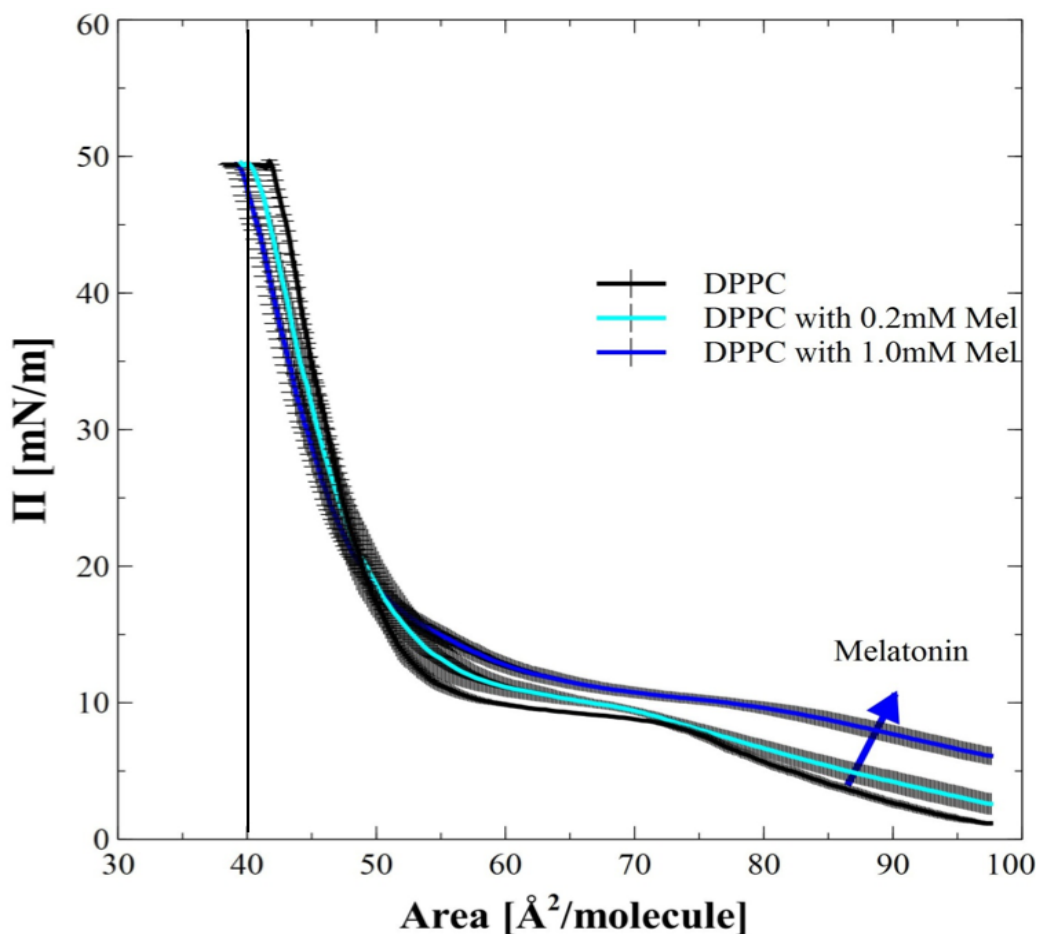


Figure 20- Melatonin in DPPC monolayers. The blue arrow depicts shifts in the isotherm with melatonin. Statistical testing at pressure 11.5 mN/m revealed that there is no significant difference between control and 0.2 mM melatonin, but with 1.0 mM melatonin, the area per molecules was increased significantly over that of control (n=3, both groups), with p=0.02, paired Student's t-test. The curves are shown as the average of three trials with standard error of the mean as the error bars. The data was obtained using materials and methods described in detail on pages 54-55 (DPPC was used with melatonin in subphase (water) at room temperature, spreading solvent was chloroform, using a micropipette, deposition volume 10.0 μl , lipid solution concentration 1mg/ml) (From [118], modified and presented with written permission).

1.0 mM melatonin significantly increased the pressure per given area at low compression pressures between 0 mN/m and 11.5 mN/m (figure 20), which is equivalent to increased area per molecule compared to control. Above the pressure of 20 mN/m, there is no significant difference between the three curves (at pressure = 45 mN/m, 1.0 mM melatonin and control were not significantly different, $p=0.17$, paired Student's t-test[126]). Repeated experiments (Figure 30E) that tested the same concentration of melatonin also revealed that there is no significant difference at the higher pressure ranges compared to control (figure 30E). The increase in pressure of the monolayer with melatonin at low pressure (high area) is much more reliable. Simply put, the molecules are pushing outward away from each other and spreading themselves out more when melatonin is present compared to when they are not. The results suggest that melatonin might be able to incorporate in between the DPPC molecules and somehow induce repulsion. Not all molecules that incorporate into the monolayer lead to spreading effects, as cholesterol, for example, has been shown to decrease molecular area of lipids through monolayer incorporation[93]. Melatonin also seems to lose its effects and may be excluded from the monolayer as the pressure increases. The diminishing effects may be indicative of a solubilizing effect on the lipid molecules into the subphase[127], [128], but also may be due to increased molecular order and tightened molecular packing by increasing head group hydration[43]. It is most likely that melatonin is simply losing its effects through being squeezed out of the monolayer, being unable to withstand the increased compression pressure brought on by the decreasing area of the trough. The squeeze out effect is associated with molecules that interact with phospholipids mainly through hydrophobic interactions[129]. The lack of strong electrostatic interaction with the lipids may be responsible for the diminishing effects at high

compression pressures. Our group's molecular dynamics simulation data, included in the published manuscript, also supports that melatonin utilizes hydrophobic interactions as the main driver in interacting with the lipids[71].

It is important to discuss bilayer equivalencies that can be inferred from the data, as values at these points may have biological relevance. The bilayer correspondent theory[91], [92] suggests that at certain parameters, monolayers may exhibit or closely match the physical properties found in bilayer membranes. Extensive theoretical discussion on this theory has led to some consensus on the precise parameters at which the monolayer may be considered bilayer equivalent. However, the matter is still being debated[130]. The most frequently cited bilayer equivalent point is the bilayer equivalent pressure, which is accepted to be at around $\Pi = 30$ mN/m[131]. Estimating the bilayer equivalent pressure is purely theoretical because bilayer lateral pressure is not experimentally measurable. Another frequently cited point is the bilayer equivalent molecular area, which for DPPC bilayers has been shown to be $\sim 64 \text{ \AA}^2$ [132]–[134].

Data on melatonin measured in the DPPC monolayer seems to suggest that all effects are lost at the bilayer equivalent pressure of 30 mN/m. Considering that there are previous publications that studied and showed melatonin's ability to interact and alter membrane properties using bilayer systems, this result was surprising. It was decided that the bilayer equivalent area ($\sim 64 \text{ \AA}^2$) should be used to estimate the bilayer equivalent effects of the data. The isotherms reached about 11- 12 mN/m pressure at the 64 \AA^2 mark, and thus 11.5 mN/m was chosen as the standard point at which to characterize and compare the isotherms. The data at the bilayer equivalent area shows that 1.0mM melatonin significantly increases the lateral pressure at this area per molecule,

which suggests a spreading effect (figure 21 inset A, also see figure 30). The spreading effect is in good agreement with the previous literature[70], [71].

Cholesterol isotherms showed the opposite effect compared to melatonin (figure 21). Inclusion of cholesterol in the DPPC monolayer resulted in decreased area per molecule at the given pressure (11.5 mN/m), and the smallest area per molecule at a given pressure was observed for the pure cholesterol monolayer. The results are in good agreement with the literature[135]. Also note that in addition to the decrease in the area, although effects were only significant starting at 20% cholesterol and greater, the shape of the isotherms also changes with increasing cholesterol content. Higher cholesterol content makes the isotherm more smooth and curved without having distinctive discontinuities or phase-separated regions. This effect is especially evident with the LE/LC phase plateau (the characteristic kink in the DPPC isotherm just below 10 mN/m) slowly diminishing as the fraction of cholesterol is increased. This effect is due to cholesterol inducing condensation of the monolayer, whereby the DPPC molecules are drawn closer to each other by cholesterol to form condensed phases, which is essentially eliminating the LE phase. Lipid condensing effects of cholesterol is well documented in the literature[71].

The elastic compressibility modulus was calculated from the isotherms (Figure 21B). Compressibility modulus is an inverse measure of the elastic compressibility. Comparing the compressibility moduli at the chosen standard 11.5 mN/m pressure reveals that the elastic compressibility modulus is inversely correlated to the pressure changes observed in the isotherms (figure 21). 33% and 100% cholesterol isotherms decreased the pressure at a given area per molecule, however, the results translated into increased elastic compressibility modulus (compared to control, $p < 0.05$). In other words, condensing the monolayer by cholesterol resulted

in a stiffer less compressible film. It was found that the two concentrations of melatonin and the two lowest concentrations of cholesterol showed compressibility moduli that were not different from control (figure 21B). However, significant ($p < 0.05$, paired Student's t-test) changes in compressibility modulus with melatonin were observed at a later repeated experiment at pressures 11.5 mN/m and 15 mN/m at the same 1.0 mM concentration (figure 31).

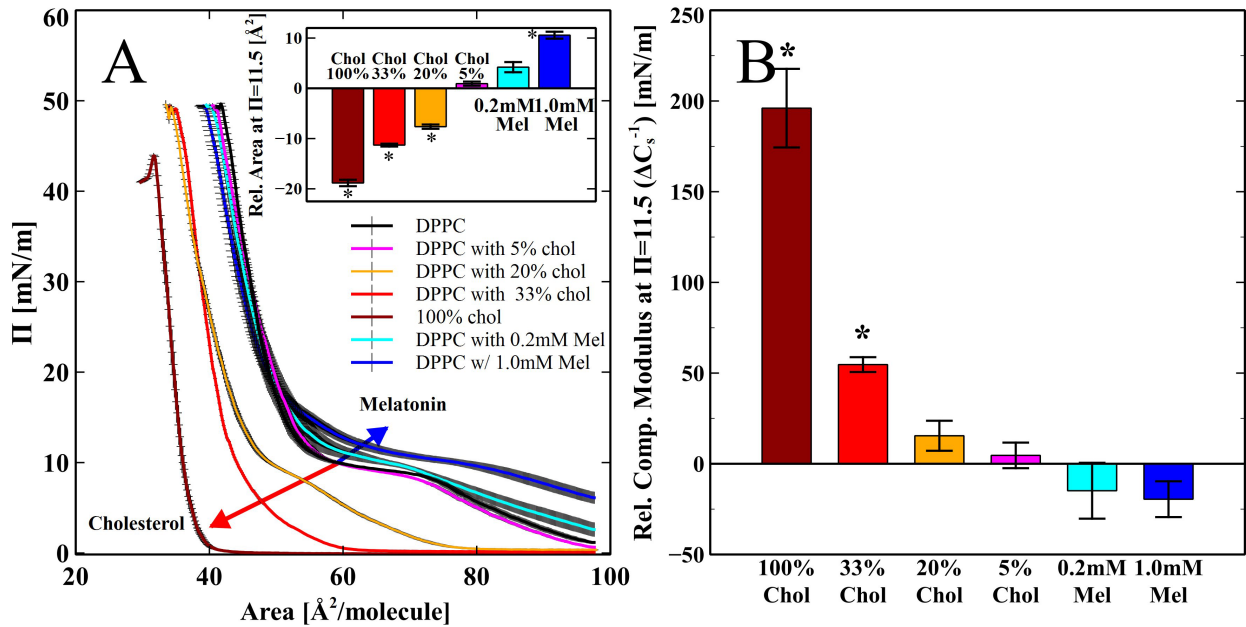


Figure 21- (A) DPPC isotherms with melatonin present in the subphase and differing molar fractions of cholesterol presented with standard error of the mean. The blue and red arrows show a trend in the shift of the isotherms for melatonin and cholesterol, respectively. Inset shows relative change in the area per molecule at pressure 11.5 mN/m, error bars indicate standard error of the mean. (B) Relative comparison of the compressibility modulus calculated from the isotherms, also measured at 11.5 mN/m. Error bars indicate standard error of the mean. In the insets, *'s indicate concentrations which give values which are significantly ($p < 0.05$ using paired Student's t-test) different from control. For figure A inset, the relative changes from control for the two melatonin concentrations were also significantly different with $p < 0.05$. Note that even though the isotherm with 1.0 mM melatonin in the subphase had showed a noticeable increase in the molecular area compared to the 0.2 mM melatonin (A, inset, $p < 0.05$), the relative change in compressibility modulus (compared to the control) for the two concentrations of melatonin and 5% and 20% cholesterol did not differ significantly (B) (From [118], modified and presented with written permission).

Next, effects of having both melatonin and cholesterol in the monolayers were measured. The mixture permutations included four different cholesterol monolayer concentrations and two concentrations of melatonin. DPPC monolayers containing cholesterol (5, 20, and 33 mol%), and a pure cholesterol monolayer (100%), were compressed with the subphase containing melatonin at 0.2 mM and 1.0 mM concentrations. The corresponding pressure vs area isotherms are shown in figure 22. Figure 22 A–D show isotherms for DPPC monolayer with progressively increasing concentrations of cholesterol from 5 to 20, 33 and 100 mol% of cholesterol.

At the beginning of the isotherms (area 98 \AA^2), all isotherms show a normalization and recovery toward the DPPC only isotherms ($p < 0.05$ Student's t-test), in terms of lipid area per molecule but only when the high concentration melatonin is present (the increase is indicated with blue arrows in figure 22). The LE to LE/LE LC phase transitions in the mixed monolayers can be seen to diminish with increasing cholesterol. The complete lack of clear LE to LE/LC phase transition in the isotherms (figure 22 C and D) with higher amounts of cholesterol (33 and 100% respectively), even with the highest concentration of melatonin present, indicates that cholesterol effects on the phase transition of the monolayers persisted and could not be countered completely by melatonin. Even though the influence of cholesterol on the shape of the isotherms was persistent, highest concentration of melatonin was able to increase the area per molecule at 11.5 mN/m for 20, 30 and 100% cholesterol isotherms ($p < 0.05$, figure 22B, C, and D, also 23A). Figure 22D contains pure cholesterol isotherms with melatonin in the subphase. Without any phospholipids present, the highest concentration of melatonin increased the area per molecule significantly ($p < 0.05$), demonstrating that it is capable of partitioning into the pure cholesterol monolayers and directly modifying the molecular arrangement of cholesterol molecules without the need for the presence of any phospholipids.

The relative molecular area and compressibility changes are shown in figure 23. The change in the area per molecule relative to pure DPPC at pressure 11.5 mN/m is shown for all cholesterol samples and at all melatonin concentrations. Data confirms that melatonin at 1.0 mM concentration significantly increases the area per molecule in control, and in cholesterol mixed/ pure cholesterol isotherms, when cholesterol is at 20% or higher concentrations. Figure 23B shows relative change in compressibility modulus, compared to pure DPPC at $\Pi = 11.5$ mN/m, for all cholesterol containing samples and at all melatonin concentrations. The data shows that melatonin significantly decreased the compressibility modulus for all cholesterol containing samples at the highest concentration, and for the 33% samples, the decrease was concentration dependent.

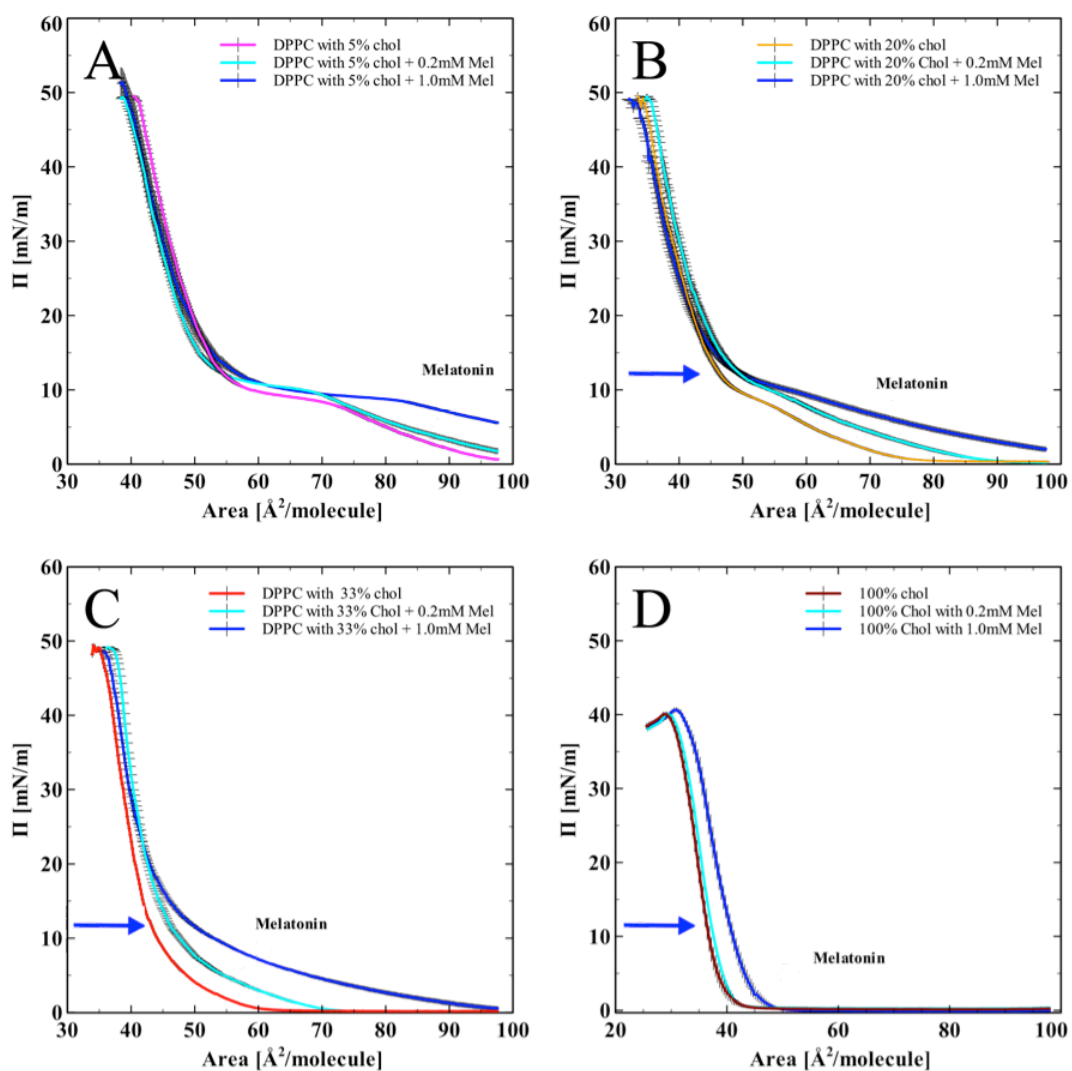


Figure 22- Compression isotherms for lipid/ cholesterol mixtures with melatonin in water subphase (0.2 mM and 1.0 mM melatonin, in water subphase). (A) DPPC with 5% cholesterol. (B) DPPC with 20% cholesterol. (C) DPPC with 33% cholesterol. (D) Pure cholesterol monolayer isotherms. Blue arrow indicates a significant shift in the area at $\Pi = 11.5$ mN/m on the addition of 1.0 mM melatonin. In figures A and B, the LE/LC phase (flat plateau) exists but in figure C the LE/LC transition is no longer visible (D is pure cholesterol). Molar fraction was used in determining the percentages of cholesterol, and subphase (water) contained melatonin, compression speed $80 \text{ cm}^2/\text{min}$ (From [118], modified and presented with written permission).

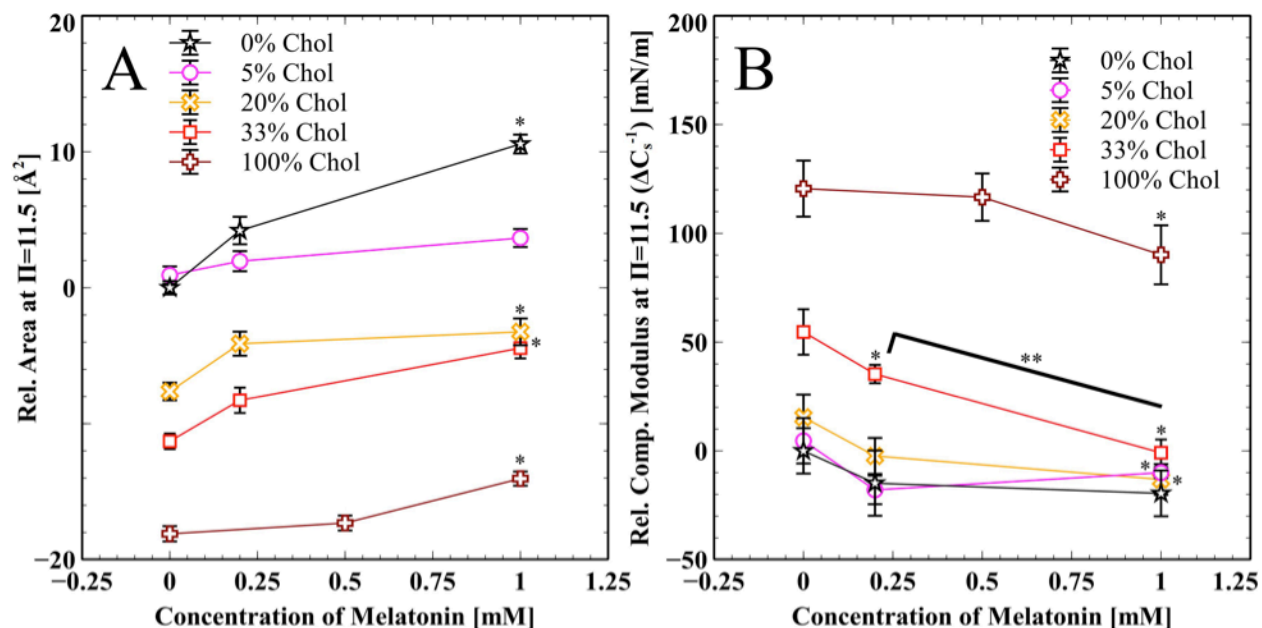


Figure 23- (A) Relative change in the area per molecule versus increased concentrations of melatonin in the subphase. Numbers were measured from the isotherms (in figure 22) at pressure $\pi= 11.5$ mN/m. Increasing melatonin in the subphase of cholesterol and or cholesterol/DPPC monolayers increased the area per molecule in all concentrations of cholesterol. (B) Relative change in the compressibility modulus in monolayers with cholesterol. The error bars denote standard error of the mean. *'s indicate $p < 0.05$ compared to control, and **'s indicate $p < 0.05$ compared to the lower concentration, determined using Student's t-test (From [118], modified and presented with written permission).

2.3.4 Discussion

Overall, the resulting changes in the lipid biophysical properties due to melatonin were an increased area per molecule and a decreased compressibility modulus in the cholesterol mixed monolayers. The results suggest that melatonin has both a spreading effect on the DPPC/cholesterol molecules, and also a softening effect on cholesterol containing monolayers. The findings are in agreement with previous reports that showed increased molecular area and decreased thickness in a 1-palmitoyl-2-oleoyl-sn-glycero-3-phosphocholine (POPC) monolayer

with melatonin, and also with another report that showed similar results in both 1,2-dioleoyl-sn-glycero-3-phosphocholine (DOPC) and DPPC bilayers.[71]

Melatonin's influence in decreasing the elastic compressibility modulus in cholesterol containing monolayers, as well as the increase in the area per molecule may involve increased water interaction with the head groups, for several reasons. It has been reported by other groups that melatonin can augment hydration of the head groups[136]. The increase in the hydration of the lipid head groups may reduce the prevalence of highly dense liquid condensed areas within the monolayer, since it increases the area per lipid that promotes the acyl chain dynamic motional freedom (i.e. fluidity) due to entropy[137]. Increased lipid molecular area and acyl chain fluidity due to hydration would naturally lead to lowering the thickness of the bilayer[138]–[140], which was also reported for melatonin[70], [71]. Simply put, increasing the spacing of the DPPC molecules may induce increased interaction with water molecules.

An especially notable result of this study is that there is evidence for direct interaction between cholesterol and melatonin (shown in figure 23). The pure cholesterol monolayer showed an increase in the area per molecule and a decrease in compressibility modulus, when the high concentration of melatonin was present in the subphase and partitioned into the monolayer. This suggests that melatonin is able to incorporate between both the phospholipids and also in between cholesterol molecules. Previously, it was known that melatonin prevented membrane fluidity decrease due to lipid peroxidation, for which only its anti-oxidative properties have been attributed to have been responsible[123], [124], [141], [142]. Our results show that melatonin interacts directly with the lipids and the cholesterol molecules, increases membrane fluidity and alleviates cholesterol's condensing effect in the membrane.

A summarizing schematic of the results is shown in figure 24. It is hypothesized that melatonin and cholesterol, when mixed in the lipid monolayer, will counteract each other's effects, resulting in a monolayer similar to the original DPPC monolayer with the characteristic molecular area for DPPC. The resulting hybrid L-B isotherms, when both melatonin and cholesterol were present in the monolayer, did show moderate recovery toward control but did not fully recover to match the normal DPPC control isotherm (figures 24B and C). Thus, attributes of cholesterol in the isotherms remained in conjunction with the increased molecular area due to melatonin. Figure 24D contains a depiction of melatonin's influence on the monolayer as not disturbing the cholesterol rich condensed domains. However, it is likely that both the cholesterol rich domains as well as the lipids are affected as melatonin had effects that increased the pressure per given area in the pure cholesterol monolayer as well as in the pure lipid monolayer.

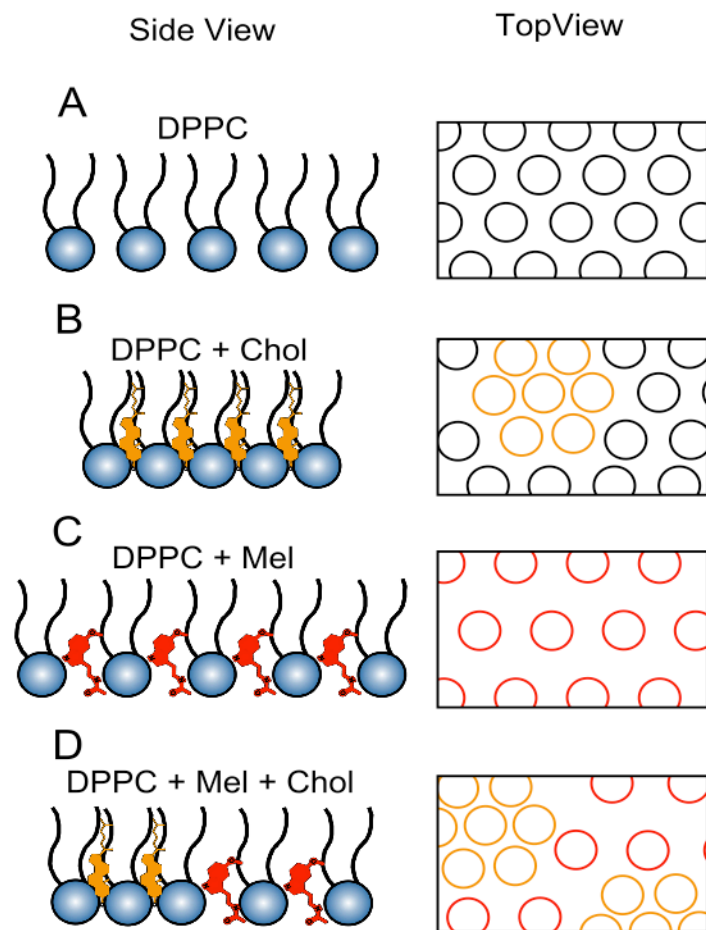


Figure 24- Schematics illustrating packing of DPPC molecules in a monolayer containing melatonin and/or cholesterol. (A) Pure DPPC monolayer showing even spacing of the phosphatidylcholine molecules spread over the air/water interface; (B) monolayer enriched with cholesterol causes the lipids to condense and form closely packed domains, decreasing overall area per lipid headgroup; (C) monolayer with melatonin, which likely locates between the headgroups increasing overall area per lipid headgroup. (D) When cholesterol and melatonin are both present, densely packed domains created by cholesterol may co-exist with widely spaced areas created by the presence of melatonin, leading to an overall area per lipid headgroup similar to the control. Side view: ball and stick schematic represents single DPPC molecules, orange and red molecules represent cholesterol and melatonin respectively; top view: circles represent space occupied by lipid groups alone (black), enriched with cholesterol (orange) and enriched with melatonin (red) From [118] presented with written permission.

2.3.5 Conclusion

Melatonin had a noticeable influence on the compressibility of DPPC monolayers in an opposing manner to that of cholesterol (Figure 23B). With melatonin present, both increase in the area per molecule as well as decrease in the compressibility modulus were observed in most of the cholesterol containing monolayers tested (5% cholesterol did not increase significantly in the molecular area, but significantly decreased in compressibility modulus). Significantly, pure cholesterol monolayers without any phospholipids also showed increased area per molecule and decreased elastic compressibility modulus with melatonin. The results indicate that both cholesterol and melatonin can co-exist in the monolayer. The possibility of competitive exclusion being part of the interaction cannot be dismissed, however, the evidence is weak compared to the co-existing and mutual influence from both of the molecules.

Our results suggest that melatonin has a direct fluidizing effect in the membrane and counteracts the condensing effect of cholesterol. The results suggest that melatonin may be actively involved in counteracting cholesterol-induced changes of membrane structure and properties. High cholesterol induced membrane changes have been associated with various diseases such as cardiovascular diseases[120], cancer[143], and Alzheimer's disease[69]. The results of our study demonstrate that melatonin's ability to provide protection against such diseases might involve, at least in part, its nonspecific receptor independent interaction with the cell membrane.

The countering effects of melatonin on cholesterol were in support of the hypothesis that melatonin's ability to alter the membrane properties may be involved in reduction of A β activity in the membrane. Membrane cholesterol has been shown to increase A β binding to the

membrane and also to enhance toxicity of A β [30]. It is possible that the membrane effect of melatonin is involved in both directly and indirectly reducing such effects. Melatonin may directly reduce A β effects by having membrane effects that are opposing to cholesterol, which is A β enhancing. Secondly, melatonin interacts with cholesterol and reduces its effect, which may indirectly reduce the associated A β effect. The significance of the biophysical effects of the molecules in affecting the effects of A β in membrane remains to be clarified.

2.4 Testing A β Binding in Langmuir Monolayers

Characterizing melatonin and cholesterol effects in the monolayer was a step toward the next phase of the project, which was to determine the consequence of such effects on A β interaction with the membrane. By directly measuring how A β interacts with the monolayers, with and without melatonin and cholesterol, it is possible to ascertain the extent to which the biophysical effects of the molecules on the monolayer may play a role in the toxic effects of A β .

For the experiments, peptide-binding assays were utilized. The assay involved injecting the peptide underneath a compressed monolayer. The monolayer was held at a constant pressure or area, usually at the bilayer equivalent pressure or bilayer equivalent area. Then, using an injection port or a bent needle syringe, the peptides are added below the monolayer and allowed to interact with the monolayer. As the peptides interact with the monolayer from the water subphase, the monolayer lateral pressure or the film area become altered, and by monitoring the changes over time, the thermodynamics of the interaction can be extracted from the observed changes. Such experiments are called 'pressure hold' or 'area hold' experiments, where either the pressure setting or the molecular area setting for the monolayer is set and held at a constant value, and changes to the other parameter induced by the introduction of the peptide molecules is monitored. The resulting data from the experiments are presented in graphs as change in area versus time or as change in pressure versus time.

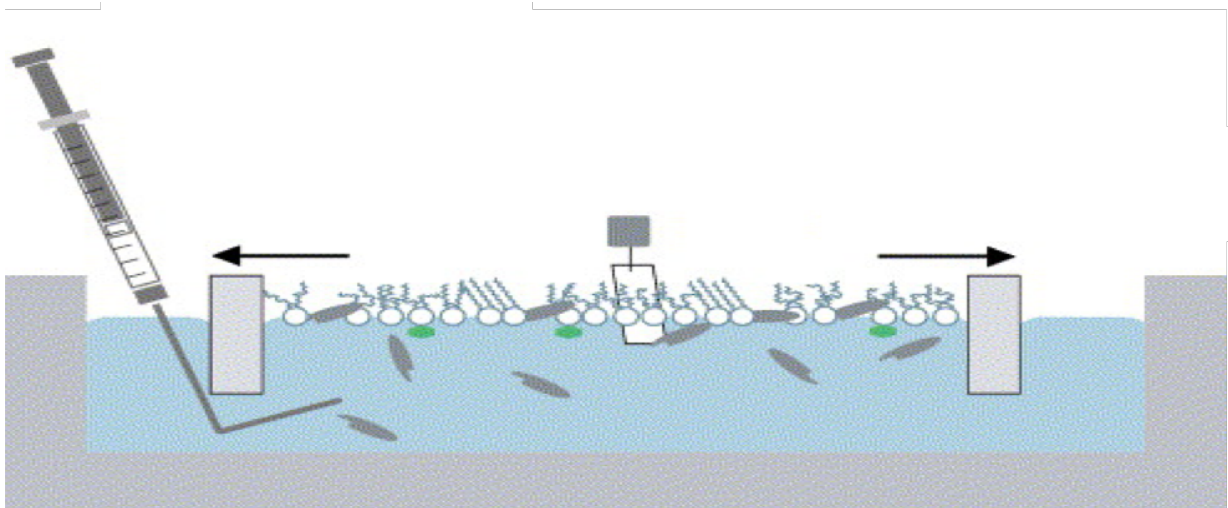


Figure 25- Schematic of a pressure hold experiment, where the change in area is measured due to addition of peptide molecules (grey) interacting with the monolayer. The black arrow depicts the direction of force inducing expansion of the trough area upon addition of peptides (Modified from [144] presented with written permission).

In an ideal case, a pressure hold experiment would yield a result where the monolayer is compressed to a pressure that corresponds to the bilayer equivalent molecular area (64\AA^2) and is held constant at that setting. Upon adding the peptide, the monolayer would undergo an increase in the area per molecule in a steady, repeatable, and predictable manner. Analyzing the increase in the molecular area over time can then be used to assess the thermodynamics of the peptide interaction. Further, adding other molecules such as melatonin or cholesterol (or both) and repeating the experiment would potentially alter the binding characteristics, and effects of the molecules on binding can thus be ascertained. Figure 26 depicts an ideal case in which the binding assay shows a flat constant control versus the experimental group showing an increase in the area compared to the control.

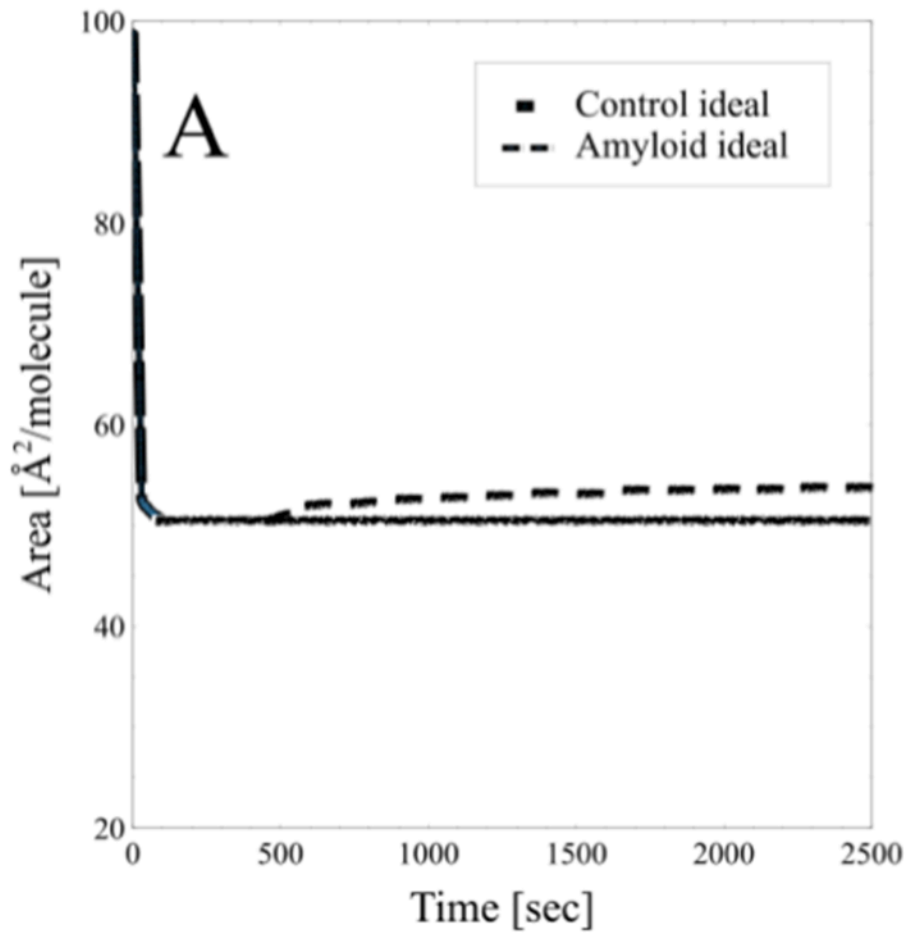


Figure 26- Illustration showing an ideal area versus time data for a pressure hold experiment. The solid line depicts a control experiment where the area is kept constant over time. The dotted line depicts a case where the amyloid peptide is incorporated into the monolayer resulting in increased area per molecule over time. Analyzing the slope of increase can be used to determine the kinetics of the interaction.

2.4.1 Materials and methods

Standard monolayer isotherms methods, as developed in the previous method development section (section 2.2) have been utilized. DPPC was purchased from Sigma-Aldrich in powder form and was used without further purification. Millipore water (resistivity > 18.2 M Ω ·cm) was used to make HEPES buffered saline (10 mM HEPES, 140 mM NaCl, pH 7.4) that was used in the subphase.

Lyophilized, powdered DPPC was dissolved in chloroform:methanol 4:1 solution (1.0 mg/ml). 10 μ l of the DPPC solution was deposited using a Hamilton syringe on to a Langmuir–Blodgett microtrough (NIMA, UK) with a subphase volume of approximately 50 ml. The compression rate for the isotherms was 80 cm²/min or 9.8 Å^2 /molecule \times min. The subphase was kept at room temperature at 24°C. A β peptide (1-42, NaOH) was purchased from rPrptide (GA, USA) as lyophilized powder. The peptides were dissolved in 0.01M NaOH and sonicated for 30 seconds in a bath type sonicator (Branson, CT, USA) and flash frozen in dry ice at 0.5 mg/ml. The peptides aliquots were kept at -20°C and thawed at room temperature just prior to injection into the monolayer subphase. A 50 μ l glass syringe (model 705 LT) with an 18 gauge, Kel-F Hub NDL, 2.65 in, point style 3 bent needle (model 90432), was used for injection (Hamilton Company, NV, USA).

2.4.2 Results and Discussion

Figure 27 shows experimental results from 5 different independent trials. The results show that unlike the ideal control case depicted in figure 26, where the control remains constant over time, the experimental data (figure 27) shows the area decreasing over time. The negative slope of the graph indicates material loss or leakage in the trough. Also, the slope varies between trials and each trial has a rate of decline that is not constant (the downward slope varies and changes slightly over time).

The results are problematic for several reasons. First, any potential increase in the area elicited by the addition of peptides will be masked by the area loss occurring in the system. It is still possible to have a control where the area declines over time, as long as the rate of decline is consistent and repeatable. An averaged value of the decline could serve as an adequate control to compare the effects of peptide binding and the resulting increased area, even though the overall final value would still be a net decrease compared to the initial. Nonetheless, the decline in the area over time is highly variable in between trials and within a trial over time. One is unlikely to be able to calculate a reliable averaged control baseline with such data.

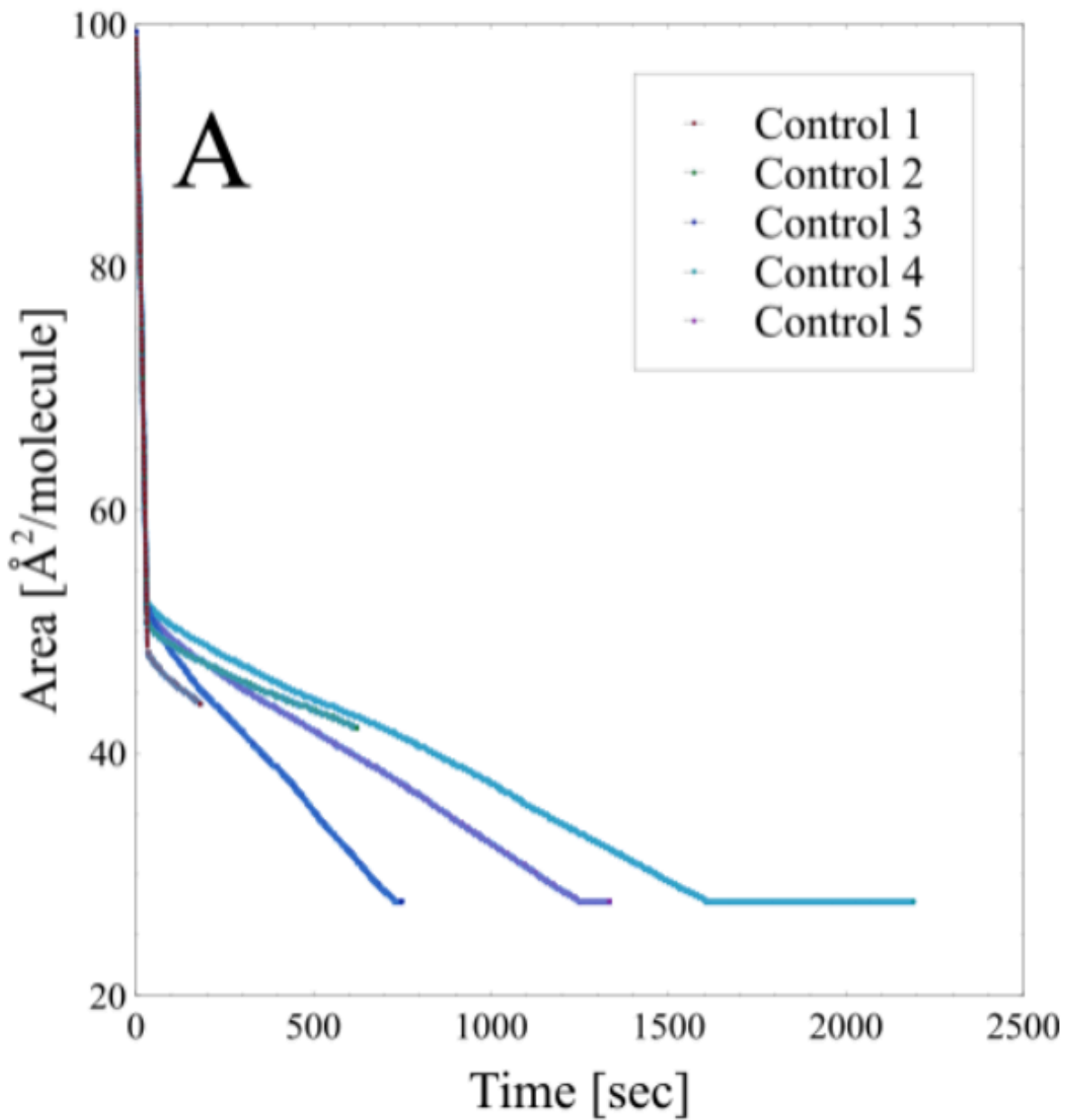


Figure 27- Results of pressure hold experiment with control DPPC monolayers. Five independent trials resulted in negative decline of the area over time. DPPC was spread using a glass syringe and chloroform:methanol 4:1 was used as the spreading solvent.

Another issue with this experiment was that the rate of leakage was much too fast. Previous publications that studied A β binding in monolayers through conducting pressure hold experiments showed that peptide incorporation time (from injection of peptide to end of changes observed in the molecular area) would need to last for around 300 minutes. Due to the constant decrease in the area, the collected preliminary data shown in figure 28 indicates that the maximum sustainable pressure hold time was only around 27 minutes (1600 seconds). In addition to the poor precision, the overall length of time may be too short to fully determine the binding interaction of the peptide used in the experiment.

There was a remote possibility that addition of the peptide would yield such a drastic increase in the molecular area over time, so much so that it would overcome the variability in the control trials. Thus, experiments with vehicle controls as well as with A β were conducted and the results are shown in figure 28. The vehicle controls included injection of the solution that normally contains A β , but without it, administered using a bent-needle syringe into the subphase. The experimental trial involved the injection including the peptide. It is evident that both the vehicle controls and the experimental fell within the variability of the control trials. Any differences produced by the peptide cannot be ascertained due to poor precision in controls.

There are several other miscellaneous considerations that may have contributed to the unfavorable results of the experiments, including not having an enclosure that controls temperature and humidity, or an anti-vibration table that may be required for such extended time dependent trials. Peptide injection ports with bath temperature controllers and subphase stirring mechanisms to ensure uniform distribution of the injected material are all widely utilized in such experiments. However, it is unclear that accounting for these factors would have helped to

overcome the leakage issues that were present due to the design and the low barrier quality of the trough.

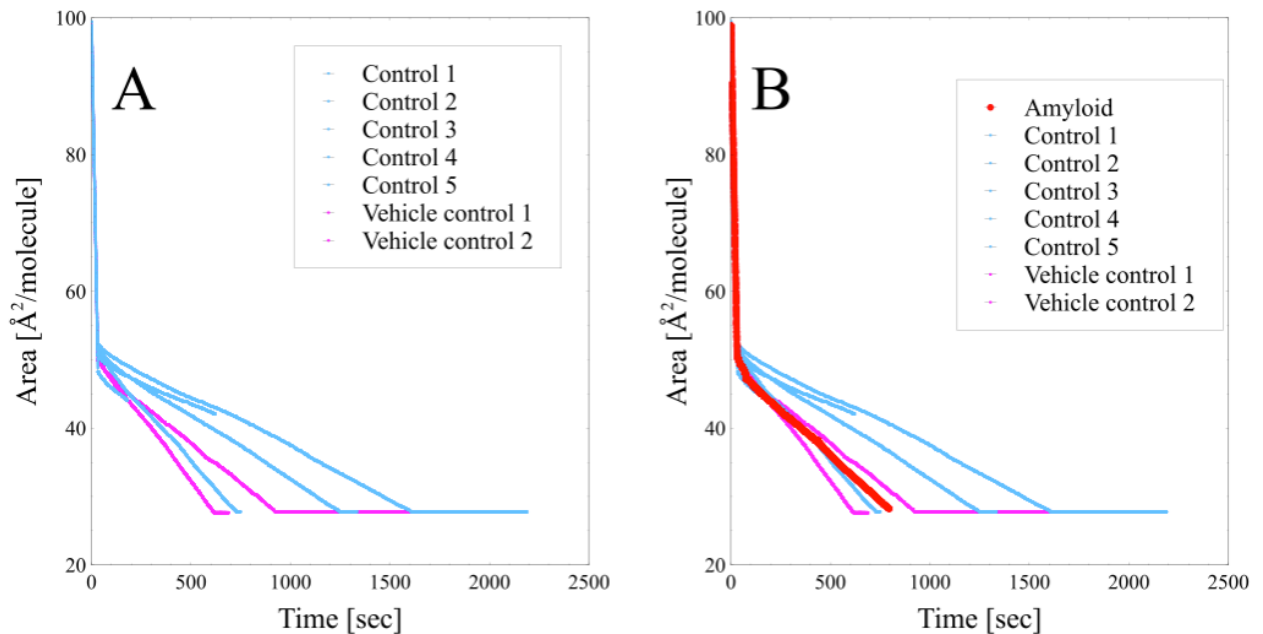


Figure 28- (A) Pressure-hold experiments with five different control DPPC monolayers and two different vehicle controls (pink lines). (B) Red line depicts a trial where A β is added. The value fell within the variability of the control trials. Vehicle control (pink lines) involved injecting the amyloid incubation solution (NaOH_(aq)) in to the buffer subphase (HEPES 10 mM, NaCl 150 mM pH 7.4) using a bent needle glass syringe.

2.4.3 Conclusion

The monolayer pressure-hold experiments to study A β binding to the membrane model were unsuccessful due to technical difficulties. The use of bent needle syringe in depositing the sodium hydroxide solution (vehicle for A β) in the subphase was a success, although it showed leakage. Technical recommendations from the trough manufacturer included the use of differently designed machines with enclosed ribbon barriers, but that was not practically possible. It was decided that other techniques, such as AFM, should be utilized to investigate the binding of A β instead.

2.5 Determining the Effects of Molecules that are Precursors to Melatonin in DPPC Monolayers

2.5.1 Introduction

Despite the results on the monolayer pressure hold experiments, the monolayer isotherm data gathered using the technique have been proven to be reliable, and of quality that well matches or surpasses the standards admissible for publications. Using the isotherm measure, it was decided to measure and compare the effects of tryptophan, serotonin, N-acetylserotonin, and melatonin on DPPC monolayers. It was a good opportunity to study and publish data on melatonin and its related molecules. Melatonin analogues may have potentially positive effects in AD, and recent publications showed that melatonin's precursor molecules have protective effects against AD and A β toxicity[145]–[147].

Melatonin is produced in the body from converting the amino acid tryptophan into serotonin, then to N-acetylserotonin (NAS), then into melatonin[51]. It may be valuable to compare the effects of these molecules, especially their ability to interact with the monolayer nonspecifically and compare the differences. Although very similar in structure, each of the molecules may employ different mechanisms in reducing AD associated effects. For instance, NAS has been shown to have anti-oxidative properties but not prevent A β aggregation[65], unlike melatonin, which is capable of both effects[69]. If NAS and melatonin affect the membrane in a similar way and they both are able to decrease A β accumulation in the membrane, it would become clear that inhibiting A β aggregation does not play a significant role in the membrane A β accumulation. If melatonin shows an advantage over NAS in terms of decreasing the A β membrane accumulation, then the difference would be attributable to melatonin's ability to decrease A β aggregation (assuming they have similar membrane effects). By characterizing the differences in the

membrane biophysical effects between the closely related molecules, it may be possible to estimate the significance of those effects in affecting the A β accumulation in the membrane.

There are other advantages to studying these molecules, in terms of their broader biological relevance. Understanding the structure specific effects of small molecules that affect the biophysical properties of the membrane lipid assemblies is an active area of research, as many biological molecules have been shown to directly interact with the membrane lipids with implications to their mechanism of action. Even certain neurotransmitters are proposed to have anesthetic properties that are suspected to result from membrane effects[44], [47], and experimental evidence of the membrane interaction of several neurotransmitters has been reported recently[148]–[152]. One of the works, by Peters and co-workers, investigated serotonin, the tryptophan derived neurotransmitter[148]. Using equilibrium dialysis measurements and also molecular dynamics (MD) simulations, they showed that serotonin strongly interacts with phosphocholine (PC) bilayer membranes. The measured high membrane partition and interaction for serotonin showed a strong influence of the electrostatically driven salt bridge formation between its positive amine group and the phosphate group of the lipid as the major driver in the lipid-serotonin interaction[148]. Wood and co-workers further showed through MD simulations that both tryptophan and serotonin had limited access to the hydrophobic bilayer core but instead interacted with the PC head groups through electrostatic interactions[151].

As a precursor to serotonin and many other biologically active compounds, L-tryptophan is also a molecule of interest for its interaction with lipids. Tryptophan is an essential amino acid that is present in significantly higher quantities in membrane proteins versus in soluble

proteins[153]. Earlier work on tryptophan in the bilayer focused on the location of the tryptophan residues in various membrane spanning proteins, as tryptophan is the most abundant amino acid residue that occurs at the bilayer water interface in stabilizing the trans-membrane regions of the proteins[153]–[155]. The location and abundance of tryptophan residues at the membrane interface have been known to act as "floats" within the bilayer, acting to stabilize the structure and function of proteins in the bilayer environment[155], [156]. Jain et al.,[157] using fluorescence spectroscopy reported that tryptophan, tryptophan derivatives, and tryptophan containing peptides were able to decrease the temperature transition of DMPC (dimyristoyl phosphocholine), which implies that they had a fluidizing effect. Also a previous monolayer study on tryptophan using vibrational spectroscopy has revealed that it increased the DPPC headgroup angle and changed the 2-dimentional-lattice structure by interacting with the PC groups through electrostatic interactions[158].

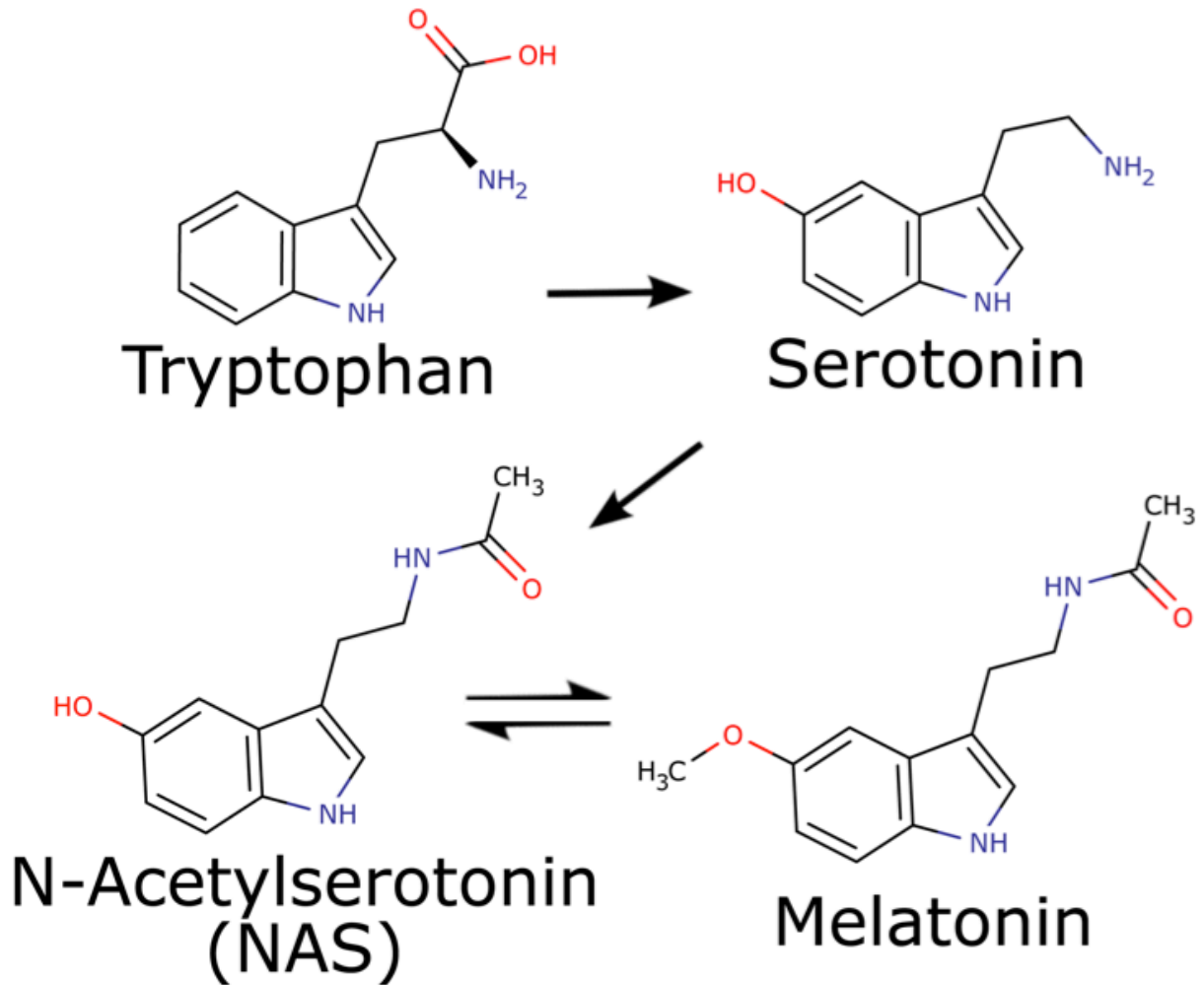


Figure 29- Molecular structures of tryptophan, serotonin, N-Acetylserotonin (NAS) and melatonin. The arrows depict the biosynthetic pathway. In physiologically relevant conditions, tryptophan is zwitterionic, and serotonin is in its amine salt form. NAS and melatonin will have no charged functional groups.

Another tryptophan derivative, the hormone melatonin, has been shown to interact non-specifically with membrane lipids[71]. Along with tryptophan and serotonin, melatonin has been referred to as having "sedative" effects[49], [159], [160]. Such effects are a hallmark of many anesthetic agents that are able to interact with the bilayer, including certain antihistamines and alcohols[40]. Ethanol, for example, has been shown to be able to thin the membrane[160]. Melatonin's anti-oxidative effects against lipid peroxidation have also been reported extensively[161], and the ability to interact with the lipid may be directly involved in this function[136]. Such effects of melatonin support the notion that a common anesthetic-like mechanism of interaction may be involved[162]. In support of this view, one of our previous publications have reported that melatonin interacts with the bilayer mainly through hydrophobic interaction[118]. The lipid interaction data for NAS has not yet been reported.

It was decided to investigate these four highly biologically relevant molecules, considering that they may all have non-specific membrane action. Tryptophan residues play an essential role in membrane proteins[153], and also its derived molecules serotonin, NAS, and melatonin may have anesthetic like mechanism of action[53], [118]. Also, because of the structural similarities, they were ideal for comparing the functional group specific effects on the interaction of the molecules to the membrane lipids.

Further, tryptophan based indole derivatives are widely used as pharmacological agents in broad areas of medicinal chemistry as anticancer, antioxidant, antirheumatoid, aldose reductase inhibitor, and anti-HIV agents[163]. The compounds are commonly suspected and in some cases known for their ability to interact with the membrane non-specifically with functional consequences. The interaction of these molecules with membrane lipids is suspected to increase

their availability within the membrane to interact with membrane bound proteins. It may also enhance their ability to interact with chemicals such as oxidative species and counter them with anti-oxidative properties, for which the indole-derived compounds are widely known[136], [163], [164] Reactive oxygen species are normally produced through many endogenous reactions including NADPH oxidase activation and oxidative phosphorylation[165]. Insight into how modifications to the tryptophan/indole backbone affects/modifies the membrane action of these compounds will broaden the understanding of the effects of these drugs and biomolecules. Although the membrane interaction of some of the tryptophan derived molecules have been reported, a biophysical structural study comparing the effects of these closely related molecules in the membrane lipid environment is highly limited.

In this study, the effects of tryptophan, serotonin, NAS and melatonin on lipid biophysical properties were assessed using the Langmuir monolayer technique. There are a few studies that looked at the effects of non-monolayer forming water-soluble pharmacological molecules in the monolayer before[43], [129], [168]-[170], but studying non-monolayer forming biological molecules such as hormones and neurotransmitters has been limited. The present study addressed a need for an experimental assessment of structure based functional group specific effects of tryptophan and its derived biological molecules on the monolayer.

2.5.2 Materials and Methods

DPPC ($\geq 99\%$), L-tryptophan ($\geq 99.5\%$), serotonin hydrochloride ($\geq 98\%$), N-acetyl-5-hydroxytryptamine (NAS, $\geq 99\%$), and melatonin ($\geq 98\%$) were purchased from Sigma-Aldrich in powder form and were used without further purification. The chemicals were directly dissolved in Millipore Water (Resistivity $> 18.2 \text{ M}\Omega\cdot\text{cm}$) by agitation to yield the final solutions

used in the monolayer subphase. Chloroform (ACS grade, EMD Chemicals, USA) /methanol (HPLC grade, Caledon Laboratories, Canada) 4:1 solution was used as the DPPC monolayer spreading solvent.

Lyophilized powdered DPPC was dissolved in chloroform:methanol 4:1 (v/v) solvent at 1.0 mg/ml. 10 μ l of the DPPC solution was deposited using a Hamilton syringe model #705 (Hamilton Company, USA) on to a Langmuir-Blodgett trough (KSVNIMA, Finland) with a subphase volume of approximately 50 ml. The compression rate for the isotherms was 80 cm^2/min or $9.8 \text{ \AA}^2/\text{molecule} \times \text{min}$. The subphase was kept at room temperature at 24 $^\circ\text{C}$. The isotherms and the compressibility data were analyzed using an in-house developed script using Matlab. Each Pressure versus area isotherm presented represents an average of a minimum of three individual experiments, with the error bars in the figures calculated as ± 2 standard deviations (SD). Uncertainties presented in the following sections are SD's unless otherwise specified. Student's t-test (as previously specified on page 57) was performed to confirm statistically significant changes[126]. Statistically significant difference was considered for p values lower than 0.05, and the tests used were paired two sample t-tests performed using StatPlus:mac software version 5.8.2.0. (AnalystSoft INC. USA)

The elastic compressibility modulus was calculated from the pressure versus area isotherm using equation (1). C_s^{-1} represents the compression modulus, where A is area in the trough isotherm, π is the pressure.

$$C_s^{-1} = -A(d\pi/dA) \quad (1)$$

In general, a lower Cs^{-1} value means an increase in the monolayer compressibility and vice versa.

2.5.3 Results and Discussion

DPPC monolayer pressure-area isotherms with tryptophan, serotonin, NAS, and melatonin in the subphase are shown in figure 30. The corresponding differences (change) in the area per molecule compared to control (ΔA) versus pressure (Π) are also shown. Briefly, all four of the tested molecules interacted with DPPC monolayers at certain pressures and concentrations. The concentrations tested here (0.1 to 10 mM) are physiologically relevant, as serotonin concentrations in the synaptic vesicles of serotonergic neurons may reach up to 270 mM, and the concentrations at the synaptic cleft may reach up to 25 mM[150]. Melatonin concentrations can reach high micromolar range[166] and millimolar range concentrations are routinely considered as pharmacologically relevant[53]. Tryptophan concentrations were also included in the physiological range considered by Sarangi et al[158].

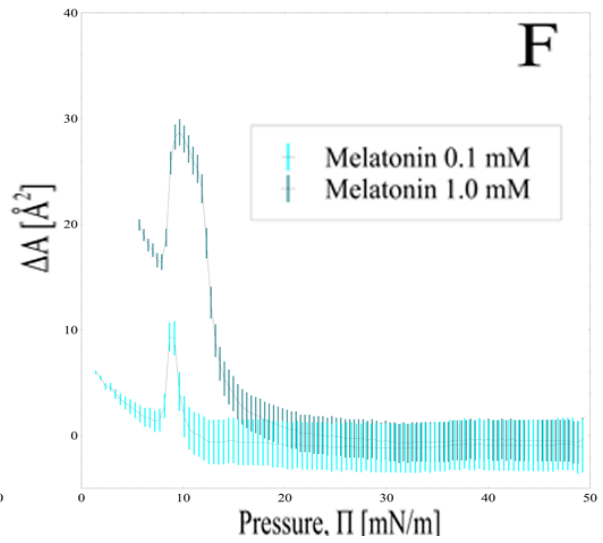
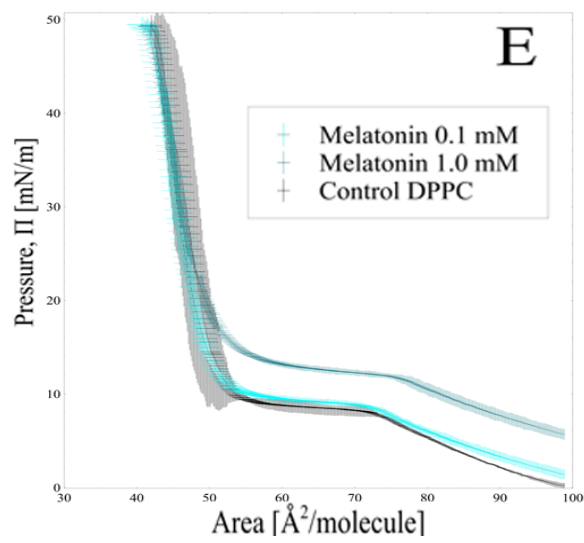
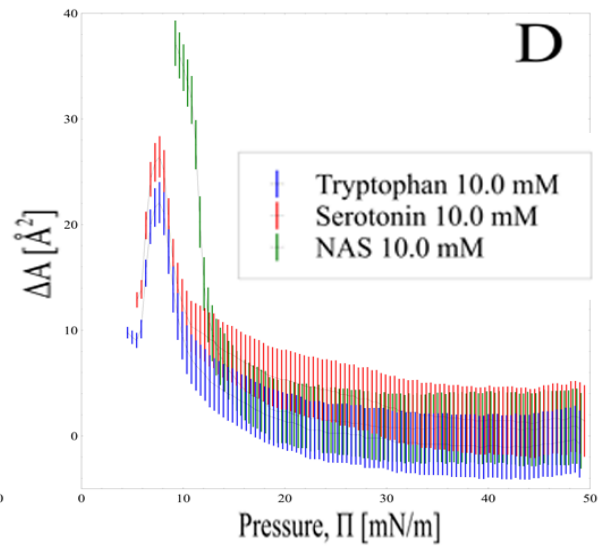
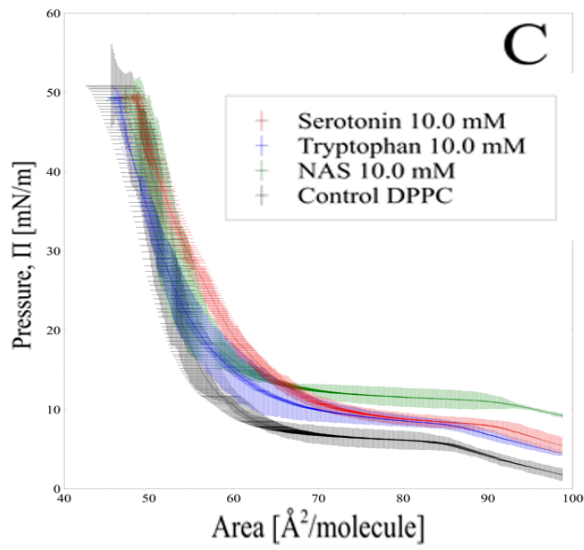
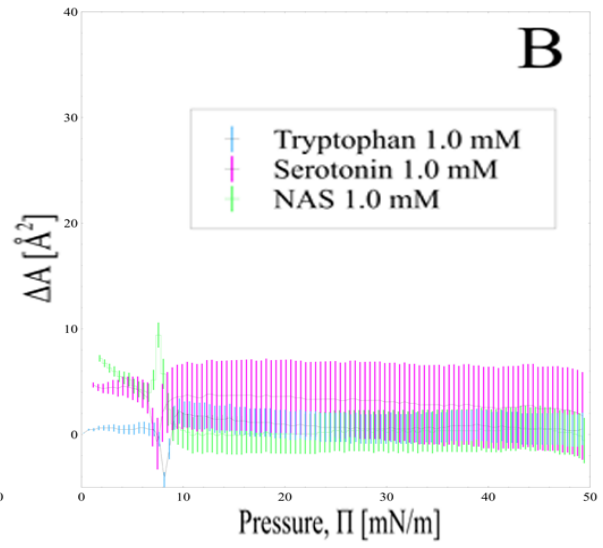
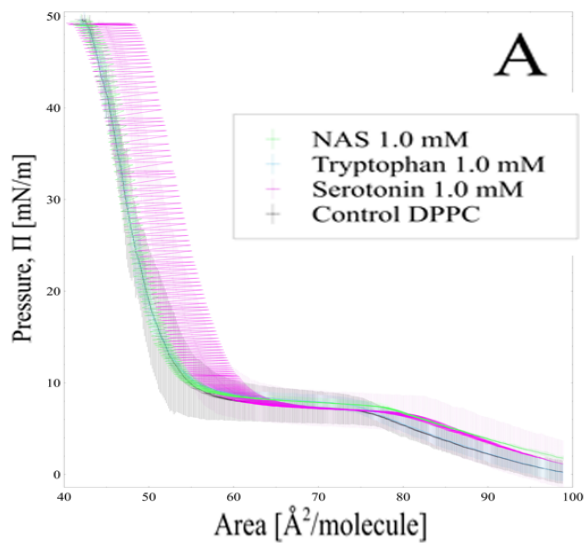


Figure 30- DPPC Langmuir monolayer isotherms (left hand side) and the difference in area per molecule compared to control (right hand side). The error bars are showing $\pm 2SD$. In each case, three curves were averaged together. Control is shown in black, serotonin in red, tryptophan in blue, NAS in green, and melatonin in cyan. (A) DPPC isotherms with 1.0 mM concentrations of serotonin (red), NAS (green), tryptophan (blue) in subphase (B) Difference in area per molecule compared to control derived from A. (C) 10.0 mM concentrations serotonin (red), NAS (green), tryptophan (blue) in subphase (D) Difference in area per molecule compared to control derived from C. (E) DPPC isotherms with 0.1 mM and 1.0 mM melatonin in subphase (F) Difference in area per molecule compared to control derived from E.

Within figure 30A, only NAS showed significant change versus control, and it was only at the very low-pressure regions near the beginning of the isotherm specifically at the area of around 96 \AA^2 (bottom right corner of the graph, $p < 0.05$, Student's t-test). Though significant, the effect quickly diminished with increasing pressure ($> 10 \text{ mN/m}$). The result indicates that NAS was able to increase the area per molecule at low pressures where the monolayer is known to be in its liquid expanded phase. The region at the beginning of the isotherms is where the pressure is low and the area per molecule is large, with the lateral pressure of the lipid molecules at its minimum and the area per molecule at its maximum. Such conditions might favor incorporation of added molecules into the monolayer with minimal hindrance. The diminishing effects with increased pressure is most likely due to the molecule (NAS) being squeezed out of the monolayer upon compression[43]. Molecules that primarily utilize the hydrophobic interaction when interacting with the lipids have been shown to display such patterns in monolayer isotherms[129], [167].

Serotonin and tryptophan did not produce significant changes ($p > 0.05$) at 1.0 mM concentration at any pressures (figure 30A,B), including at the bilayer equivalent pressure of 30

mN/m where effects of molecules in monolayers are often assessed. Although the bilayer equivalent pressure is the most commonly used parameter to relate monolayer effects to bilayers, the pressure value of 30 mN/m is still under debate[130]. Thus, in addition to the equivalent pressure, many groups also consider the bilayer equivalent molecular area. The commonly accepted experimentally determined value for DPPC molecule area in a bilayer is 64 \AA^2 [132]. When comparing values at the bilayer equivalent area, the three compounds at 1.0 mM also showed insignificant changes compared to control (figure 30A,B) matching the null results observed at the bilayer equivalent pressure of 30 mN/m.

The peaks and the valleys observed around pressure 8 mN/m in figure 30B are due to having an offset in the LE to LE/LC phase transition points (the kinks preceding plateau regions found in the isotherms, figure 30A) between each of the isotherms and the control. The liquid expanded (LE) to liquid expanded/liquid condensed (LE/LC) transition normally occurs between pressures 8-10 mN/m[88]. In figure 30B, only NAS showed a peak in the ΔA graph (as opposed to valleys with serotonin and tryptophan), which meant that the phase transition occurred at a higher pressure than the normal pressure with NAS, most likely due to having larger area per molecule compared to control. The result implies that NAS had a spreading effect.

The effects of the three molecules on the monolayers were clearly evident when the concentration was increased to 10.0 mM (figure 30C,D). In figure 30C, tryptophan, NAS, and serotonin all showed significant effects on the monolayer at the beginnings of the isotherms compared to control ($p < 0.05$). At this higher concentration, the three compounds showed significantly different change in area relative to control (ΔA , figure 30D), and also between each other ($p < 0.05$) at the beginning of the isotherms. Also, both low and high concentrations of

melatonin showed significantly different peak heights at the 8-10 mN/m region (figure 30F) again indicating a significant difference from control and from each other. Thus overall, the compounds with high concentrations all had a spreading effect on the monolayer. Relative to control, NAS and melatonin showed significant area change in both low and high concentrations, whereas tryptophan and serotonin showed significant changes only at the high concentration. Nevertheless, it is evident that the effects were not sustained with increased pressure, indicated by the fact that all of the curves converge with the control (likely due to molecules being squeezed out of the monolayer). Even NAS, which had the greatest effect in increasing the area per molecule at lower pressures ($p < 0.05$, paired Student's t-test) compared to serotonin and tryptophan, also followed the same trend of losing its effects at higher pressures much like the others (figure 30D).

In high concentration groups, at low-pressure regions (figure 30C, bottom right corner), serotonin's effects were significant compared to control ($p < 0.05$), and they were not significantly different from the effects of tryptophan. Collectively, both serotonin and tryptophan showed significantly lower effects compared to NAS ($p < 0.05$). Moving toward higher-pressure regions (within figure 30C, left side), at the bilayer equivalent pressure 30 mN/m, all molecules showed insignificant effects compared to control. Using molecular dynamics simulations, Peters et al. and Wood et al., showed that serotonin primarily interacts with the lipid headgroup through forming a salt-bridge [148], [151]. This implied that there would be a maximum saturation point for serotonin in relation to the number of binding sites available in the lipid molecules. Likewise, the similar values of ΔA from both the 1.0 mM and the 10.0mM serotonin indicates that a point of maximum influence had been reached at the lower concentration, implying that the

lipid/serotonin interaction involves a mechanism that results in a stoichiometric saturation. Thus the data supports the previously reported electro-static salt bridge driven interaction of serotonin. In a previous report, Peters et al. also determined the minimum distance between the lipid head groups and serotonin to be between 2 to 9 Å[148]. Our data suggests that at the commonly accepted bilayer equivalent pressure, serotonin increases the area per molecule by about 3 Å².

The bilayer equivalent area also marked a spot where NAS's effects were not significantly different from serotonin's effects (figure 30 C). This was in contrast to NAS having had significantly greater values at higher areas per molecule (>73 Å²/molecule) compared to serotonin. It may be possible to describe NAS as having experienced a quicker squeeze-out effect with increasing pressure compared to serotonin. The difference may have been due to the two molecules employing different interaction mechanisms. Considering that serotonin and tryptophan isotherms are within experimental uncertainty (except at the very beginning of the isotherm, figure 30C and D), and NAS is considered to display a quicker squeeze-out effect at higher molecular areas, it might be possible that the both serotonin and tryptophan employ similar interaction mechanism that differs from that of NAS. Since the squeeze-out effect seen with NAS is considered characteristic of molecules that employ hydrophobic interactions[129], it might be possible that tryptophan and serotonin utilize a different lipid interaction mechanism, most likely involving electrostatic contributions when interacting with the lipids[151]. Nonetheless, at pressures greater than 15 mN/m, the effects of both tryptophan and serotonin have disappeared completely by displaying the squeeze-out effect as it did for NAS, which might mean that hydrophobic interactions are basically present in all three compounds.

Many previous reports have shown that melatonin is able to interact with membrane lipids[70], [118]. Of the four tested compounds, it is the most modified molecule furthest away from tryptophan within the brain biosynthetic pathway. It is also the most hydrophobic molecule tested with the lowest aqueous solubility. Unlike the other three molecules as shown in figure 30C, it is not possible to attain and test melatonin at 10.0 mM concentration in aqueous solution. However, the effects of melatonin in monolayers were so strong that changes in the area per molecule that are insignificantly different could be observed with 10x lower concentrations compared to the other molecules. Melatonin isotherms at concentrations of 0.1 mM and 1.0 mM are shown in figure 30E.

In low concentration groups, melatonin at 0.1 mM concentration showed an increase in pressure at a given area versus control at high areas ($p < 0.05$), which was not significantly different from the results obtained for 1.0 mM concentration of NAS (figure 30A). When comparisons are made in the high concentration group (figure 30C vs figure 30E), 1.0 mM melatonin managed to increase the initial pressure of the monolayer that was not significantly different compared to the 10.0 mM concentration effects of serotonin and tryptophan. The initial isotherm pressure for NAS had the highest value both significantly above control and the rest of the molecules ($p < 0.05$ vs control and also vs all three compounds). However, melatonin had similar effects at a 10x lower concentration.

At the bilayer equivalent area of 64 \AA^2 , high concentration groups of all four of the tested molecules showed significant changes compared to control ($p < 0.05$), and they were not significantly different from each other. Taking into account that melatonin's concentration was 10x less than the rest, it may be suggested that the order of influence at the bilayer equivalent

area might have been Melatonin > Serotonin/ NAS / Tryptophan. Comparing the effects at the start of the isotherms, NAS had the most pronounced effect ($p < 0.05$ against all other groups, paired Student's t-test). Even with NAS having the greatest result, taking into consideration the order of magnitude lower concentration of melatonin, it could still be considered that melatonin had the strongest influence at the start of the isotherms as well (Melatonin > NAS > Serotonin = Tryptophan). The comparisons roughly follow the biochemical modification pathway of tryptophan in reverse order (figure 29). It may be relevant to note that molecules might exert fewer local and more general effects when further modified away from tryptophan. Accordingly, serotonin with fewer modifications from tryptophan has more local effects as a neurotransmitter, as opposed to the highly modified melatonin, which has broad range of effects as a hormone. Nonetheless, at pressures > 15 mN/m, (which includes the bilayer equivalent pressure) no significant difference vs control could be ascertained for any of the compounds.

The overall shapes of the isotherms for all groups are similar in that the effects of the molecules are at their maximum in lower pressure regions, and the effects gradually diminish as the pressure increases. The rate of diminishing effects may be different for each compound, and the slower diminishing trend observed for serotonin compared to NAS may be attributable to its increased electrostatic interactions with the membrane lipids[151].

Compressibility moduli for the four compounds (figure 31) were derived from the averaged isotherms (figure 30 A,C,E). Compressibility modulus (C_s^{-1}) correlates directly with the bending modulus and the bulk modulus; it is a measure of the stiffness of the monolayer[87], [125]. A monolayer's ability to store mechanical energy as stress is reflective of its stiffness. Also as a second derivative of the surface free energy vs the area, it is expected to show discontinuities at

both first and second order transitions[168]. This is useful for confirming any shift in the phase transition point. In terms of comparing results, the effects at the bilayer equivalent pressure of 30mN/m will again be considered. However, comparing the effects at the bilayer equivalent area ($\sim 64 \text{ \AA}^2$, which usually occurs at a pressure considerably lower than 30mN/m) will be difficult to consider, since the area measure is not present in the compressibility modulus data. Judging from the isotherms (figure 30A,C,E), at the bilayer equivalent area ($\sim 64 \text{ \AA}^2$) the isotherms tend to have pressure values between 11.5 mN/m to 15 mN/m. Thus these two pressure values might be useful as indirect estimates for the bilayer equivalent area. So compressibility results are compared, using paired Student's t-test, at three different pressures: at the bilayer equivalent pressure of 30 mN/m, and also at 11.5 mN/m and 15 mN/m, with the last two pressures approximately representing the bilayer equivalent area.

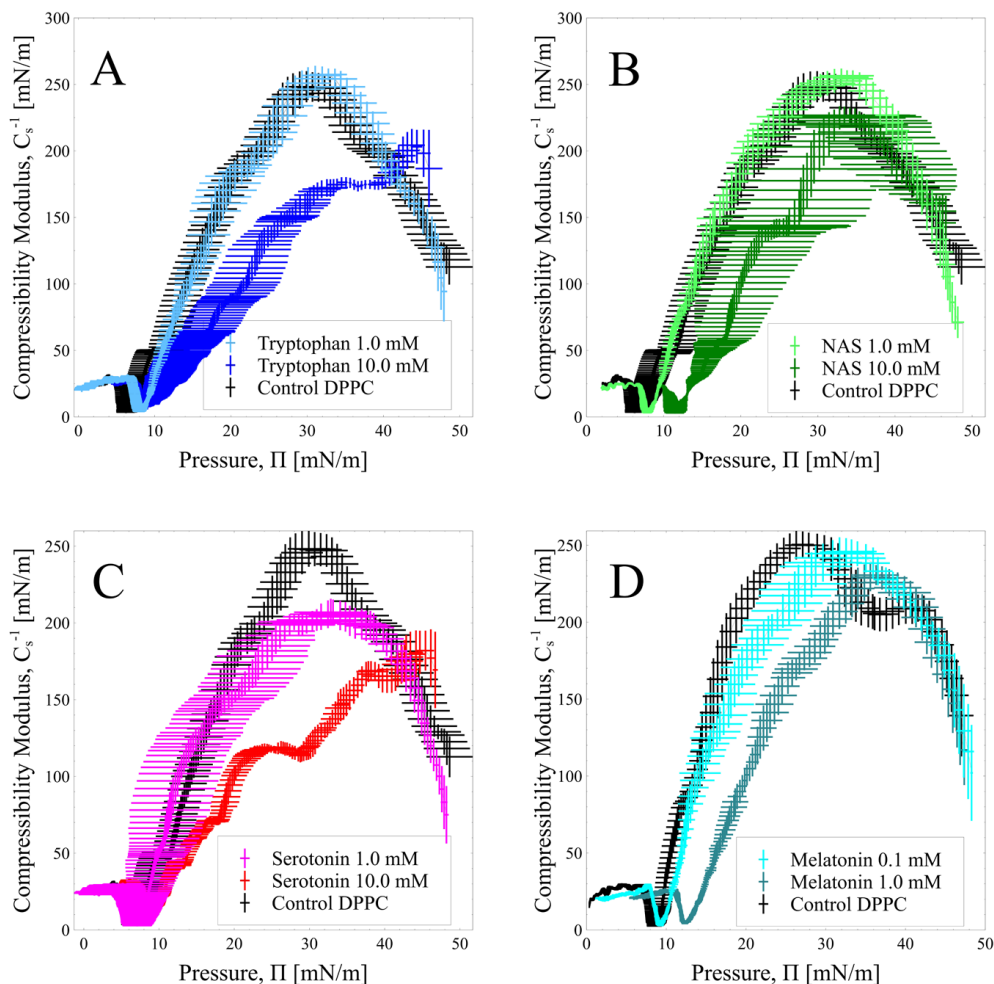


Figure 31- Compressibility modulus C_s^{-1} (mN/m) versus pressure Π (mN/m), calculated from the isotherms (figure 30 A,C,E). (A) Tryptophan, (B) NAS, (C) Serotonin, (D) Melatonin. Black lines are controls, the lighter colors (sky blue for tryptophan, pink for serotonin, light green for NAS and light teal for melatonin) in each group denote low concentrations, the darker colors (dark blue for tryptophan, red for serotonin, dark green for NAS and dark teal for melatonin) denote higher concentrations used within each group. The high concentrations for the two charged molecules tryptophan (zwitterionic) and serotonin (cationic, amine salt) show a pattern of compressibility modulus change (flat almost liner increase over the pressure range) that is different compared to the pattern seen with uncharged NAS and melatonin (compressibility modulus follows the control curve shape overall). Each curve contains an average of $n=3$ trials, presented with $\pm 2SD$. Individual isotherms ($n=3$ for each line) were converted to compressibility modulus and then the average and SD's were determined with $\pm 2SD$ plotted.

The compressibility modulus results show that all of the tested molecules at the low concentration (0.1 mM for melatonin, 1.0 mM for the rest) remained within experimental uncertainty compared to control at pressures 11.5 mN/m, 15.0 mN/m, and 30.0 mN/m. However, high concentration samples showed significantly different values compared to control ($p < 0.05$, paired Student's t-test) in at least one of the three tested pressures.

Tryptophan at 10.0 mM showed lowered compressibility modulus at 30 mN/m ($p < 0.05$, compared to control). The results imply that the monolayer is less stiff and thus became more fluid with the presence of tryptophan. The difference, however was not significant in the lower pressures tested (11.5 mN/m and 15.0 mN/m).

Similar results are observed for serotonin as the similarities in the molecular structures may have resulted in comparable effects on the monolayer. With 10 mM concentration at 30 mN/m, serotonin decreased ($p < 0.05$) the compressibility modulus compared to control. The similar results for both tryptophan and serotonin is not surprising, as Wood et al.,[151] using molecular dynamics simulations, had shown that both tryptophan and serotonin are able to interact with POPC (1-palmitoyl-2-oleoyl-sn-glycero-3-phosphocholine) by salt-bridge, hydrogen bonds, and cation- π interactions, which are electrostatic interactions. They also noted that both these molecules were unable to permeate through the membrane hydrophobic core.

Both serotonin and tryptophan did not change the compressibility at pressures below 30.0 mN/m (no change compared to control at 15.0 mN/m or at 11.5 mN/m). The results contrasted with NAS and melatonin, as they showed significant difference relative to control at lower pressures but not at the higher 30mN/m pressure. NAS and melatonin yielded

significantly different compressibility modulus changes at a pressure of 11.5 mN/m compared to control ($p < 0.05$, but not different compared to each other). A significant reduction in compressibility modulus with melatonin was also seen at 15 mN/m pressures ($p < 0.05$). Neither NAS nor melatonin showed significant effects at 30.0 mN/m. The overall effects of NAS and melatonin can be said to be similar in that both the compounds decreased the stiffness of the monolayer and changed the monolayer to be in a more fluid (expanded state) only at low pressure ranges (< 15 mN/m for melatonin and < 11.5 mN/m for NAS with no significant difference between the two). Again, melatonin results were with 10x lower concentration compared to NAS.

The contrasting compressibilities shown by NAS and melatonin compared to tryptophan and serotonin are probably due to the differences in the lipid interaction mechanism. It may be important to note that both NAS and melatonin are known to cross the blood-brain barrier and bilayers [169], [170], whereas serotonin and tryptophan have not been shown to cross bilayers [151]. The findings suggest that melatonin and NAS are hydrophobically driven when interacting with membrane lipids, as non-charged molecules (NAS and melatonin) are able to pass through the hydrophobic core of the membrane, whereas tryptophan and serotonin with electrostatic interactions of their charged groups may not be able to cross the bilayer.

In terms of differences within each pair, melatonin had effects that matched (no significant difference) that of NAS at 10x lower concentrations, and likewise, there was no significant difference between tryptophan and serotonin. However, it was reported previously that tryptophan may have a less strong of an interaction compared to serotonin with lipids, due to

its carboxylic acid group destabilizing the tryptophan-lipid interaction through preferential interaction with water[151].

In the compressibility modulus graphs (figure 31), there is a minimum point that occurs for each curve at between 6-12 mN/m pressures. This point denotes an LE to LE/LC phase transition[171] (figure 31, all panels). Both melatonin and NAS shifted the points to significantly higher pressures compared to control ($p < 0.05$), but serotonin and tryptophan did not. The shift or the delay in the onset of the phase transition to a higher pressure may correspond with the relative hydrophobicity of the molecules, as less hydrophobic molecules tryptophan and serotonin, did not change the minimum points significantly. The results indicate that the hydrophobicity of the interacting substance might be an important factor in the molecular packing density and the LE to LE/LC transition.

Melatonin, as the most hydrophobic molecule of the group, had the greatest effects in delaying the LE to LE/LC phase transition, concentration considering, as NAS had comparable (not significantly different) results but with 10x greater concentration than melatonin. The difference is remarkable considering that NAS and melatonin differ by only one functional group. NAS has a hydroxyl and melatonin has a methoxy group at the 5th position of the indole backbone (figure 29). This difference makes melatonin much more hydrophobic compared to NAS and also much more potent in affecting the monolayer. Our previous work on melatonin supports the hypothesis that hydrophobic interaction might be an important main driver of melatonin's interaction with DPPC and cholesterol[118]. Further, a different pattern of results seen with serotonin and tryptophan compared to NAS and melatonin also indicates that the interaction of tryptophan and serotonin with lipids might be

different than that of NAS and melatonin, most likely due to involving differences in electrostatic interactions.

2.5.4 Conclusions

The mode and the extent of interaction of the four related tryptophan derived bio molecules within the DPPC monolayer were measured using the Langmuir monolayer technique. It was determined that NAS and melatonin likely utilized hydrophobic interactions as the main driver in their incorporation within the monolayer, and melatonin's interaction was enhanced by an order of magnitude with the presence of a more hydrophobic methoxy functional group compared to the hydroxyl group on NAS. The interaction contrasted with that for tryptophan and serotonin. Melatonin and NAS both showed significant effects on compressibility modulus at low pressures, but insignificant effects at 30 mN/m compared to control. On the other hand, tryptophan and serotonin displayed insignificant effects at low pressures, but at a higher pressure (30 mN/m) they had significant effects compared to control. The difference observed might be attributable to electrostatic interactions of tryptophan (zwitterionic) and serotonin (amine salt). At the bilayer equivalent area, all four compounds had significant effects of increasing the area per molecule compared to control ($p < 0.05$, paired Student's t-test). The effects between the different molecules were insignificant, but since melatonin had 10 times less concentration compared to the rest, it can be said that melatonin had the strongest effect comparatively.

By characterizing the changes in the monolayer using the Langmuir monolayer technique, it was possible to qualitatively and quantitatively differentiate the interactions of the structurally related tryptophan and its derivatives with the phospholipids. Improvements were

made that increased the precision of isotherm measurements, and averaged isotherms with standard deviations were presented. The data presented here may add to the overall understanding of the non-specific interactions of these biologically pertinent molecules that may be playing a role in their diverse range of function. The methods and technique presented may also serve as a platform for characterizing non-specific membrane interactions of other biologically and pharmacologically relevant molecules.

Chapter 3

Atomic Force Microscopy Study of Supported Bilayers

3.1 Introduction

It was important that the hypotheses of this thesis be tested using a bilayer membrane model, since it is a closer representative of the real plasma membrane, compare to the monolayer. In this chapter, results are outlined from AFM imaging combined with AFM force spectroscopy studies on supported phospholipid bilayer membranes that were created through the process of vesicle fusion.

3.1.1 Atomic Force Microscopy (AFM)

AFM is a member of a family of scanning probe microscopy (SPM) techniques that are capable of gathering surface topographical information at nanometer and even atomic resolutions. AFM is a mechanical scanning device utilizing a sharpened probe (a cantilever needle) that physically interacts with the surface and creates 3-dimensional data. As the cantilever moves along the surface and interacts with the surface, a laser beam detects the fine movement of the tip and the image of the surface is produced (figure 32). It is also highly versatile especially for life sciences since special preparation of samples is not required for scans, which can be performed in air or in liquid.

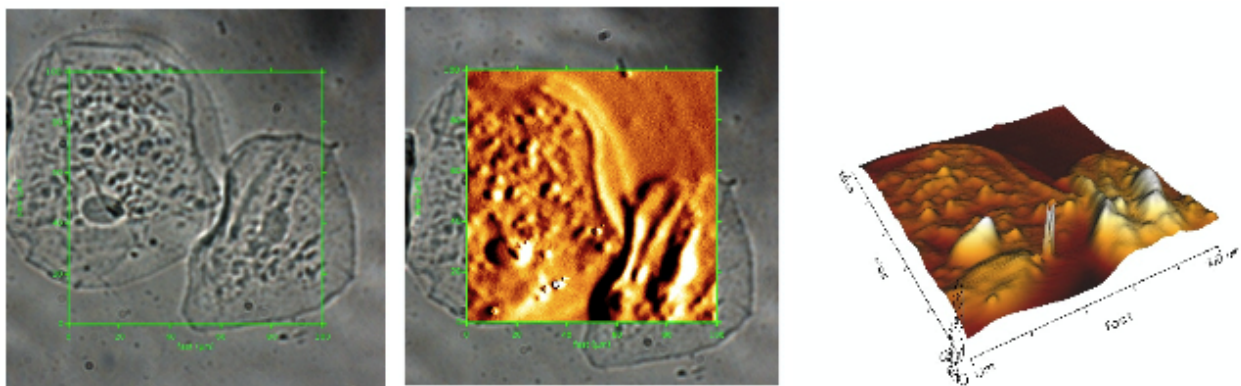
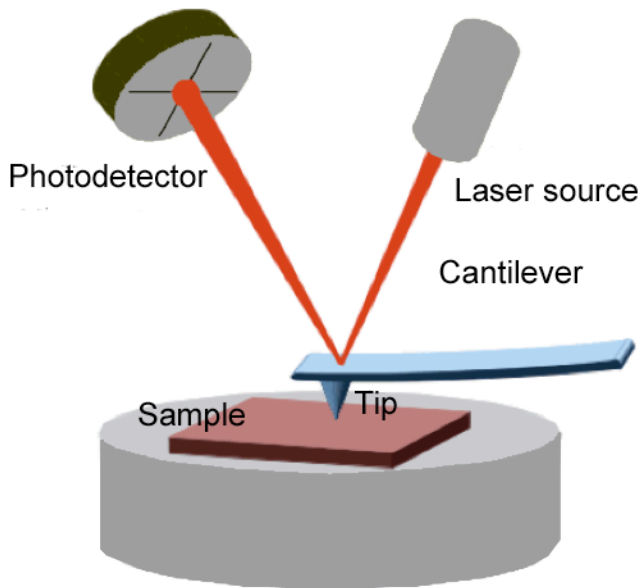


Figure 32- (Top) Cartoon of an AFM cantilever/tip and the sample, the movement of the cantilever is detected by the laser beam. (Bottom) Example illustration of a combined optical and AFM overlay sample images (100 x 100 μm , green square) of human epithelial cells. Optical microscopy picture (bottom left) shows two cells and subsequent AFM overlay imaging (in orange bottom center) reveals the 3-dimensional surface structure (bottom right). The AFM image in bottom center is an amplitude image, and the height scale for the 3-D AFM rendering (bottom right) is shown at the bottom left corner, height scale range 0.2-1.0 μm .

There are three imaging modes: contact mode, intermittent contact mode, and non-contact mode. The differences between the imaging modes can be explained by examining the atomic forces involved at the sample surface. Fundamental to the technique are the atomic forces present near the sample surface that are being detected by the tip, and the technique is thus named after them.

As the tip approaches the surface of any given sample, various attractive and repulsive forces act on the tip. Some forces lead to the tip being attracted toward the surface of the sample, which causes the tip to bend down toward the sample, or the forces prevent or hold onto the tip from moving away from the surface. Examples of forces that can induce attraction include covalent and hydrogen bonds, capillary forces, and solvation forces. Repulsive forces occur due to electron wave overlap (Pauli exclusion principle) or ionic repulsion. There are long-range forces (up to 100 nm) comprised of electrostatic, magnetic, and Van der Waals forces involved as well that can be both attractive and/or repulsive[172], [173].

The effective role of the forces at the tip-sample interface, in practical summation, can be graphed in a force versus distance graph. When the tip is far away from the surface, the forces are not strong enough to affect the deflection of the cantilever (no interaction). However as the tip approaches the sample (tip-sample separation decreases) attractive forces can dominate, which pulls the tip toward the surface (downward slope in the force versus distance graph). When the tip becomes even closer to the surface, the contact regime is established, meaning expulsion forces push the tip away causing the cantilever to deflect upward (figure 33).

The three modes of imaging work in different force regimes. Contact and intermittent contact mode imaging operate at the repulsive region, where the tip is close enough to the sample that it is bent upward and is constantly being repelled by the sample. For the two modes, the operator manually selects the exact amount of force being exerted by the tip while scanning within the repulsive region. Non-contact mode will scan the surface while the tip is in the attractive region, which is further away from the surface than the contact/intermittent contact imaging modes. This mode is ideal for measuring long-range forces, rather than the short-range chemical forces experienced in the contact/intermittent contact regime (figure 33).

In essence, AFM imaging consists of choosing a certain force threshold for the tip to be in and keeping the force experienced by the tip constant at or near the surface of the sample while performing a line-by-line raster scan of the surface. Some practical limitations in this approach of generating images are that the tip is most likely interacting laterally with the surface due to the nature of raster scanning involving sideways movement of the tip, which can lead to unwanted tip-sample interactions (much like drawing lines in the sand). Also, because the force threshold is set by the user/operator, the measured sample height could be over or underestimated, depending on the force exerted by the tip and the softness and flexibility of the sample material.

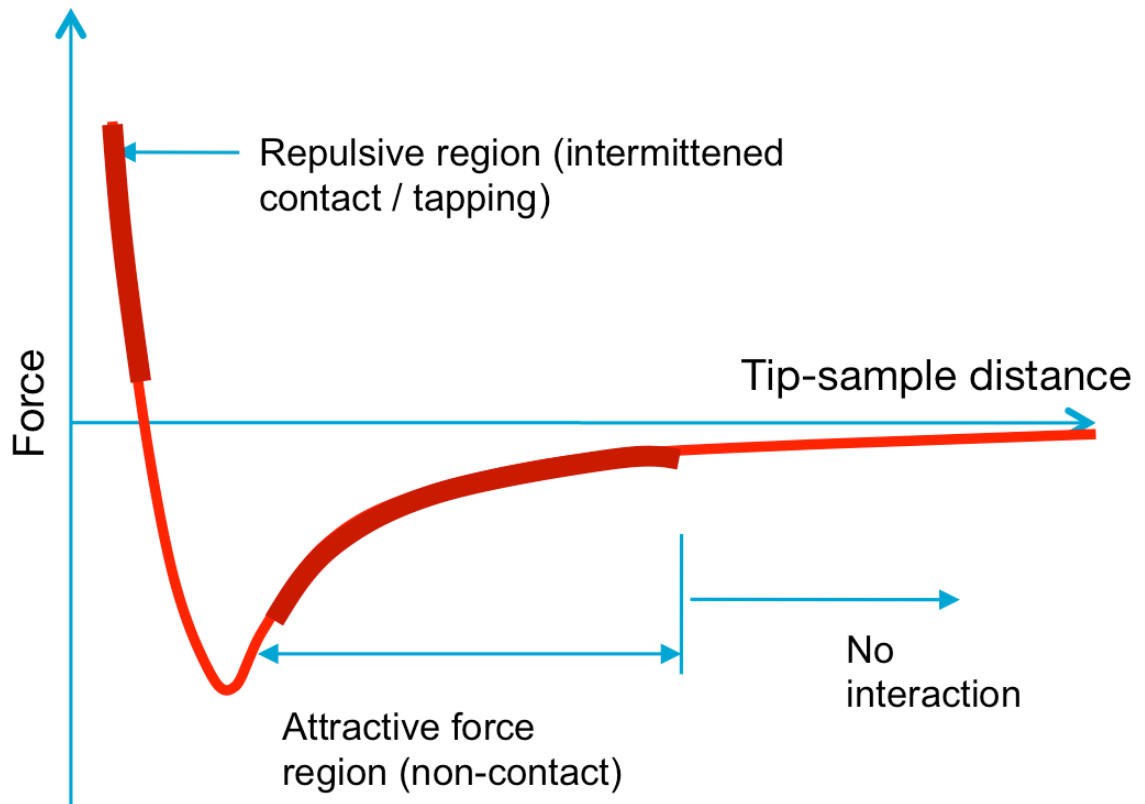


Figure 33- Force versus tip-sample distance graph, describing the summation of forces experienced by the tip at or near the sample surface. The force is high when the tip is closer to the surface (repulsive region). As the tip moves away from the surface (tip sample distance increase) the force decreases to a minimum and then attractive forces become dominant (at non-contact region). Moving the tip further away from the surface leads to very low to no detectable forces acting on the tip (no interaction).

3.1.2 AFM Force Spectroscopy

In force spectroscopy mode, the AFM tip is moved vertically down to the sample and then backed out. This generates a full range of force versus distance data (a force versus distance curve, or force curve for short) between the sample and the tip. By analyzing the forces (measured in piconewton scales) required to compress, breakthrough, and adhere to the sample, it is possible to determine various material properties of the sample. In order to calculate the force in the force vs distance curves (figure 34), the spring constant (K) of the cantilever is calculated using the thermal fluctuation method[174]. This step is also referred to as "force calibration".

This mode is also advantageous compared to imaging, as imaging parameters restrict the tip to a specific limited force region within the tip-sample interaction range. This means that choosing a different parameter could result in different characterization of the same sample. The spectroscopy mode circumvents this problem by taking account of the full range of forces experienced by the tip at a single point of the sample. Instead of performing a raster scan, many force curves can be taken using a grid pattern, and analyzing the spectroscopy data over the grid area can be used to generate images as well as compute the material properties of the sample. The grid technique, also called 'force volume mode' is often used to measure the various material properties of a bilayer, such as elastic compressivity, rupture depth and breakthrough rupture force.

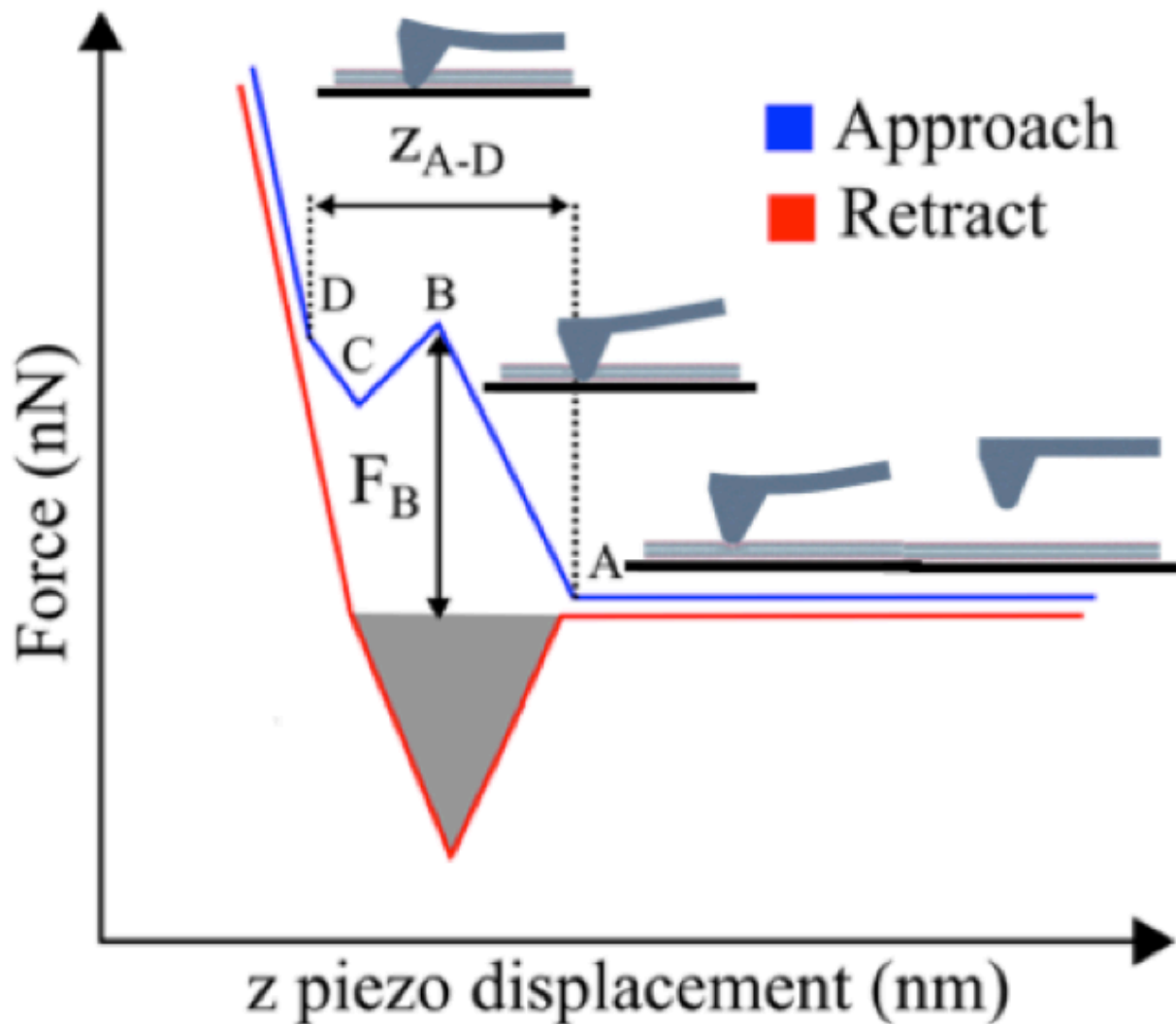


Figure 34- Force spectroscopy vertical deflection (force) versus height (displacement) graph. Point A depicts the point of contact between the tip and the sample, point B denotes the maximum force exerted in indenting the sample, point C is after the tip had broken through the sample, point D is the point at which the tip is pressing on the substrate underneath the sample. F_B denotes breakthrough force, which is indentation force required to compress the sample to cause rupture or failure. Z_{A-D} is breakthrough depth, which is calculated as the distance from the tip sample contact point to the substrate.

3.1.3 Vesicle Fusion

Vesicle fusion describes the technique of forming model lipid bilayer membrane structures supported on a flat substrate, such as mica or glass. The vesicle fusion technique involves two steps. First, membrane phospholipid molecules are formed into lipid vesicles (hollow spherical bilayer self-assembly) in solution. This step is usually done through sonication or filtration. Then the solution containing the vesicles is deposited on a flat substrate such as mica, and the vesicles can rupture and form a uniform bilayer covering the surface.

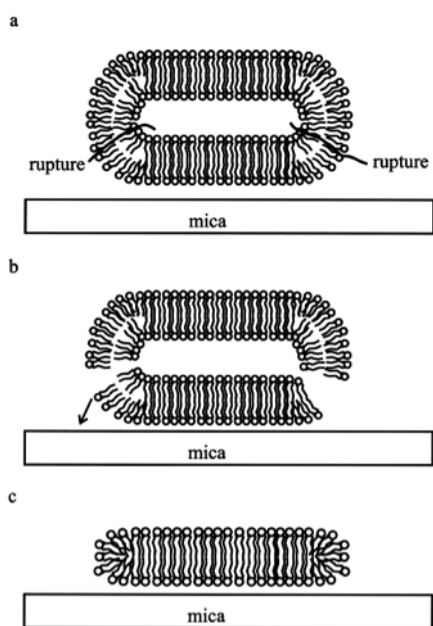


Figure 35- Schematic diagram of vesicle fusion process, reproduced from [175] presented with written permission.

The conditions in which vesicle fusion occur can be manipulated to produce a stable supported vesicle layer, instead of a supported bilayer. Nonetheless, the process of vesicle fusion is a spontaneous uncontrolled event that is not yet fully characterized or understood precisely.

3.2 AFM Experiments to Assess Bilayers

In order to study supported bilayers, several experiments were conducted. The first step was to assess supported bilayers by AFM imaging.

3.2.1 Bilayer Imaging

First, DPPC supported bilayers were made by following the protocols already employed in the lab. The traditional protocol, as outlined in previous literature, gave bilayers with varying degrees of defects, which are holes present in a patchy coverage of a bilayer. The bilayer making protocol was geared toward producing bilayers with defects (holes) that reveal not only the presence of the bilayer patches but also their thickness compared to the underlying substrate.

Adding melatonin to the sample gave a very slight change in the bilayer thickness (< 0.5 nm), which was estimated from the cross sectional height measured from the AFM images. However, measuring the bilayer thickness using the cross sectional height measure was not reliable, especially for measuring such soft pliable samples. The operator sets the force exerted by the tip arbitrarily in generating AFM images, and the force also is often changed during imaging. The control bilayer thickness measured using AFM imaging and other comparable techniques are shown in Table 1. In the literature, thickness values for DPPC ranges from 4.8 to 10.0 nm, for DOPC 3.6 to 8.0 nm. The difference between the two different phases of lipids (fluid phase DOPC and gel phase DPPC mixed in the same sample) was reported to range from 0 to 2.0 nm. The variability in the control thickness values found in the literature confirmed the observed variability during the experiments (Table 1). The usually reported experimental variability was evident in the differences observed with and without melatonin (figure 36). The thickness values observed for the images shown in figure 36 were 6.24 ± 0.31 nm for DPPC, and 6.67 ± 0.82

SEM, n=10 for DPPC with melatonin (2.0 mM), so they were not significantly different. Although an increase in a different lipid bilayer (DMPC) thickness of around 0.5 nm with melatonin has been previously reported using AFM[70], it was not possible to measure such a small change in the thickness with melatonin with this method. We can place an estimated upper limit on the thickness change of 5.2 nm. The accuracy and precision of the controlled thickness measure needed to be improved in order to differentiate smaller changes in membrane thickness. Because of the force between the tip and the sample is rather arbitrarily set (force setpoint) and varied during imaging, and the height cross section measurements reflect that, it was decided that using a force spectroscopy method might be better suited for measuring changes in the bilayer thickness since it circumvents the use of force setpoint.

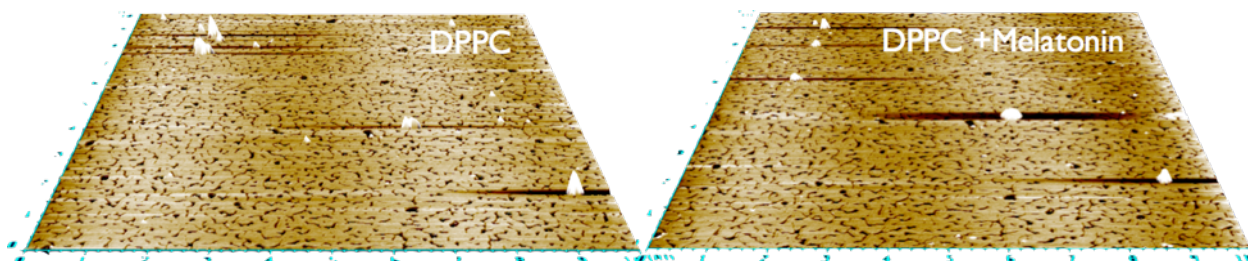


Figure 36- DPPC bilayers with and without melatonin. Visual changes (changes in the size of defects, new domain formation, etc.) are not observed with melatonin added (2.0 mM). Changes may be present but they are not detected using AFM imaging. DPPC deposited in water at room temperature.

Table 1- Reported literature values for DPPC and DOPC bilayer thickness using different techniques. X-ray diffraction techniques are often compared to AFM results, however, the numbers represent the lipid thickness only without the hydration shell [200]-[202]

First Author, year	Lipid	Method	Thickness	Thickness difference
Leonenko 2004 [176]	DPPC DOPC	AFM	DPPC 5.5±0.2 nm DOPC 5.5±0.1nm	0.0 nm
Picas 2012 [177]	DPPC DOPC	AFM	DPPC 5.3±0.4 nm DOPC 4.1±0.2 nm	1.2 nm
Milheit 2002 [178]	DPPC DOPC	AFM	DPPC ~6.5 nm	0.97±0.14 nm
Deleu 2013 [179]	DPPC DOPC	AFM	-	1.1±0.1 nm
Seantier 2008 [180]	DPPC DOPC	AFM	-	0.9 nm
Geocondi 2001 [181]	DPPC DOPC	AFM	-	1.21±0.03 nm (n=28)
Geocondi 2010 [182]	DPPC DOPC	AFM	DPPC 10 nm DOPC 8 nm	2.0 nm
Choucair 2007 [183]	DPPC DOPC	AFM	-	1.4±0.3nm
Mingeot-Leclercq 2008 [184]	DPPC DOPC	AFM	-	1.1±0.1 nm
Kirat 2010 [185]	DPPC	AFM	5.5±0.1 nm	-

Yarrow 2011 [186]	DPPC	AFM	5.2-5.4 nm	-
Rinia 2002 [187]	DPPC	AFM	~6 nm	-
Mou 1996 [188]	DPPC	AFM	5.6 nm	-
Keller 2005 [189]	DPPC	AFM	5.0 nm	-
Wacklin 2011 [190]	DPPC	QCM/neutron reflectivity	4.8 nm	-
Dekkiche 2010 [191]	DOPC	AFM	~4.5 nm	-
Munford 2005 [192]	DOPC	AFM	~5 nm	-
Grant 2002 [193]	DOPC	AFM	4.4 nm	-
Gallova 2004 [194]	DOPC	Small angle neutron scattering	4.52±0.24 nm	-
Drolle 2013 [71]	DPPC DOPC	Small angle neutron scattering	39.2 Å 33.9 Å	5.3 Å
Gandhavadi 2002 [195]	DOPC	x-ray diffraction	36.0 Å	-
Pan 2009 [196]	DOPC	x-ray diffraction	36.8 Å	-
Tristram- Nagle 1998 [197]	DOPC	x-ray diffraction	45.3 Å	-

3.2.2 Force Spectroscopy Experiment 1

To complement the results from AFM imaging and other methods, next we used atomic force spectroscopy to test its suitability to address physical properties of supported bilayers. Careful control force experiments on proper bilayer preparations are required to perform such experiments, and these have never been presented in the literature before. Such experiments are important for the future goal to address effect of melatonin on the bilayers. Bilayers with defects were created by vesicle fusion (as per the protocol utilized at the time being, also in the preceding AFM imaging section, that was only able to reliably produce them), and force spectroscopy was done on selected areas of bilayers.

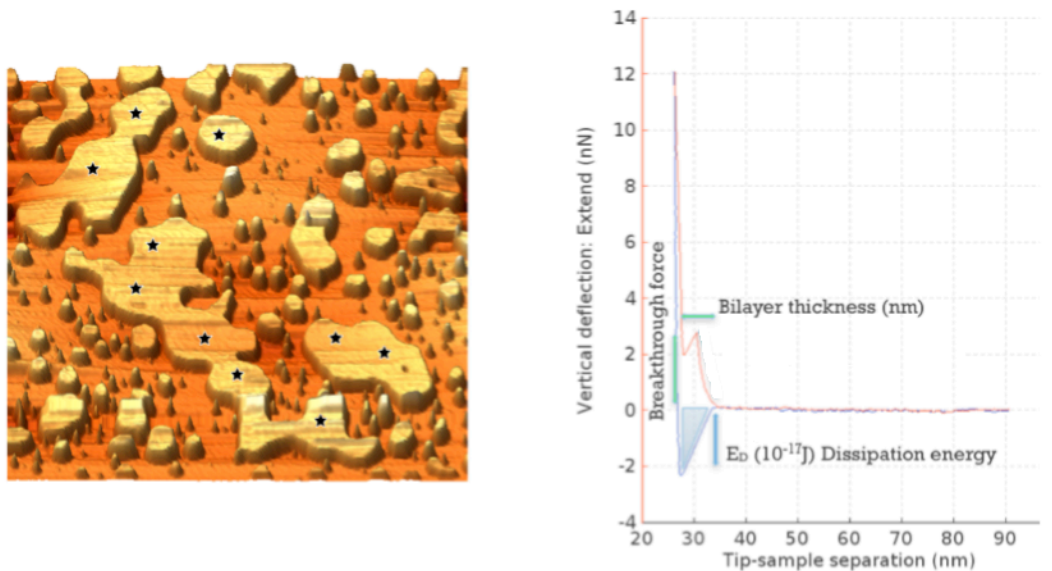
3.2.2.1 Experiment 1- Methods

Flat intact bilayer islands away from defects (or holes) in the sample were selected for conducting force spectroscopy measurements (figure 37). Bilayer edges were avoided as guided by the literature[198] to avoid getting a lower force value and induce an overall greater variability in the results due to edge effects. A total of two bilayer samples were used- one for each of the two times of incubation, 1 hour and 24 hours. Each bilayer sample was prepared in pure water (control), imaged to select 10 different central locations on bilayer patches and force spectroscopy curves were gathered (100 curves from each spot, 10 spots, so a total of 1000 curves). The number of raw curves gathered is denoted to as "N" numbers. Out of the N number of curves, only a proportion of the curves gave analyzable breakthrough events that are having the characteristic breakthrough discontinuities as reported in the literature (Fig 34). The number of useable curves collected is denoted as the "n" number.

From the n number of curves, breakthrough thickness, breakthrough force (BT-force or F_B), and dissipation energy (E_D) were observed and calculated. These values were determined using the manufacturer's AFM software (JPK Instruments, Germany). MAC II cantilevers (Agilent Technologies, USA) with spring constant $k=2.4$ N/m were used without further modification. Bilayer samples were in water. JPK Nanowizard II AFM was used.

3.2.2.2 Experiment 1- Results

Data from the experiment is presented in figure 37. There was no change in the BT-force between the 1 hour and the 24 hour sample, no significant changes in BT-force (F_B), thickness (nm) and dissipation energy (E_D) were observed. The n numbers used for the data were, for 1 hour DPPC, $n=10$, and for 24 hour DPPC $n=9$. The N number for each of the groups was $N=1000$.



1 Hour	Thickness (nm)	F_B (nN)	$E_D(10^{-17})$ (J)
DPPC	5.68 ± 0.61	0.57 ± 0.36	2.17 ± 1.12
24 Hour	Thickness (nm)	F_B (nN)	$E_D(10^{-17})$ (J)
DPPC	6.24 ± 0.31	0.59 ± 0.17	0.76 ± 0.21

Figure 37- Force spectroscopy data of DPPC bilayer. Numbers are reported with \pm SD, The top left image shows patches of DPPC bilayer where the tip was directed to break through (Ten different spots marked by black stars indicate how different central locations within the bilayer islands were chosen to collect the force curves. A sample force-distance curve (graph top right) shows the parts of the curve from where the values shown in the tables were obtained. The table values show changes after 1 and 24 hours incubation. The number of curves analyzed for 1 hour DPPC, $n=10$, 24 hour DPPC $n=9$. Unmodified MAC II cantilevers were used on DPPC bilayer samples in water. The top right schematic shows how the thickness (nm) F_B and E_D values were obtained from the BT-force curve. Thickness was the measure of the width of the breakthrough part of the curve, F_B was the BT-force, which was the height of the breakthrough transition of the curve. E_D was the dissipation energy calculated using the area under the adhesion portion of the retract curve.

3.2.2.3 Experiment 1- Discussion

No significant changes were observed with time (between 1 vs 24 hours of incubation) in terms of measurable bilayer properties (breakthrough thickness, breakthrough force and dissipation energy as shown by student's t test (95% confidence interval). The differences in values in each of the three parameters measured were 0.56 ± 0.61 nm for thickness, 0.02 ± 0.36 nN for BT-force (F_B), and 1.41 ± 1.12 J for dissipation energy (E_D). The specific values for the three properties measured were obtained from the curves as shown in figure 37- thickness was measured as the width of the breakthrough curve on the force vs tip-sample separation graph (measured on the x-axis), force was measured as the height of the breakthrough as measured on the y-axis within the graph. Dissipation energy was the area of the adhesion curve on the retract portion of the curve.

It might be important to consider that the results were obtained from a small fraction of the total number of force curves taken, and the analyzable n number of curves used were as low as $n=9$ out of $N=1000$. The relatively small n numbers suggested that it was possible that the obtained results were from rare anomalous events only, rather than from events that are normally present most commonly during interaction between the tip and the sample. The low yield of forces is a well-known phenomenon [203], however, the result would need to be repeated extensively in order to obtain a greater number of the low proportion of n numbers to N. Because this may be difficult and time consuming, using another lipid model was considered.

The reasons for having such low n numbers may have been that it was difficult to consistently choose intact bilayer areas for obtaining usable breakthrough forces by manually adjusting the tip positioning. This process of manually selecting specific areas within patches of bilayers has

been widely utilized in AFM bilayer force spectroscopy studies that were published before by Garcia-Manyes[198], [199] and Franz et al.[200]. However, there are limitations with this approach. In order to select the correct bilayer patch to conduct force spectroscopy, the sample must be imaged beforehand to capture its topography. The process of imaging the bilayer would shift the bilayer patch or the islands to adopt a different shape or be moved to a slightly different location. Choosing a precise location from which to collect the curves must be made under assumption that the imaged bilayer had not been altered too much from the process of imaging.

3.2.2.4 Experiment 1- Conclusion

Time of incubation (between 1 and 24 h) did not lead to statistically significant changes in the BT-force, thickness and dissipation energy. Due to low n numbers obtained in the experiment 1, it was decided that another type of lipid should be utilized for future experiments.

3.2.3 Force Spectroscopy Experiment 2

Another strategy to improve the usable force yield was to increase the bilayer coverage. First, having defect free bilayers would minimize the variability arising from tip interacting only with the substrate, as the bilayer would completely cover the entire surface. Secondly, it would minimize bilayer edge effects (the molecules are less confined and loosely associated), which can be different from the areas near the center of the bilayer patch. Lastly, a completely intact and uniform surface can better serve as a controlled surface on which to easily observe and discern the effects of different molecules of interest, such as the A β peptides, interacting with the bilayer surface.

The DPPC bilayer making protocol that was being utilized up to this point had been only effective in producing bilayers with defects. The procedures had been intentionally developed this way, as having defects in the bilayer is useful in verifying the presence of the bilayer and also convenient in measuring the cross sectional height, which roughly corresponds to the thickness of the bilayer. Although good for imaging, force spectroscopy experiments may now require defect free samples.

Having a defect-free bilayer would normally have some downsides, as the image of it would just appear flat resembling that of the substrate (mica) with nothing on it. It is certainly very difficult to ascertain the presence of a bilayer on the sample if it is completely defect free. Also completely defect free bilayers are notoriously difficult to reproduce using vesicle fusion, especially using gel phase lipids, such as DPPC. Because it is difficult to produce intact bilayers with DPPC (figure 37 as well as 45 for examples of DPPC bilayers), it was decided that using another lipid bilayer system (DOPC) might be necessary to obtain defect-free bilayer samples.

In addition to creating defect free bilayers with DOPC, a different AFM machine was tried, partly due to a scheduling conflict with other external experiments (had to go from JPK AFM to Agilent AFM). The logic behind the switch was that as long as the difference between control samples were measured using one system under same conditions, the results would be valid. Both of the AFM machines have been featured in several different previous force spectroscopy publications (not necessarily bilayer BT-force) that were done by other groups [201]–[203].

3.2.3.1 Experiment 2- Background

One of the most popular ways of addressing the difficulties with having completely featureless nature of defect-free bilayers is to produce samples with two or more lipid types mixed that would have different height contrast. As shown in table 1, DOPC and DPPC mixtures are used frequently in defect free bilayer studies. DOPC represents a "fluid" phase lipid, and DPPC represents a "gel" phase lipid[36]. In such mixed gel and fluid bilayers, the gel phase lipids form a protruding domain above the fluid phase DOPC (although some publications suggest that no difference should be seen between the bilayers of the two lipids, see table 1). There are several studies featuring protocols in producing a DOPC/DPPC bilayer mixture [184], [204](papers shown in table 1). The methods were followed as outlined in the papers to produce the mixed bilayer shown in figure 38.

70:30 DOPC:DPPC

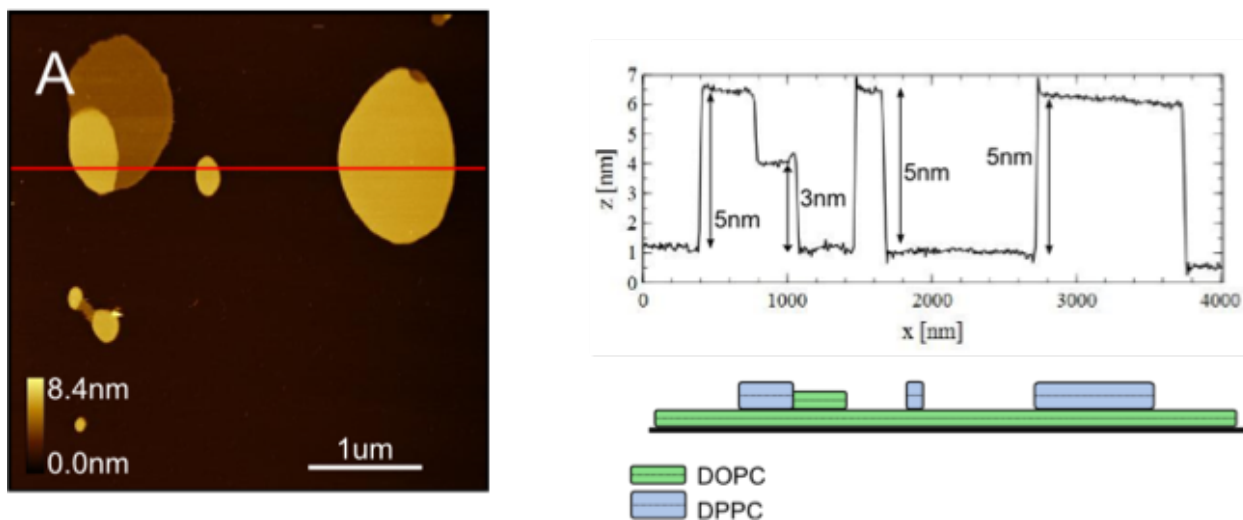


Figure 38- AFM image of the DOPC and DPPC mixed (70:30) bilayer. The higher (yellow) domains are hypothesized to be composed of DPPC (cross sectional schematic is shown in bottom right). The dark brown background area in the image is assumed to be composed of DOPC. The cross sectional heights of the domains are shown in the top right. The 5 nm height domains correspond to DPPC regions, and 3 nm regions to DOPC (presumably). BT-forces were only taken from the dark brown background region, consisting of DOPC only. The presence of DPPC domains was intended only to aid in the verification of the intact, defect free underlying DOPC bilayer (Courtesy Dr. Attwood, presented with written permission, unpublished).

3.2.3.2 Experiment 2- Method

The bilayer sample shown in figure 38 was used to conduct a force spectroscopy study, and the results are shown in table 2. A total of 2 trials have been conducted. The trials involved one tip and one sample and data from two different areas collected in sequence. T-tests were conducted to compare trials 1 versus 2. MAC II cantilevers ($k=2.4$) were used without any modification. Agilent 5500 AFM (Agilent Technologies, USA) was used.

3.2.3.3 Experiment 2- Results

The two control trials were significantly different ($p<0.05$ Student's t-test). The results showed that there is a significant difference in BT-force and decreased in the Z_{A-D} depths between different areas within the same sample.

Table 2- BT-force data on the DOPC regions of the samples using various parameters

Data set	N	n %	speed nm s^{-1}	\bar{F}_B nN	\bar{Z}_{A-B} nm	\bar{Z}_{B-C} nm	\bar{Z}_{C-D} nm	\bar{Z}_{A-D} nm
1:DOPC	411	82	100.2	7.48 ± 0.05	1.87 ± 0.01	1.54 ± 0.01	0.70 ± 0.01	4.10 ± 0.01
*2:DOPC	397	79	100.2	7.13 ± 0.05	1.66 ± 0.01	1.52 ± 0.01	0.75 ± 0.01	3.92 ± 0.02

The table shows raw data with SEM. Independent trials 1, 2 were conducted using one tip and one sample with forces measured for different sample regions without removing the tip from the solution. N= total number of force curves, n% the percentage of the total number of curves that were used to calculate the values, F_B = Force breakthrough, Z denotes the distance between different points (subscript letters) assigned within the breakthrough event. Data from each group (same shade trials) were combined together in calculating the average values. MAC mode type II cantilevers with nominal spring constant $k=2.4$ N/m were used for all sets with no tip surface modification, in water. * Denotes $p<0.05$ Student's t-test for both between the individual trials. The Z_{A-B} , Z_{B-C} , Z_{C-D} , and Z_{A-D} denote distance between different parts of the breakthrough curve, as shown previously in figure 34 (Courtesy Dr. Attwood, modified and presented with written permission, unpublished).

3.2.3.4 Experiment 2- Discussion

When data within Table 2 is analyzed, trial 1 were significantly different from 2 ($p < 0.05$ Student's t-test). Control BT-forces from seemingly the same control bilayer sample gave different force and depth results just by conducting forces on different areas. The possible causes for the difference in forces were that the different areas actually contained different lipids, as the sample bilayer was a mixture of lipids

The bilayer samples had topography that had been never reported in the literature before, as papers featuring DOPC/DPPC bilayers show defect free bilayers with two different domains, one lower and one higher [171], (table 1). In the literature, the height difference between the low fluid and high gel phase domains is almost unanimously agreed to be ~ 1 nm. The sample (figure 38) had 3 different domains with height differences of $\sim 3-5$ nm. It was proposed that the high domains were the results of multilayer (multiple bilayer) formations. Also, the seemingly anomalous high domains were completely avoided and force spectroscopy data was only collected on the lowest of the domains. The lowest domain was presumed to only contain DOPC (lowest and the thinnest bilayer domain), however, further evidence suggest this assumption may have been incorrect (figure 39).

The problem here was that the thickness determined using BT-force curves (< 4.0 nm, table 2) did not correlate well with reported DOPC thickness measured using other methods (> 5.0 nm) [199, 202]. It was possible that degradation of DOPC could be responsible for obtaining a reduced thickness with the BT-force results. For future experiments, it was decided that only fresh DOPC solution made on the same day would be used for conducting force experiments. Also, DOPC only lipid samples without any DPPC mixed in together would be used in future

experiments. Making such provisions did eventually produce AFM thickness results that correlated well with others in the literature [209].

3.2.3.5 Experiment 2- Conclusion

A significant difference in BT-force and depth were observed in two different areas within a control bilayer sample. The mixed bilayer sample was questionable because they did not match any of the previously published data on mixed bilayers with the different domains [171], [184], [199]. It was possible that the results were due to having various domains and mixtures of lipids within the sampled areas. Thus a decision was made to make changes to both the bilayer protocol and BT-force protocols to reconfirm the result.

3.2.4 Bilayer Protocol Redevelopment

Redeveloping protocols began with reexamination of the DOPC/DPPC mixed bilayer protocols. It was discovered that there were two main misconceptions or knowledge gaps in the literature. First, there was a widely held dogmatic assumption that the DOPC and DPPC domain heights, as measured by the AFM image cross sectional measure, must differ by around 1 nm in mixed bilayers. Further, the assumption of ~1 nm height difference was based on the two lipids automatically phase separating and being sorted by their difference in chemistry (due to line tension)[205] upon deposition onto the substrate, even though they are intermixed within the vesicle solution. There are several indicators that suggest that this assumption may not be adequately substantiated in the literature. There are many other papers that suggest or report hybrid domains of mixed composition (a third mixed composition domain, rather than just two pure non mixed areas), the presence of which was dependent on sonication protocol and thermal history of the vesicle solution[183], [206]. Our own AFM experimental data gathered from

observing DOPC and DPPC bilayers mixing on mica also supported intermixing of the bilayer components, rather than phase separation of the mixtures (figure 39). The literature on mixed bilayer systems do not adequately mention or address the intermixing of the lipid components clearly with direct experimental evidence (it is simply inferred or assumed), and it needs to be further explained and tested to improve the reproducibility and credibility of the published data.

Also, there were several misconceptions in the bilayer protocol literature. The first was that the presence of divalent cations is absolutely required for successful vesicle rupture and fusion[184]. The second was that careful thermal cycling of DPPC would not result in any extra domain formation within DPPC bilayers[204]. The following sections feature the published experimental data that definitively disproved these two prevailing misconceptions in producing supported bilayers. The results suggested, despite the wide availability of protocols and papers in existence, that there are still many unknowns in the mixed bilayer protocol and in the literature that discusses it. Because there were increased complexity in using and producing mixed bilayer compositions, it was decided that working with single component bilayers, although they are too simple to be significantly relevant biologically, might be best in obtaining reliable controlled results.

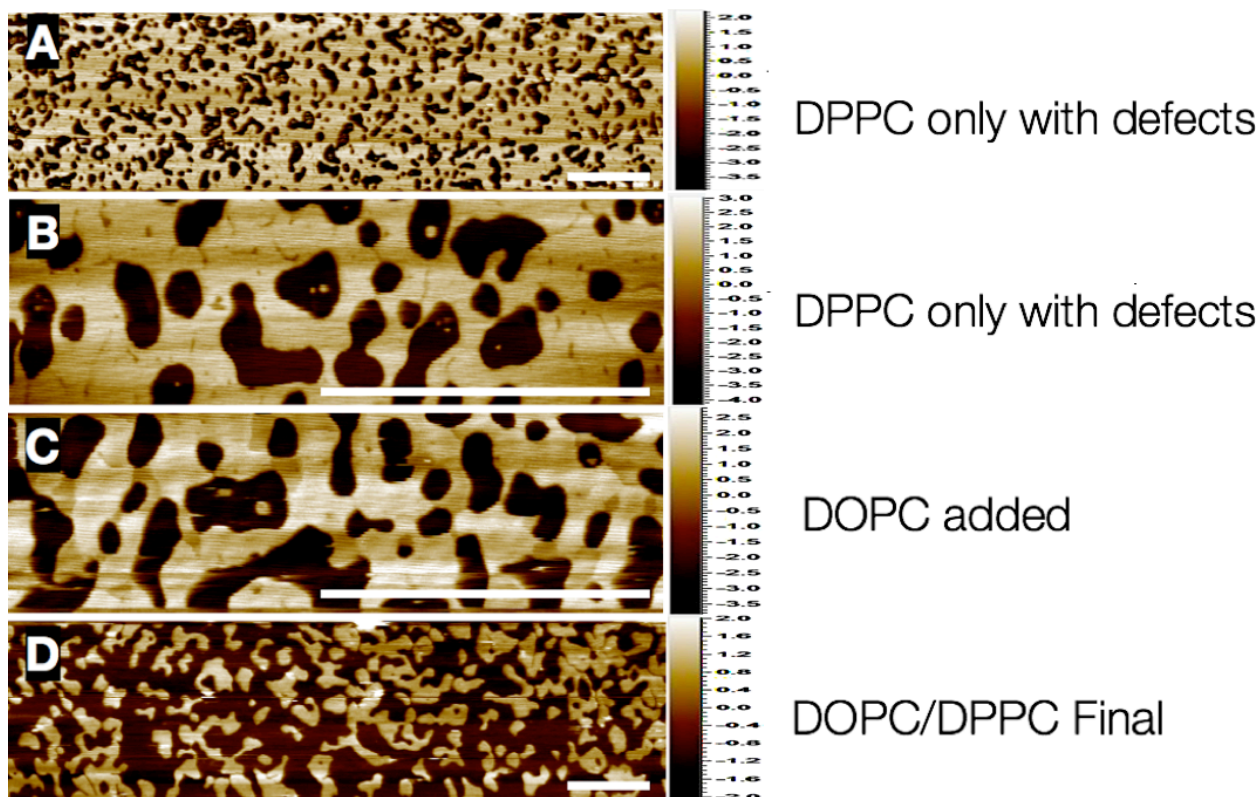


Figure 39- Images showing how DPPC and DOPC molecules intermix and form domains. Scale bar 1.0 μm . (A) DPPC bilayer with defects. (B) Same as image A but zoomed in. The image shows DPPC bilayers have a lower height domain, shown in darker brown color that span between the defects, which are shown as large darkest colored areas. (C) Image of the DPPC domains when DOPC is added to the sample. Instead of filling in the defects and staying separated, DOPC binds and mixes in with the existing DPPC bilayers and forms secondary domains. The height difference between the lower and higher domains is around ~ 1 nm, corresponding to the reported literature domain height difference between DOPC and DPPC. (D) Final mixed DOPC/DPPC bilayer after 2 hours. The higher domain shape, size and density are all altered from the initial DPPC only state shown in A. Changes in the shapes and heights of the domains indicate that the two different lipids do not stay completely separated but that they are intermixing and forming complex intermediary steps in forming mixed composition bilayers. The domain height difference is $\sim 1.8\text{nm}$, which is much greater than the usual value reported in the literature ($\leq 1\text{nm}$ for DOPC-DPPC systems, table 1, AFM measurements).

3.2.4.1 Producing Single Component DOPC Bilayers

It was decided that using single composition bilayers might be better than using mixed compositions for BT forces due to the decreased complexity. Among single composition bilayers, using fluid phase bilayers, such as those made with DOPC to produce defect free bilayers for BT-force spectroscopy, had several advantages. First, it was less likely for DOPC than DPPC to form extra features on top of the bilayer, since DOPC forms a less ridged bilayer that is less likely to support and sustain an extra layer on top of itself (a double bilayer layering effect). Secondly, DOPC bilayers were more dynamic than DPPC in that the patches in the bilayer (small defects) would often close off and self seal over time (dynamic nature of supported bilayers is a well-established phenomenon)[175]. Figure 40 shows AFM topography images of DPPC and DOPC bilayers supported on mica and imaged in water.

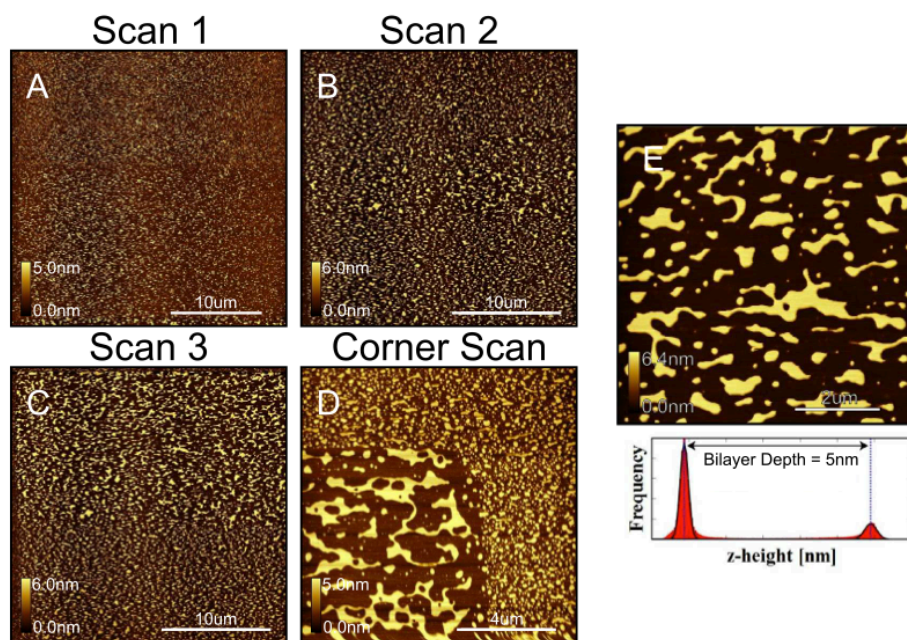


Figure 40 - AFM images of DOPC bilayer patches illustrating the delicate, fluidic nature of DOPC. Sparsely covered sample of DOPC on mica (scan 1) was scanned successively over the same area. As can be seen, the tip drags the lipid together, forming successively larger patches, with the space between them growing. The effect is most obvious when the boundary between a previously scanned area and an untouched area is observed, such as at the corner. By using computer software to calculate and remove undulations arising from imperfections in the piezo movement in the plane of the raw image data (flattening the image), and using a custom Matlab code, the frequency versus z-height of pixels that belong to the mica area (dark brown) and also in bilayer areas (yellow) were assessed, and we are able to observe two distinct populations, representing the mica surface and the top surface of the bilayer (red Gaussian distributions, bottom right). By fitting two Gaussian distributions and then subtracting the difference between the peak heights, we find that the bilayer depth is 5 nm. The precision of this measurement is very high (standard error of the mean <math><0.02\%</math>), however the largest uncertainty in this measurement is due to the force setpoint. By scanning with a higher force, it is easy to compress the bilayer, measuring slightly less than the “true” depth. By scanning with a low force, it is possible that contributions from repulsive forces play a role, resulting in an overestimation of the height of the bilayer. It is thus probable that quantitative approach to depth measurement of soft bilayer systems can only be achieved by analyzing force distance curves (From [204], presented with written permission).

There were downsides to using DOPC. DOPC has unsaturated lipid tails, and the double bond is vulnerable to oxidative damage. DPPC with saturated tails are much more stable in air and also in water. Thus DOPC required greater care in storing and producing the vesicle solution, as well as after it was deposited into a supported bilayer. DOPC vesicle solutions were produced daily and this took extra time and also potentially increased variability in the results during repeated trials. Nonetheless, it was possible to optimize the protocol to produce defect free DOPC bilayers (figure 41). The details of the protocol are as follows.

DOPC Bilayer Preparation

Stock Solution Preparation:

1. Open the ampule containing 25 mg DOPC in chloroform.
2. Transfer the entire ampule directly to a 20 ml glass vial. Add an extra 1000 μ l of chloroform to the ampule and wash out to the glass vial so as to remove all lipids.
3. Evaporate the solvents under a stream of nitrogen until visibly dry (approximately 10–15 min).
4. Add 6 ml chloroform/methanol (2:1) and split into even aliquots to 6 small glass vials (capacity 4 ml each). Each stock vial therefore contains 4.17 mg DOPC.
5. Top with nitrogen and store at -20°C .

Liposome Preparation:

1. Transfer one of the 1000 μ l stock aliquots to a clean 20 ml glass vial. Wash out the small vial with an extra 1600 μ l chloroform/methanol (2:1) and add this to the 20 ml vial as well to make 2 mM and ensure no lipid is lost.
2. Evaporate solvents with a continuous stream of nitrogen. After \sim 15 min all should be visibly dry. Continue for an extra 15 min to ensure all solvents are evaporated (30 min total).
3. Bubble nitrogen gas through \sim 20 ml of Millipore water for \sim 15 min to remove the oxygen.
4. Add de-oxygenated Millipore water to make 0.5 mg/ml. The lipid should quickly start to swell, separate from the glass vial and form an inhomogeneous suspension of cloudy material. Also add a stir bar and top the vial with nitrogen.
5. Stir using magnetic stirrer for 30 min at 1100 rpm (the solution should appear homogeneous and milky).
6. Place the solution at 4°C and allow to swell for 1 hour.
7. Stir using magnetic stirrer at 1100 rpm for 30 min at room temperature.
8. Place the vial in the middle of the sonicator where cavitation is greatest. The most powerful region of any bath sonicator can be found easily by placing a sheet of aluminium foil on the surface of the water and sonicating for \sim 10 min, a large hole should appear at the region of most intense power. Sonicate for 30 min, during which there was a slight inadvertent heating of the water (start temperature is \sim 23°C, finish temperature is \sim 31°C. The solution should appear completely clear after sonication. If using higher concentrations of lipid, the solution may take longer to go to clarity.

9. Store the liposome solution at 4°C until needed.

Vesicle Fusion:

1. Remove the liposome solution from the fridge and stir at 1100 rpm for ~ 45 sec.
2. Place 300 µl of cold solution directly into the AFM fluid cell containing freshly cleaved mica.
3. Wait 15 min.
4. Wash with 10 ml water through a syringe by slowly allowing the fluid cell to overflow so as to prevent sample de-wetting.

Typically the above protocol will give a continuous bilayer of DOPC. However, slight decreases in the concentration (e.g., a little extra lipid lost during preparation of the liposome solution) may mean that a complete bilayer is not formed. In this case it was found that it is best to prepare several samples that have been incubated for slightly longer and shorter periods of time and image these using the AFM. By capturing the state of bilayer coverage at various points in time, it is then possible to be certain that for a given incubation time a complete bilayer was formed. In some cases, a complete bilayer may not form even for extended incubation times. In this case, another approach can be taken whereby a higher concentration of lipid (1 mg/ml) liposome solution is prepared. This solution can then be sequentially diluted to find the optimum concentration to form a complete bilayer.

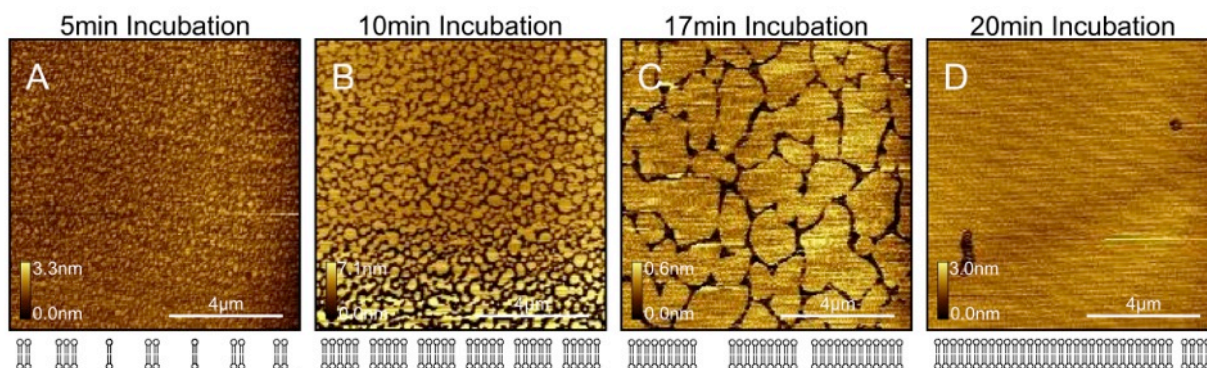


Figure 41- Time series of DOPC bilayer formation. Four separate samples of DOPC bilayers on mica were prepared that were incubated for (A) 5 min (B) 10 min (C) 17 min and (D) 20 min. Below each image is an illustration of the state of the lipid coverage across the mica surface. The time series experiment is a good way of determining that a complete single bilayer covers the mica surface. Without doing the time series experiment, it is very difficult to distinguish a complete single bilayer from multilayer or even bare mica. In addition, when faced with a DOPC sample with partial patchy coverage, it is a simple task to prepare a new sample with a slightly increased incubation time that will result in continuous coverage. All images were taken in pure water at room temperature (From [204], presented with written permission).

Once a continuous DOPC bilayer is produced, it was useful to verify the presence of the bilayer through dewetting the sample. Supported bilayer structure is sustained by the balance between the hydrophobic bonding of the phospholipid acyl chains and hydrophilic expansion of the phospholipid head groups[87]. Drying the sample overwhelms the balance and leads to detachment of some of the bilayer from the substrate (forming defects). As illustrated in figure 42, this technique is useful to verify the presence of the bilayer, however, it is a destructive process and should be performed sparingly. Also, increasing the volume or strength of the washing stream at the rinsing step of the bilayer preparation does not produce defects or have any other perceivable effects. Although transient aeration during such maneuvers may result in partial dewetting of the sample, which then would produce defects in the sample.

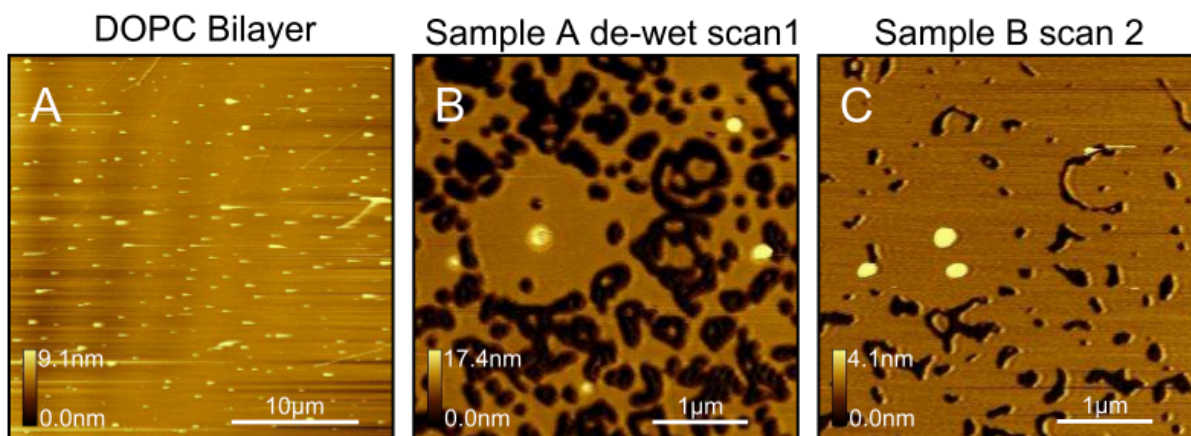


Figure 42- Illustration of the dewetting test used to confirm bilayer coverage. (A) A sample is prepared using DOPC liposomes. Apart from some protrusions the sample is defect-free, making a confirmation of the state of the sample (mica, single bilayer, multilayer) difficult (B) Sample instantaneously dewetted and then rehydrated. The holes confirm the presence of a single bilayer (C) After a short period the holes begin to close, demonstrating again the fluidic nature of DOPC. All images were taken in pure water at room temperature (From [204], presented with written permission).

3.2.4.2 Producing Single Component DPPC bilayers

The steps taken in producing DOPC bilayers was extended to produce DPPC bilayers. Producing defect free DPPC bilayers proved to be a much more difficult task, mainly due to the fact that DPPC is a gel phase lipid at room temperature. Only at above its melting transition temperature of 42°C, would it behave similarly to DOPC in terms of its deposition characteristics, and causing it to melt involved heating and cooling the sample (thermal fluctuation to turn into fluid phase then go back to solid or gel phase). The procedure induced fusion of the vesicles, however, differing degree of defects and domains appeared depending on the cooling rate (Figure 43). The domains and defects remained stable at room temperature for an extended period of time. Also, not heating enough and leaving it below its transition temperature yielded various incompletely fused structures (figure 44).

The overall dilemma in creating a full coverage of defect free DPPC bilayer was that there must be a balance between adding heat to cause fusion of the vesicles and yet minimize temperature induced defect and domain formation from the heating. The key to creating a workable DPPC bilayer was in finding the optimal conditions at which the fusion of vesicles can be maximized while the domain and defect formation is minimized. Eliminating all features on DPPC bilayers was not achievable.

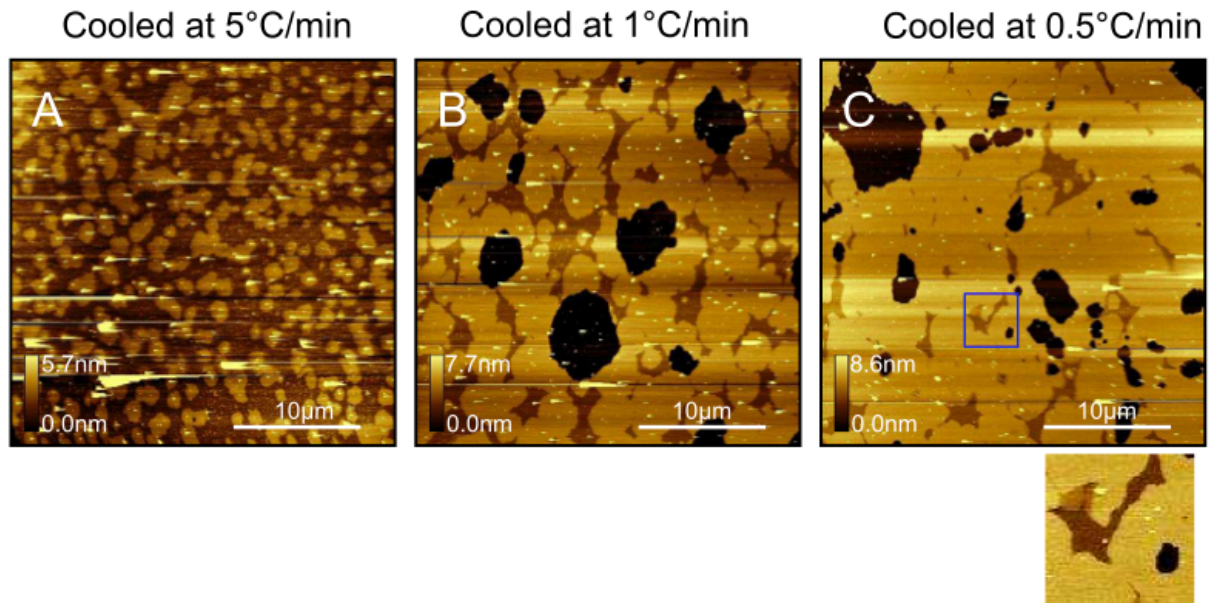


Figure 43- Effect of cooling rate on DPPC bilayers in water. All samples were prepared by incubation with DPPC liposome solution in water at 60 °C and incubation for 5 min followed by cooling to room temperature at (A) 5°C/min (B) 1°C/min (C) 0.5°C/min. The region enclosed by the blue box has been enlarged and is shown below C. For this image of DPPC at room temperature, we see three different types of domains with the lower two being 1.1 nm and 0.6 nm below the upper most domain (From [204], presented with written permission).

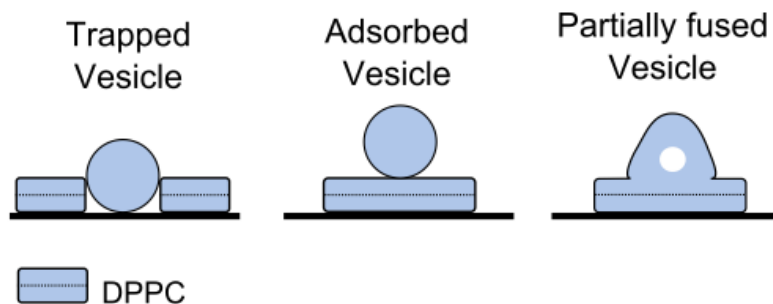
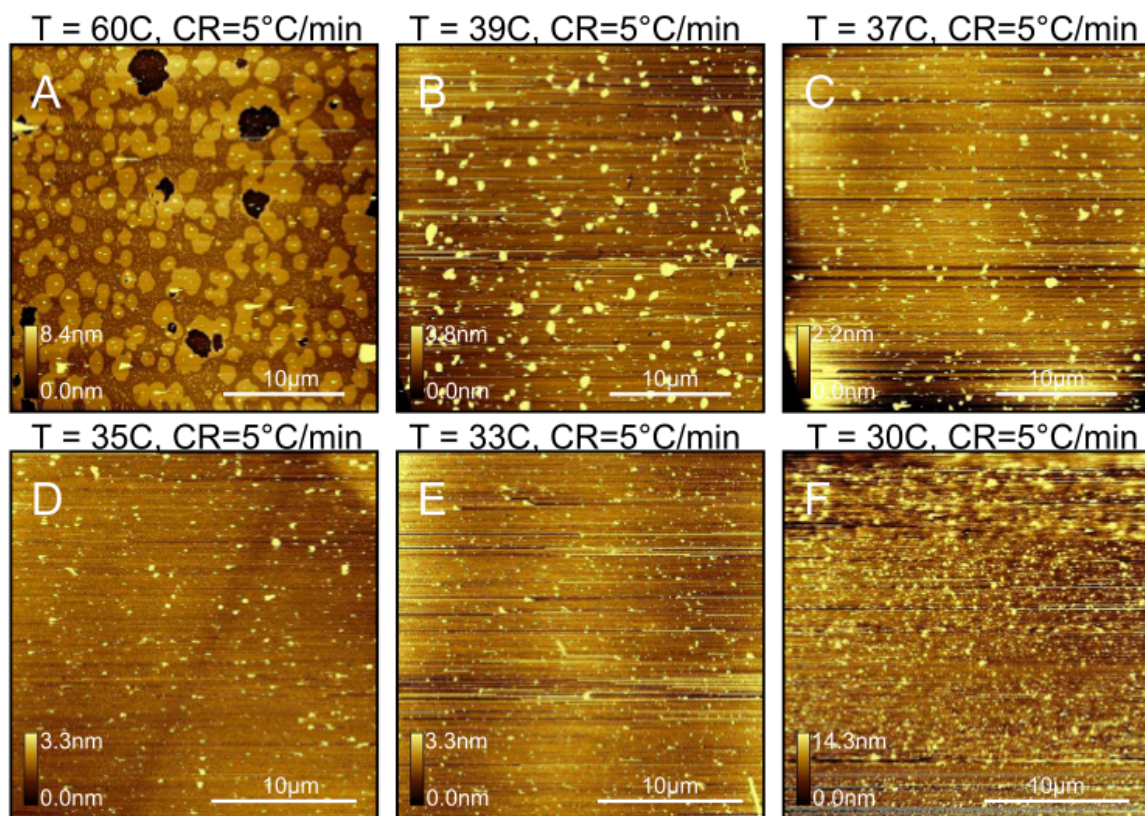


Figure 44- Effect of mica temperature during deposition. All samples were prepared with a cooling rate of 5°C/min. Mica temperature during deposition was:(A) 60°C (B) 39°C (C) 37°C (D) 35°C (E) 33°C (F) 30°C. Lower domains decrease dramatically as a proportion of total lipid coverage between 60°C and 39°C, after which a slow decrease is observed to 33°C. At 30°C we mostly observe unfused vesicles. Protrusions thought to be trapped vesicles are seen for all samples but dominate for temperatures below 60°C. Schematic (bottom) illustrates the various under-fused DPPC structures present in the images (From [204], presented with written permission).

Some of the specific factors that were tested in creating a defect free DPPC supported bilayers included the sample heating rate, cooling rate, peak temperature, initial temperature, time of incubation, solution ionic strength, solution temperature, solution pH, and details in rinsing (temperature, harshness). The individual factors were tested one at a time for its effects on the final bilayer product. This step in the process was especially difficult and time consuming as the factors individually as well as in combination in various possible permutations had to be tested and confirmed for bilayer features and reproducibility. Countless different samples were created and imaged testing various combinations of conditions and factors. In the end, it was not possible to create a completely homogenous defect free supported bilayer of DPPC. The final product, with the best compromise between maximum amount of coverage and least amount of defects and domains, which was also unequivocally reproducible, is shown in figure 45. The final procedure used is as follows.

150 μ l of DPPC vesicle solution at 1 mg/ml concentration was added to the AFM liquid cell containing 150 μ l of HEPES saline buffer (10 mM HEPES, 140 mM NaCl, pH 7.4) that was heated to 60°C. The sample was kept for 2 minutes at 60°C. With the heater on, the sample was rinsed to overflow with 10 ml of Milipore water (resistivity > 18.2 M Ω -cm, at room temperature) using a syringe. Remaining water in the liquid cell (contains a volume of ~1 ml) was flushed and replaced with the buffer using a micropipette with a total of 10 ml of the buffer by fluid replacement, pipetted in and out 1 ml at a time (x10 times). After the rinse, the sample (still at 60°C) was cooled to 45°C at 1.0 Kelvin/min cooling rate, then from 45°C to room temperature the cooling rate used was reduced to 0.5 Kelvin/min

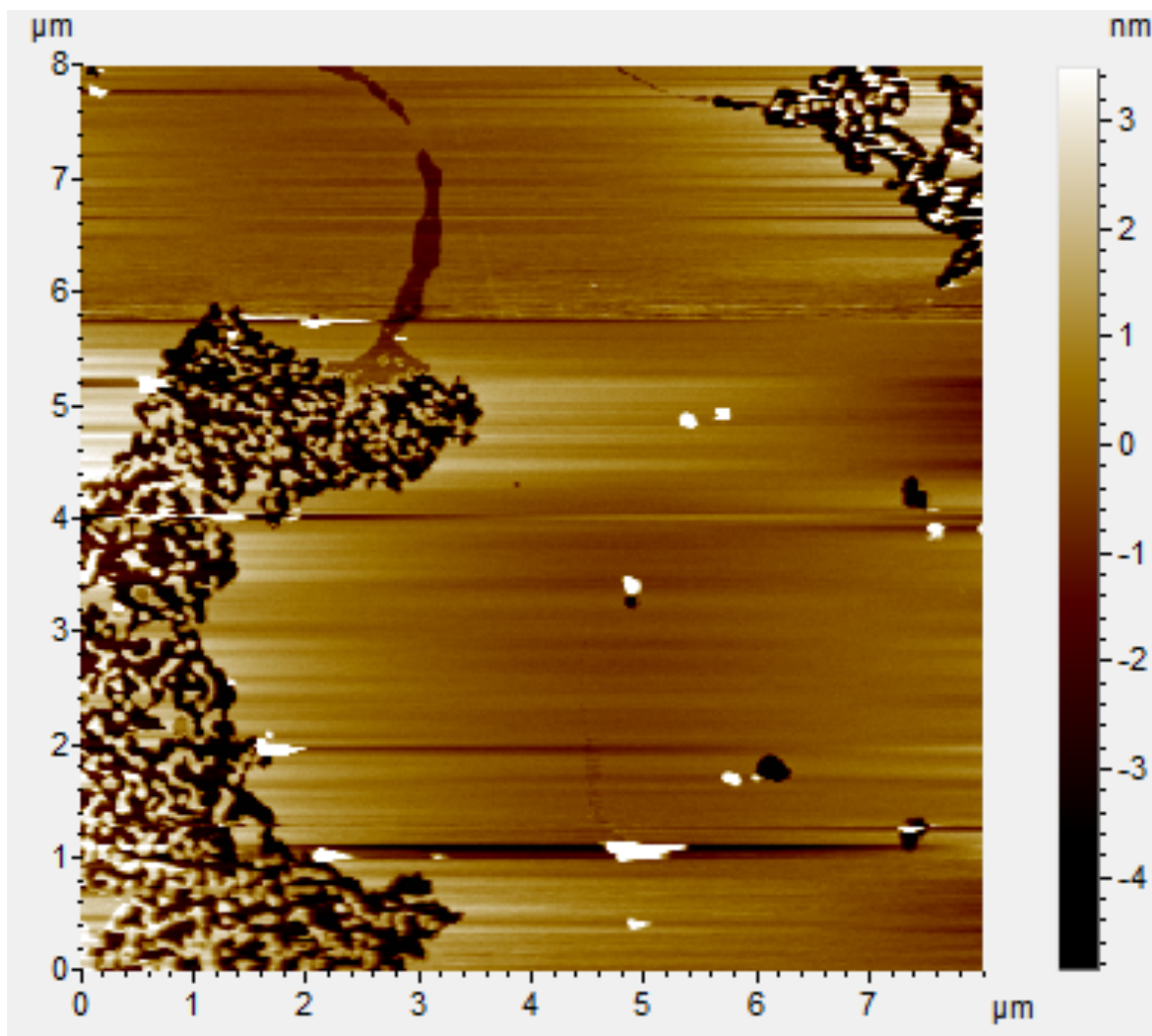


Figure 45- DPPC bilayer with the best compromise between having the least amount of defects and domains with the largest area coverage. The sample still contains defects (darkest brown), domains (medium brown), as well as extra deposits of lipids on top (white blobs). The DPPC vesicle solution at room temperature (1.0 mg/ml) was deposited onto an AFM liquid sample holder at 60°C for 1 minute, rinsed with a 10 ml of buffer with a syringe and cooled gradually from 60°C to 50°C at 1 Kelvin/min, then 50°C to 35°C at 0.5 Kelvin/min. Cooling from 35°C to room temperature (24°C) was done with the AFM sample heater off. Both the vesicle solution and sample were in buffer (HEPES 10 mM, NaCl 150 mM, pH 7.4).

3.2.5 Force Spectroscopy Experiment 3 - Force Spectroscopy on Supported DOPC Bilayers

Refinements made in bilayer making protocols insured the production of mostly defect free bilayers that can be used for BT-force spectroscopy experiments (Figure 41 D). Now that producing completely homogenous bilayer samples was possible with DOPC, it was preferred over using DPPC bilayers (Figure 45). Several trials of BT-force experiments were conducted on DOPC bilayers.

3.2.5.1 Experiment 3- Methods

Control BT-force curves were collected using a grid of 256 squares in a 4.0 μm by 4.0 μm defect free bilayer area. A grid or a map was utilized to avoid bilayer recovery time dependence from taking multiple curves from the same spot. The collected 256 curves were analyzed for the BT-force, and breakthrough depth (BT-depth). The BT-force from the 256 curves formed a Gaussian distribution and the data was plotted on a force versus time graph as a single point presenting the mean force with the standard error of the mean (one data point in the graph represents the average and SEM from a map of 256 curves, distribution shown in figure 46).

A total of three different trials were conducted. Each trial involved using a single tip and one separately prepared bilayer sample. In each trial, a series of force maps (for an example for a data from just one force map, see figure 46) were collected in one of the samples over a course of 100 minutes. Unmodified gold (NPG) cantilevers with spring constant $k= 0.06 \text{ N/m}$ were used with JPK Nanowizard II AFM (JPK Instruments, Germany).

3.2.5.2 Experiment 3- Results

The results are shown in figure 47. Control BT-force values were different from the three independent trials depending on the particular tip of the same type being used. The absolute force value per a given tip differed. The absolute force values were trial A 2.44 ± 0.5 nN, trial B 1.98 ± 0.5 nN and trial C 4.10 ± 0.2 nN. Two sample t-tests with unequal variances were performed in between each of the trials, trials A vs B gave $p = 0.02$, and A vs C gave $p = 1.6 \times 10^{-6}$. B vs C gave $p = 1.5 \times 10^{-10}$ (all $p < 0.05$, see figure 47 also table 3). Thickness number are not presented in figure, but for trial A it was 8.27 ± 4.8 nm, trial B 7.99 ± 6.2 nm and trial B 7.47 ± 2.3 nm. No significant differences were observed for the thickness in between the trials ($p > 0.05$ for all trials)

The variations in forces within a map (distributions shown in figure 46, represents error within each data point shown in figure 47) were overall smaller compared to shifts in the average values (difference between data points) that varied over time (figure 47). BT-force values for control, even though they were relatively stable over time, always changed from tip to tip and also even within a tip when used on a different occasion; the same tip could give a different, but stable, BT-forces on a different day on a different DOPC bilayer sample. Also the trials shown in figure 47 C showed a much higher force compared to the other trials but overall for reasons unknown.

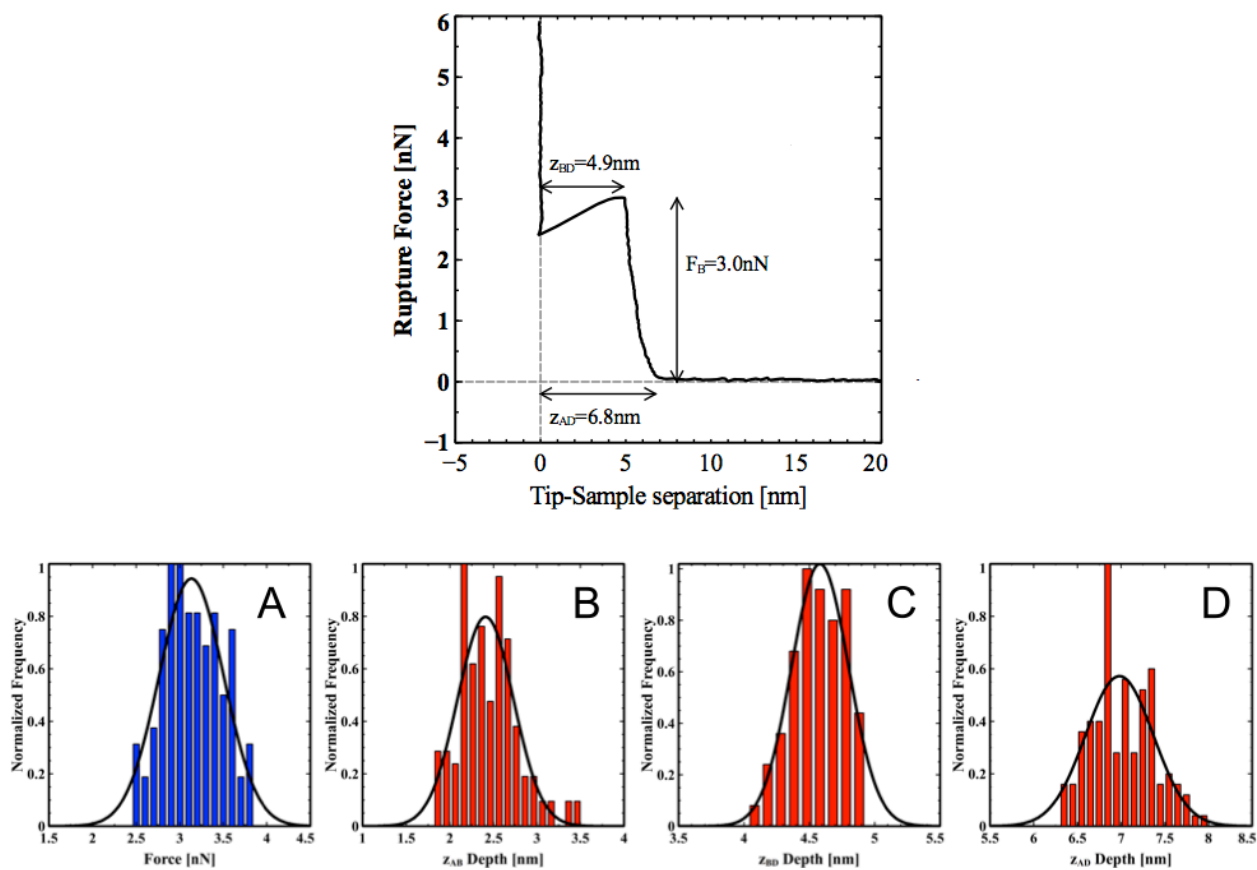


Figure 46- Example BT-force and the values estimated from the curves (top image). 256 of these curves are collected in a grid pattern and the values from the curves are plotted on graphs as Gaussian distributions. The mean values of each distribution is depicted as a single point in a force vs time graphs, such as the one shown in figure 47, or a single point in depth vs time graph (not shown). (A) Force distribution (B) the z_{A-B} depth (C) z_{B-D} depth (D) z_{A-D} depth. DOPC bilayer was prepared in water using the procedures outlined in section 3.2.4.1. The cantilever used was an unmodified NPG lever with spring constant around 0.06 N/m. Only control sample measures are presented. For distribution, non-linear least squares fitting algorithm (Levenberg-Marquardt) was used that was implemented in Matlab software (From [204], presented with written permission).

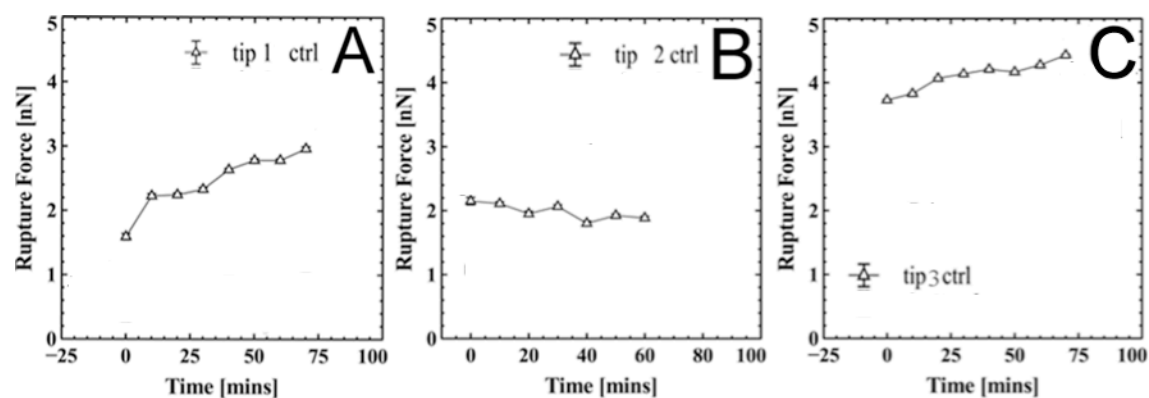


Figure 47- Force versus time graphs of breakthrough (rupture) force spectroscopy results with control DOPC from three different trials A, B, and C. Each trial utilized one tip and one sample (separately prepared control bilayer sample per each trial). Unmodified NPG- gold-coated leavers ($k=0.06$ N/m) were used for these trials. Each data point represents an average \pm SEM of 256 curves from a force map, conducted in water at room temperature.

3.2.5.3 Experiment 3- Discussion

The change in rupture force was noticeable between each data point over the time course of the experiments, in all three trials (figures 47). The absolute BT-forces for control varied from 1.9 to 4.1 nN even though the same types of tip and sample were used. The differences in the data points within each trial indicate that there is a time dependent change in force that exists with this technique, and this result also corresponds with the results obtained in force experiment 2. Another issue observed is the force change that is tip dependent, even though the tips used were from the one box of tips of the same manufactured type (they were all NPG levers from the same box). It was plausible that all of the tips could be undergoing a time dependent change from repeated use over time throughout the trials, such that the forces would vary depending on the changes in the tip shape or the structure over time.

Some factors that might be involved that created the tip-to-tip variation in BT-forces could be that different tips (of the same type) may have different radii curvatures due to manufacturing variations, and also there could be a slight variations in the location of the AFM laser spot that is on the tip could create the difference in the force values. It is also possible that the silicon cantilever material of the tips could have varying minute physical defects, which may have caused different force values.

3.2.5.4 Experiment 3- Conclusion

Control forces taken using three different but same type of tips gave different force values. The force values also fluctuated over time within one tip and one sample. The results correspond with the results of experiment 2, in that they both indicate time dependent change occurs with BT-forces. The results overall show that different control forces can be obtained using this technique

depending on the various experimental factors, but how the specific factors had affected the forces remains unknown.

3.2.6 Summary of Force Spectroscopy Results

A total of three experiments have been conducted to measure breakthrough force on bilayers using force spectroscopy. Table 3 is a summary comparison of all of the experiments. Procedural variations exist between the experiments to study different factors involved in control BT-forces. Significant differences in forces were measured in exp. 2 and 3 that depended on the particular tip used and the experiment time. Bilayer incubation time however, which was tested in exp. 1, was not a factor that changed the BT-forces, as the resulting differences in exp. 1 for thickness, BT-force and dissipation energy were all statistically insignificant.

Table 3- Summary Comparison of Force Spectroscopy Data Set Results

Force Data Set	Exp. 1 (Figure 37)	Exp. 2 (Table 2)	Exp.3 (Figure 47)
Tested Factor	Effects of bilayer incubation time on forces	Effects of different areas of the sample on forces	Using different tips (of the same type) on forces, and time dependence of forces
Experimental Protocol	<ul style="list-style-type: none"> • One tip used for two control samples, samples incubated for 1 and 24 hours 	<ul style="list-style-type: none"> • One tip used with one control sample • Two trials per sample collected - two different areas on the sample without removing the tip 	<ul style="list-style-type: none"> • One tip used with one control sample • Force measured over time • Repeated with three different (same type) tips
Outcome	Varying time did not lead to changes in BT-forces (p=0.32)	Different areas gave different BT-forces	BT-forces changed over time/ Different tips gave different BT-forces.

The factors that created the differences in forces have been identified, but how exactly they created the changes in forces are unclear. It is also possible that there could be other unidentified factors involved other than the two currently identified that are able to cause changes in forces. Further experiments are needed to increase the understanding of the different factors involved in technique, in terms of how they change the observed BT-forces in supported bilayers. As a future suggestion, conducting additional experiments based on exp.3 but with various different tip types and lipids may be ideal to confirm results.

3.2.7 Concluding Remarks for AFM Force Experiments

Technical improvements were made throughout the section including creating defect free bilayers and successfully reproducing analyzable breakthrough force data in control bilayers. Incubation time, tip variation and sample areas have been successfully identified as factors that can produce variability in results, which maybe useful information for future experiments.

Due to the highly time consuming nature of these experiments, more work is planned in the future to study the effect on melatonin by BT-forces methods in a separate project by another student. The developed protocols and control experiments presented in the current work will provide a valuable foundation for future work.

3.3 Imaging Amyloid- β ($A\beta$) Accumulation on Bilayers

Many previous publications have utilized AFM imaging to study accumulation of $A\beta$ on supported bilayers[83], [183], [207]–[212]. The amounts of $A\beta$ present on bilayers as well as its effect on its physical integrity were of great interest since they may be relevant to the cell toxicity of $A\beta$. Many previous papers had studied the effects of $A\beta$ (1-40) on various different composition bilayers including DPPC, DOPC and brain lipid extract bilayers[209], [210], [213], [214]. A number of recent papers had investigated $A\beta$ (1-42) [83], [183], [207], [209], [212], which is known to be much more toxic than the 1-40 fragment, and thus is of greater interest in the AD pathophysiology compared to the 1-40. One of the reasons for the previous studies using the 1-40 fragment over the 1-42, even though known to be less toxic, would be that the 1-40 fragment made very drastically observable changes to the bilayer surface topography compared to that observed with 1-42[207]. The results are counterintuitive as increased damage to the bilayer is often assumed to correlate with increased overall toxicity. However, this correlation may not be true, at least in studies using AFM, because the more toxic 1-42 fragment has been shown to cause minimal to very low bilayer topographical disturbance [183], [207]. However, cell and animal studies have repeatedly confirmed that the 1-42 fragment should be the most toxic compared to the other fragments[8], [21], [215].

Nevertheless, AFM bilayer studies featuring the 1-42 fragment showed that it is capable of accumulating on various bilayers and also capable of inducing low levels of detectable damage to the bilayer surface[207]. Furthermore, it showed preferential accumulation on gel phase DPPC bilayer domains over the fluid phase DOPC [183]. This result was also interesting, since the average cell membrane, with all of its multiple of components, is known to be in fluid phase at

physiological conditions. It has been shown that cholesterol enriched domains (that have somewhat similar physical properties to gel phase domains but also have a distinct electrostatic nature) induce preferential binding of A β [212]. Another AFM study testing A β (1-42) on brain extract enriched with cholesterol reported increased disturbance and binding compared to samples without added cholesterol [207].

It was decided that for assessing melatonin's effects, AFM imaging of two different bilayer types would be performed to characterize A β (1-42) accumulation and bilayer surface structure disturbance (damaging effects). The first type used was brain extract membrane. Studying the A β effect on supported bilayers made up of brain lipid extract was advantageous due to its biological relevance. The composition of the bilayer would be very close to the physiological membranes found in brain neural tissue. Also the majority of the available data in the literature was on brain extract, meaning that comparisons and verifications could be made in interpreting our results. The second bilayer choice was DPPC. Work by Choucair et al., studying the A β (1-42) peptide with AFM showed that A β preferentially accumulates on DPPC domains versus DOPC in a mixed bilayer system[183]. Thus, choosing to utilize DPPC in the study essentially guaranteed the observation of accumulation of the A β , which was advantageous for several reasons. First, the gel phase lipid, as mentioned above, is often utilized as a raft model component since its physical properties resemble that of cholesterol enriched bilayers. Using DPPC gel phase bilayer platform as a surrogate for cholesterol lipid raft model made sense due to the relative simplicity of producing it and also its closeness to the raft membrane model. Secondly, knowing that DPPC promotes accumulation of A β made it an appropriate choice as a control starting point to test against effects of melatonin. The hypothesis being tested is that melatonin would probably

decrease the accumulation of A β on the bilayer by fluidizing the gel or the lipid raft phase (Lo phase) bilayers.

3.3.1 Materials and Methods

Brain extract bilayer (porcine) in chloroform was purchased from Avanti Polar Lipids (AL, USA). The same procedures used for preparing DOPC bilayers were used in preparing brain extract bilayers (shown in section 3.2.4.1), since both brain extract lipids and DOPC are in fluid phase at room temperature. DPPC was purchased from Sigma-Aldrich in powder form and the procedure for forming supported bilayers is outlined in section 3.2.4.2. Melatonin was purchased from Sigma and was used without further purification. Melatonin was directly dissolved in the buffer to 2.0 mM.

A β (1-42) NaOH was purchased from rPeptide (GA, USA) in lyophilized powder form and used without further purification. 500 μ g of A β in NaOH is brought to room temperature to avoid condensation[216] and dissolved in 0.01M NaOH to 1mg/ml concentration[217]. The peptide is sonicated for 1 minute in a bath sonicator to disassociate larger aggregates[218]. 69.5 μ l of the solution is aliquoted into 14 different Eppendorf vials and snap frozen in dry ice, then kept at -20°C[210]. Before experiments, a vial containing the frozen solution is thawed at room temperature and added to the AFM liquid cell to the final concentration of 5- 15 μ M. The A β preparation yielded very small monomeric to very low oligomeric (most likely dimer or trimers) species according to size, as verified by AFM image cross sections, consistently for up to 15 days (figure 48).

Several different AFM cantilevers were utilized for liquid imaging. MAC mode type II cantilevers (silicon tip) with the nominal spring constant of 2.4 N/m (Agilent Technologies, USA), DNP-S cantilevers (silicon nitride) with spring constant 0.02 N/m (Bruker, USA), SNL levers with spring constant 0.02 N/m (sharpened silicon, Bruker, USA), and NPG levers (Gold coated, Bruker, USA) with spring constant of 0.02 N/m were utilized. The gold-coated levers were also chemically modified with PEG, using the tip modification procedure outlined in appendix A.

Experimental procedure included creating an appropriate bilayer and imaging the surface first as control. After a minimum of three different areas has been imaged, then A β or A β +melatonin was added to the bilayer. The sample was left to incubate at room temperature (24°C) and rinsed at varying predetermined times to stop the aggregation progress and imaged to assess membrane damage. Time dependent *in situ* imaging trials were also conducted, however, for those experiments the presence of A β in solution (from not being able to rinse away) made the imaging highly difficult due to frequent contamination of the tip (see page 152, figure 49). All bilayer samples were imaged at room temperature in buffer (HEPES 10 mM, NaCl 150mM, pH 7.4).

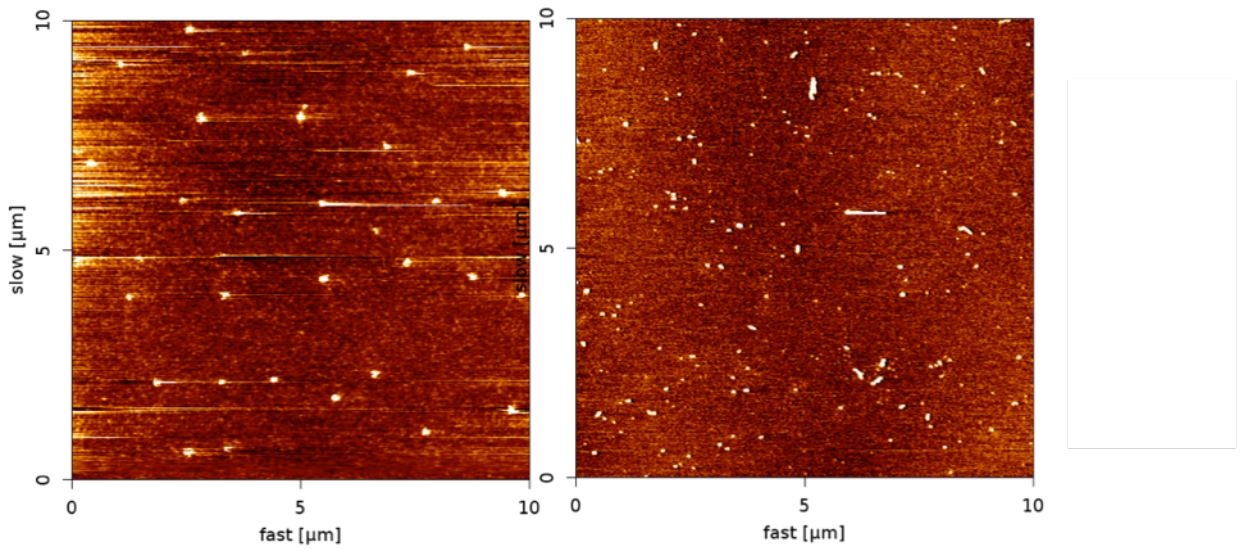


Figure 48- A β preparation thawed and deposited on mica, imaged in air. Left image shows samples from day 1 and right image shows samples from day 15. Overall, the size and shape of the aggregate is preserved and no fibrillar or larger aggregates have developed between the two samples. 5 μ l of the amyloid solution was deposited on mica, left for 5 minutes, rinsed with 100 μ l of water, and dried with a stream of nitrogen, sample imaged in air at room temperature with NCH-50 cantilever with nominal $k= 42$ N/m imaged using intermittent contact mode.

3.3.2 Results and Discussion

3.3.2.1 Brain Extract Bilayer and A β

Brain extract bilayers were created and A β (1-42) was added in three different concentrations (5, 10, 15 μ M). The samples were incubated and imaged at several different times (immediate after the addition of A β , 2, 6, and 24 hours, the results are shown in figure 49).

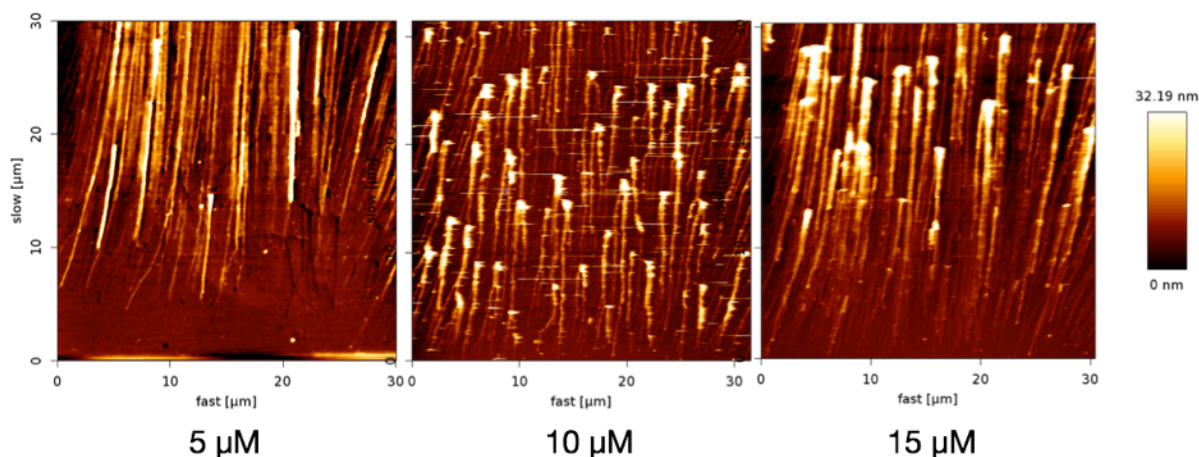


Figure 49- A β (1-42) on brain extract bilayers in 3 different concentrations. Images taken after 24 hours. All images are 30 μ m by 30 μ m in size. A β is shown as white blobs. The trails or tails behind the aggregates are created by the tip moving across the image horizontally in a line-by-line scan (scanning fast left and right moving slowly one line at a time from bottom to top), which results in gradual upward push or line by line nudging of the aggregates upward, every time a horizontal line scan is performed. The moving aggregates always have tails that are perpendicular to the fast scan direction, and parallel to the slow scan direction. Sample imaged using intermittent contact mode in buffer (HEPES 10 mM, NaCl 150mM, pH 7.4). NPG levers (Gold coated, Bruker, USA) with the spring constant of 0.02 N/m were utilized. The gold-coated levers were also chemically modified with PEG thiols.

Overall, concentration dependent effects on the accumulation of A β on the bilayer surface were not obvious, even at shorter times of incubations. The main difference between the

concentrations is that the final sizes of the aggregates are greater in the higher concentration samples compared to the lower concentration ones (figure 49). Surface coverage was comparable. Further precise quantitative assessment of the samples was highly challenging, as A β seemed to not be strongly bound to the bilayer. Imaging the samples caused the aggregates (white blobs) to shift across the images and drag trails behind them as they were being moved in the direction of the imaging tip. The mobile aggregates are shown in figures 50 and 51.

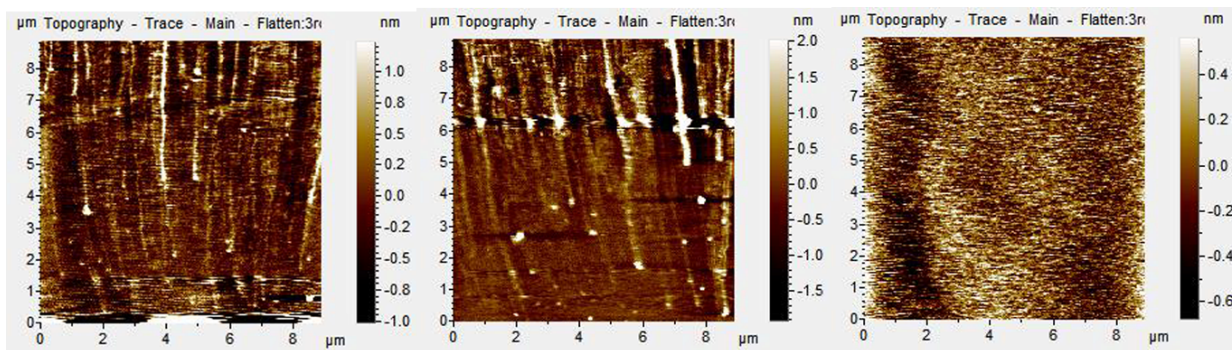


Figure 50- Sequential images of 10 μM A β on brain extract bilayer taken from the same area. After repeated scans, A β is completely removed from the brain extract bilayer through scanning. Image sizes 8 μm^2 , incubation time 24 hours. Sample imaged using intermittent contact mode in buffer (HEPES 10 mM, NaCl 150mM, pH 7.4). Vertical height scales are shown to the right of each image. NPG levers (Gold coated, Bruker, USA) with the spring constant of 0.02 N/m were utilized. The gold-coated levers were also chemically modified with PEG thiols.

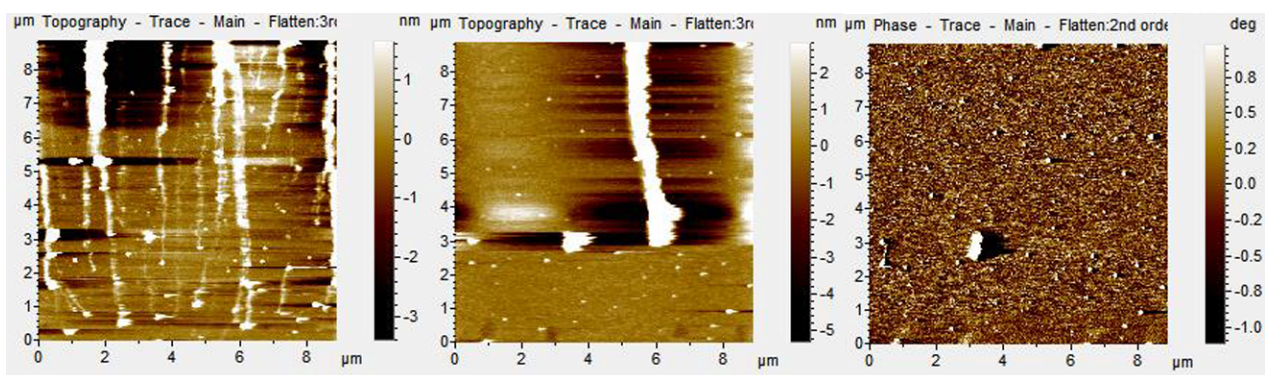


Figure 51- Even at the highest concentration of A β tested (18 μM) incubated for 48 hours (longest incubation time tested), the aggregates are still mobile and can be swept clean from the bilayer surface through scanning. Sequential images from left to right, image size 8 μm^2 . Sample imaged using intermittent contact mode in buffer (HEPES 10 mM, NaCl 150mM, pH 7.4). Vertical height scales are shown to the right of each image. NPG levers (Gold coated, Bruker, USA) with the spring constant of 0.02 N/m were utilized. The gold-coated levers were also chemically modified with PEG thiols.

After numerous trials (figure 50 and 51), the results indicated that A β does not strongly bind to the brain extract and that scanning the surface would change the surface coverage of them depending on the number of scans performed over the area and also depending on the setpoint (force applied) by the tip while scanning (figures 49-51). Adding melatonin to the system to try to ascertain any measurable changes caused by it was unsuccessful, because with melatonin, the A β blobs also displayed similar shifting characteristics that made it impossible to statistically measure the surface coverage amount accurately. Also, the highly mobile aggregates on the surface (figure 52) changed shape and measurable height during a scan, making it impossible to estimate the accumulated aggregate size. The bilayer also appeared clean and damage free after being cleared of all aggregates from repeated scans, much like the control samples.

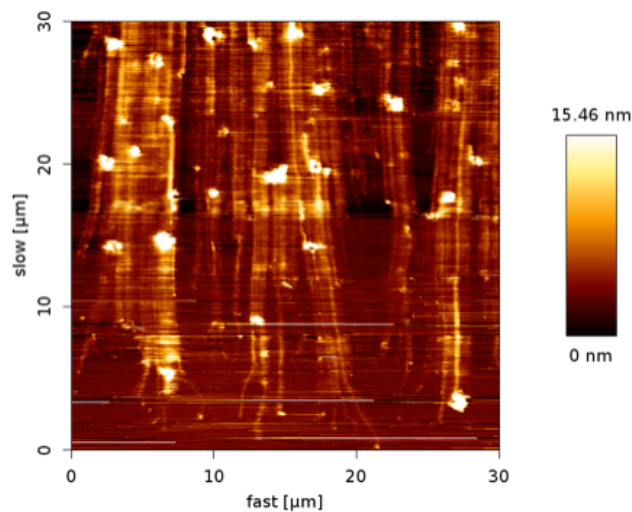


Figure 52- 5 μ M A β added to brain extract bilayer in 2.0 mM melatonin solution. The left streaks on the aggregates are due to their being pushed by the tip (moved the aggregates upward from bottom to top). The over results resembles that of the control and no discernable changes could be observed or measured due to having easily movable aggregates; the very first scanned image of the area is shown. Sample imaged using intermittent contact mode in buffer (HEPES 10 mM, NaCl 150mM, pH 7.4). NPG levers (Gold coated, Bruker, USA) with the spring constant of 0.02 N/m were utilized. The gold-coated levers were also chemically modified with PEG thiols.

Further continuation and conducting repeat trials in the same system seem futile, since it was unclear if there were any obvious differences produced with melatonin. Even if there were changes in the accumulation with melatonin, it was not possible to precisely quantify the difference.

A decision was made to utilize DPPC bilayers instead of the brain extract, since A β had been shown to preferentially and measurably bind to DPPC bilayers[183], [210], more strongly than to brain extract and the studies were done using the same method (AFM). Also, the brain extract samples were highly prone to degradation and biological contamination and it was extremely difficult to maintain the integrity of the sample for longer than 24 hours (In many trials, defect and extra contaminations would spontaneously appear over time, figure 53). DPPC bilayers were much more stable overtime and did not show perceivable changes in the control topography within the time periods tested.

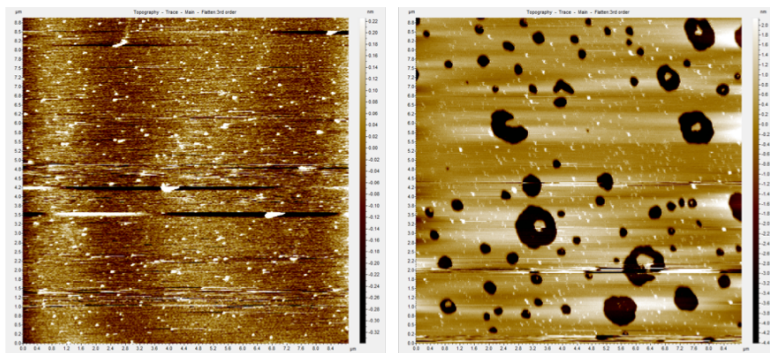


Figure 53- Control brain extract bilayer at 1 hr (left) and after 24 hours (right). Even after insuring meticulous control of the incubation conditions, brain extract bilayers showed spontaneous changes in their topography, making them less suitable for the time dependent A β accumulation studies. Samples imaged using intermittent contact mode in buffer (HEPES 10 mM, NaCl 150mM, pH 7.4), NPG levers (Gold coated, Bruker, USA) with the spring constant of 0.02 N/m were utilized. The gold-coated levers were also chemically modified with PEG thiols.

3.3.2.2 DPPC Bilayer and A β

DPPC bilayers were created with the protocol outlined in section 3.2.4.2. As expected, A β was more strongly bound to DPPC compared to the brain extract as it took more scans to rid of all aggregates from the surface compared to the brain extract samples. However, unlike the fluid brain extract that can form a completely flat defect free bilayer, DPPC coverage could not be as ideal due to its deposition characteristics discussed in section 3.2.4.2. Defects in the DPPC bilayer acted as nucleation sites for A β to preferentially bind and aggregate on, compared to the flat top surface of the bilayer as well as the lower flat domain areas (figure 54).

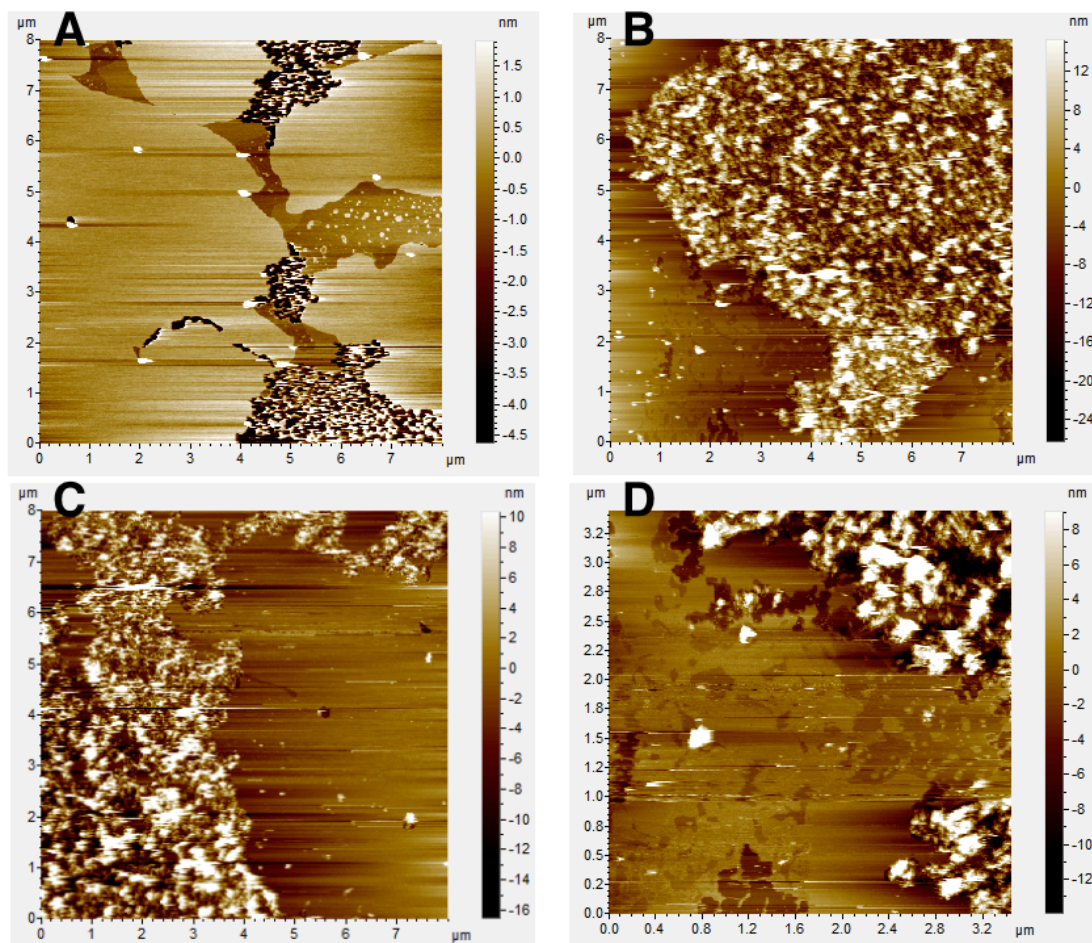


Figure 54- (A) Image of a control DPPC bilayer with extended intact bilayer areas but also containing defects (black areas) as well as lower domains (darker brown). (B) Image contains Aβ at 12 μM incubated for 6 hours. There is a definite preference for Aβ (white blobs) to accumulate and cover the areas with defects compared to the flat bilayer regions. (C) Same sample as B but in a different area. The amount of amyloid accumulation per image depends on the location within the sample where the image is taken, due to varying sizes of areas with defects. (D) Zoomed image of the same sample (3.4 μm²) shows that amyloid aggregates are preferentially located around bilayer defects, as opposed to the top surface of the bilayer (lower domains in darker brown and high domains in light brown). Only the darkest black areas (defects or holes in the bilayer) are covered by the amyloid aggregates. Samples imaged using intermittent contact mode in buffer (HEPES 10 mM, NaCl 150mM, pH 7.4), NPG levers (Gold coated, Bruker, USA) with the spring constant of 0.02 N/m were utilized. The gold-coated levers were also chemically modified with PEG thiols.

There were several challenges in quantifying the accumulation of A β on the bilayers. Adding more amyloid would result in high surface coverage that led to frequent tip contamination. Tip contamination results in image artifacts (determined by presence of exactly repeating shapes, evidence of tip sticking and dragging the sample as is evident as streaks or white lines, or tails around features in the direction of the tip), false extra features in the images as well as misrepresenting the sizes and shapes of the actual features. Tip contamination was reduced through the use of modified gold levers with the tips covered in PEG-thiol groups (Appendix A), which is one of the most inert coatings known for the use in AFM. Having low concentrations of A β could drastically reduce tip contamination, however, this approach also reduced the number of aggregates that could be analyzed. The final concentration of A β was chosen at 12 μ M, which gave optimum accumulation of the aggregates, and were imaged with modified gold levers to yield images without artifacts.

Even when the difficulties in imaging were overcome, there were other issues. First, the amounts of A β added and present on the surfaces between samples could not be kept constant, as the volume of liquid in the AFM liquid cell could not be determined precisely. This was due to the fact that submerging the scanner into the sample to obtain the image of the sample before the addition of amyloid would displace the liquid volume inside the AFM liquid cell and also varying amounts of evaporation would occur during imaging (it takes about 20 minutes per image). Even if the exact amount of A β being added and the volume of buffer in the AFM sample cell could be known, addition of A β to the bilayer surface could not be controlled to ensure even coverage or application, since the amyloid solution had to be added drop by drop

using a micropipette. Thus, depending on the area covered and also on the concentration variability, differing amounts of A β were added to sample surfaces unevenly.

In figure 55, DPPC samples with 1, 6 and 24 hours incubation with A β are shown. The first hour sample shows the least amount of A β (left image), but the 6 hours sample (middle image) seems to show more A β bound around the bilayer defects compared to the longer incubated 24 hour sample (right image). The 24 hours sample shows more A β on the flat intact surfaces of the bilayer compared to the 6 hour sample, but around the defect areas, the amount of A β still appears to be less than that of the 6 hour sample.

Possible explanations for such a result could be that such patterns are accurate, or more likely it is due to these images being taken from three independent samples. In order to obtain sufficiently low uncertainty, every parameter from the volume of the buffer in the liquid cell to the amount of A β being added, and the homogeneity of the added mixture must be as equal as possible. All these factors must be precisely controlled for multiple samples, in order to produce samples that contain the same amount of A β that can be cross-compared.

The results shown in figure 55 represent the best-effort standardized samples with equal treatments. Due to experimental uncertainty that could not be controlled further (random errors in the volume of liquid inside the cell, uniformity in adding the concentrated A β solution), the samples still showed some variability. In addition, the DPPC surface had unevenly distributed defects and domains that led to uneven distribution of A β . Another issue with images was that the tip was moving the aggregates around (figure 56). Also, all samples needed to be made independently, as samples needed to be rinsed before being imaged, otherwise the tip

contamination would be too great to generate images with minimum amount of artifacts (no matter what tip we used, including PEG thiol coated tips that are known to be the least attractive with peptides, image artifacts due to intermittent contamination of the tip was, though minimized, still unavoidable. Image artifacts are shown as straight white thin lines in the image). In essence, it was not possible to determine, with any confidence, if a sample had more or less accumulation of A β aggregates as a function of incubation time, because A β was added across the sample unevenly, different samples had variable areas of bilayer defects to which A β had an affinity, and the scanning action of the technique used to image the number of deposits moved the aggregates

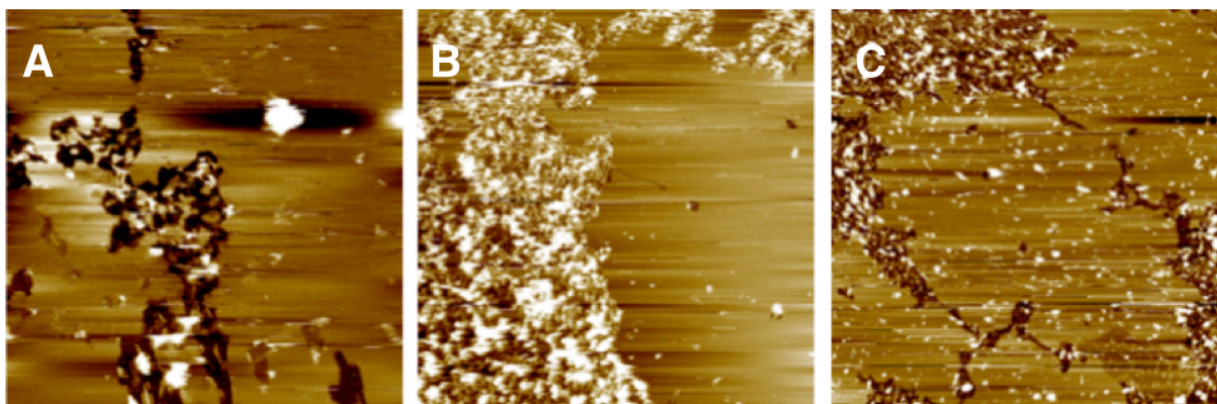


Figure 55- (A) DPPC bilayers with A β at 12 μ M, incubated for 1 hour, (B) 6 hours and (C) 24 hours. The 6 hour sample B shows the greatest amount of A β accumulation in the areas with defects, but the 24 hour sample C shows more A β aggregates on the flat defect free areas. Images taken using intermittent contact mode with NPG (gold coated) levers modified with PEG thiols, imaged at room temperature in buffer (HEPES 10 mM, NaCl 150mM, pH 7.4), from three independent samples.

Quantifying the differences in the samples is complicated by the fact that even though A β binds more strongly to DPPC compared to the brain extract, the aggregates are still not stably

affixed to the bilayer. Figure 56 shows a sample that has been incubated with A β for 2 hours. The two images are of the same spot except the image on the right has a clean square area in the middle of the image. The cleaned area is created by repeated scans, and an image of a larger final area that includes the original area is shown. With A β on DPPC, it is possible to image the accumulation of A β on the surface to a reasonable degree. However, as seen in the figure, even the slightest increase in the force between the tip and the sample will result in clearing the aggregates and or result in underestimation of the sizes or heights of the aggregates (decreasing force would result in the opposite).

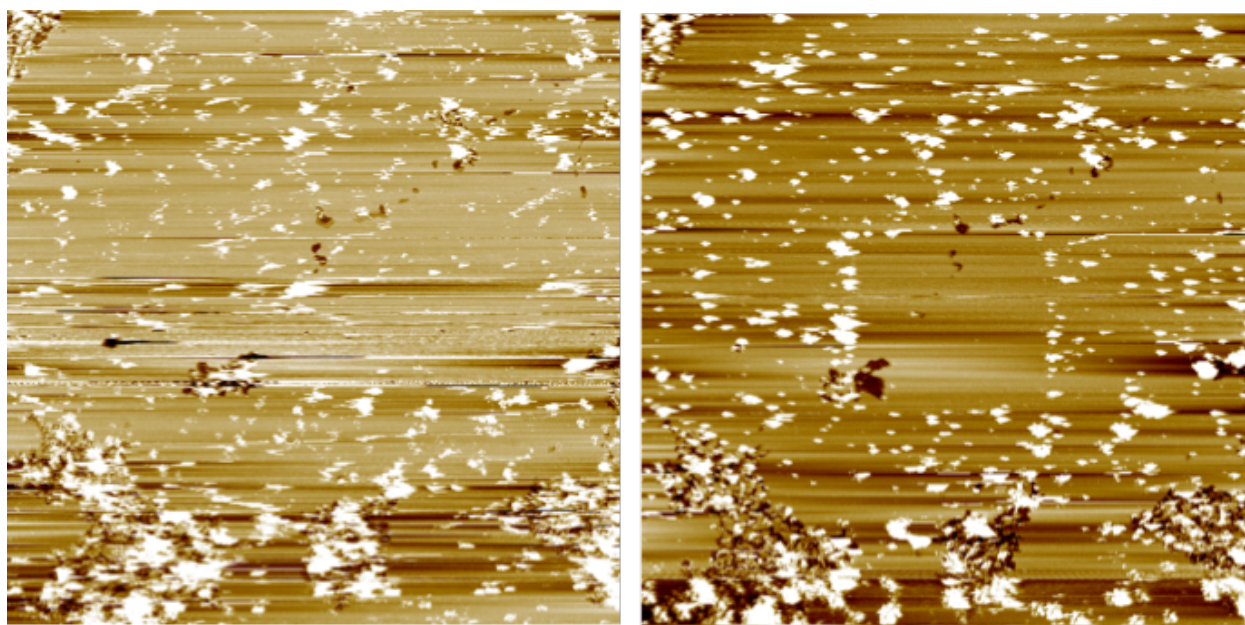


Figure 56- DPPC with A β incubated for 2 hours. Left image shows the first scan of the area, and right image shows the same area but after a small scan was performed in the middle (one pass using the same force). Scanning the sample clears the surface of the aggregates gradually in every single pass. Image parameters were kept constant throughout (large image area 8 μm^2). Even the very first pass of the region reduces the amount of aggregates present. Images taken with NPG (gold coated) levers modified with PEG thiols, at room temperature in buffer (HEPES 10 mM, NaCl 150mM, pH 7.4) using intermittent contact mode.

In addition, further complicating the matter is the presence of the aggregates in the defect areas where there are holes and breaks in the bilayer. It is quite obvious that A β prefers to accumulate in and around these areas (figure 54). However, because the holes extending below the top plane of the bilayer mask the size of the aggregates, it was not possible to reliably compare the vertical height of the aggregates in these areas, where the majority of the aggregates were located (figures 54 and 55, white blobs in image).

Nevertheless, it was still possible that adding melatonin would yield such drastic differences in the A β accumulation that the results may stand out beyond these various factors that caused variability. When samples with melatonin were imaged, the level of A β accumulation in different melatonin samples was not consistent. Results from one of the trials are shown in figure 57, and there were more A β present in the 2 hour sample compared to the 6 or 24 hour samples. Inconsistencies in the accumulation of A β were similar to those in control samples. Also, it appeared that with melatonin, there were increased surface coverage and larger aggregate sizes present compared to control. However, the differences in the surface accumulation of A β between the two groups were difficult to ascertain from the images, because scanning altered the surface features (figure 58) also in control and melatonin samples. It made the quantifiable information present on the images (the number of features, height of the features, width and lengths of the features, etc.) variable. Also, the feature sizes and surface coverage were constantly shifting from one scan to the next.

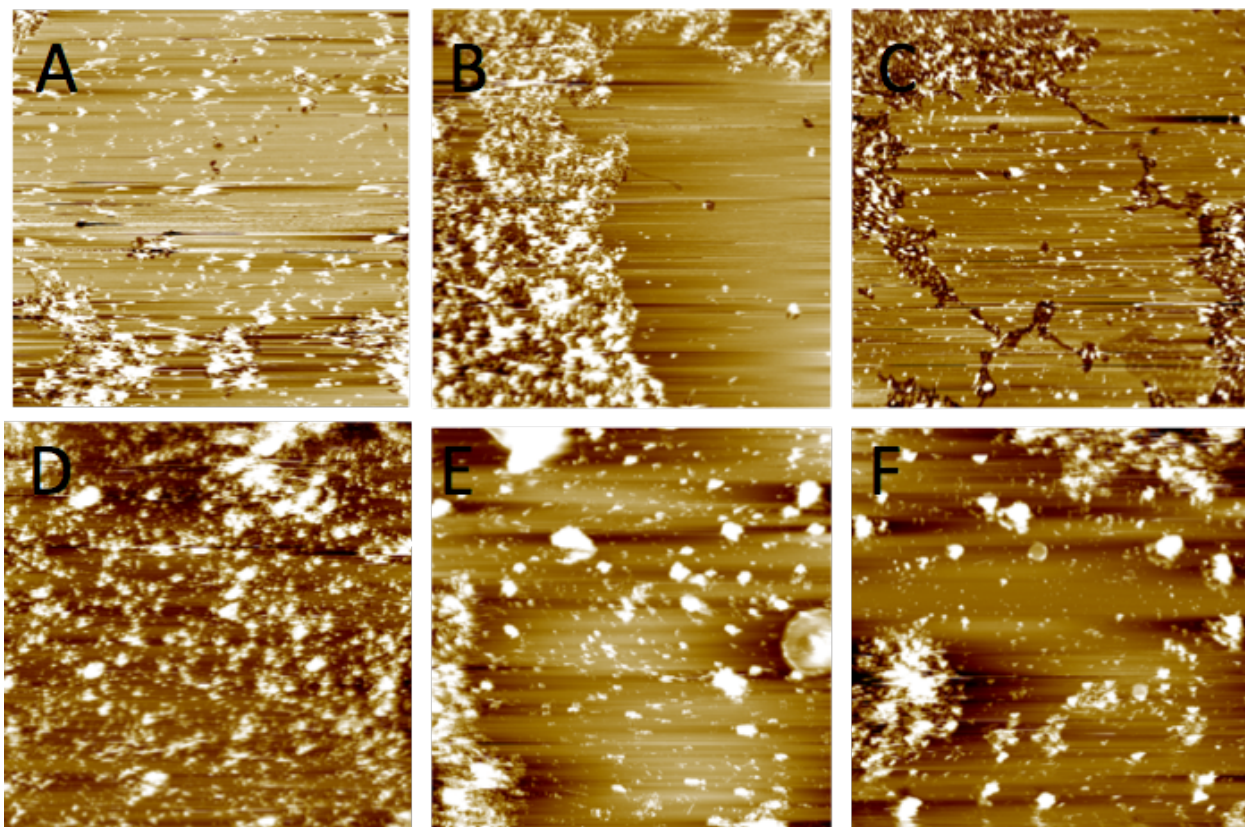


Figure 57- Top images are control DPPC bilayers with A β incubated for (A) 2 hours, (B) 6 hours and (C) 24 hours. Bottom row samples incubated with 2.0 mM melatonin for (D) 2 hours, (E) 6 hours and (F) 24 hours. (All images size 8 μm^2). The difference in the accumulation of A β could not be measured reliably due to factors discussed in the text. Images taken with NPG (gold-coated) levers modified with PEG thiols, imaged at room temperature in buffer (HEPES 10 mM, NaCl 150mM, pH 7.4) using intermittent contact mode.

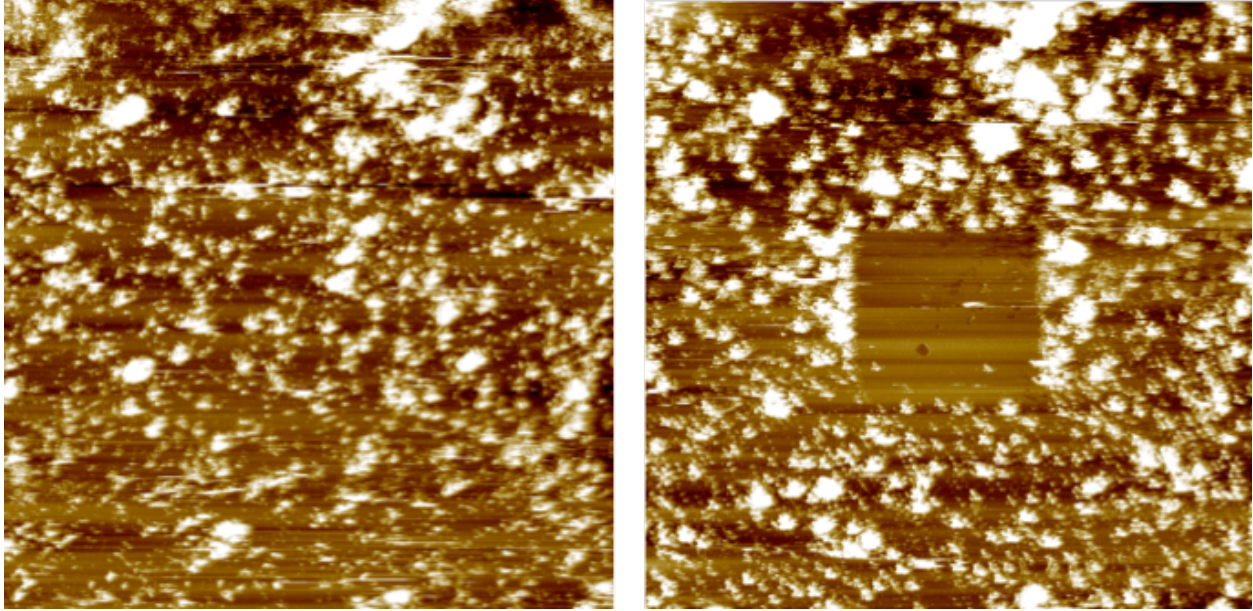


Figure 58- DPPC bilayer with A β incubated for 2 hours with 2.0 mM melatonin. The two images are identical, except the image on the right has been scanned in the center repeatedly. It was evident that every single pass of the area removed some aggregates until the area became completely clear, meaning that even the very first scan of the sample might be removing aggregates from the surface. Scanning parameters were kept constant but multiples images were taken on one spot until the aggregates were moved. Imaged using intermittent contact mode, at room temperature in buffer (HEPES 10 mM, NaCl 150mM, pH 7.4), taken with NPG (gold-coated) levers modified with PEG thiols, image size 8 μm^2 .

Repeated trials with and without melatonin resulted in samples that displayed highly varied images among all samples, in terms of bilayer surface features as well as amounts of defects and domains (figure 59). Having reliable quantification of A β accumulation in melatonin samples would be highly unlikely due to shifting aggregates and non-uniform surface distribution/coverage that also changed depending on scanning frequency and parameters.

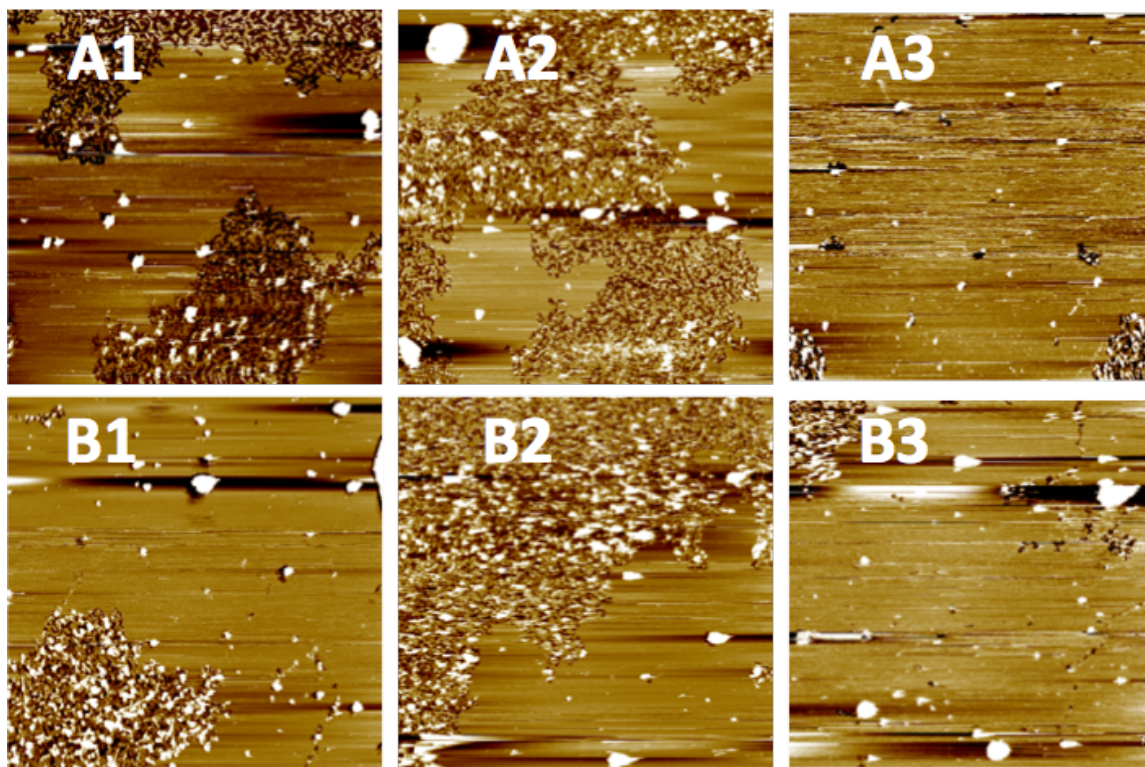


Figure 59- Three different trials of 1 hour incubation without melatonin (top row) and with melatonin (bottom row). (A1) Control from trial 1, (A2) control from trial 2 and (A3) control from trial 3. (B1) sample from trial 1 incubated with melatonin, (B2) sample from trial 2 with melatonin, (B3) sample from trial 3 with melatonin (All images are 8 μm^2). The order of experiments was A1, B1, A2, B2, A3, and B3. Six independent samples imaged with NPG (gold-coated) levers modified with PEG thiols, imaged at room temperature in buffer (HEPES 10 mM, NaCl 150mM, pH 7.4) using intermittent contact mode.

3.3.3 Summary and Conclusion

Assessment of A β accumulation on brain extract and DPPC bilayers was conducted. Brain extract bilayer samples showed accumulation of round amorphous A β aggregates on the surface, however the aggregates were loosely bound and highly mobile. Repeatedly scanning the sample resulted in clearing of the aggregates and revealed intact, and to the best of knowledge, damage free brain extract bilayer. The results were comparable with previous studies where only a very small limited amount of defects were observed with A β (1-42) on brain extract bilayers[207].

A β accumulation on DPPC showed smaller aggregates compared to the ones observed on brain extract. They were amorphous and round in shape similar to the ones found on the brain extract, and they were bound to the bilayer more strongly. However, repeated scanning of an area also caused clearing of the aggregates that revealed the DPPC bilayer underneath that was also observably damage free. Samples were highly diverse in terms of the bilayer topography (bilayer defects and domains), which were favored by A β . Accumulation also depended on scanning parameters and frequency, which is impossible to keep constant between different samples but only possible within a sample to a very limited degree (most often parameters had to be changed multiple times during a single scan of an image). With all of the factors combined, it is concluded that the very slight differences observed qualitatively in melatonin samples compared to control might be the result of uncertainties or variations in the samples and assessment, rather than due to the presence or absence of melatonin.

In conclusion, the imaging experiments were inconclusive due to having non-uniform bilayer samples and also due to unstable aggregates that are moved by the tip. However, an amyloid oligomer incubation procedure was successfully developed.

Chapter 4

Collaborative Works

4.1 Introduction

Collaborative work has been performed to obtain complementary data in support of the hypotheses presented in this thesis as well as to make contributions in other closely related research projects. Many different methods have been utilized including fluorescence microscopy (FM), and cell viability testing of cell cultures (mouse hippocampal cells, retinal ganglion cells). *In silico* molecular dynamics simulations data were also utilized to support and discuss of the findings presented in the previous chapters. Some of the collaborative work presented here has been published in peer-reviewed journals, and many are currently being prepared for submissions to various peer-reviewed journals. The published data are presented with written permission (see Statement of Contributions).

4.2 Investigating A β Deposits on Human Retina

Characterization A β deposits in human retina was performed using FM and AFM. The work was conducted as part of a project in Dr. Campbell's group. The main motivation of the project was to utilize and modify the biophysical techniques used in the main part of the study to identify and characterize deposits of A β present in human retinas. The importance of the goal lies in the fact that the retina is a neural tissue that is considered to be a direct extension of the brain with parallel characteristics and features. Thus, it was possible that the neuro-pathophysiological featured found in the brains of AD patients may also be present in the retina. The retina is high accessible for direct assessment using ophthalmological methods, compared to the brain. Examining the retina for signs of AD could effectively serve as a disease diagnostic and assessment strategy.

FM combined with AFM was used to identify and characterize A β deposits in human retinas. Briefly, epifluorescence microscopy utilizes fluorophores, which are chemical compounds that are able to absorb the energy of photons at a specific wavelength of light and release the energy back with a different lower energy, longer wavelength of light. The released light or emitted light has a specific color (wavelength). The spectral differences (wavelength and frequency difference) between the absorbed (excitation light) and emitted lights are specific for a given fluorophore and are also specific to the configuration and the surrounding environment of the fluorophore. For instance, a fluorophore named thioflavin can undergo a detectable spectral shift when bound to A β aggregates. By attaching fluorophores to the molecules or structures of interest, it is possible to identify, track, and characterize them through fluorescence visualization.

As a preliminary step, A β is deposited on to a flat clean substrate (specially cleaned glass using aqua regia) and imaged using the FM-AFM combination (figure 60). The technique, although not novel, was new to the lab and was specifically setup and tested for this purpose. The results demonstrated the capabilities of the setup in detecting and characterizing A β aggregates in the retina using the thioflavin T fluorophore (Sigma-Aldrich). A β (1-42) NaOH purchased from rPeptide (GA, USA) was used without further purification. A β was incubated in buffer (10 mM HEPES saline 150 mM NaCl, pH 7.4) for 24 hours, thioflavin T solution in ethanol (5%) was added to A β and A β was deposited on to glass, dried and imaged in air (figure 61). Preliminary control experiments were prepared and conducted solely by the author. Human retina experiments were conducted in collaboration (see Statement of Contributions).

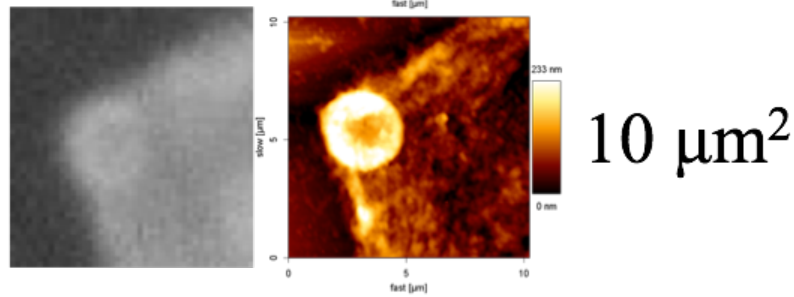
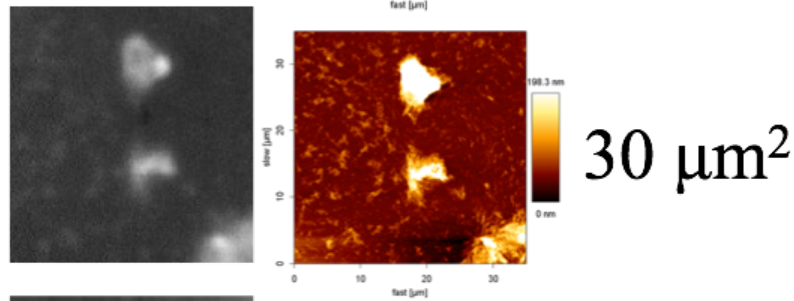
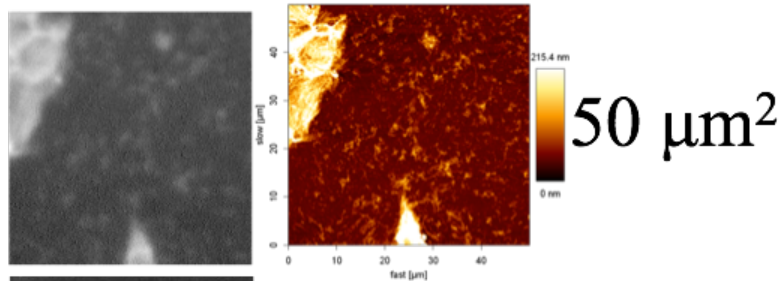
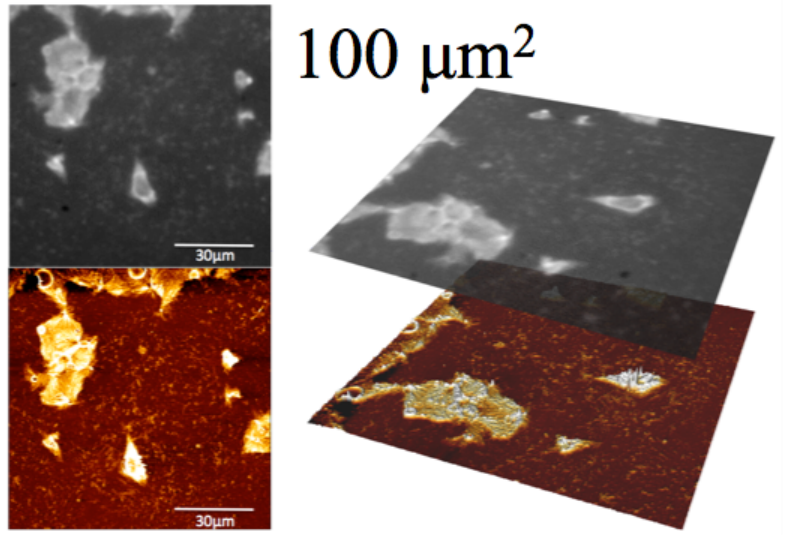


Figure 60- Testing the combined FM (grey scale) and AFM (yellow-brown) imaging of A β aggregates in different resolutions deposited on glass. The FM and AFM images can be overlaid on top of each other as shown in top right with the 100 μm^2 images. Imaged using intermittent contact mode in air using NCH probes with nominal spring constant of 42 N/m.

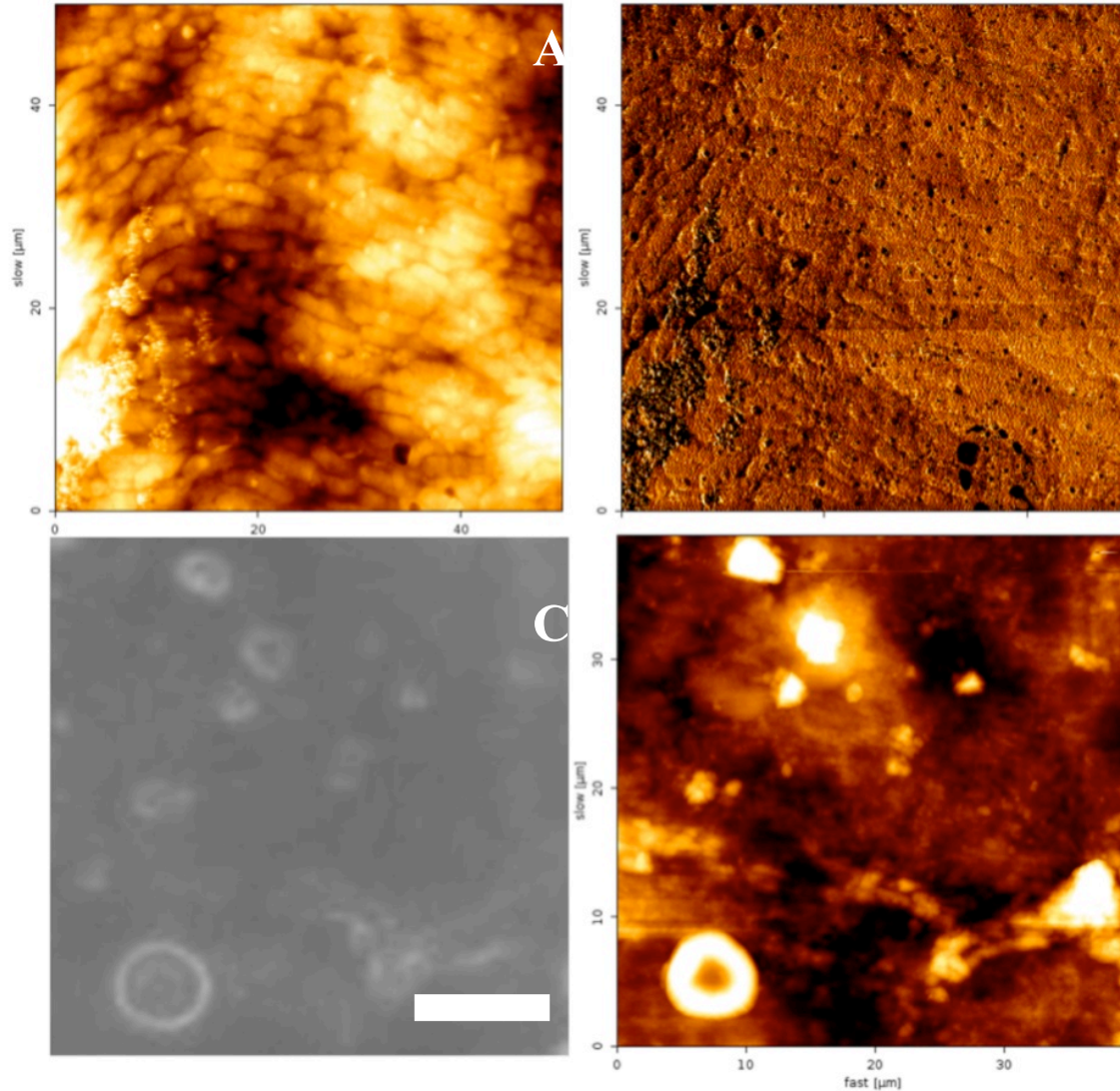


Figure 61- Images of post-mortem human retinas. (A) AFM topography image of the inner limiting membrane within the human retina harvested from a control subject. No large deposits are found, and also shows tube like tracks of the underlying nerve fiber layer (stratum opticum). (B) AFM phase image of the same spot as image A indicates the uniform material property of the inner limiting membrane covering the nerve fiber layer. (C) Grey scale fluorescence imaging of the inner limiting membrane within the retina harvested from an AD patient. Sample is fluorescently labeled with thioflavin S for A β , and large deposits of labeled aggregates are present, scale bar 10 μm (D) AFM topography image of the corresponding fluorescent spot shown in C. Amyloid deposits correspond with the fluorescent staining and are similar to amyloid deposits on glass. AFM imaging was performed in air using intermittent contact mode using NCH levers with nominal spring constant of 42 N/m.

4.3 Cell Viability Testing with A β and Melatonin

The capability of melatonin in preventing and reducing A β toxicity is central to this thesis. Although there are quite a few papers that have provided evidence for the cell protection of melatonin against A β , this fact is still gaining acceptance and is not yet universally accepted. The results of these experiments provided experimental support for melatonin's ability to protect the cells from A β toxicity. Showing melatonin's cell protection was important in justifying the foundational reasons for the overall project. Also extended experiments using cyclodextrin (cholesterol harvesting molecule) were performed to give relevant biological insight at the cellular level, and the results were used to determine the direction of other parallel experiments conducted within the thesis.

Assessing the physical properties of A β aggregates are critical for controlling their toxicity[21]. It is challenging to precisely control and reproduce specifically aggregated species of A β for use in cell viability tests. Among many different A β incubation protocols, three different approaches were chosen and performed. The aggregates were imaged using AFM to ascertain the effects of the different incubation protocols. The variations in the protocol ranged from pretreatment with DMSO, separation with centrifugation, and no treatment. The results are shown in figure 62.

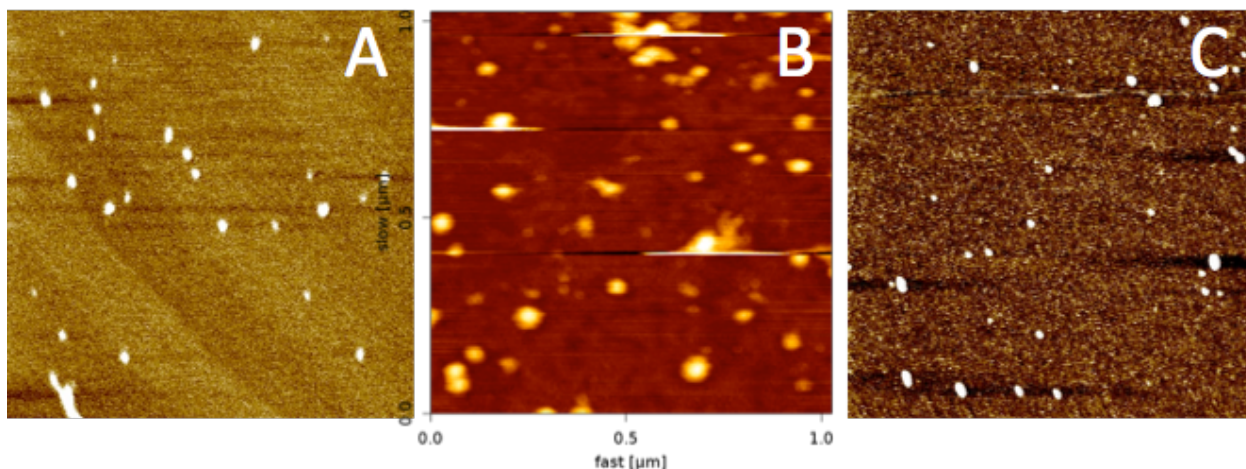


Figure 62- Representative images of three different A β aggregate samples incubated in cell culture media. (A) Predissolved A β in DMSO, incubated in cell culture media. Image size is 5 μm^2 (B) A β aggregates from a centrifuged supernatant, transferred and incubated in cell culture media. Image size is 1.2 μm^2 (C) no pretreatment A β aggregates incubated in media. Image size is 5 μm^2 . Sample preparation for AFM imaging entailed incubating A β with various pretreatments in cell culture media, depositing 25 μl of the solution on to freshly cleaved mica, wait 5 minutes, rinsed with 50 μl of water three times, then dried with nitrogen. Images taken in intermittent contact mode using NCH levers with spring constant $k \sim 42$ N/m.

Overall, the different pretreatments yielded comparably shaped A β aggregates. Samples with no pretreatment or DMSO pretreatment of A β showed 4-5nm aggregates. The samples that were centrifuged showed much smaller, amorphous layer of particles (presumably monomers or very low number oligomers). Control samples without amyloid showed small 1-2nm aggregates, as well as large 10-40 nm blobs. The DMSO and centrifuged control samples both showed <40 nm large features. The control samples also showed a thin layer of compounds, presumably of media additives (HyClone media), as a layer 0.5-1 nm thick lining the substrate. These extra features present in control samples were excluded from consideration when assessing amyloid samples. The results from this work helped to finalize the protocols used in amyloid cell viability studies. The results from the cell studies are presented in Appendix B.

4.4 Dynamic Light Scattering (DLS)

DLS experiments were aimed at characterizing the unilamellar vesicle solutions being used for depositing supported bilayer samples. For obtaining repeatable results in producing supported bilayer samples, it was crucial that the quality of the vesicle solution, containing unilamellar vesicles made through bath sonication, be of consistent quality. The usual method of quality control for the vesicle solutions (end point determination of the finished product at the end of the sonication cycle) was to inspect it with the naked eye and determine the clarity and the transparency of the solution. However, for obvious reasons, the quality of the dispersion could not be precisely controlled and determined this way.

Using dynamic light scattering, particle (vesicle) size and its distribution were measured for six different DPPC vesicle solutions each prepared in slightly different ways. The variables for the solutions included the length of time of sonication, temperature during sonication, concentration and overall volume.

The results of the experiment are shown in figure 63. The sensitivity of the measurement was too low (± 10 nm) to characterize and differentiate the vesicle solutions in terms of the size distribution of the vesicles they contain, which had average diameters around 74 nm. The uncertainties in the measurements were greater than the differences between the sample solutions, and it was not possible to determine the precise differences between the sample solutions. So relying on the DLS measurements as quality control for the solutions each time they were produced seemed unfeasible. A decision was made to rigorously setup detailed solution making procedures and meticulously execute the steps every time, in order to maintain the solution quality constant each and every time. The intent of conducting DLS experiment was

also to characterize the effects of time on the solution during long-term storage. The solutions often became cloudy over time and also change in their deposition characteristics as well as in the produced bilayer quality. If shelf life of solutions (the length of time in which the distribution of vesicles in solution remains unchanged) could be adequately determined, then a working solution that produces good supported bilayer samples could be reliably kept and reused overtime. The detection sensitivity of the DLS machine, however, was not high enough to determine the subtle differences in the various solutions that were differently aged. Since shelf life could not be determined, the only way to ensure consistent solution quality was to produce them fresh in exactly the same way every time, and use it within a set time (usually within 24 hours).

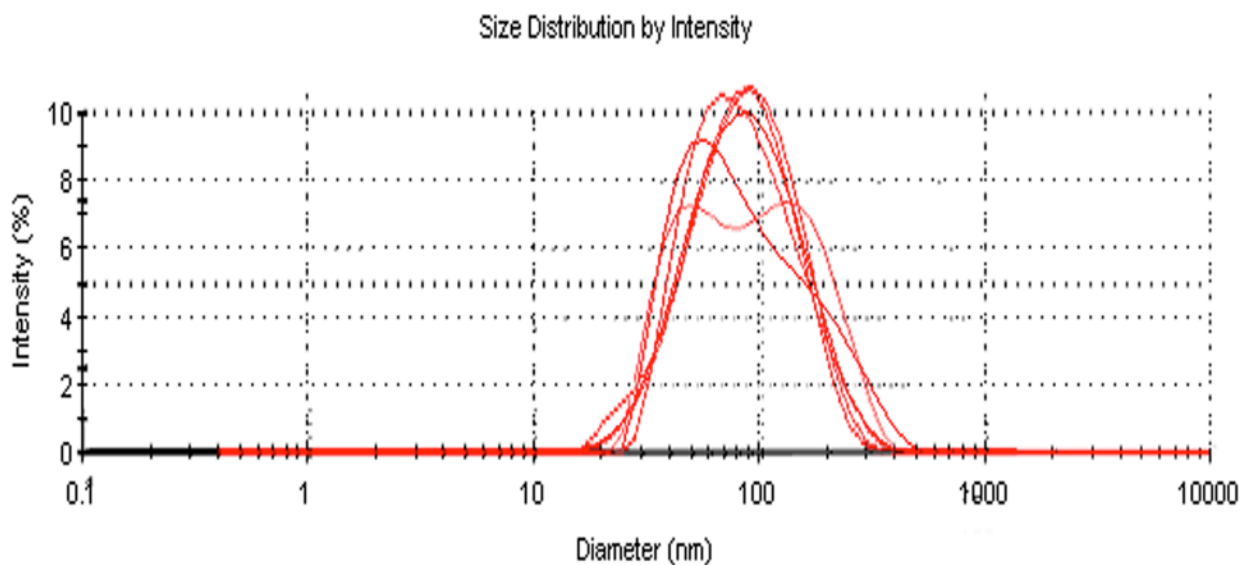


Figure 63- DLS measurements of DPPC vesicle solutions, showing size distribution by intensity for six unilamellar vesicle different solutions. The z average (intensity-weighted average) diameters for the trials were between 73.4- 78.4 nm with standard errors of the mean of ± 10 nm.

4.5 Other Contributions- Molecular Dynamics Simulations

This section features collaborative work on molecular dynamics (MD) simulations. Specific contributions made in this section are outlined in detail in the "Statement of Contributions" section at the beginning of the thesis (Pages iii-v).

MD simulations were conducted and the results clarified the location of melatonin in respect to the phospholipids in a membrane model environment. It also characterized the interaction of melatonin as mainly hydrophobicity driven, rather than electrostatic. Comparisons to how cholesterol and phospholipids interact with each other in contrast to melatonin were also made using this technique. The data showed that at 12% concentration, melatonin is able to have a countering influence compared to 20% cholesterol in a lipid monolayer [71], [118]. In section 2.3.3, figures 22B and 23, the monolayer experiment results showed that 20% concentration of cholesterol in the monolayer had condensing effects that was countered by 1.0 mM melatonin in the subphase. However, with the experimental monolayer technique, it is not possible to determine the concentration of melatonin directly inside the monolayer rather than just in the subphase, so it is difficult to make a direct quantitative comparison with the simulations data.

Chapter 5

Summary and Conclusions

5.1 Summary

Increasing evidence suggests that A β interaction with the cell membrane may be an important factor in AD. The hormone melatonin had been shown to have protective effects in AD, which may involve its ability to interact and change the lipid membrane structural properties. The primary goal of the research was to characterize the membrane effects of melatonin on binding and accumulation of A β .

Langmuir monolayers were employed as the first membrane model, as the technique and the model were advantageous in measuring the area per molecule and changes in the lateral expansion and contraction of membrane lipid molecules (membrane surface area). After a period of successful method refinement, the effects of melatonin, cholesterol, and A β were measured in DPPC monolayers. The results showed that melatonin may be able to interact with membrane lipids in a way that is countering the effects of cholesterol. Effects of A β binding in monolayers were also measured, however, the results showed high variability and dependence on experimental conditions. An extended study using the method involving other melatonin related biological molecules, tryptophan, NAS, and serotonin, showed that the tested related molecules were capable of interacting with the membrane monolayer at physiologically relevant concentrations, and differences in the interactions could be successfully measured and characterized using the technique.

The next phase of the project involved creating supported lipid bilayers to conduct BT-forces. The supported bilayer membrane model platform served as a close analogue resembling the real cell plasma membrane in terms of its basic physicochemical configuration. Even though extensive data exists in the literature on supported bilayers, the methods and procedures outlined produced variable results in planned experiments. A great deal of effort and time was spent in devising protocols for producing supported bilayers in a consistent and reproducible manner.

Once the bilayer making protocols were successfully established, AFM BT-force spectroscopy was conducted to characterize various structural parameters of bilayers. Protocols were developed to successfully conduct force versus time experiments on defect free bilayer samples. Experiments showed that control BT-force values may fluctuate depending on various factors, and repeated experiments will be needed with varying tip types and lipid mixtures. Due to the time consuming nature of these experiments, more work is planned to study the effect on melatonin with BT-force spectroscopy in a separate future project. The developed protocols and control experiments presented in the current work provide a valuable foundation for the future work.

In order to obtain additional supplementary data for the project, many other techniques have also been utilized in collaboration with other research groups. MD simulations were utilized to gather complementary data that could further the understanding of melatonin's interaction with membrane phospholipids at the atomic and molecular scales. DLS was utilized to supplement and improve the supported bilayer sample making protocols. Also, in order to extend the relevance of the project to the cellular level, complementary cell studies through conducting cell viability assays were performed. In support of the assumptions made in the hypothesis of the

project, the results of the cell studies verified and confirmed the effects of melatonin and A β on various cell types.

Collaborative work involving studying the human retina for characterizing and identifying A β deposits was also conducted. The retina study served as a pioneering platform for developing a potential AD diagnostic strategy by studying the retinal tissue as a brain tissue surrogate. Setting up and developing protocols for using FM-AFM combination approach was an important first step in collecting the first set of preliminary data for the project.

5.2 Conclusion

The project had an ambitious goal of characterizing melatonin's effects on the structure and properties of model lipid membrane and membrane interaction with A β in relation to its toxicity. The monolayer experiments showed that melatonin is able to interact with phospholipids in ways that oppose cholesterol, and also it is able to directly interact with cholesterol in a membrane model environment. Additional experiments also showed that melatonin and its related biological precursor molecules, tryptophan, NAS and serotonin ($p < 0.05$ paired t-test against control at bilayer equivalent area) are able to directly interact with membrane phospholipids and alter the physical properties of the membrane model assemblies. The results indicated and characterized the capacity of these small molecules to directly affect the membrane, which is a less commonly recognized factor in cellular and molecular biology. The results supported further appreciation of the existence of direct membrane action of molecules.

Membrane actions of melatonin on A β binding and incorporation was investigated but could not be quantified due to experimental uncertainties. Verification of melatonin's molecular effects

on bilayer membranes and any direct consequence of such effects on A β toxicity and other related cellular processes will need further investigation. However, during the process of investigation, various methodological improvements were made in monolayer isotherm experiments, in the protocol for making supported bilayers and in conducting control BT-force spectroscopy, which provided a foundation for future experiments.

Collaborative work involved both emerging and traditional methods in conducting biological research. It utilized traditional biological techniques to study effects of melatonin in cell cultures and developed new protocols for studying amyloid- β in real human tissues. The work broadened the scope of the thesis, and I was able to experience and learn the different methods in the field. The studies helped advance the research field by inventing new approaches and protocols to investigate biologically motivated problems.

In conclusion, this project contributed to the field of membrane nanobiophysics through verifying and characterizing the effects of small biological molecules in model membranes, and also by improving and refining the various techniques utilized. The results and the technical improvements made in this work will foster future work that will help with further development of the field.


Copyright Permissions

SPRINGER LICENSE TERMS AND CONDITIONS

May 19, 2014

This is a License Agreement between Youngjik Choi ("You") and Springer ("Springer") provided by Copyright Clearance Center ("CCC"). The license consists of your order details, the terms and conditions provided by Springer, and the payment terms and conditions.

All payments must be made in full to CCC. For payment instructions, please see information listed at the bottom of this form.

License Number	
License date	May 19, 2014
Licensed content publisher	Springer
Licensed content publication	Springer eBook
Licensed content title	Potential Applications of Langmuir-Blodgett Films
Licensed content author	G. G. Roberts
Licensed content date	Jan 1, 1990
Type of Use	Thesis/Dissertation
Portion	Figures
Author of this Springer article	No
Order reference number	None
Original figure numbers	3.4.1
Title of your thesis / dissertation	Nanoscale Characterization of Melatonin and Amyloid Beta in Model Membranes- in Relation to Alzheimer's Disease
Expected completion date	May 2014
Estimated size(pages)	250
Total	0.00 USD
Terms and Conditions	

Introduction

The publisher for this copyrighted material is Springer Science + Business Media. By clicking "accept" in connection with completing this licensing transaction, you agree that the following terms and conditions apply to this transaction (along with the Billing and Payment terms and conditions established by Copyright Clearance Center, Inc. ("CCC"), at the time that you opened your Rightslink account and that are available at any time at <http://myaccount.copyright.com>).

Limited License

With reference to your request to reprint in your thesis material on which Springer Science and Business Media control the copyright, permission is granted, free of charge, for the use indicated in your enquiry.

Licenses are for one-time use only with a maximum distribution equal to the number that you identified in the licensing process.

This License includes use in an electronic form, provided its password protected or on the university's intranet or repository, including UMI (according to the definition at the Sherpa website: <http://www.sherpa.ac.uk/romeo/>). For any other electronic use, please contact Springer at (permissions.dordrecht@springer.com or permissions.heidelberg@springer.com).

The material can only be used for the purpose of defending your thesis limited to university-use only. If the thesis is going to be published, permission needs to be re-obtained (selecting "book/textbook" as the type of use).

Although Springer holds copyright to the material and is entitled to negotiate on rights, this license is only valid, subject to a courtesy information to the author (address is given with the article/chapter) and provided it concerns original material which does not carry references to other sources (if material in question appears with credit to another source, authorization from that source is required as well).

Permission free of charge on this occasion does not prejudice any rights we might have to charge for reproduction of our copyrighted material in the future.

Altering/Modifying Material: Not Permitted

You may not alter or modify the material in any manner. Abbreviations, additions, deletions and/or any other alterations shall be made only with prior written authorization of the author(s) and/or Springer Science + Business Media. (Please contact Springer at (permissions.dordrecht@springer.com or permissions.heidelberg@springer.com))

Reservation of Rights

Springer Science + Business Media reserves all rights not specifically granted in the combination of (i) the license details provided by you and accepted in the course of this licensing transaction, (ii) these terms and conditions and (iii) CCC's Billing and Payment terms and conditions.

Copyright Notice:Disclaimer

You must include the following copyright and permission notice in connection with any reproduction of the licensed material: "Springer and the original publisher /journal title, volume, year of publication, page, chapter/article title, name(s) of author(s), figure number(s), original copyright notice) is given to the publication in which the material was originally published, by adding; with kind permission from Springer Science and Business Media"

Warranties: None

Example 1: Springer Science + Business Media makes no representations or warranties with respect to the licensed material.

Example 2: Springer Science + Business Media makes no representations or warranties with respect to the licensed material and adopts on its own behalf the limitations and disclaimers established by CCC on its behalf in its Billing and Payment terms and conditions for this licensing transaction.

Indemnity

You hereby indemnify and agree to hold harmless Springer Science + Business Media and CCC, and their respective officers, directors, employees and agents, from and against any and all claims arising out of your use of the licensed material other than as specifically authorized pursuant to this license.

No Transfer of License

This license is personal to you and may not be sublicensed, assigned, or transferred by you to any other person without Springer Science + Business Media's written permission.

No Amendment Except in Writing

This license may not be amended except in a writing signed by both parties (or, in the case of Springer Science + Business Media, by CCC on Springer Science + Business Media's behalf).

Objection to Contrary Terms

Springer Science + Business Media hereby objects to any terms contained in any purchase order, acknowledgment, check endorsement or other writing prepared by you, which terms are inconsistent with these terms and conditions or CCC's Billing and Payment terms and conditions. These terms and conditions, together with CCC's Billing and Payment terms and conditions (which are incorporated herein), comprise the entire agreement between you and Springer Science + Business Media (and CCC) concerning this licensing transaction. In the event of any conflict between your obligations established by these terms and conditions and those established by CCC's Billing and Payment terms and conditions, these terms and conditions shall control.

Jurisdiction

All disputes that may arise in connection with this present License, or the breach thereof, shall be settled exclusively by arbitration, to be held in The Netherlands, in accordance with Dutch law, and to be conducted under the Rules of the 'Netherlands Arbitrage Instituut' (Netherlands Institute of Arbitration).**OR:**

All disputes that may arise in connection with this present License, or the breach thereof, shall be settled exclusively by arbitration, to be held in the Federal Republic of Germany, in accordance with German law.

Other terms and conditions:

v1.3

If you would like to pay for this license now, please remit this license along with your

payment made payable to "COPYRIGHT CLEARANCE CENTER" otherwise you will be invoiced within 48 hours of the license date. Payment should be in the form of a check or money order referencing your account number and this invoice number 501306727. Once you receive your invoice for this order, you may pay your invoice by credit card. Please follow instructions provided at that time.

**Make Payment To:
Copyright Clearance Center
Dept 001
P.O. Box 843006
Boston, MA 02284-3006**

For suggestions or comments regarding this order, contact RightsLink Customer Support: customercare@copyright.com or +1-877-622-5543 (toll free in the US) or +1-978-646-2777.


Gratis licenses (referencing \$0 in the Total field) are free. Please retain this printable license for your reference. No payment is required.

NATURE PUBLISHING GROUP LICENSE TERMS AND CONDITIONS

Mar 18, 2014

This is a License Agreement between Youngjik Choi ("You") and Nature Publishing Group ("Nature Publishing Group") provided by Copyright Clearance Center ("CCC"). The license consists of your order details, the terms and conditions provided by Nature Publishing Group, and the payment terms and conditions.

All payments must be made in full to CCC. For payment instructions, please see information listed at the bottom of this form.

License Number	
License date	Mar 18, 2014
Licensed content publisher	Nature Publishing Group
Licensed content publication	Nature Reviews Molecular Cell Biology
Licensed content title	Membrane lipids: where they are and how they behave
Licensed content author	Gerrit van Meer, Dennis R. Voelker and Gerald W. Feigenson
Licensed content date	Feb 1, 2008
Volume number	9
Issue number	2
Type of Use	reuse in a dissertation / thesis
Requestor type	academic/educational
Format	print and electronic
Portion	figures/tables/illustrations
Number of figures/tables/illustrations	1
High-res required	no
Figures	Figure, Box1
Author of this NPG article	no
Your reference number	
Title of your thesis / dissertation	NANOSCALE CHARACTERIZATION OF MELATONIN AND AMYLOID BETA IN MODEL MEMBRANES - IN RELATION TO ALZHEIMER'S DISEASE
Expected completion date	Apr 2014
Estimated size (number of	250

pages)

Total 0.00 USD

[Terms and Conditions](#)

Terms and Conditions for Permissions

Nature Publishing Group hereby grants you a non-exclusive license to reproduce this material for this purpose, and for no other use, subject to the conditions below:

1. NPG warrants that it has, to the best of its knowledge, the rights to license reuse of this material. However, you should ensure that the material you are requesting is original to Nature Publishing Group and does not carry the copyright of another entity (as credited in the published version). If the credit line on any part of the material you have requested indicates that it was reprinted or adapted by NPG with permission from another source, then you should also seek permission from that source to reuse the material.
2. Permission granted free of charge for material in print is also usually granted for any electronic version of that work, provided that the material is incidental to the work as a whole and that the electronic version is essentially equivalent to, or substitutes for, the print version. Where print permission has been granted for a fee, separate permission must be obtained for any additional, electronic re-use (unless, as in the case of a full paper, this has already been accounted for during your initial request in the calculation of a print run). NB: In all cases, web-based use of full-text articles must be authorized separately through the 'Use on a Web Site' option when requesting permission.
3. Permission granted for a first edition does not apply to second and subsequent editions and for editions in other languages (except for signatories to the STM Permissions Guidelines, or where the first edition permission was granted for free).
4. Nature Publishing Group's permission must be acknowledged next to the figure, table or abstract in print. In electronic form, this acknowledgement must be visible at the same time as the figure/table/abstract, and must be hyperlinked to the journal's homepage.
5. The credit line should read:
Reprinted by permission from Macmillan Publishers Ltd: [JOURNAL NAME] (reference citation), copyright (year of publication)
For AOP papers, the credit line should read:
Reprinted by permission from Macmillan Publishers Ltd: [JOURNAL NAME], advance online publication, day month year (doi: 10.1038/sj.[JOURNAL ACRONYM].XXXXX)

Note: For republication from the *British Journal of Cancer*, the following credit lines apply.

Reprinted by permission from Macmillan Publishers Ltd on behalf of Cancer Research UK: [JOURNAL NAME] (reference citation), copyright (year of publication) For AOP papers, the credit line should read:
Reprinted by permission from Macmillan Publishers Ltd on behalf of Cancer Research UK: [JOURNAL NAME], advance online publication, day month year (doi: 10.1038/sj.[JOURNAL ACRONYM].XXXXX)

6. Adaptations of single figures do not require NPG approval. However, the adaptation should be credited as follows:

Example 1: Springer Science + Business Media makes no representations or warranties with respect to the licensed material.

Example 2: Springer Science + Business Media makes no representations or warranties with respect to the licensed material and adopts on its own behalf the limitations and disclaimers established by CCC on its behalf in its Billing and Payment terms and conditions for this licensing transaction.

Indemnity

You hereby indemnify and agree to hold harmless Springer Science + Business Media and CCC, and their respective officers, directors, employees and agents, from and against any and all claims arising out of your use of the licensed material other than as specifically authorized pursuant to this license.

No Transfer of License

This license is personal to you and may not be sublicensed, assigned, or transferred by you to any other person without Springer Science + Business Media's written permission.

No Amendment Except in Writing

This license may not be amended except in a writing signed by both parties (or, in the case of Springer Science + Business Media, by CCC on Springer Science + Business Media's behalf).

Objection to Contrary Terms

Springer Science + Business Media hereby objects to any terms contained in any purchase order, acknowledgment, check endorsement or other writing prepared by you, which terms are inconsistent with these terms and conditions or CCC's Billing and Payment terms and conditions. These terms and conditions, together with CCC's Billing and Payment terms and conditions (which are incorporated herein), comprise the entire agreement between you and Springer Science + Business Media (and CCC) concerning this licensing transaction. In the event of any conflict between your obligations established by these terms and conditions and those established by CCC's Billing and Payment terms and conditions, these terms and conditions shall control.

Jurisdiction

All disputes that may arise in connection with this present License, or the breach thereof, shall be settled exclusively by arbitration, to be held in The Netherlands, in accordance with Dutch law, and to be conducted under the Rules of the 'Netherlands Arbitrage Instituut' (Netherlands Institute of Arbitration).**OR:**

All disputes that may arise in connection with this present License, or the breach thereof, shall be settled exclusively by arbitration, to be held in the Federal Republic of Germany, in accordance with German law.

Other terms and conditions:

v1.3

If you would like to pay for this license now, please remit this license along with your

Adapted by permission from Macmillan Publishers Ltd: [JOURNAL NAME] (reference citation), copyright (year of publication)

Note: For adaptation from the *British Journal of Cancer*, the following credit line applies.

Adapted by permission from Macmillan Publishers Ltd on behalf of Cancer Research UK: [JOURNAL NAME] (reference citation), copyright (year of publication)

7. Translations of 401 words up to a whole article require NPG approval. Please visit <http://www.macmillanmedicalcommunications.com> for more information. Translations of up to a 400 words do not require NPG approval. The translation should be credited as follows:

Translated by permission from Macmillan Publishers Ltd: [JOURNAL NAME] (reference citation), copyright (year of publication).

Note: For translation from the *British Journal of Cancer*, the following credit line applies.

Translated by permission from Macmillan Publishers Ltd on behalf of Cancer Research UK: [JOURNAL NAME] (reference citation), copyright (year of publication)

We are certain that all parties will benefit from this agreement and wish you the best in the use of this material. Thank you.

Special Terms:

v1.1

If you would like to pay for this license now, please remit this license along with your payment made payable to "COPYRIGHT CLEARANCE CENTER" otherwise you will be invoiced within 48 hours of the license date. Payment should be in the form of a check or money order referencing your account number and this invoice number RLNK501254325.

Once you receive your invoice for this order, you may pay your invoice by credit card. Please follow instructions provided at that time.

**Make Payment To:
Copyright Clearance Center
Dept 001
P.O. Box 843006
Boston, MA 02284-3006**

For suggestions or comments regarding this order, contact RightsLink Customer Support: customercare@copyright.com or +1-877-622-5543 (toll free in the US) or +1-978-646-2777.

Gratis licenses (referencing \$0 in the Total field) are free. Please retain this printable license for your reference. No payment is required.

payment made payable to "COPYRIGHT CLEARANCE CENTER" otherwise you will be invoiced within 48 hours of the license date. Payment should be in the form of a check or money order referencing your account number and this invoice number 501306727. Once you receive your invoice for this order, you may pay your invoice by credit card. Please follow instructions provided at that time.

**Make Payment To:
Copyright Clearance Center
Dept 001
P.O. Box 843006
Boston, MA 02284-3006**

For suggestions or comments regarding this order, contact RightsLink Customer Support: customercare@copyright.com or +1-877-622-5543 (toll free in the US) or +1-978-646-2777.


Gratis licenses (referencing \$0 in the Total field) are free. Please retain this printable license for your reference. No payment is required.

**NATURE PUBLISHING GROUP LICENSE
TERMS AND CONDITIONS**

Mar 18, 2014

This is a License Agreement between Youngjik Choi ("You") and Nature Publishing Group ("Nature Publishing Group") provided by Copyright Clearance Center ("CCC"). The license consists of your order details, the terms and conditions provided by Nature Publishing Group, and the payment terms and conditions.

All payments must be made in full to CCC. For payment instructions, please see information listed at the bottom of this form.

License Number	
License date	Mar 18, 2014
Licensed content publisher	Nature Publishing Group
Licensed content publication	Nature
Licensed content title	Emerging roles for lipids in shaping membrane-protein function
Licensed content author	Rob Phillips, Tristan Ursell, Paul Wiggins and Pierre Sens
Licensed content date	May 20, 2009
Volume number	459
Issue number	7245
Type of Use	reuse in a dissertation / thesis
Requestor type	academic/educational
Format	print and electronic
Portion	figures/tables/illustrations
Number of figures/tables/illustrations	1
High-res required	no
Figures	Figure 1
Author of this NPG article	no
Your reference number	
Title of your thesis / dissertation	NANOSCALE CHARACTERIZATION OF MELATONIN AND AMYLOID BETA IN MODEL MEMBRANES - IN RELATION TO ALZHEIMER'S DISEASE
Expected completion date	Apr 2014
Estimated size (number of	250

pages)

Total 0.00 USD

[Terms and Conditions](#)

Terms and Conditions for Permissions

Nature Publishing Group hereby grants you a non-exclusive license to reproduce this material for this purpose, and for no other use, subject to the conditions below:

1. NPG warrants that it has, to the best of its knowledge, the rights to license reuse of this material. However, you should ensure that the material you are requesting is original to Nature Publishing Group and does not carry the copyright of another entity (as credited in the published version). If the credit line on any part of the material you have requested indicates that it was reprinted or adapted by NPG with permission from another source, then you should also seek permission from that source to reuse the material.
2. Permission granted free of charge for material in print is also usually granted for any electronic version of that work, provided that the material is incidental to the work as a whole and that the electronic version is essentially equivalent to, or substitutes for, the print version. Where print permission has been granted for a fee, separate permission must be obtained for any additional, electronic re-use (unless, as in the case of a full paper, this has already been accounted for during your initial request in the calculation of a print run). NB: In all cases, web-based use of full-text articles must be authorized separately through the 'Use on a Web Site' option when requesting permission.
3. Permission granted for a first edition does not apply to second and subsequent editions and for editions in other languages (except for signatories to the STM Permissions Guidelines, or where the first edition permission was granted for free).
4. Nature Publishing Group's permission must be acknowledged next to the figure, table or abstract in print. In electronic form, this acknowledgement must be visible at the same time as the figure/table/abstract, and must be hyperlinked to the journal's homepage.
5. The credit line should read:
Reprinted by permission from Macmillan Publishers Ltd: [JOURNAL NAME] (reference citation), copyright (year of publication)
For AOP papers, the credit line should read:
Reprinted by permission from Macmillan Publishers Ltd: [JOURNAL NAME], advance online publication, day month year (doi: 10.1038/sj.[JOURNAL ACRONYM].XXXXX)

Note: For republication from the *British Journal of Cancer*, the following credit lines apply.

Reprinted by permission from Macmillan Publishers Ltd on behalf of Cancer Research UK: [JOURNAL NAME] (reference citation), copyright (year of publication) For AOP papers, the credit line should read:
Reprinted by permission from Macmillan Publishers Ltd on behalf of Cancer Research UK: [JOURNAL NAME], advance online publication, day month year (doi: 10.1038/sj.[JOURNAL ACRONYM].XXXXX)

6. Adaptations of single figures do not require NPG approval. However, the adaptation should be credited as follows:

Adapted by permission from Macmillan Publishers Ltd: [JOURNAL NAME] (reference citation), copyright (year of publication)

Note: For adaptation from the *British Journal of Cancer*, the following credit line applies.

Adapted by permission from Macmillan Publishers Ltd on behalf of Cancer Research UK: [JOURNAL NAME] (reference citation), copyright (year of publication)

7. Translations of 401 words up to a whole article require NPG approval. Please visit <http://www.macmillanmedicalcommunications.com> for more information. Translations of up to a 400 words do not require NPG approval. The translation should be credited as follows:

Translated by permission from Macmillan Publishers Ltd: [JOURNAL NAME] (reference citation), copyright (year of publication).

Note: For translation from the *British Journal of Cancer*, the following credit line applies.

Translated by permission from Macmillan Publishers Ltd on behalf of Cancer Research UK: [JOURNAL NAME] (reference citation), copyright (year of publication)

We are certain that all parties will benefit from this agreement and wish you the best in the use of this material. Thank you.

Special Terms:

v1.1

If you would like to pay for this license now, please remit this license along with your payment made payable to "COPYRIGHT CLEARANCE CENTER" otherwise you will be invoiced within 48 hours of the license date. Payment should be in the form of a check or money order referencing your account number and this invoice number RLNK501254321.

Once you receive your invoice for this order, you may pay your invoice by credit card. Please follow instructions provided at that time.

**Make Payment To:
Copyright Clearance Center
Dept 001
P.O. Box 843006
Boston, MA 02284-3006**

For suggestions or comments regarding this order, contact RightsLink Customer Support: customercare@copyright.com or +1-877-622-5543 (toll free in the US) or +1-978-646-2777.

Gratis licenses (referencing \$0 in the Total field) are free. Please retain this printable license for your reference. No payment is required.

REPRINTS AND PERMISSIONS

Welcome to our Permissions and Reprints Guidelines page. Here you will find information about how to request permission to reproduce content published in our journals and web publications in new works as well as information on how to order print and e-copies of individual articles.

DO I NEED REPRINTS OR PERMISSION?

ORDERING REPRINTS

- › Author Reprints
- › Commercial Reprints
- › Ordering Commercial Reprints, E–prints, Translations
- › Commercial Reprints Alerting Service
- › Multiple article reprints
- › Issue reprints

REQUESTING PERMISSION

- › Permission for Authors
- › Submitting your permission request
- › What if Rightslink can't process my permission request?
- › How do I get permission to distribute copies of articles for classroom use?
- › How do I get permission to reproduce content in my thesis or dissertation?

REPRINTS OR PERMISSION?

If you wish to distribute copies of a single article to others, you might consider purchasing reprints. Our reprint service will enable you to purchase print copies of individual articles as well as e–prints. Custom reprint options are also available. If you are an Author seeking reprints of your article, [click here](#) for further information about Author Reprints. If you are not an author, [click here](#) for further information about Commercial Reprints.

If you wish to take material from *Science's* journals or websites (figures, extracts, abstracts, even full-text articles) and incorporate them into new works (for example, newsletters, journal articles, book chapters, posters, presentations, reports, film, etc.), you will need to obtain copyright permission. [Click here](#) to go to the instructions for requesting permission to reproduce/republish material from *Science's* journals and websites.

If you are not currently a subscriber and simply wish to obtain a single copy of an article for your own personal review, you may purchase either a fax copy of a single article or a PDF, or you may purchase 24-hour access to the article and its supplemental online materials by [clicking here](#) and selecting the preferred option.

ORDERING REPRINTS

Author Reprints*

Author reprints are administered and produced by Sheridan Reprints. For information or to place an order, [click here](#) and use our Author Reprint order form, or contact:

Cindy Eyler
The Sheridan Press
450 Fame Avenue

Hanover, PA 17331
Phone: (800) 635-7181
Fax: (717) 633-8929

E-mail: cindy.eyler@sheridan.com

***Author reprints are solely for the author's personal, noncommercial use. For other uses, including use by an author's employer, see Commercial Reprints below.**

Commercial Reprints

Science and its sister journals contain some of the most highly cited and influential articles in the world.

AAAS commercial reprints are high quality, with specially designed covers and customization options. The reprints are an exact replica of the published article. All reprints are printed double-sided on premium 70# glossy paper in multiples of 100 copies. Title page covers may be included. These covers include the journal's logo, article title, author name(s), and citation information. Alternatively, if not subject to copyright restrictions, the issue cover of the desired journal may be added for an additional fee.

Reprints are saddle stitched unless the article is 3-4 pages, in which case the reprint is folded. Customers may purchase standard reprints in black and white or in color. Articles containing color may be purchased in black and white for which conversion charges will apply. Please be sure to carefully consider whether you can accept a color article in black and white.

Shrink-wrapping in bundles is recommended and offered at a small additional cost.

Customization options are available at extra cost:

- › Addition of disclaimer text and product codes
- › Addition of product information
- › Addition of a company name and/or logo
- › Addition of supplemental online material
- › Addition of a reproduction of the journal cover within which the article was published (when not restricted by copyright)

Orders can be shipped to more than one shipping location.

Standard reprints are shipped within 8-12 business days from proof approval. Rush Schedule Reprints are shipped within 5-7 business days from proof approval for an additional fee. Note: Customizations increase processing time.

Reprints are shipped via Federal Express Standard or comparable service. Note: FEDEX does not ship to all countries and territories. For the most current information, see the FEDEX website at <http://www.fedex.com>.

The price of reprints depends on the number of pages in the article, the number of reprints ordered, whether the reprints contain color, if additional permission needs to be secured, and whether you require any custom options such as the addition of your product information or logo.

Every reprint requires the approval of the customer prior to printing and billing. Proofs will be provided by our reprint vendor, or from an AAAS Commercial Reprints Representative.

Ordering Commercial Reprints, E-Prints, Translations

Please contact Beth Ann Rocheleau at 803-359-4578 / aaas@rockwaterinc.com.

Commercial Reprints Alerting Service

If you would like to receive a monthly e-mail alert highlighting recently published content of commercial interest, please go to: <http://www.sciencemag.org/cgi/alerts/main> to sign up for the alert.

To have our agent monitor your alerts and notify you when new content is published that may be of interest to you, please contact Beth Ann Rocheleau 803-359-4578 / aaas@rockwaterinc.com

Multiple Article Reprints

To reprint an entire supplement, please contact Beth Ann Rocheleau at 803-359-4578 / aaas@rockwaterinc.com for availability and pricing.

To combine various articles into a reprint collection, including sponsorship opportunities, please contact your regional sales representative or our Director of Worldwide Advertising bmoran@aaas.org

2. Your complete mailing address, phone number, and fax number

Identify the content you wish to use:

1. AAAS publication title (*Science*; *Science Classic*; *ScienceNOW*; *Science Careers*; *Science Signaling* (or STKE); *Science Translational Medicine*; *Science Express*; *AIDScience*; or SAGE KE)
2. Article title
3. Authors' names
4. Volume number, issue date, page numbers (provide all that apply)
5. Specific figure numbers or portion of text (or supply a photocopy)

Include the following information about your intended use:

1. Type of work in which our material will be used (e.g., book, journal, newsletter, poster, etc.)
2. Title of work in which *Science* material will appear
3. Title of article/chapter (if you are using the material in a journal, newspaper, newsletter, or book)
4. Author(s)/editor(s)
5. Expected publication date (or volume and issue number for journals)
6. Publishing company
7. Retail price (for books only)
8. Print run (for books only)
9. Intended audience for the work

If you wish to reprint the material on the World Wide Web (in cases where content is available online, we may grant linking privileges rather than republication rights), please also include the following:

1. Your website's URL
2. Website's sponsoring organization/company
3. Whether the sponsor is a for-profit or nonprofit organization
4. Description of the purpose and nature of your website
5. Description of the website's visitors (customers, scholars, professors, etc.)
6. Whether the site is password protected

If you wish to reproduce the material for purposes other than those described above, please write a description of your project, including the title of your project, the number of copies to be made, the format (e.g., print copies, PowerPoint presentation, poster, media kit, etc.), targeted recipients, expected distribution date, and proposed selling price.

Please e-mail your request to permissions@aaas.org. All requests are reviewed and responded to in the order of receipt. All responses will be e-mailed, and, if permission is granted, the terms and conditions and any permissions fees will be e-mailed as an attachment. Our turnaround time ranges between 2 and 15 business days, depending upon the volume of requests we receive and the complexity of your particular request.

For educational photocopies (coursepacks, classroom handouts, electronic classroom use) contact:

Copyright Clearance Center
APS Customer Service
222 Rosewood Dr.
Danvers, MA 01923
Phone: (978) 750-8400
Fax: (978) 750-4470

Reproducing AAAS Material in your Thesis or Dissertation

NOTE: If you are the Original Author of the AAAS article being reproduced, please refer to your License to Publish for rules on reproducing your paper in a dissertation or thesis. AAAS permits the use of content published in its journals *Science*, *Science Technical Medicine*, and *Science Signaling*, but only provided the following criteria are met.

1. If you are using figure(s)/table(s), permission is granted for use in print and electronic versions of your dissertation or thesis.
2. A full text article may be used only in print versions of a dissertation or thesis. AAAS does not permit the reproduction of full text articles in electronic versions of theses or dissertations.
3. The following credit line must be printed along with the AAAS material: "From [Full Reference Citation]. Reprinted with permission from AAAS."
4. All required credit lines and notices must be visible any time a user accesses any part of the AAAS material and must appear on any printed copies that an authorized user might make.
5. The AAAS material may not be modified or altered except that figures and tables may be modified with permission from the author. Author permission for any such changes must be secured prior to

to discuss options and pricing.

Issue Reprints

Complete journal issue reprints are not available. To order back issues, please go to [click here](#) for availability and pricing.

REQUESTING PERMISSIONS

Permission is required before reproducing any content (text, photos, tables, figures) from:

- › *Science*
- › *Science Careers*
- › *Science Classic* (digital archive of *Science* issues published 1880 – 1996)
- › *Science Express*
- › *ScienceNOW*
- › *Science Signaling*/STKE
- › *Science Translational Medicine*
- › AIDScience
- › SAGE KE

Permission for Authors

If you are the author of the article that was published in a *Science* journal or on a *Science* website, you retain the rights to make a number of uses of your paper and its contents as automatically permitted under AAAS's License to Publish. Please [click here](#) and see our Information for Authors document for a detailed description of these rights. If you wish to use your paper in ways that are not covered under the License to Publish, please submit your request to our Permissions Department in accordance with the guidelines below.

Submit Your Permission Request Using Rightslink

If you are seeking permission to copy/reproduce/republish content from *Science*, *Science Signaling*, or *Science Translational Medicine* and are not the author of that content, you may use the Copyright Clearance Center's Rightslink® service. If you are seeking permission to use content from one of the other AAAS publications listed above, please see our [Special Request Guidelines](#) below for further instructions.

With Copyright Clearance Center's Rightslink® service it is faster and easier than ever before to secure permission for material from *Science* to be republished in your thesis, journal article, book, newsletter, or other publication. Simply visit www.sciencemag.org and locate your desired content (we suggest using the journal's Advanced Search engine). Once you have found the article you are looking for:

- › Click on either the article abstract/summary or the Full Text view
- › Click on the Get Permission or Reprints link which appears in the menu bar on the left side of your screen
- › Once you are in Rightslink®, create an account if you do not already have one
- › Select the use you wish to make
- › Click to accept the terms and conditions

Confirmation of your permission and a copy of the permission terms and conditions will be sent to you instantly via e-mail.

If you have questions about using the Rightslink® service, please contact Customer Support at (877) 622-5543 (toll free) or (978) 777-9929, or e-mail customer@copyright.com.

If you are unable to locate the material you wish to use or you are unable to secure the rights you are seeking, please e-mail us at permissions@aaas.org, providing the details outlined below.

Special Request Guidelines

While Rightslink® processes the most commonly requested uses, Rightslink® does not grant permissions for all types of uses. You might be directed to contact the AAAS Permissions Department directly, depending upon your request. If you are prompted to contact us, please e-mail us the following details (note: the more details you provide, the faster your request is likely to be processed):

1. Your name, institute, and title

your use.

6. AAAS must publish the full paper prior to your use of any of its text or figures.
7. If the AAAS material covered by this permission was published in *Science* during the years 1974–1994, you must also obtain permission from the author, who may grant or withhold permission, and who may or may not charge a fee if permission is granted. See original article for author's address. This condition does not apply to news articles.
8. If you are an Original Author on the AAAS article being reproduced, please refer to your License to Publish for rules on reproducing your paper in a dissertation or thesis.

Permission covers the distribution of your dissertation or thesis on demand by a third party distributor (e.g. ProQuest / UMI), provided the AAAS material covered by this permission remains in situ and is not distributed by that third party outside of the context of your Thesis/Dissertation.

Permission does not apply to figures/photos/artwork or any other content or materials included in your work that are credited to non-AAAS sources. If the requested material is sourced to or references non-AAAS sources, you must obtain authorization from that source as well before using that material. You agree to hold harmless and indemnify AAAS against any claims arising from your use of any content in your work that is credited to non-AAAS sources.

By using the AAAS Material identified in your request, you agree to abide by all the terms and conditions herein.

AAAS makes no representations or warranties as to the accuracy of any information contained in the AAAS material covered by this permission, including any warranties of merchantability or fitness for a particular purpose.


Questions about these terms can be directed to the AAAS Permissions department at permissions@aaas.org.

NATURE PUBLISHING GROUP LICENSE TERMS AND CONDITIONS

Mar 18, 2014

This is a License Agreement between Youngjik Choi ("You") and Nature Publishing Group ("Nature Publishing Group") provided by Copyright Clearance Center ("CCC"). The license consists of your order details, the terms and conditions provided by Nature Publishing Group, and the payment terms and conditions.

All payments must be made in full to CCC. For payment instructions, please see information listed at the bottom of this form.

License Number	
License date	Mar 18, 2014
Licensed content publisher	Nature Publishing Group
Licensed content publication	Nature Reviews Neuroscience
Licensed content title	Linking lipids to Alzheimer's disease: cholesterol and beyond
Licensed content author	Gilbert Di Paolo and Tae-Wan Kim
Licensed content date	Mar 30, 2011
Volume number	12
Issue number	5
Type of Use	reuse in a dissertation / thesis
Requestor type	academic/educational
Format	print and electronic
Portion	figures/tables/illustrations
Number of figures/tables/illustrations	1
High-res required	no
Figures	Figure 2-a
Author of this NPG article	no
Your reference number	
Title of your thesis / dissertation	NANOSCALE CHARACTERIZATION OF MELATONIN AND AMYLOID BETA IN MODEL MEMBRANES - IN RELATION TO ALZHEIMER'S DISEASE
Expected completion date	Apr 2014
Estimated size (number of	250

pages)

Total 0.00 USD

[Terms and Conditions](#)

Terms and Conditions for Permissions

Nature Publishing Group hereby grants you a non-exclusive license to reproduce this material for this purpose, and for no other use, subject to the conditions below:

1. NPG warrants that it has, to the best of its knowledge, the rights to license reuse of this material. However, you should ensure that the material you are requesting is original to Nature Publishing Group and does not carry the copyright of another entity (as credited in the published version). If the credit line on any part of the material you have requested indicates that it was reprinted or adapted by NPG with permission from another source, then you should also seek permission from that source to reuse the material.
2. Permission granted free of charge for material in print is also usually granted for any electronic version of that work, provided that the material is incidental to the work as a whole and that the electronic version is essentially equivalent to, or substitutes for, the print version. Where print permission has been granted for a fee, separate permission must be obtained for any additional, electronic re-use (unless, as in the case of a full paper, this has already been accounted for during your initial request in the calculation of a print run). NB: In all cases, web-based use of full-text articles must be authorized separately through the 'Use on a Web Site' option when requesting permission.
3. Permission granted for a first edition does not apply to second and subsequent editions and for editions in other languages (except for signatories to the STM Permissions Guidelines, or where the first edition permission was granted for free).
4. Nature Publishing Group's permission must be acknowledged next to the figure, table or abstract in print. In electronic form, this acknowledgement must be visible at the same time as the figure/table/abstract, and must be hyperlinked to the journal's homepage.
5. The credit line should read:
Reprinted by permission from Macmillan Publishers Ltd: [JOURNAL NAME] (reference citation), copyright (year of publication)
For AOP papers, the credit line should read:
Reprinted by permission from Macmillan Publishers Ltd: [JOURNAL NAME], advance online publication, day month year (doi: 10.1038/sj.[JOURNAL ACRONYM].XXXXX)

Note: For republication from the *British Journal of Cancer*, the following credit lines apply.

Reprinted by permission from Macmillan Publishers Ltd on behalf of Cancer Research UK: [JOURNAL NAME] (reference citation), copyright (year of publication) For AOP papers, the credit line should read:
Reprinted by permission from Macmillan Publishers Ltd on behalf of Cancer Research UK: [JOURNAL NAME], advance online publication, day month year (doi: 10.1038/sj.[JOURNAL ACRONYM].XXXXX)

6. Adaptations of single figures do not require NPG approval. However, the adaptation should be credited as follows:

Adapted by permission from Macmillan Publishers Ltd: [JOURNAL NAME] (reference citation), copyright (year of publication)

Note: For adaptation from the *British Journal of Cancer*, the following credit line applies.

Adapted by permission from Macmillan Publishers Ltd on behalf of Cancer Research UK: [JOURNAL NAME] (reference citation), copyright (year of publication)

7. Translations of 401 words up to a whole article require NPG approval. Please visit <http://www.macmillanmedicalcommunications.com> for more information. Translations of up to a 400 words do not require NPG approval. The translation should be credited as follows:

Translated by permission from Macmillan Publishers Ltd: [JOURNAL NAME] (reference citation), copyright (year of publication).

Note: For translation from the *British Journal of Cancer*, the following credit line applies.

Translated by permission from Macmillan Publishers Ltd on behalf of Cancer Research UK: [JOURNAL NAME] (reference citation), copyright (year of publication)

We are certain that all parties will benefit from this agreement and wish you the best in the use of this material. Thank you.

Special Terms:

v1.1

If you would like to pay for this license now, please remit this license along with your payment made payable to "COPYRIGHT CLEARANCE CENTER" otherwise you will be invoiced within 48 hours of the license date. Payment should be in the form of a check or money order referencing your account number and this invoice number RLNK501254316.

Once you receive your invoice for this order, you may pay your invoice by credit card. Please follow instructions provided at that time.

**Make Payment To:
Copyright Clearance Center
Dept 001
P.O. Box 843006
Boston, MA 02284-3006**

For suggestions or comments regarding this order, contact RightsLink Customer Support: customercare@copyright.com or +1-877-622-5543 (toll free in the US) or +1-978-646-2777.

Gratis licenses (referencing \$0 in the Total field) are free. Please retain this printable license for your reference. No payment is required.

Company Info

- At a glance
- Elsevier locations
- Mission
- Senior management
- Experts ▶
- Subject information
- Publishing guidelines ▶
- Corporate responsibility ▶
- Open access ▼
 - Open access journals
 - Open access articles
 - Open archives
 - Green open access
- Funding body agreements
- Institutional agreements
- Policies**
- Elsevier and open access
- Universal access ▶
- Company history ▶
- Annual reports
- Press releases ▶
- Conferences
- Exhibitions
- Content innovation ▶
- Careers
- Social Media

Elsevier user license

Articles published under an Elsevier user license are protected by copyright and may be used for non-commercial purposes. Users may access, download, copy, display, redistribute, adapt, translate, text mine and data mine the articles provided that users:

- Cite the article using an appropriate bibliographic citation (i.e. author(s), journal, article title, volume, issue, page numbers, DOI and the link to the definitive published version on ScienceDirect)
- Use the article for non-commercial purposes
- Maintain the integrity of the article
- Retain copyright notices and links to these terms and conditions so it is clear to other users what can and cannot be done with the article
- Ensure that, for any content in the article that is identified as belonging to a third party, any re-use complies with the copyright policies of that third party
- Any translations, for which a prior translation agreement with Elsevier has not been established, must prominently display the statement: "This is an unofficial translation of an article that appeared in an Elsevier publication. Elsevier has not endorsed this translation."

For permission to use documents beyond permitted here, visit our [Support & Contact website](#).

This is a non commercial license where the use of published articles for commercial purposes is prohibited.

Commercial purposes include:
Copying or downloading articles, or linking to such postings, for further redistribution, sale or licensing, for a fee
Copying, downloading or posting by a site or service that incorporates advertising with such content
The inclusion or incorporation of article content in other works or services (other than normal quotations with an appropriate citation) that is then available for sale or licensing, for a fee
Use of articles or article content (other than normal quotations with appropriate citation) by for-profit organizations for promotional purposes, whether for a fee or otherwise.
Use for the purposes of monetary reward by means of sale, resale, license, loan, transfer or other form of commercial exploitation.



**ELSEVIER LICENSE
TERMS AND CONDITIONS**

Mar 18, 2014

This is a License Agreement between Youngjik Choi ("You") and Elsevier ("Elsevier") provided by Copyright Clearance Center ("CCC"). The license consists of your order details, the terms and conditions provided by Elsevier, and the payment terms and conditions.

All payments must be made in full to CCC. For payment instructions, please see information listed at the bottom of this form.

Supplier	Elsevier Limited The Boulevard, Langford Lane Kidlington, Oxford, OX5 1GB, UK
Registered Company Number	1982084
Customer name	Youngjik Choi
Customer address	430 Ashby Court Waterloo, ON N2T1H1
License number	[REDACTED]
License date	Mar 18, 2014
Licensed content publisher	Elsevier
Licensed content publication	Biochimica et Biophysica Acta (BBA) - Biomembranes
Licensed content title	Analysis of nanoprobe penetration through a lipid bilayer
Licensed content author	Fei Liu, Dan Wu, Roger D. Kamm, Ken Chen
Licensed content date	August 2013
Licensed content volume number	1828
Licensed content issue number	8
Number of pages	7
Start Page	1667
End Page	1673
Type of Use	reuse in a thesis/dissertation
Portion	figures/tables/illustrations
Number of figures/tables/illustrations	1

Format	both print and electronic
Are you the author of this Elsevier article?	No
Will you be translating?	No
Title of your thesis/dissertation	NANOSCALE CHARACTERIZATION OF MELATONIN AND AMYLOID BETA IN MODEL MEMBRANES - IN RELATION TO ALZHEIMER'S DISEASE
Expected completion date	Apr 2014
Estimated size (number of pages)	250
Elsevier VAT number	GB 494 6272 12
Permissions price	0.00 USD
VAT/Local Sales Tax	0.00 USD / 0.00 GBP
Total	0.00 USD
Terms and Conditions	

INTRODUCTION

1. The publisher for this copyrighted material is Elsevier. By clicking "accept" in connection with completing this licensing transaction, you agree that the following terms and conditions apply to this transaction (along with the Billing and Payment terms and conditions established by Copyright Clearance Center, Inc. ("CCC"), at the time that you opened your Rightslink account and that are available at any time at <http://myaccount.copyright.com>).

GENERAL TERMS

2. Elsevier hereby grants you permission to reproduce the aforementioned material subject to the terms and conditions indicated.

3. Acknowledgement: If any part of the material to be used (for example, figures) has appeared in our publication with credit or acknowledgement to another source, permission must also be sought from that source. If such permission is not obtained then that material may not be included in your publication/copies. Suitable acknowledgement to the source must be made, either as a footnote or in a reference list at the end of your publication, as follows:

“Reprinted from Publication title, Vol /edition number, Author(s), Title of article / title of chapter, Pages No., Copyright (Year), with permission from Elsevier [OR APPLICABLE SOCIETY COPYRIGHT OWNER].” Also Lancet special credit - “Reprinted from The Lancet, Vol. number, Author(s), Title of article, Pages No., Copyright (Year), with permission from Elsevier.”

4. Reproduction of this material is confined to the purpose and/or media for which permission is hereby given.

5. Altering/Modifying Material: Not Permitted. However figures and illustrations may be altered/adapted minimally to serve your work. Any other abbreviations, additions, deletions and/or any other alterations shall be made only with prior written authorization of Elsevier Ltd. (Please contact Elsevier at permissions@elsevier.com)
6. If the permission fee for the requested use of our material is waived in this instance, please be advised that your future requests for Elsevier materials may attract a fee.
7. Reservation of Rights: Publisher reserves all rights not specifically granted in the combination of (i) the license details provided by you and accepted in the course of this licensing transaction, (ii) these terms and conditions and (iii) CCC's Billing and Payment terms and conditions.
8. License Contingent Upon Payment: While you may exercise the rights licensed immediately upon issuance of the license at the end of the licensing process for the transaction, provided that you have disclosed complete and accurate details of your proposed use, no license is finally effective unless and until full payment is received from you (either by publisher or by CCC) as provided in CCC's Billing and Payment terms and conditions. If full payment is not received on a timely basis, then any license preliminarily granted shall be deemed automatically revoked and shall be void as if never granted. Further, in the event that you breach any of these terms and conditions or any of CCC's Billing and Payment terms and conditions, the license is automatically revoked and shall be void as if never granted. Use of materials as described in a revoked license, as well as any use of the materials beyond the scope of an unrevoked license, may constitute copyright infringement and publisher reserves the right to take any and all action to protect its copyright in the materials.
9. Warranties: Publisher makes no representations or warranties with respect to the licensed material.
10. Indemnity: You hereby indemnify and agree to hold harmless publisher and CCC, and their respective officers, directors, employees and agents, from and against any and all claims arising out of your use of the licensed material other than as specifically authorized pursuant to this license.
11. No Transfer of License: This license is personal to you and may not be sublicensed, assigned, or transferred by you to any other person without publisher's written permission.
12. No Amendment Except in Writing: This license may not be amended except in a writing signed by both parties (or, in the case of publisher, by CCC on publisher's behalf).
13. Objection to Contrary Terms: Publisher hereby objects to any terms contained in any purchase order, acknowledgment, check endorsement or other writing prepared by you, which terms are inconsistent with these terms and conditions or CCC's Billing and Payment terms and conditions. These terms and conditions, together with CCC's Billing and Payment terms and conditions (which are incorporated herein), comprise the entire agreement between you and publisher (and CCC) concerning this licensing transaction. In the event of any conflict between your obligations established by these terms and conditions and those established by CCC's Billing and Payment terms and conditions, these terms and conditions

shall control.

14. **Revocation:** Elsevier or Copyright Clearance Center may deny the permissions described in this License at their sole discretion, for any reason or no reason, with a full refund payable to you. Notice of such denial will be made using the contact information provided by you. Failure to receive such notice will not alter or invalidate the denial. In no event will Elsevier or Copyright Clearance Center be responsible or liable for any costs, expenses or damage incurred by you as a result of a denial of your permission request, other than a refund of the amount(s) paid by you to Elsevier and/or Copyright Clearance Center for denied permissions.

LIMITED LICENSE

The following terms and conditions apply only to specific license types:

15. **Translation:** This permission is granted for non-exclusive world **English** rights only unless your license was granted for translation rights. If you licensed translation rights you may only translate this content into the languages you requested. A professional translator must perform all translations and reproduce the content word for word preserving the integrity of the article. If this license is for use 1 or 2 figures then permission is granted for non-exclusive world rights in all languages.

16. **Posting licensed content on any Website:** The following terms and conditions apply as follows: Licensing material from an Elsevier journal: All content posted to the web site must maintain the copyright information line on the bottom of each image; A hyper-text must be included to the Homepage of the journal from which you are licensing at <http://www.sciencedirect.com/science/journal/xxxxx> or the Elsevier homepage for books at <http://www.elsevier.com>; Central Storage: This license does not include permission for a scanned version of the material to be stored in a central repository such as that provided by Heron/XanEdu.

Licensing material from an Elsevier book: A hyper-text link must be included to the Elsevier homepage at <http://www.elsevier.com>. All content posted to the web site must maintain the copyright information line on the bottom of each image.

Posting licensed content on Electronic reserve: In addition to the above the following clauses are applicable: The web site must be password-protected and made available only to bona fide students registered on a relevant course. This permission is granted for 1 year only. You may obtain a new license for future website posting.

For journal authors: the following clauses are applicable in addition to the above: Permission granted is limited to the author accepted manuscript version* of your paper.

***Accepted Author Manuscript (AAM) Definition:** An accepted author manuscript (AAM) is the author's version of the manuscript of an article that has been accepted for publication and which may include any author-incorporated changes suggested through the processes of submission processing, peer review, and editor-author communications. AAMs do not include other publisher value-added contributions such as copy-editing, formatting, technical enhancements and (if relevant) pagination.

You are not allowed to download and post the published journal article (whether PDF or HTML, proof or final version), nor may you scan the printed edition to create an electronic version. A hyper-text must be included to the Homepage of the journal from which you are licensing at <http://www.sciencedirect.com/science/journal/xxxxx>. As part of our normal production process, you will receive an e-mail notice when your article appears on Elsevier's online service ScienceDirect (www.sciencedirect.com). That e-mail will include the article's Digital Object Identifier (DOI). This number provides the electronic link to the published article and should be included in the posting of your personal version. We ask that you wait until you receive this e-mail and have the DOI to do any posting.

Posting to a repository: Authors may post their AAM immediately to their employer's institutional repository for internal use only and may make their manuscript publicly available after the journal-specific embargo period has ended.

Please also refer to Elsevier's Article Posting Policy for further information.

18. **For book authors** the following clauses are applicable in addition to the above: Authors are permitted to place a brief summary of their work online only. You are not allowed to download and post the published electronic version of your chapter, nor may you scan the printed edition to create an electronic version. Posting to a repository: Authors are permitted to post a summary of their chapter only in their institution's repository.

20. **Thesis/Dissertation:** If your license is for use in a thesis/dissertation your thesis may be submitted to your institution in either print or electronic form. Should your thesis be published commercially, please apply for permission. These requirements include permission for the Library and Archives of Canada to supply single copies, on demand, of the complete thesis and include permission for UMI to supply single copies, on demand, of the complete thesis. Should your thesis be published commercially, please apply for permission.

Elsevier Open Access Terms and Conditions

Elsevier publishes Open Access articles in both its Open Access journals and via its Open Access articles option in subscription journals.

Authors publishing in an Open Access journal or who choose to make their article Open Access in an Elsevier subscription journal select one of the following Creative Commons user licenses, which define how a reader may reuse their work: Creative Commons Attribution License (CC BY), Creative Commons Attribution – Non Commercial - Share Alike (CC BY NC SA) and Creative Commons Attribution – Non Commercial – No Derivatives (CC BY NC ND)

Terms & Conditions applicable to all Elsevier Open Access articles:

Any reuse of the article must not represent the author as endorsing the adaptation of the article nor should the article be modified in such a way as to damage the author's honour or

reputation.

The author(s) must be appropriately credited.

If any part of the material to be used (for example, figures) has appeared in our publication with credit or acknowledgement to another source it is the responsibility of the user to ensure their reuse complies with the terms and conditions determined by the rights holder.

Additional Terms & Conditions applicable to each Creative Commons user license:

CC BY: You may distribute and copy the article, create extracts, abstracts, and other revised versions, adaptations or derivative works of or from an article (such as a translation), to include in a collective work (such as an anthology), to text or data mine the article, including for commercial purposes without permission from Elsevier

CC BY NC SA: For non-commercial purposes you may distribute and copy the article, create extracts, abstracts and other revised versions, adaptations or derivative works of or from an article (such as a translation), to include in a collective work (such as an anthology), to text and data mine the article and license new adaptations or creations under identical terms without permission from Elsevier

CC BY NC ND: For non-commercial purposes you may distribute and copy the article and include it in a collective work (such as an anthology), provided you do not alter or modify the article, without permission from Elsevier

Any commercial reuse of Open Access articles published with a CC BY NC SA or CC BY NC ND license requires permission from Elsevier and will be subject to a fee.

Commercial reuse includes:

- Promotional purposes (advertising or marketing)
- Commercial exploitation (e.g. a product for sale or loan)
- Systematic distribution (for a fee or free of charge)

Please refer to Elsevier's Open Access Policy for further information.

21. Other Conditions:

v1.7

If you would like to pay for this license now, please remit this license along with your payment made payable to "COPYRIGHT CLEARANCE CENTER" otherwise you will be invoiced within 48 hours of the license date. Payment should be in the form of a check

**or money order referencing your account number and this invoice number
RLNK501254270.
Once you receive your invoice for this order, you may pay your invoice by credit card.
Please follow instructions provided at that time.**

**Make Payment To:
Copyright Clearance Center
Dept 001
P.O. Box 843006
Boston, MA 02284-3006**

**For suggestions or comments regarding this order, contact RightsLink Customer
Support: customercare@copyright.com or +1-877-622-5543 (toll free in the US) or +1-
978-646-2777.**

**Gratis licenses (referencing \$0 in the Total field) are free. Please retain this printable
license for your reference. No payment is required.**



Title / Keyword	<input type="text"/>	Journal	<input type="text" value="all"/>	Volume	<input type="text"/>	<input type="button" value="Clear"/>
Author	<input type="text"/>	Section	<input type="text" value="---"/>	Issue	<input type="text"/>	
Article Type	<input type="text" value="all"/>	Special Issue	<input type="text" value="---"/>	Page	<input type="text"/>	<input type="button" value="Search"/>

MDPI Open Access Information and Policy

All articles published by MDPI are made immediately available worldwide under an open access license. This means:

everyone has free and unlimited access to the full-text of *all* articles published in MDPI journals, and everyone is free to re-use the published material if proper accreditation/citation of the original publication is given.

open access publication is supported by the authors' institutes or research funding agencies by payment of a comparatively low Article Processing Charge (APC) for accepted articles.

External Open Access Resources

MDPI is a [RoMEO green publisher](#) — RoMEO is a database of Publishers' copyright and self-archiving policies hosted by the [University of Nottingham](#)

Those who are new to the concept of open access might find the following websites or 'Open Access 101' video informative:

[Wikipedia article on 'Open Access'](#)
[Peter Suber's 'Open Access Overview'](#)
[Information Platform Open Access \[in English, in German\]](#)
[SHERPA's 'Authors and Open Access'](#)

Meaning of Open Access

In accordance with major definitions of open access in scientific literature (namely the Budapest, Berlin, and Bethesda declarations), MDPI defines *open access* by the following conditions:

- peer-reviewed literature is freely available without subscription or price barriers,
- literature is immediately released in open access format (no embargo period), and
- published material can be re-used without obtaining permission as long as a correct citation to the original publication is given.

Until 2008, most articles published by MDPI contained the note: "© year by MDPI (<http://www.mdpi.org>). Reproduction is permitted for noncommercial purposes". During 2008, MDPI journals started to publish articles under the [Creative Commons Attribution License](#). All articles published by MDPI before and during 2008 should now be considered as having been released under the post-2008 Creative Commons Attribution License.

This means that all articles published in MDPI journals, including data, graphics, and supplements, can be linked from external sources, scanned by search engines, re-used by text mining applications or websites, blogs, etc. free of charge under the sole condition of proper accreditation of the source and original publisher. MDPI believes that open access publishing fosters the exchange of research results amongst scientists from different disciplines, thus facilitating interdisciplinary research. Open access publishing also provides access to research results to researchers worldwide, including those from developing countries, and to an interested general public. Although MDPI publishes all of its journals under the open access model, we believe that open access is an enriching part of the scholarly communication process that can and should co-exist with other forms of communication and publication, such as society-based publishing and conferencing activities.

Important Note: some articles (especially *Reviews*) may contain figures, tables or text taken from other publications, for which MDPI does not hold the copyright or the right to re-license the published material. Please note that you should inquire with the original copyright holder (usually the original publisher or authors), whether or not this material can be re-used.

Advantages of Open Access for Authors

The High Availability and Visibility of our open access articles is guaranteed through the free and unlimited accessibility of the publication over the Internet. Everyone can freely access and download the full text of all articles published with MDPI: readers of open access journals, *i.e.*, mostly other researchers, do not need to pay any subscription or pay-per-view charges to read articles published by MDPI. Open access publications are also more likely to be included in search engines and indexing databases.

The Higher Citation Impact of open access articles results from their high publicity and availability. Open access publications are demonstrably more frequently cited [1,2].

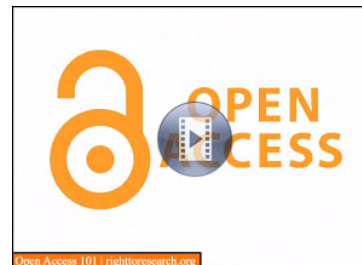
Lower Publishing Costs: Open access publishers cover their costs for editorial handling and editing of a paper by charging authors' institutes or research funding agencies. The cost of handling and producing an article is covered through the one-time payment of an [article processing charge \(APC\)](#) for each accepted article. The APCs of open access publishers are only a fraction of the average income per paper earned by traditional, subscription-based publishers. MDPI's [article processing charge \(APC\)](#) is the same, irrespective of article length, because we wish to encourage publication of long papers with complete results and full experimental or computational details [3].

Faster Publication in MDPI's open access journals is achieved by online-only availability. Accepted articles are typically published online more rapidly in MDPI journals than those of traditional, subscription-based and printed journals are [4].

Links and Notes

1. Open access citation impact advantage: http://en.wikipedia.org/wiki/Open_access#Authors_and_researchers. For example, a standard research paper "Shutalev, A.D.; Kishko, E.A.; Sivova, N.V.; Kuznetsov, A.Y. *Molecules* **1998**, *3*, 100-106" has been cited 51 times, the highest number among all the papers published so far by the same author.
2. Lin, S.-K. *Editorial: Non-Open Access and Its Adverse Impact on Molecules*. *Molecules* **2007**, *12*, 1436-1437 (PDF format 16 K, HTML format).
3. Recently a research paper of 30 pages has been published: *Molecules* **2008**, *13*(5), 1081-1110.

SPARC Open Access 101 Video



Acknowledgements to be used by RSC authors

Authors of RSC books and journal articles can reproduce material (for example a figure) from the RSC publication in a non-RSC publication, including theses, without formally requesting permission providing that the correct acknowledgement is given to the RSC publication. This permission extends to reproduction of large portions of text or the whole article or book chapter when being reproduced in a thesis.

The acknowledgement to be used depends on the RSC publication in which the material was published and the form of the acknowledgements is as follows:

- For material being reproduced from an article in *New Journal of Chemistry* the acknowledgement should be in the form:
 - [Original citation] - Reproduced by permission of The Royal Society of Chemistry (RSC) on behalf of the Centre National de la Recherche Scientifique (CNRS) and the RSC
- For material being reproduced from an article *Photochemical & Photobiological Sciences* the acknowledgement should be in the form:
 - [Original citation] - Reproduced by permission of The Royal Society of Chemistry (RSC) on behalf of the European Society for Photobiology, the European Photochemistry Association, and RSC
- For material being reproduced from an article in *Physical Chemistry Chemical Physics* the acknowledgement should be in the form:
 - [Original citation] - Reproduced by permission of the PCCP Owner Societies
- For material reproduced from books and any other journal the acknowledgement should be in the form:
 - [Original citation] - Reproduced by permission of The Royal Society of Chemistry

The acknowledgement should also include a hyperlink to the article on the RSC website.

The form of the acknowledgement is also specified in the RSC agreement/licence signed by the corresponding author.

Except in cases of republication in a thesis, this express permission does not cover the reproduction of large portions of text from the RSC publication or reproduction of the whole article or book chapter.


A publisher of a non-RSC publication can use this document as proof that permission is granted to use the material in the non-RSC publication.

**ELSEVIER LICENSE
TERMS AND CONDITIONS**

Jan 01, 2014

This is a License Agreement between Youngjik Choi ("You") and Elsevier ("Elsevier") provided by Copyright Clearance Center ("CCC"). The license consists of your order details, the terms and conditions provided by Elsevier, and the payment terms and conditions.

All payments must be made in full to CCC. For payment instructions, please see information listed at the bottom of this form.

Supplier	Elsevier Limited The Boulevard, Langford Lane Kidlington, Oxford, OX5 1GB, UK
Registered Company Number	1982084
Customer name	Youngjik Choi
Customer address	430 Ashby Court Waterloo, ON n2t1h1
License number	
License date	Jan 01, 2014
Licensed content publisher	Elsevier
Licensed content publication	Biochimica et Biophysica Acta (BBA) - Biomembranes
Licensed content title	Effect of melatonin and cholesterol on the structure of DOPC and DPPC membranes
Licensed content author	E. Drolle, N. Kučerka, M.I. Hoopes, Y. Choi, J. Katsaras, M. Karttunen, Z. Leonenko
Licensed content date	September 2013
Licensed content volume number	1828
Licensed content issue number	9
Number of pages	8
Start Page	2247
End Page	2254
Type of Use	reuse in a thesis/dissertation
Portion	full article
Format	both print and electronic
Are you the author of this Elsevier article?	Yes
Will you be translating?	No

Title of your thesis/dissertation	NANOSCALE CHARACTERIZATION OF MELATONIN AND AMYLOID BETA IN MODEL MEMBRANES - IN RELATION TO ALZHEIMER'S DISEASE
Expected completion date	Apr 2014
Estimated size (number of pages)	250
Elsevier VAT number	GB 494 6272 12
Permissions price	0.00 USD
VAT/Local Sales Tax	0.00 USD / 0.00 GBP
Total	0.00 USD
Terms and Conditions	

INTRODUCTION

1. The publisher for this copyrighted material is Elsevier. By clicking "accept" in connection with completing this licensing transaction, you agree that the following terms and conditions apply to this transaction (along with the Billing and Payment terms and conditions established by Copyright Clearance Center, Inc. ("CCC"), at the time that you opened your Rightslink account and that are available at any time at <http://myaccount.copyright.com>).

GENERAL TERMS

2. Elsevier hereby grants you permission to reproduce the aforementioned material subject to the terms and conditions indicated.
3. Acknowledgement: If any part of the material to be used (for example, figures) has appeared in our publication with credit or acknowledgement to another source, permission must also be sought from that source. If such permission is not obtained then that material may not be included in your publication/copies. Suitable acknowledgement to the source must be made, either as a footnote or in a reference list at the end of your publication, as follows:

“Reprinted from Publication title, Vol /edition number, Author(s), Title of article / title of chapter, Pages No., Copyright (Year), with permission from Elsevier [OR APPLICABLE SOCIETY COPYRIGHT OWNER].” Also Lancet special credit - “Reprinted from The Lancet, Vol. number, Author(s), Title of article, Pages No., Copyright (Year), with permission from Elsevier.”
4. Reproduction of this material is confined to the purpose and/or media for which permission is hereby given.
5. Altering/Modifying Material: Not Permitted. However figures and illustrations may be altered/adapted minimally to serve your work. Any other abbreviations, additions, deletions and/or any other alterations shall be made only with prior written authorization of Elsevier Ltd. (Please contact Elsevier at permissions@elsevier.com)
6. If the permission fee for the requested use of our material is waived in this instance, please be advised that your future requests for Elsevier materials may attract a fee.
7. Reservation of Rights: Publisher reserves all rights not specifically granted in the combination of (i) the license details provided by you and accepted in the course of this

5. **Altering/Modifying Material: Not Permitted.** However figures and illustrations may be altered/adapted minimally to serve your work. Any other abbreviations, additions, deletions and/or any other alterations shall be made only with prior written authorization of Elsevier Ltd. (Please contact Elsevier at permissions@elsevier.com)
6. If the permission fee for the requested use of our material is waived in this instance, please be advised that your future requests for Elsevier materials may attract a fee.
7. **Reservation of Rights:** Publisher reserves all rights not specifically granted in the combination of (i) the license details provided by you and accepted in the course of this licensing transaction, (ii) these terms and conditions and (iii) CCC's Billing and Payment terms and conditions.
8. **License Contingent Upon Payment:** While you may exercise the rights licensed immediately upon issuance of the license at the end of the licensing process for the transaction, provided that you have disclosed complete and accurate details of your proposed use, no license is finally effective unless and until full payment is received from you (either by publisher or by CCC) as provided in CCC's Billing and Payment terms and conditions. If full payment is not received on a timely basis, then any license preliminarily granted shall be deemed automatically revoked and shall be void as if never granted. Further, in the event that you breach any of these terms and conditions or any of CCC's Billing and Payment terms and conditions, the license is automatically revoked and shall be void as if never granted. Use of materials as described in a revoked license, as well as any use of the materials beyond the scope of an unrevoked license, may constitute copyright infringement and publisher reserves the right to take any and all action to protect its copyright in the materials.
9. **Warranties:** Publisher makes no representations or warranties with respect to the licensed material.
10. **Indemnity:** You hereby indemnify and agree to hold harmless publisher and CCC, and their respective officers, directors, employees and agents, from and against any and all claims arising out of your use of the licensed material other than as specifically authorized pursuant to this license.
11. **No Transfer of License:** This license is personal to you and may not be sublicensed, assigned, or transferred by you to any other person without publisher's written permission.
12. **No Amendment Except in Writing:** This license may not be amended except in a writing signed by both parties (or, in the case of publisher, by CCC on publisher's behalf).
13. **Objection to Contrary Terms:** Publisher hereby objects to any terms contained in any purchase order, acknowledgment, check endorsement or other writing prepared by you, which terms are inconsistent with these terms and conditions or CCC's Billing and Payment terms and conditions. These terms and conditions, together with CCC's Billing and Payment terms and conditions (which are incorporated herein), comprise the entire agreement between you and publisher (and CCC) concerning this licensing transaction. In the event of any conflict between your obligations established by these terms and conditions and those

established by CCC's Billing and Payment terms and conditions, these terms and conditions shall control.

14. **Revocation:** Elsevier or Copyright Clearance Center may deny the permissions described in this License at their sole discretion, for any reason or no reason, with a full refund payable to you. Notice of such denial will be made using the contact information provided by you. Failure to receive such notice will not alter or invalidate the denial. In no event will Elsevier or Copyright Clearance Center be responsible or liable for any costs, expenses or damage incurred by you as a result of a denial of your permission request, other than a refund of the amount(s) paid by you to Elsevier and/or Copyright Clearance Center for denied permissions.

LIMITED LICENSE

The following terms and conditions apply only to specific license types:

15. **Translation:** This permission is granted for non-exclusive world **English** rights only unless your license was granted for translation rights. If you licensed translation rights you may only translate this content into the languages you requested. A professional translator must perform all translations and reproduce the content word for word preserving the integrity of the article. If this license is to re-use 1 or 2 figures then permission is granted for non-exclusive world rights in all languages.

16. **Website:** The following terms and conditions apply to electronic reserve and author websites:

Electronic reserve: If licensed material is to be posted to website, the web site is to be password-protected and made available only to bona fide students registered on a relevant course if:

This license was made in connection with a course,

This permission is granted for 1 year only. You may obtain a license for future website posting,

All content posted to the web site must maintain the copyright information line on the bottom of each image,

A hyper-text must be included to the Homepage of the journal from which you are licensing at <http://www.sciencedirect.com/science/journal/xxxxx> or the Elsevier homepage for books at <http://www.elsevier.com> , and

Central Storage: This license does not include permission for a scanned version of the material to be stored in a central repository such as that provided by Heron/XanEdu.

17. **Author website** for journals with the following additional clauses:

All content posted to the web site must maintain the copyright information line on the bottom of each image, and the permission granted is limited to the personal version of your paper. You are not allowed to download and post the published electronic version of your article (whether PDF or HTML, proof or final version), nor may you scan the printed edition to create an electronic version. A hyper-text must be included to the Homepage of the journal from which you are licensing at <http://www.sciencedirect.com/science/journal/xxxxx> . As part of our normal production process, you will receive an e-mail notice when your

article appears on Elsevier's online service ScienceDirect (www.sciencedirect.com). That e-mail will include the article's Digital Object Identifier (DOI). This number provides the electronic link to the published article and should be included in the posting of your personal version. We ask that you wait until you receive this e-mail and have the DOI to do any posting.

Central Storage: This license does not include permission for a scanned version of the material to be stored in a central repository such as that provided by Heron/XanEdu.

18. Author website for books with the following additional clauses:

Authors are permitted to place a brief summary of their work online only.

A hyper-text must be included to the Elsevier homepage at <http://www.elsevier.com>. All content posted to the web site must maintain the copyright information line on the bottom of each image. You are not allowed to download and post the published electronic version of your chapter, nor may you scan the printed edition to create an electronic version.

Central Storage: This license does not include permission for a scanned version of the material to be stored in a central repository such as that provided by Heron/XanEdu.

19. Website (regular and for author): A hyper-text must be included to the Homepage of the journal from which you are licensing at <http://www.sciencedirect.com/science/journal/xxxxx>. or for books to the Elsevier homepage at <http://www.elsevier.com>

20. Thesis/Dissertation: If your license is for use in a thesis/dissertation your thesis may be submitted to your institution in either print or electronic form. Should your thesis be published commercially, please reapply for permission. These requirements include permission for the Library and Archives of Canada to supply single copies, on demand, of the complete thesis and include permission for UMI to supply single copies, on demand, of the complete thesis. Should your thesis be published commercially, please reapply for permission.

21. Other Conditions:

v1.6

If you would like to pay for this license now, please remit this license along with your payment made payable to "COPYRIGHT CLEARANCE CENTER" otherwise you will be invoiced within 48 hours of the license date. Payment should be in the form of a check or money order referencing your account number and this invoice number RLNK501189484.

Once you receive your invoice for this order, you may pay your invoice by credit card. Please follow instructions provided at that time.

**Make Payment To:
Copyright Clearance Center
Dept 001
P.O. Box 843006**

Boston, MA 02284-3006

For suggestions or comments regarding this order, contact RightsLink Customer Support: customercare@copyright.com or +1-877-622-5543 (toll free in the US) or +1-978-646-2777.

Gratis licenses (referencing \$0 in the Total field) are free. Please retain this printable license for your reference. No payment is required.

Bibliography

- [1] A. Association, *Alzheimer's disease facts and figures*. Chicago, IL: Alzheimer's Association, 2012.
- [2] A. B. Rodgers, *Alzheimer's Disease: Unraveling the Mystery*, vol. 120, no. 25. U.S. Department of Health and Human Services NIH Publication Number: 08-3782, 2008.
- [3] D. P. Cardinali, A. M. Furio, and L. I. Brusco, "Clinical aspects of melatonin intervention in Alzheimer's disease progression.," *Curr. Neuropharmacol.*, vol. 8, no. 3, pp. 218–27, Sep. 2010.
- [4] J. Diamond, *Alzheimer's disease : What's it all about? Where do we stand in the search for a cure?*. Toronto, ON, Canada: Alzheimer Society of Canada, 2011.
- [5] F. M. LaFerla, K. N. Green, and S. Oddo, "Intracellular amyloid-beta in Alzheimer's disease.," *Nat. Rev. Neurosci.*, vol. 8, no. 7, pp. 499–509, Jul. 2007.
- [6] G. Di Paolo and T. Kim, "Linking lipids to Alzheimer's disease: cholesterol and beyond.," *Nat. Rev. Neurosci.*, vol. 12, no. 5, pp. 284–96, May 2011.
- [7] E. D. Roberson and L. Mucke, "100 years and counting: prospects for defeating Alzheimer's disease.," *Science*, vol. 314, no. 5800, pp. 781–4, Nov. 2006.
- [8] E. Karran, M. Mercken, and B. De Strooper, "The amyloid cascade hypothesis for Alzheimer's disease: an appraisal for the development of therapeutics.," *Nat. Rev. Drug Discov.*, vol. 10, no. 9, pp. 698–712, Sep. 2011.
- [9] C. Haass and D. J. Selkoe, "Soluble protein oligomers in neurodegeneration: lessons from the Alzheimer's amyloid beta-peptide.," *Nat. Rev. Mol. Cell Biol.*, vol. 8, no. 2, pp. 101–12, Feb. 2007.
- [10] Y. Huang and L. Mucke, "Alzheimer mechanisms and therapeutic strategies.," *Cell*, vol. 148, no. 6, pp. 1204–22, Mar. 2012.
- [11] A. Maltsev, S. Bystryak, and O. Galzitskaya, "The role of β -amyloid peptide in neurodegenerative diseases.," *Ageing Res. Rev.*, vol. 10, no. 4, pp. 440–52, Sep. 2011.
- [12] M. Goedert and M. G. Spillantini, "A century of Alzheimer's disease.," *Science*, vol. 314, no. 5800, pp. 777–81, Nov. 2006.
- [13] A. Belkacemi and C. Ramassamy, "Time sequence of oxidative stress in the brain from transgenic mouse models of Alzheimer's disease related to the amyloid- β cascade.," *Free Radic. Biol. Med.*, vol. 52, no. 3, pp. 593–600, Mar. 2012.

- [14] S. Sisodia and P. H. St George-Hyslop, “gamma-Secretase, Notch, Abeta and Alzheimer’s disease: where do the presenilins fit in?,” *Nat. Rev. Neurosci.*, vol. 3, no. 4, pp. 281–90, Apr. 2002.
- [15] G. Bu, “Apolipoprotein E and its receptors in Alzheimer’s disease: pathways, pathogenesis and therapy.,” *Nat. Rev. Neurosci.*, vol. 10, no. 5, pp. 333–44, May 2009.
- [16] C. Reitz, C. Brayne, and R. Mayeux, “Epidemiology of Alzheimer disease.,” *Nat. Rev. Neurol.*, vol. 7, no. 3, pp. 137–52, Mar. 2011.
- [17] A. Aguzzi and T. O’Connor, “Protein aggregation diseases: pathogenicity and therapeutic perspectives.,” *Nat. Rev. Drug Discov.*, vol. 9, no. 3, pp. 237–48, Mar. 2010.
- [18] G. Shankar, S. Li, T. Mehta, A. Garcia-Munoz, N. Shepardson, I. Smith, F. M. Brett, M. Farrell, M. Rowan, C. Lemere, C. Regan, D. Walsh, B. Sabatini, and D. Selkoe, “Amyloid-beta protein dimers isolated directly from Alzheimer’s brains impair synaptic plasticity and memory.,” *Nat. Med.*, vol. 14, no. 8, pp. 837–42, Aug. 2008.
- [19] F. Chiti and C. M. Dobson, “Protein misfolding, functional amyloid, and human disease.,” *Annu. Rev. Biochem.*, vol. 75, pp. 333–66, Jan. 2006.
- [20] J. Bieschke, M. Herbst, T. Wiglenda, R. Friedrich, A. Boeddrich, F. Schiele, D. Kleckers, J. Lopez del Amo, B. Grüning, Q. Wang, M. Schmidt, R. Lurz, R. Anwyl, S. Schnoegl, M. Fändrich, R. Frank, B. Reif, S. Günther, D. Walsh, and E. Wanker, “Small-molecule conversion of toxic oligomers to nontoxic β -sheet-rich amyloid fibrils.,” *Nat. Chem. Biol.*, vol. 8, no. 1, pp. 93–101, Jan. 2012.
- [21] I. Benilova, E. Karran, and B. De Strooper, “The toxic A β oligomer and Alzheimer’s disease: an emperor in need of clothes.,” *Nat. Neurosci.*, vol. 15, no. 3, pp. 349–57, Mar. 2012.
- [22] A. Jan, D. Hartley, and H. Lashuel, “Preparation and characterization of toxic Abeta aggregates for structural and functional studies in Alzheimer’s disease research.,” *Nat. Protoc.*, vol. 5, no. 6, pp. 1186–209, Jun. 2010.
- [23] J. Laurén, D. Gimbel, H. Nygaard, J. Gilbert, and S. Strittmatter, “Cellular prion protein mediates impairment of synaptic plasticity by amyloid-beta oligomers.,” *Nature*, vol. 457, no. 7233, pp. 1128–32, Feb. 2009.
- [24] A. Thathiah and B. De Strooper, “The role of G protein-coupled receptors in the pathology of Alzheimer’s disease.,” *Nat. Rev. Neurosci.*, vol. 12, no. 2, pp. 73–87, Feb. 2011.

- [25] J. Palop and L. Mucke, "Amyloid-beta-induced neuronal dysfunction in Alzheimer's disease: from synapses toward neural networks.," *Nat. Neurosci.*, vol. 13, no. 7, pp. 812–8, Jul. 2010.
- [26] R. Williamson, A. Usardi, D. P. Hanger, and B. H. Anderton, "Membrane-bound beta-amyloid oligomers are recruited into lipid rafts by a fyn-dependent mechanism.," *FASEB J.*, vol. 22, no. 5, pp. 1552–9, May 2008.
- [27] X. Yang, S. Askarova, and J. C. Lee, "Membrane biophysics and mechanics in Alzheimer's disease.," *Mol. Neurobiol.*, vol. 41, no. 2–3, pp. 138–48, Jun. 2010.
- [28] S. Askarova, X. Yang, and J. C. Lee, "Impacts of membrane biophysics in Alzheimer's disease: from amyloid precursor protein processing to $\text{A}\beta$ Peptide-induced membrane changes.," *Int. J. Alzheimers. Dis.*, vol. 2011, no. 134971, pp. 1–12, Jan. 2011.
- [29] S. Butterfield and H. Lashuel, "Amyloidogenic protein-membrane interactions: mechanistic insight from model systems.," *Angew. Chem. Int. Ed. Engl.*, vol. 49, no. 33, pp. 5628–54, Aug. 2010.
- [30] J. Rushworth and N. M. Hooper, "Lipid Rafts: Linking Alzheimer's Amyloid- β Production, Aggregation, and Toxicity at Neuronal Membranes.," *Int. J. Alzheimers. Dis.*, vol. 2011 (1), no. 603052, pp. 1–14, Jan. 2010.
- [31] A. Y. Abramov, M. Ionov, E. Pavlov, and M. R. Duchon, "Membrane cholesterol content plays a key role in the neurotoxicity of β -amyloid: implications for Alzheimer's disease.," *Aging Cell*, vol. 10, no. 4, pp. 595–603, Aug. 2011.
- [32] R. Ehehalt, P. Keller, C. Haass, C. Thiele, and K. Simons, "Amyloidogenic processing of the Alzheimer beta-amyloid precursor protein depends on lipid rafts.," *J. Cell Biol.*, vol. 160, no. 1, pp. 113–23, Jan. 2003.
- [33] J. Fantini and N. Yahi, "Molecular insights into amyloid regulation by membrane cholesterol and sphingolipids: common mechanisms in neurodegenerative diseases.," *Expert Rev. Mol. Med.*, vol. 12, no. e27, pp. 1–22, Jan. 2010.
- [34] M. P. Mattson, "Pathways towards and away from Alzheimer's disease.," *Nature*, vol. 430, no. 7000, pp. 631–9, Aug. 2004.
- [35] J. R. Steiner, M. Irizarry, N. Scarmeas, S. Raju, J. Brandt, M. Albert, D. Blacker, B. Hyman, and Y. Stern, "Distinct Pools of Amyloid in Alzheimer Disease Affected Brain," *Arch Neurol.*, vol. 65, no. 7, pp. 906–912, 2008.
- [36] G. Van Meer, D. R. Voelker, and G. W. Feigenson, "Membrane lipids: where they are and how they behave.," *Nat. Rev. Mol. Cell Biol.*, vol. 9, no. 2, pp. 112–24, Feb. 2008.

- [37] A. G. Lee, "How lipids affect the activities of integral membrane proteins.," *Biochim. Biophys. Acta*, vol. 1666, no. 1–2, pp. 62–87, Nov. 2004.
- [38] R. Phillips, T. Ursell, P. Wiggins, and P. Sens, "Emerging roles for lipids in shaping membrane-protein function.," *Nature*, vol. 459, no. 7245, pp. 379–85, May 2009.
- [39] A. M. Seddon, D. Casey, R. V Law, A. Gee, R. H. Templer, and O. Ces, "Drug interactions with lipid membranes.," *Chem. Soc. Rev.*, vol. 38, no. 9, pp. 2509–19, Sep. 2009.
- [40] J. K. Seydel and M. Wiese, *Drug-Membrane Interactions*, vol. 15. Weinheim, FRG: Wiley-VCH Verlag GmbH & Co. KGaA, 2002, pp. 217–289.
- [41] S. Kane and S. Floyd, "Interaction of local anesthetics with phospholipids in Langmuir monolayers," *Phys. Rev. E*, vol. 62, no. 6, pp. 8400–8408, Dec. 2000.
- [42] H. Jerabek, G. Pabst, M. Rappolt, and T. Stockner, "Membrane-mediated effect on ion channels induced by the anesthetic drug ketamine.," *J. Am. Chem. Soc.*, vol. 132, no. 23, pp. 7990–7, Jun. 2010.
- [43] C. Nunes, G. Brezesinski, C. Pereira-Leite, J. L. F. C. Lima, S. Reis, and M. Lúcio, "NSAIDs interactions with membranes: a biophysical approach.," *Langmuir*, vol. 27, no. 17, pp. 10847–58, Sep. 2011.
- [44] H. M. Seeger, M. L. Gudmundsson, and T. Heimburg, "How anesthetics, neurotransmitters, and antibiotics influence the relaxation processes in lipid membranes.," *J. Phys. Chem. B*, vol. 111, no. 49, pp. 13858–66, Dec. 2007.
- [45] R. S. Cantor, "Breaking the Meyer-Overton rule: predicted effects of varying stiffness and interfacial activity on the intrinsic potency of anesthetics.," *Biophys. J.*, vol. 80, no. 5, pp. 2284–97, May 2001.
- [46] F. Esteves, C. Moutinho, and C. Matos, "Correlation between octanol/water and liposome/water distribution coefficients and drug absorption of a set of pharmacologically active compounds.," *J. Liposome Res.*, vol. 23, no. 2, pp. 83–93, Jun. 2013.
- [47] P. S. Milutinovic, L. Yang, R. S. Cantor, E. I. Eger, and J. M. Sonner, "Anesthetic-like modulation of a gamma-aminobutyric acid type A, strychnine-sensitive glycine, and N-methyl-d-aspartate receptors by coreleased neurotransmitters.," *Anesth. Analg.*, vol. 105, no. 2, pp. 386–92, Aug. 2007.
- [48] E. Matsubara, T. BryantThomas, J. Pacheco Quinto, T. Henry, B. Poeggeler, D. Herbert, F. CruzSanchez, Y. Chyan, M. Smith, G. Perry, M. Shoji, K. Abe, A. Leone, I. GrundkeIkbal, G. Wilson, J. Ghiso, C. Williams, L. Refolo, and M. Pappolla, "Melatonin

- increases survival and inhibits oxidative and amyloid pathology in a transgenic model of Alzheimer's disease," *J. Neurochem.*, vol. 85, no. 5, pp. 1101–8, May 2003.
- [49] A. Brzezinski, "Melatonin in Humans," *N. Engl. J. Med.*, vol. 336, no. 3, pp. 186–195, Jan. 1997.
- [50] M. Karasek, "Melatonin, human aging, and age-related diseases.," *Exp. Gerontol.*, vol. 39, no. 11–12, pp. 1723–9, 2004.
- [51] G. Oxenkrug and R. Ratner, "N-acetylserotonin and aging-associated cognitive impairment and depression.," *Aging Dis.*, vol. 3, no. 4, pp. 330–8, Aug. 2012.
- [52] K. Yeleswaram, L. G. McLaughlin, J. O. Knipe, and D. Schabdach, "Pharmacokinetics and oral bioavailability of exogenous melatonin in preclinical animal models and clinical implications.," *J. Pineal Res.*, vol. 22, no. 1, pp. 45–51, Jan. 1997.
- [53] V. Srinivasan, S. R. Pandi-Perumal, D. P. Cardinali, B. Poeggeler, and R. Hardeland, "Melatonin in Alzheimer's disease and other neurodegenerative disorders.," *Behav. Brain Funct.*, vol. 2, no. 4, p. 15, Jan. 2006.
- [54] R. Y. Liu, J. N. Zhou, J. van Heerikhuize, M. A. Hofman, and D. F. Swaab, "Decreased melatonin levels in postmortem cerebrospinal fluid in relation to aging, Alzheimer's disease, and apolipoprotein E-epsilon4/4 genotype.," *J. Clin. Endocrinol. Metab.*, vol. 84, no. 1, pp. 323–7, Jan. 1999.
- [55] J. Zhou, R. Liu, W. Kamphorst, M. A. Hofman, and D. F. Swaab, "Early neuropathological Alzheimer's changes in aged individuals are accompanied by decreased cerebrospinal fluid melatonin levels," *J. Pineal Res.*, vol. 35, no. 2, pp. 125–130, Sep. 2003.
- [56] J. Kang, M. M. Lim, R. J. Bateman, J. J. Lee, L. P. Smyth, J. R. Cirrito, N. Fujiki, S. Nishino, and D. M. Holtzman, "Amyloid-beta dynamics are regulated by orexin and the sleep-wake cycle.," *Science*, vol. 326, no. 5955, pp. 1005–7, Nov. 2009.
- [57] M. A. Pappolla, M. Sos, R. A. Omar, R. J. Bick, D. L. Hickson-Bick, R. J. Reiter, S. Efthimiopoulos, and N. K. Robakis, "Melatonin prevents death of neuroblastoma cells exposed to the Alzheimer amyloid peptide.," *J. Neurosci.*, vol. 17, no. 5, pp. 1683–90, Mar. 1997.
- [58] G. Masilamoni, P. Jesudason, S. Dhandayuthapani, B. Ashok, S. Vignesh, C. Jebaraj, S. Paul, and R. Jayakumar, "The neuroprotective role of melatonin against amyloid beta peptide injected mice.," *Free Radic. Res.*, vol. 42, no. 7, pp. 661–73, Jul. 2008.

- [59] M. Gunasingh, J. Philip, B. Ashok, R. Kirubakaran, C. Jebaraj, J. Davis, S. Vignesh, S. Dhandayuthapani, and R. Jayakumar, "Melatonin prevents amyloid protofibrillar induced oxidative imbalance and biogenic amine catabolism.," *Life Sci.*, vol. 83, no. 3–4, pp. 96–102, Jul. 2008.
- [60] Y. Cheng, Z. Feng, Q. Zhang, and J. Zhang, "Beneficial effects of melatonin in experimental models of Alzheimer disease.," *Acta Pharmacol. Sin.*, vol. 27, no. 2, pp. 129–39, Feb. 2006.
- [61] Z. Feng and J. Zhang, "Melatonin reduces amyloid beta-induced apoptosis in pheochromocytoma (PC12) cells.," *J. Pineal Res.*, vol. 37, no. 4, pp. 257–66, Nov. 2004.
- [62] G. Benítez-King, "Melatonin as a cytoskeletal modulator: implications for cell physiology and disease.," *J. Pineal Res.*, vol. 40, no. 1, pp. 1–9, Jan. 2006.
- [63] K. Clapp-Lilly, M. Smith, G. Perry, and L. Duffy, "Melatonin reduces interleukin secretion in amyloid- β stressed mouse brain slices," *Chem. Biol. Interact.*, vol. 134, no. 1, pp. 101–107, Mar. 2001.
- [64] F. Severcan, I. Sahin, and N. Kazanci, "Melatonin strongly interacts with zwitterionic model membranes-evidence from Fourier transform infrared spectroscopy and differential scanning calorimetry.," *Biochim. Biophys. Acta*, vol. 1668, no. 2, pp. 215–22, Mar. 2005.
- [65] M. Pappolla, P. Bozner, C. Soto, H. Shao, N. K. Robakis, M. Zagorski, B. Frangione, and J. Ghiso, "Inhibition of Alzheimer beta-fibrillogenesis by melatonin.," *J. Biol. Chem.*, vol. 273, no. 13, pp. 7185–8, Mar. 1998.
- [66] B. Poeggeler, L. Miravalle, M. G. Zagorski, T. Wisniewski, Y. J. Chyan, Y. Zhang, H. Shao, T. Bryant-Thomas, R. Vidal, B. Frangione, J. Ghiso, and M. A. Pappolla, "Melatonin reverses the profibrillogenic activity of apolipoprotein E4 on the Alzheimer amyloid Abeta peptide.," *Biochemistry*, vol. 40, no. 49, pp. 14995–5001, Dec. 2001.
- [67] M. A. Westerman, D. Cooper-Blacketer, A. Mariash, L. Kotilinek, T. Kawarabayashi, L. H. Younkin, G. A. Carlson, S. G. Younkin, and K. H. Ashe, "The relationship between Abeta and memory in the Tg2576 mouse model of Alzheimer's disease.," *J. Neurosci.*, vol. 22, no. 5, pp. 1858–67, Mar. 2002.
- [68] J. Quinn, D. Kulhanek, J. Nowlin, R. Jones, D. Praticò, J. Rokach, and R. Stackman, "Chronic melatonin therapy fails to alter amyloid burden or oxidative damage in old Tg2576 mice: implications for clinical trials.," *Brain Res.*, vol. 1037, no. 1–2, pp. 209–13, Mar. 2005.
- [69] S. A. Rosales-Corral, D. Acuña-Castroviejo, A. Coto-Montes, J. A. Boga, L. C. Manchester, L. Fuentes-Broto, A. Korkmaz, S. Ma, D.-X. Tan, and R. J. Reiter,

- “Alzheimer’s disease: pathological mechanisms and the beneficial role of melatonin.,” *J. Pineal Res.*, vol. 52, no. 2, pp. 167–202, Mar. 2012.
- [70] V. de Lima, M. Caro, M. Munford, B. Desbat, E. Dufourc, A. Pasa, and T. Creczynski-Pasa, “Influence of melatonin on the order of phosphatidylcholine-based membranes.,” *J. Pineal Res.*, vol. 49, no. 2, pp. 169–75, Sep. 2010.
- [71] E. Drolle, N. Kučerka, M. I. Hoopes, Y. Choi, J. Katsaras, M. Karttunen, and Z. Leonenko, “Effect of melatonin and cholesterol on the structure of DOPC and DPPC membranes.,” *Biochim. Biophys. Acta*, vol. 1828, no. 9, pp. 2247–54, Sep. 2013.
- [72] Z. Feng and J. Zhang, “Protective effect of melatonin on beta-amyloid-induced apoptosis in rat astrogloma C6 cells and its mechanism.,” *Free Radic. Biol. Med.*, vol. 37, no. 11, pp. 1790–801, Dec. 2004.
- [73] Y. Shen, S. Xu, W. Wei, X. Wang, H. Wang, and X. Sun, “Melatonin blocks rat hippocampal neuronal apoptosis induced by amyloid beta-peptide 25-35,” *J. Pineal Res.*, vol. 32, no. 3, pp. 163–167, Apr. 2002.
- [74] M. Ionov, V. Burchell, B. Klajnert, M. Bryszewska, and a Y. Abramov, “Mechanism of neuroprotection of melatonin against beta-amyloid neurotoxicity.,” *Neuroscience*, vol. 180, pp. 229–37, Apr. 2011.
- [75] D. Bongiorno, L. Ceraulo, M. Ferrugia, F. Filizzola, A. Ruggirello, and V. T. Liveri, “Localization and interactions of melatonin in dry cholesterol/lecithin mixed reversed micelles used as cell membrane models.,” *J. Pineal Res.*, vol. 38, no. 4, pp. 292–8, May 2005.
- [76] M. Pappolla, M. Simovich, T. Bryant-Thomas, Y. Chyan, B. Poeggeler, M. Dubocovich, R. Bick, G. Perry, F. Cruz-Sanchez, and M. Smith, “The neuroprotective activities of melatonin against the Alzheimer beta-protein are not mediated by melatonin membrane receptors,” *J. Pineal Res.*, vol. 32, no. 3, pp. 135–142, Apr. 2002.
- [77] M. J. Duncan, J. S. Takahashi, and M. L. Dubocovich, “Characteristics and autoradiographic localization of 2-[125I]iodomelatonin binding sites in Djungarian hamster brain.,” *Endocrinology*, vol. 125, no. 2, pp. 1011–8, Aug. 1989.
- [78] B. Keshet, J. Gray, and T. Good, “Structurally distinct toxicity inhibitors bind at common loci on β -amyloid fibril.,” *Protein Sci.*, vol. 19, no. 12, pp. 2291–304, Dec. 2010.
- [79] G. Roberts, *Langmuir-Blodgett films*. New York : Plenum Press, 1990, p. 425.
- [80] KSV-Instruments, “Langmuir and Langmuir-Blodgett Films what and how?,” LTD., KSV Instruments, Helsinki, Finland, Application Note #107.

- [81] R. Veldhuizen, K. Nag, S. Orgeig, and F. Possmayer, "The role of lipids in pulmonary surfactant.," *Biochim. Biophys. Acta*, vol. 1408, no. 2–3, pp. 90–108, Nov. 1998.
- [82] E. J. Acosta, R. Gitiafroz, Y. Y. Zuo, Z. Policova, P. N. Cox, M. L. Hair, and a W. Neumann, "Effect of humidity on lung surfactant films subjected to dynamic compression/expansion cycles.," *Respir. Physiol. Neurobiol.*, vol. 155, no. 3, pp. 255–67, Mar. 2007.
- [83] F. Hane, E. Drolle, and Z. Leonenko, "Effect of cholesterol and amyloid- β peptide on structure and function of mixed-lipid films and pulmonary surfactant BLES: an atomic force microscopy study.," *Nanomedicine*, vol. 6, no. 6, pp. 808–14, Dec. 2010.
- [84] P. Wydro and K. Hac-Wydro, "Thermodynamic description of the interactions between lipids in ternary Langmuir monolayers: the study of cholesterol distribution in membranes.," *J. Phys. Chem. B*, vol. 111, no. 10, pp. 2495–502, Mar. 2007.
- [85] R. Maget-Dana, "The monolayer technique: a potent tool for studying the interfacial properties of antimicrobial and membrane-lytic peptides and their interactions with lipid membranes," *Biochim. Biophys. Acta - Biomembr.*, vol. 1462, no. 1–2, pp. 109–140, Dec. 1999.
- [86] D. Marsh, "Lateral pressure in membranes," *Biochim. Biophys. Acta - Rev. Biomembr.*, vol. 1286, no. 3, pp. 183–223, Oct. 1996.
- [87] D. Marsh, "Lateral pressure profile, spontaneous curvature frustration, and the incorporation and conformation of proteins in membranes.," *Biophys. J.*, vol. 93, no. 11, pp. 3884–99, Dec. 2007.
- [88] G. Ma and H. C. Allen, "DPPC Langmuir monolayer at the air-water interface: probing the tail and head groups by vibrational sum frequency generation spectroscopy.," *Langmuir*, vol. 22, no. 12, pp. 5341–9, Jun. 2006.
- [89] S. Baoukina, L. Monticelli, H. J. Risselada, S. J. Marrink, and D. P. Tieleman, "The molecular mechanism of lipid monolayer collapse.," *Proc. Natl. Acad. Sci. U. S. A.*, vol. 105, no. 31, pp. 10803–8, Aug. 2008.
- [90] L. Zhao and S. Feng, "Effects of cholesterol component on molecular interactions between paclitaxel and phospholipid within the lipid monolayer at the air-water interface.," *J. Colloid Interface Sci.*, vol. 300, no. 1, pp. 314–26, Aug. 2006.
- [91] J. F. Nagle, "Theory of lipid monolayer and bilayer chain-melting phase transitions," *Faraday Discuss. Chem. Soc.*, vol. 81, no. 81, p. 151, Jan. 1986.

- [92] S. Feng, “Interpretation of Mechanochemical Properties of Lipid Bilayer Vesicles from the Equation of State or Pressure–Area Measurement of the Monolayer at the Air–Water or Oil–Water Interface,” *Langmuir*, vol. 15, no. 4, pp. 998–1010, Jan. 1999.
- [93] K. Kim, S. Q. Choi, Z. A. Zell, T. M. Squires, and J. A. Zasadzinski, “Effect of cholesterol nanodomains on monolayer morphology and dynamics.,” *Proc. Natl. Acad. Sci. U. S. A.*, vol. 110, no. 33, pp. E3054–60, Aug. 2013.
- [94] O. Coban, J. Popov, M. Burger, D. Vobornik, and L. J. Johnston, “Transition from nanodomains to microdomains induced by exposure of lipid monolayers to air.,” *Biophys. J.*, vol. 92, no. 8, pp. 2842–53, Apr. 2007.
- [95] M. Edidin, “The state of lipid rafts: from model membranes to cells.,” *Annu. Rev. Biophys. Biomol. Struct.*, vol. 32, pp. 257–83, Jan. 2003.
- [96] C. Ege and K. Lee, “Insertion of Alzheimer’s A beta 40 peptide into lipid monolayers.,” *Biophys. J.*, vol. 87, no. 3, pp. 1732–40, Sep. 2004.
- [97] A. Izmitli, C. Schebor, M. P. McGovern, A. S. Reddy, N. L. Abbott, and J. J. de Pablo, “Effect of trehalose on the interaction of Alzheimer’s A β -peptide and anionic lipid monolayers.,” *Biochim. Biophys. Acta*, vol. 1808, no. 1, pp. 26–33, Jan. 2011.
- [98] C. Alonso, A. Waring, and J. Zasadzinski, “Keeping lung surfactant where it belongs: protein regulation of two-dimensional viscosity.,” *Biophys. J.*, vol. 89, no. 1, pp. 266–73, Jul. 2005.
- [99] E. Maltseva, A. Kerth, A. Blume, H. Möhwald, and G. Brezesinski, “Adsorption of amyloid beta (1-40) peptide at phospholipid monolayers.,” *ChemBiochem*, vol. 6, no. 10, pp. 1817–24, Oct. 2005.
- [100] M. Eeman, A. Berquand, Y. F. Dufrière, M. Paquot, S. Dufour, and M. Deleu, “Penetration of surfactin into phospholipid monolayers: nanoscale interfacial organization.,” *Langmuir*, vol. 22, no. 26, pp. 11337–45, Dec. 2006.
- [101] T. Brehmer, A. Kerth, W. Graubner, M. Malesevic, B. Hou, T. Brüser, and A. Blume, “Negatively charged phospholipids trigger the interaction of a bacterial Tat substrate precursor protein with lipid monolayers.,” *Langmuir*, vol. 28, no. 7, pp. 3534–41, Mar. 2012.
- [102] H. P. Ta, K. Berthelot, B. Couлары-Salin, B. Desbat, J. Géan, L. Servant, C. Cullin, and S. Lecomte, “Comparative studies of nontoxic and toxic amyloids interacting with membrane models at the air-water interface.,” *Langmuir*, vol. 27, no. 8, pp. 4797–807, Apr. 2011.

- [103] S. L. Duncan and R. G. Larson, "Comparing experimental and simulated pressure-area isotherms for DPPC.," *Biophys. J.*, vol. 94, no. 8, pp. 2965–86, Apr. 2008.
- [104] K. Sabatini, J. Mattila, F. M. Megli, and P. K. J. Kinnunen, "Characterization of two oxidatively modified phospholipids in mixed monolayers with DPPC.," *Biophys. J.*, vol. 90, no. 12, pp. 4488–99, Jun. 2006.
- [105] D. O. Shah and J. H. Schulman, "Influence of calcium, cholesterol, and unsaturation on lecithin monolayers.," *J. Lipid Res.*, vol. 8, no. 3, pp. 215–26, May 1967.
- [106] C. Yuan and L. J. Johnston, "Atomic force microscopy studies of ganglioside GM1 domains in phosphatidylcholine and phosphatidylcholine/cholesterol bilayers.," *Biophys. J.*, vol. 81, no. 2, pp. 1059–69, Aug. 2001.
- [107] E. Berring, K. Borrenpohl, S. Fliesler, and A. B. Serfis, "A comparison of the behavior of cholesterol and selected derivatives in mixed sterol-phospholipid Langmuir monolayers: a fluorescence microscopy study.," *Chem. Phys. Lipids*, vol. 136, no. 1, pp. 1–12, Jul. 2005.
- [108] K. Kim, C. Kim, and Y. Byun, "Preparation of a Dipalmitoylphosphatidylcholine/Cholesterol Langmuir–Blodgett Monolayer That Suppresses Protein Adsorption," *Langmuir*, vol. 17, no. 16, pp. 5066–5070, Aug. 2001.
- [109] K. Gong, S. Feng, M. L. Go, and P. H. Soew, "Effects of pH on the stability and compressibility of DPPC/cholesterol monolayers at the air–water interface," *Colloids Surfaces A Physicochem. Eng. Asp.*, vol. 207, no. 1–3, pp. 113–125, Jul. 2002.
- [110] O. Edholm and J. F. Nagle, "Areas of molecules in membranes consisting of mixtures.," *Biophys. J.*, vol. 89, no. 3, pp. 1827–32, Sep. 2005.
- [111] M. C. Wiener, R. M. Suter, and J. F. Nagle, "Structure of the fully hydrated gel phase of dipalmitoylphosphatidylcholine.," *Biophys. J.*, vol. 55, no. 2, pp. 315–25, Mar. 1989.
- [112] N. J. Hardy, T. H. Richardson, and F. Grunfeld, "Minimising monolayer collapse on Langmuir troughs," *Colloids Surfaces A Physicochem. Eng. Asp.*, vol. 284–285, pp. 202–206, Aug. 2006.
- [113] P. Dynarowicz-Łatka and K. Hac-Wydro, "Interactions between phosphatidylcholines and cholesterol in monolayers at the air/water interface.," *Colloids Surf. B. Biointerfaces*, vol. 37, no. 1–2, pp. 21–5, Aug. 2004.
- [114] H. Y. Saad and W. I. Higuchi, "Water solubility of cholesterol," *J. Pharm. Sci.*, vol. 54, no. 8, pp. 1205–6, Aug. 1965.

- [115] L. A. Worthman, K. Nag, P. J. Davis, and K. M. Keough, "Cholesterol in condensed and fluid phosphatidylcholine monolayers studied by epifluorescence microscopy.," *Biophys. J.*, vol. 72, no. 6, pp. 2569–80, Jun. 1997.
- [116] C. Yuan and L. J. Johnston, "Phase evolution in cholesterol/DPPC monolayers: atomic force microscopy and near field scanning optical microscopy studies.," *J. Microsc.*, vol. 205, no. Pt 2, pp. 136–46, Mar. 2002.
- [117] O. Albrecht, H. Gruler, and E. Sackmann, "Pressure-composition phase diagrams of cholesterol/lecithin, cholesterol/phosphatidic acid, and lecithin/phosphatidic acid mixed monolayers: A Langmuir film balance study.," *J. Colloid Interface Sci.*, vol. 79, no. 2, pp. 319–338, Feb. 1981.
- [118] Y. Choi, S. J. Attwood, M. I. Hoopes, E. Drolle, M. Karttunen, and Z. Leonenko, "Melatonin directly interacts with cholesterol and alleviates cholesterol effects in dipalmitoylphosphatidylcholine monolayers.," *Soft Matter*, vol. 10, no. 1, pp. 206–13, Jan. 2014.
- [119] M. Demierre, P. D. Higgins, S. B. Gruber, E. Hawk, and S. Lippman, "Statins and cancer prevention.," *Nat. Rev. Cancer*, vol. 5, no. 12, pp. 930–42, Dec. 2005.
- [120] S. Tengattini, R. J. Reiter, D. Tan, M. P. Terron, L. F. Rodella, and R. Rezzani, "Cardiovascular diseases: protective effects of melatonin.," *J. Pineal Res.*, vol. 44, no. 1, pp. 16–25, Jan. 2008.
- [121] H. Tamura, Y. Nakamura, A. Narimatsu, Y. Yamagata, A. Takasaki, R. J. Reiter, and N. Sugino, "Melatonin treatment in peri- and postmenopausal women elevates serum high-density lipoprotein cholesterol levels without influencing total cholesterol levels.," *J. Pineal Res.*, vol. 45, no. 1, pp. 101–5, Aug. 2008.
- [122] E. J. Costa, C. S. Shida, M. H. Biaggi, A. S. Ito, and M. T. Lamy-Freund, "How melatonin interacts with lipid bilayers: a study by fluorescence and ESR spectroscopies.," *FEBS Lett.*, vol. 416, no. 1, pp. 103–6, Oct. 1997.
- [123] J. J. García, R. J. Reiter, G. G. Ortiz, C. S. Oh, L. Tang, B. P. Yu, and G. Escames, "Melatonin enhances tamoxifen's ability to prevent the reduction in microsomal membrane fluidity induced by lipid peroxidation.," *J. Membr. Biol.*, vol. 162, no. 1, pp. 59–65, Mar. 1998.
- [124] J. J. García, R. R. J. R. Reiter, J. J. M. Guerrero, G. Escames, B. P. Yu, C. S. Oh, and A. Muñoz-Hoyos, "Melatonin prevents changes in microsomal membrane fluidity during induced lipid peroxidation.," *FEBS Lett.*, vol. 408, no. 3, pp. 297–300, May 1997.

- [125] Z. Wang and S. Yang, "Effects of fullerenes on phospholipid membranes: a langmuir monolayer study.," *Chemphyschem*, vol. 10, no. 13, pp. 2284–9, Sep. 2009.
- [126] D. W. Zimmerman, "Teacher's Corner: A Note on Interpretation of the Paired-Samples t Test," *J. Educ. Behav. Stat.*, vol. 22, no. 3, pp. 349–360, Jan. 1997.
- [127] T. Schmidt, L. Caseli, T. Nobre, M. Zaniquelli, and O. Oliveira, "Interaction of horseradish peroxidase with Langmuir monolayers of phospholipids," *Colloids Surfaces A Physicochem. Eng. Asp.*, vol. 321, no. 1–3, pp. 206–210, May 2008.
- [128] M. Subirade, C. Salesse, D. Marion, and M. Pézolet, "Interaction of a nonspecific wheat lipid transfer protein with phospholipid monolayers imaged by fluorescence microscopy and studied by infrared spectroscopy.," *Biophys. J.*, vol. 69, no. 3, pp. 974–88, Oct. 1995.
- [129] S. Kundu, H. Chakraborty, M. Sarkar, and A. Datta, "Interaction of Oxicam NSAIDs with lipid monolayer: anomalous dependence on drug concentration.," *Colloids Surf. B. Biointerfaces*, vol. 70, no. 1, pp. 157–61, Apr. 2009.
- [130] R. Oliveira, E. Schneck, S. Funari, M. Tanaka, and B. Maggio, "Equivalent aqueous phase modulation of domain segregation in myelin monolayers and bilayer vesicles.," *Biophys. J.*, vol. 99, no. 5, pp. 1500–9, Oct. 2010.
- [131] D. Marsh, "Comment on interpretation of mechanochemical properties of lipid bilayer vesicles from the equation of state or pressure-area measurement of the monolayer at the air-water or oil-water interface.," *Langmuir*, vol. 22, no. 6, pp. 2916–9; discussion 2920–2, Mar. 2006.
- [132] J. F. Nagle and S. Tristram-Nagle, "Structure of lipid bilayers," *Biochim. Biophys. Acta - Rev. Biomembr.*, vol. 1469, no. 3, pp. 159–195, Nov. 2000.
- [133] A. N. Dickey and R. Faller, "How alcohol chain-length and concentration modulate hydrogen bond formation in a lipid bilayer.," *Biophys. J.*, vol. 92, no. 7, pp. 2366–76, Apr. 2007.
- [134] T. Hsu, D. L. Leiske, L. Rosenfeld, J. M. Sonner, and G. G. Fuller, "3-Hydroxybutyric acid interacts with lipid monolayers at concentrations that impair consciousness.," *Langmuir*, vol. 29, no. 6, pp. 1948–55, Mar. 2013.
- [135] B. L. Stottrup and S. L. Keller, "Phase behavior of lipid monolayers containing DPPC and cholesterol analogs.," *Biophys. J.*, vol. 90, no. 9, pp. 3176–83, May 2006.
- [136] S. B. Akkas, S. Inci, F. Zorlu, and F. Severcan, "Melatonin affects the order, dynamics and hydration of brain membrane lipids," *J. Mol. Struct.*, vol. 836, pp. 207–215, 2007.

- [137] A. Borba, F. Lairion, A. Disalvo, and R. Fausto, “Interaction of nicotinamide and picolinamide with phosphatidylcholine and phosphatidylethanolamine membranes: a combined approach using dipole potential measurements and quantum chemical calculations.,” *Biochim. Biophys. Acta*, vol. 1788, no. 12, pp. 2553–62, Dec. 2009.
- [138] R. J. Mashl, H. L. Scott, S. Subramaniam, and E. Jakobsson, “Molecular simulation of dioleoylphosphatidylcholine lipid bilayers at differing levels of hydration.,” *Biophys. J.*, vol. 81, no. 6, pp. 3005–15, Dec. 2001.
- [139] E. A. Disalvo, F. Lairion, F. Martini, E. Tymczyszyn, M. Frías, H. Almaleck, and G. J. Gordillo, “Structural and functional properties of hydration and confined water in membrane interfaces.,” *Biochim. Biophys. Acta*, vol. 1778, no. 12, pp. 2655–70, Dec. 2008.
- [140] E. R. Pinnick, S. Erramilli, and F. Wang, “Computational investigation of lipid hydration water of L α 1-palmitoyl-2-oleoyl- sn -glycero-3-phosphocholine at three hydration levels,” *Mol. Phys.*, vol. 108, no. 15, pp. 2027–36, Aug. 2010.
- [141] J. J. García, R. J. Reiter, J. Pié, G. G. Ortiz, J. Cabrera, R. M. Sáinz, and D. Acuña-Castroviejo, “Role of pinoline and melatonin in stabilizing hepatic microsomal membranes against oxidative stress.,” *J. Bioenerg. Biomembr.*, vol. 31, no. 6, pp. 609–16, Dec. 1999.
- [142] M. Karbownik, R. J. Reiter, W. Qi, J. J. Garcia, D. X. Tan, L. C. Manchester, and Vijayalaxmi, “Protective effects of melatonin against oxidation of guanine bases in DNA and decreased microsomal membrane fluidity in rat liver induced by whole body ionizing radiation.,” *Mol. Cell. Biochem.*, vol. 211, no. 1–2, pp. 137–44, Aug. 2000.
- [143] V. ijayalaxmi, C. Thomas, R. Reiter, and T. Herman, “Melatonin: From Basic Research to Cancer Treatment Clinics,” *J. Clin. Oncol.*, vol. 20, no. 10, pp. 2575–2601, May 2002.
- [144] Y. Ishitsuka, D. Pham, A. Waring, R. Lehrer, and K. Lee, “Insertion selectivity of antimicrobial peptide protegrin-1 into lipid monolayers: effect of head group electrostatics and tail group packing.,” *Biochim. Biophys. Acta*, vol. 1758, no. 9, pp. 1450–60, Sep. 2006.
- [145] H. N. Noristani, A. Verkhatsky, and J. J. Rodríguez, “High tryptophan diet reduces CA1 intraneuronal β -amyloid in the triple transgenic mouse model of Alzheimer’s disease.,” *Ageing Cell*, vol. 11, no. 5, pp. 810–22, Oct. 2012.
- [146] J. R. Cirrito, B. M. Disabato, J. L. Restivo, D. K. Verges, W. D. Goebel, A. Sathyan, D. Hayreh, G. D’Angelo, T. Benzinger, H. Yoon, J. Kim, J. C. Morris, M. a Mintun, and Y. I. Sheline, “Serotonin signaling is associated with lower amyloid- β levels and plaques in

- transgenic mice and humans.,” *Proc. Natl. Acad. Sci. U. S. A.*, vol. 108, no. 36, pp. 14968–73, Sep. 2011.
- [147] S. Bachurin, G. Oxenkrug, N. Lermontova, A. Afanasiev, B. Beznosko, G. Vankin, E. Shevtzova, T. Mukhina, and T. Serkova, “N-acetylserotonin, melatonin and their derivatives improve cognition and protect against beta-amyloid-induced neurotoxicity.,” *Ann. N. Y. Acad. Sci.*, vol. 890, pp. 155–66, Jan. 1999.
- [148] G. H. Peters, C. Wang, N. Cruys-Bagger, G. F. Velardez, J. J. Madsen, and P. Westh, “Binding of serotonin to lipid membranes.,” *J. Am. Chem. Soc.*, vol. 135, no. 6, pp. 2164–71, Mar. 2013.
- [149] C. Wang, F. Ye, G. F. Velardez, G. H. Peters, and P. Westh, “Affinity of four polar neurotransmitters for lipid bilayer membranes.,” *J. Phys. Chem. B*, vol. 115, no. 1, pp. 196–203, Jan. 2011.
- [150] K. Jodko-Piorecka and G. Litwinienko, “First experimental evidence of dopamine interactions with negatively charged model biomembranes.,” *ACS Chem. Neurosci.*, vol. 4, no. 7, pp. 1114–22, Jul. 2013.
- [151] I. Wood, M. F. Martini, and M. Pickholz, “Similarities and differences of serotonin and its precursors in their interactions with model membranes studied by molecular dynamics simulation,” *J. Mol. Struct.*, vol. 1045, pp. 124–130, Aug. 2013.
- [152] A. Orłowski, M. Grzybek, A. Bunker, M. Pasenkiewicz-Gierula, I. Vattulainen, P. T. Männistö, and T. Róg, “Strong preferences of dopamine and L-dopa towards lipid head group: importance of lipid composition and implication for neurotransmitter metabolism,” *J. Neurochem.*, vol. 122, no. 4, pp. 681–690, Aug. 2012.
- [153] W. M. Yau, W. C. Wimley, K. Gawrisch, and S. H. White, “The preference of tryptophan for membrane interfaces.,” *Biochemistry*, vol. 37, no. 42, pp. 14713–8, Oct. 1998.
- [154] M. Schiffer, C. Chang, and F. Stevens, “The function of tryptophan residues in membrane proteins,” *Protein Eng. Des. Sel.*, vol. 5, no. 3, pp. 213–214, Apr. 1992.
- [155] E. H. Clark, J. M. East, and A. G. Lee, “The role of tryptophan residues in an integral membrane protein: diacylglycerol kinase.,” *Biochemistry*, vol. 42, no. 37, pp. 11065–73, Sep. 2003.
- [156] A. Holt, R. de Almeida, T. Nyholm, L. Loura, A. Daily, R. Staffhorst, D. Rijkers, R. Koeppel, M. Prieto, and A. Killian, “Is there a preferential interaction between cholesterol and tryptophan residues in membrane proteins?,” *Biochemistry*, vol. 47, no. 8, pp. 2638–49, Feb. 2008.

- [157] M. K. Jain, J. Rogers, L. Simpson, and L. M. Gierasch, "Effect of tryptophan derivatives on the phase properties of bilayers.," *Biochim. Biophys. Acta*, vol. 816, no. 1, pp. 153–62, Jun. 1985.
- [158] N. K. Sarangi and A. Patnaik, "Unraveling tryptophan modulated 2D DPPC lattices: an approach toward stimuli responsiveness of the pulmonary surfactant.," *J. Phys. Chem. B*, vol. 115, no. 46, pp. 13551–62, Nov. 2011.
- [159] R. Wyatt, "Effects of L-Tryptophan (a natural sedative) on human sleep," *Lancet*, vol. 296, no. 7678, pp. 842–846, Oct. 1970.
- [160] F. Stetter and T. Hugel, "The nanomechanical properties of lipid membranes are significantly influenced by the presence of ethanol.," *Biophys. J.*, vol. 104, no. 5, pp. 1049–55, Mar. 2013.
- [161] V. Srinivasan, S. R. Pandi-Perumal, D. W. Spence, A. Moscovitch, I. Trakht, G. M. Brown, and D. P. Cardinali, "Potential use of melatonergic drugs in analgesia: mechanisms of action.," *Brain Res. Bull.*, vol. 81, no. 4–5, pp. 362–71, Mar. 2010.
- [162] R. S. Cantor, "Receptor desensitization by neurotransmitters in membranes: are neurotransmitters the endogenous anesthetics?," *Biochemistry*, vol. 42, no. 41, pp. 11891–7, Oct. 2003.
- [163] S. Süzen, "Antioxidant activities of synthetic indole derivatives and possible activity mechanisms," *Bioact. Heterocycles V*, no. July, pp. 145–178, 2007.
- [164] R. Reiter, L. Tang, J. J. Garcia, and A. Muñoz-Hoyos, "Pharmacological actions of melatonin in oxygen radical pathophysiology," *Life Sci.*, vol. 60, no. 25, pp. 2255–2271, May 1997.
- [165] C. K. Sen, "The general case for redox control of wound repair," *Wound Repair Regen.*, vol. 11, no. 6, pp. 431–438, Nov. 2003.
- [166] R. Hardeland, "Melatonin, hormone of darkness and more: occurrence, control mechanisms, actions and bioactive metabolites.," *Cell. Mol. Life Sci.*, vol. 65, no. 13, pp. 2001–18, Jul. 2008.
- [167] S. M. Roy, A. S. Bansode, and M. Sarkar, "Effect of increase in orientational order of lipid chains and head group spacing on non steroidal anti-inflammatory drug induced membrane fusion.," *Langmuir*, vol. 26, no. 24, pp. 18967–75, Dec. 2010.
- [168] A. Gopal and K. Y. C. Lee, "Morphology and Collapse Transitions in Binary Phospholipid Monolayers," *J. Phys. Chem. B*, vol. 105, no. 42, pp. 10348–10354, Oct. 2001.

- [169] G. Tosini, K. Baba, C. K. Hwang, and P. M. Iuvone, “Melatonin : An underappreciated player in retinal physiology and pathophysiology,” *Exp. Eye Res.*, vol. 103, pp. 82–89, 2012.
- [170] S. Rosales-Corral, D. Acuna-Castroviejo, D. X. Tan, G. López-Armas, J. Cruz-Ramos, R. Munoz, V. G. Melnikov, L. C. Manchester, and R. J. Reiter, “Accumulation of exogenous amyloid-beta peptide in hippocampal mitochondria causes their dysfunction: a protective role for melatonin.,” *Oxid. Med. Cell. Longev.*, vol. 2012, p. 843649, Jan. 2012.
- [171] J. M. Smaby, V. S. Kulkarni, M. Momsen, and R. E. Brown, “The Interfacial Elastic Packing Interactions of Galactosylceramides ,” vol. 70, no. February, pp. 868–877, 1996.
- [172] F. J. Giessibl, “Advances in atomic force microscopy,” *Rev. Mod. Phys.*, vol. 75, no. 3, pp. 949–983, Jul. 2003.
- [173] E. Meyer, H. J. Hug, and R. Bennewitz, *Scanning probe microscopy : the lab on a tip*. New York: Springer, 2004.
- [174] R. Lévy and M. Maaloum, “Measuring the spring constant of atomic force microscope cantilevers: thermal fluctuations and other methods,” *Nanotechnology*, vol. 13, no. 1, pp. 33–37, Feb. 2002.
- [175] Z. Leonenko, A. Carnini, and D. Cramb, “Supported planar bilayer formation by vesicle fusion: the interaction of phospholipid vesicles with surfaces and the effect of gramicidin on bilayer properties using atomic force microscopy,” *Biochim. Biophys. Acta - Biomembr.*, vol. 1509, no. 1–2, pp. 131–147, Dec. 2000.
- [176] Z. Leonenko, E. Finot, H. Ma, T. Dahms, and D. Cramb, “Investigation of temperature-induced phase transitions in DOPC and DPPC phospholipid bilayers using temperature-controlled scanning force microscopy.,” *Biophys. J.*, vol. 86, no. 6, pp. 3783–93, Jun. 2004.
- [177] L. Picas, F. Rico, and S. Scheuring, “Direct measurement of the mechanical properties of lipid phases in supported bilayers.,” *Biophys. J.*, vol. 102, no. 1, pp. L01–3, Jan. 2012.
- [178] P. Milhiet, M. Giocondi, O. Baghdadi, F. Ronzon, C. Le Grimellec, and B. Roux, “AFM Detection of GPI Protein Insertion into DOPC/DPPC Model Membranes,” *Single Mol.*, vol. 3, no. 2–3, pp. 135–140, Jun. 2002.
- [179] M. Deleu, J. Lorent, L. Lins, R. Brasseur, N. Braun, K. El Kirat, T. Nylander, Y. F. Dufrêne, and M. Mingeot-Leclercq, “Effects of surfactin on membrane models displaying lipid phase separation.,” *Biochim. Biophys. Acta*, vol. 1828, no. 2, pp. 801–15, Feb. 2013.

- [180] B. Seantier, M. Giocondi, C. Grimellec, and P. Milhiet, "Probing supported model and native membranes using AFM," *Curr. Opin. Colloid Interface Sci.*, vol. 13, no. 5, pp. 326–337, Oct. 2008.
- [181] E. Lesniewska, P. Milhiet, M. Zinke-allmang, C. Le Grimellec, M. Giocondi, V. Vié, and C. Le Grimellec, "Phase topology and growth of single domains in lipid bilayers," *Langmuir*, vol. 17, no. 5, pp. 1653–1659, 2001.
- [182] M. Giocondi, D. Yamamoto, E. Lesniewska, P. Milhiet, T. Ando, and C. Le Grimellec, "Surface topography of membrane domains.," *Biochim. Biophys. Acta*, vol. 1798, no. 4, pp. 703–18, Apr. 2010.
- [183] A. Choucair, M. Chakrapani, B. Chakravarthy, J. Katsaras, and L. J. Johnston, "Preferential accumulation of Aβ(1-42) on gel phase domains of lipid bilayers: an AFM and fluorescence study.," *Biochim. Biophys. Acta*, vol. 1768, no. 1, pp. 146–54, Jan. 2007.
- [184] M. Mingeot-Leclercq, M. Deleu, R. Brasseur, and Y. F. Dufrêne, "Atomic force microscopy of supported lipid bilayers.," *Nat. Protoc.*, vol. 3, no. 10, pp. 1654–9, Jan. 2008.
- [185] K. El Kirat, S. Morandat, and Y. F. Dufrêne, "Nanoscale analysis of supported lipid bilayers using atomic force microscopy.," *Biochim. Biophys. Acta*, vol. 1798, no. 4, pp. 750–65, Apr. 2010.
- [186] F. Yarrow and B. Kuipers, "AFM study of the thermotropic behaviour of supported DPPC bilayers with and without the model peptide WALP23.," *Chem. Phys. Lipids*, vol. 164, no. 1, pp. 9–15, Jan. 2011.
- [187] H. Rinia, J. Boots, D. Rijkers, R. Kik, M. M. Snel, R. Demel, A. Killian, J. van der Eerden, and B. de Kruijff, "Domain Formation in Phosphatidylcholine Bilayers Containing Transmembrane Peptides: Specific Effects of Flanking Residues †," *Biochemistry*, vol. 41, no. 8, pp. 2814–2824, Feb. 2002.
- [188] J. Mou, D. M. Czajkowsky, and Z. Shao, "Gramicidin A aggregation in supported gel state phosphatidylcholine bilayers," *Biochemistry*, vol. 35, no. 10, pp. 3222–3226, 1996.
- [189] D. Keller, N. Larsen, I. Møller, and O. Mouritsen, "Decoupled Phase Transitions and Grain-Boundary Melting in Supported Phospholipid Bilayers," *Phys. Rev. Lett.*, vol. 94(2), no. 025701, pp. 1–4, Jan. 2005.
- [190] H. P. Wacklin, "Composition and asymmetry in supported membranes formed by vesicle fusion," *Langmuir*, vol. 27, no. 12, pp. 7698–7707, 2011.

- [191] F. Dekkiche, M. Corneci, A. Trunfio-Sfarghiu, B. Munteanu, Y. Berthier, W. Kaabar, and J. Rieu, “Stability and tribological performances of fluid phospholipid bilayers: effect of buffer and ions.,” *Colloids Surf. B. Biointerfaces*, vol. 80, no. 2, pp. 232–9, Oct. 2010.
- [192] M. Munford, V. Lima, T. Vieira, G. Heinzelmann, T. Creczynski-Pasa, and A. Pasa, “AFM in-situ characterization of supported phospholipid layers formed by vesicle fusion,” *Microsc. Microanal.*, vol. 11, no. SUPPL. 3, pp. 90–93, 2005.
- [193] L. M. Grant and F. Tiberg, “Normal and lateral forces between lipid covered solids in solution: correlation with layer packing and structure.,” *Biophys. J.*, vol. 82, no. 3, pp. 1373–85, Mar. 2002.
- [194] J. Gallová, D. Uhríková, a Islamov, a Kuklin, and P. Balgavý, “Effect of cholesterol on the bilayer thickness in unilamellar extruded DLPC and DOPC liposomes: SANS contrast variation study.,” *Gen. Physiol. Biophys.*, vol. 23, no. 1, pp. 113–28, Mar. 2004.
- [195] M. Gandhavadi, D. Allende, A. Vidal, S. A. Simon, and T. J. McIntosh, “Structure, composition, and peptide binding properties of detergent soluble bilayers and detergent resistant rafts,” *Biophys. J.*, vol. 82, no. 3, pp. 1469–1482, 2002.
- [196] J. Pan, D. P. Tieleman, J. F. Nagle, N. Kučerka, and S. Tristram-Nagle, “Alamethicin in lipid bilayers: Combined use of X-ray scattering and MD simulations,” *Biochim. Biophys. Acta - Biomembr.*, vol. 1788, no. 6, pp. 1387–1397, 2009.
- [197] S. Tristram-Nagle, H. I. Petrache, and J. F. Nagle, “Structure and interactions of fully hydrated dioleoylphosphatidylcholine bilayers,” *Biophys. J.*, vol. 75, no. 2, pp. 917–925, 1998.
- [198] S. Garcia-manyes, L. Redondo-Morata, G. Oncins, and F. Sanz, “Nanomechanics of Lipid Bilayers : Heads or Tails ?,” *J. Am. Chem. Soc.*, vol. 132, no. 14, pp. 12874–12886, Sep. 2010.
- [199] S. Garcia-Manyes and F. Sanz, “Nanomechanics of lipid bilayers by force spectroscopy with AFM: a perspective.,” *Biochim. Biophys. Acta*, vol. 1798, no. 4, pp. 741–9, Apr. 2010.
- [200] V. Franz, S. Loi, H. Müller, E. Bamberg, and H.-J. Butt, “Tip penetration through lipid bilayers in atomic force microscopy,” *Colloids Surfaces B Biointerfaces*, vol. 23, no. 2–3, pp. 191–200, Feb. 2002.
- [201] M. C. Strus, C. I. Cano, R. Byron Pipes, C. V. Nguyen, and A. Raman, “Interfacial energy between carbon nanotubes and polymers measured from nanoscale peel tests in the atomic force microscope,” *Compos. Sci. Technol.*, vol. 69, no. 10, pp. 1580–1586, Aug. 2009.

- [202] S. Ip, J. K. Li, and G. C. Walker, "Phase segregation of untethered zwitterionic model lipid bilayers observed on mercaptoundecanoic-acid-modified gold by AFM imaging and force mapping.," *Langmuir*, vol. 26, no. 13, pp. 11060–70, Jul. 2010.
- [203] J. Zhang, R. Wang, X. Yang, W. Lu, X. Wu, X. Wang, H. Li, and L. Chen, "Direct observation of inhomogeneous solid electrolyte interphase on MnO anode with atomic force microscopy and spectroscopy.," *Nano Lett.*, vol. 12, no. 4, pp. 2153–7, Apr. 2012.
- [204] S. J. Attwood, Y. Choi, and Z. Leonenko, "Preparation of DOPC and DPPC Supported Planar Lipid Bilayers for Atomic Force Microscopy and Atomic Force Spectroscopy.," *Int. J. Mol. Sci.*, vol. 14, no. 2, pp. 3514–39, Jan. 2013.
- [205] S. Morandat and K. El Kirat, "Exploring the Properties and Interactions of Supported Lipid Bilayers on the Nanoscale by Atomic Force Microscopy.," in *Microscopy: Science, Technology, Applications And Education*, Vol. 3., A. Mendez-Vilas and J. Diaz, Eds. Formatex Research Center, 2010, pp. 1925–39.
- [206] E. I. Goksu and M. L. Longo, "Ternary lipid bilayers containing cholesterol in a high curvature silica xerogel environment.," *Langmuir*, vol. 26, no. 11, pp. 8614–24, Jun. 2010.
- [207] C. M. Yip, A. Darabie, and J. McLaurin, "Abeta42-peptide assembly on lipid bilayers.," *J. Mol. Biol.*, vol. 318, no. 1, pp. 97–107, Apr. 2002.
- [208] K. Sasahara, K. Morigaki, and K. Shinya, "Effects of membrane interaction and aggregation of amyloid β -peptide on lipid mobility and membrane domain structure.," *Phys. Chem. Chem. Phys.*, vol. 15, no. 23, pp. 8929–39, Jun. 2013.
- [209] K. Burke, E. Yates, and J. Legleiter, "Biophysical insights into how surfaces, including lipid membranes, modulate protein aggregation related to neurodegeneration.," *Front. Neurol.*, vol. 4, no. March, p. 17, Jan. 2013.
- [210] K. Sheikh, C. Giordani, J. McManus, M. Hovgaard, and S. Jarvis, "Differing modes of interaction between monomeric A β (1-40) peptides and model lipid membranes: an AFM study.," *Chem. Phys. Lipids*, vol. 165, no. 2, pp. 142–50, Mar. 2012.
- [211] A. Relini, O. Cavalleri, R. Rolandi, and A. Gliozzi, "The two-fold aspect of the interplay of amyloidogenic proteins with lipid membranes.," *Chem. Phys. Lipids*, vol. 158, no. 1, pp. 1–9, Mar. 2009.
- [212] E. Drolle, R. M. Gaikwad, and Z. Leonenko, "Nanoscale electrostatic domains in cholesterol-laden lipid membranes create a target for amyloid binding.," *Biophys. J.*, vol. 103, no. 4, pp. L27–9, Aug. 2012.

- [213] C. M. Yip and J. McLaurin, "Amyloid-beta peptide assembly: a critical step in fibrillogenesis and membrane disruption.," *Biophys. J.*, vol. 80, no. 3, pp. 1359–71, Mar. 2001.
- [214] J. Legleiter, "Assessing A β aggregation state by atomic force microscopy.," *Methods Mol. Biol.*, vol. 670, pp. 57–70, Jan. 2011.
- [215] A. M. Klein, N. W. Kowall, and R. J. Ferrante, "Neurotoxicity and oxidative damage of beta amyloid 1-42 versus beta amyloid 1-40 in the mouse cerebral cortex.," *Ann. N. Y. Acad. Sci.*, vol. 893, pp. 314–20, Jan. 1999.
- [216] J. Legleiter, *Alzheimer's Disease and Frontotemporal Dementia*, vol. 670. Totowa, NJ: Humana Press, 2011, pp. 57–70.
- [217] A. K. Buell, C. M. Dobson, and M. E. Welland, "Measuring the kinetics of amyloid fibril elongation using quartz crystal microbalances.," *Methods Mol. Biol.*, vol. 849, pp. 101–19, Jan. 2012.
- [218] Y. Fezoui, D. M. Hartley, J. D. Harper, R. Khurana, D. M. Walsh, M. M. Condron, D. J. Selkoe, P. T. Lansbury, a L. Fink, and D. B. Teplow, "An improved method of preparing the amyloid beta-protein for fibrillogenesis and neurotoxicity experiments.," *Amyloid*, vol. 7, no. 3, pp. 166–78, Sep. 2000.

Appendix A Tip Modification

AFM Tip Modification Procedure

1. NPG gold coated cantilevers were purchased from Bruker AFM Probes (CA, USA)
2. Transfer a cantilever into 20 ml glass scintillation vials with 2.0 ml ethanol
3. Incubate for 10 minutes at room temperature
4. Transfer the cantilever into another 20 ml glass scintillation vial with 2.0 ml water (Millipore, $>18.2 \text{ M}\Omega\cdot\text{cm}$)
5. Incubate for 10 minutes
6. Take the tip out of the vial, place it onto a freshly cleaved mica and place it inside the UV ozone clear for 60 minutes
7. After 60 minutes, put the tip in a 20 ml glass scintillation vial that contains 2 ml of ethanol and 1 mg/ml of the desired thiol compound, which were either 11-mercapto-1-undecanol (Sigma-Aldrich), or HS-(CH₂)₁₁-EG6-OH (Prochemia, Poland)
8. Leave the cantilever in thiol/ ethanol solution for 24 hours at room temperature, protect the vial and cantilever from light by wrapping the glass vial with aluminum foil.
9. After 24 hours of incubation, rinse the tip by dipping it into a 20 ml glass vial containing 2 ml of ethanol
10. Wait 2 minutes

11. Transfer and rinse the cantilever by dipping it into 2.0 ml of water in a 20 ml glass scintillation vial
12. Wait 2 minutes
13. The tip is now ready to be used for AFM force experiments, keep the cantilever under water or buffer as much as possible and only use it for one set of force experiments.

Appendix B Cell Viability Study

The results from the hippocampal neuronal cultures were not conclusive (data not shown). The tested A β aggregate production protocol in section 4.3 was used on SH-SY5Y cells. The results showed that the A β was most toxic at between 2-5 μ M concentrations (figure E-1). Testing A β toxicity on RGC-5 celled showed that 50 μ M melatonin treatment significantly reduced cell death caused by 2 μ M A β treatment, as measured via the MTT reduction assay (figure E-2). Extended experiments involving methyl- β -cyclodextrin (BCD or CD) in various combinations with melatonin were also performed to study the effects of cholesterol reduction in melatonin's effects (figure E-3). Melatonin showed positive effects against A β , however, BCD showed inherent toxicity that is further exacerbated by the presence of melatonin. Also the results were not statistically significant versus A β only, which negated any potential protective effects from CD or CD and melatonin together.

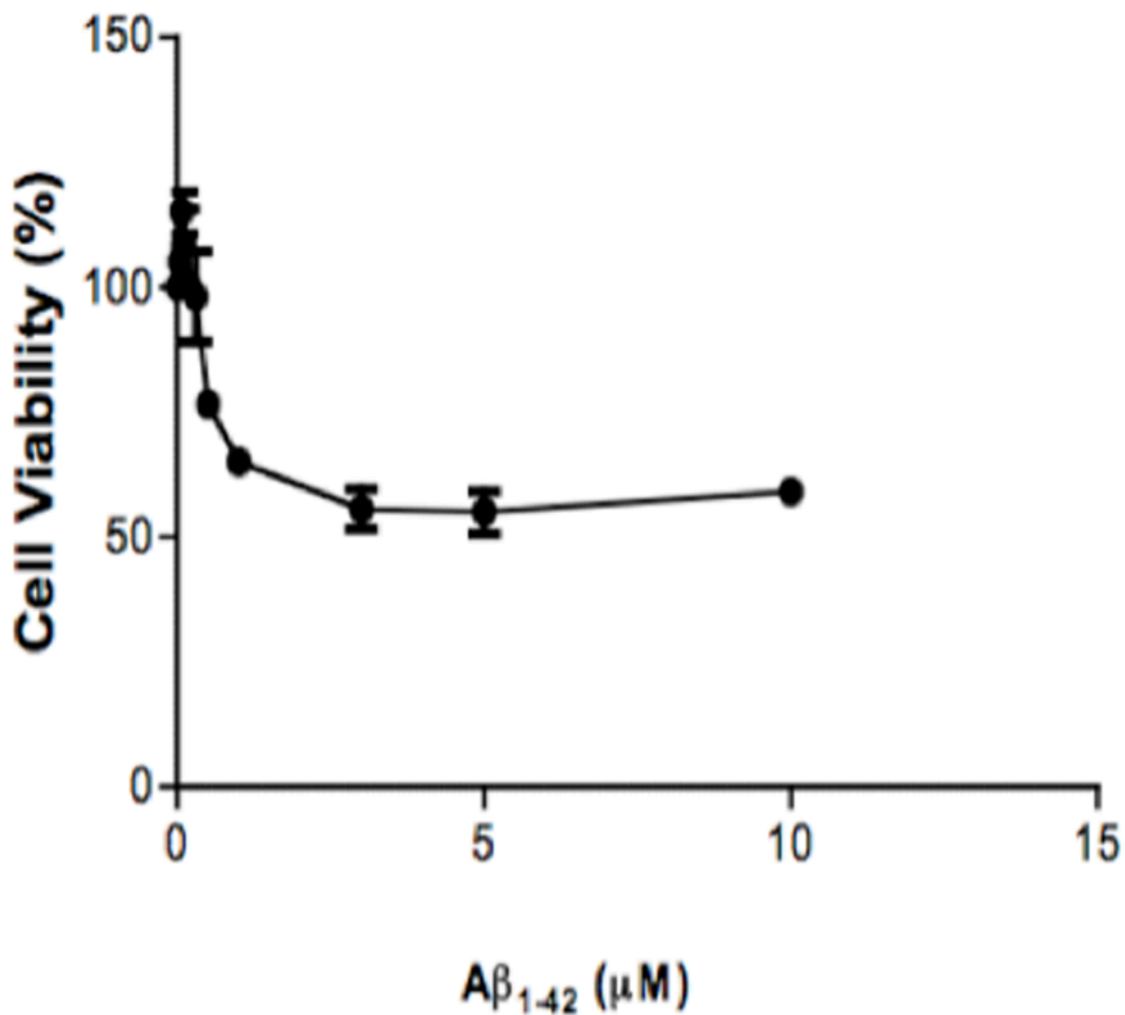


Figure E-1 - Aβ toxicity in SH-SY5Y cells. ($0.5-1 \times 10^5/\text{ml}$) were treated with 10 nM to 10 μM Aβ (1-42) for 24 hours and the cell viability was measured using the MTT assay. Data presented are the mean with standard error of the mean of 2 independent experiment with each condition repeated in triplicate per experiment. The maximum toxicity of the Aβ preparation used for the experiment occurred at concentrations between 2.5 to 5 μM of Aβ. (Data and figure credit: L. Liu)

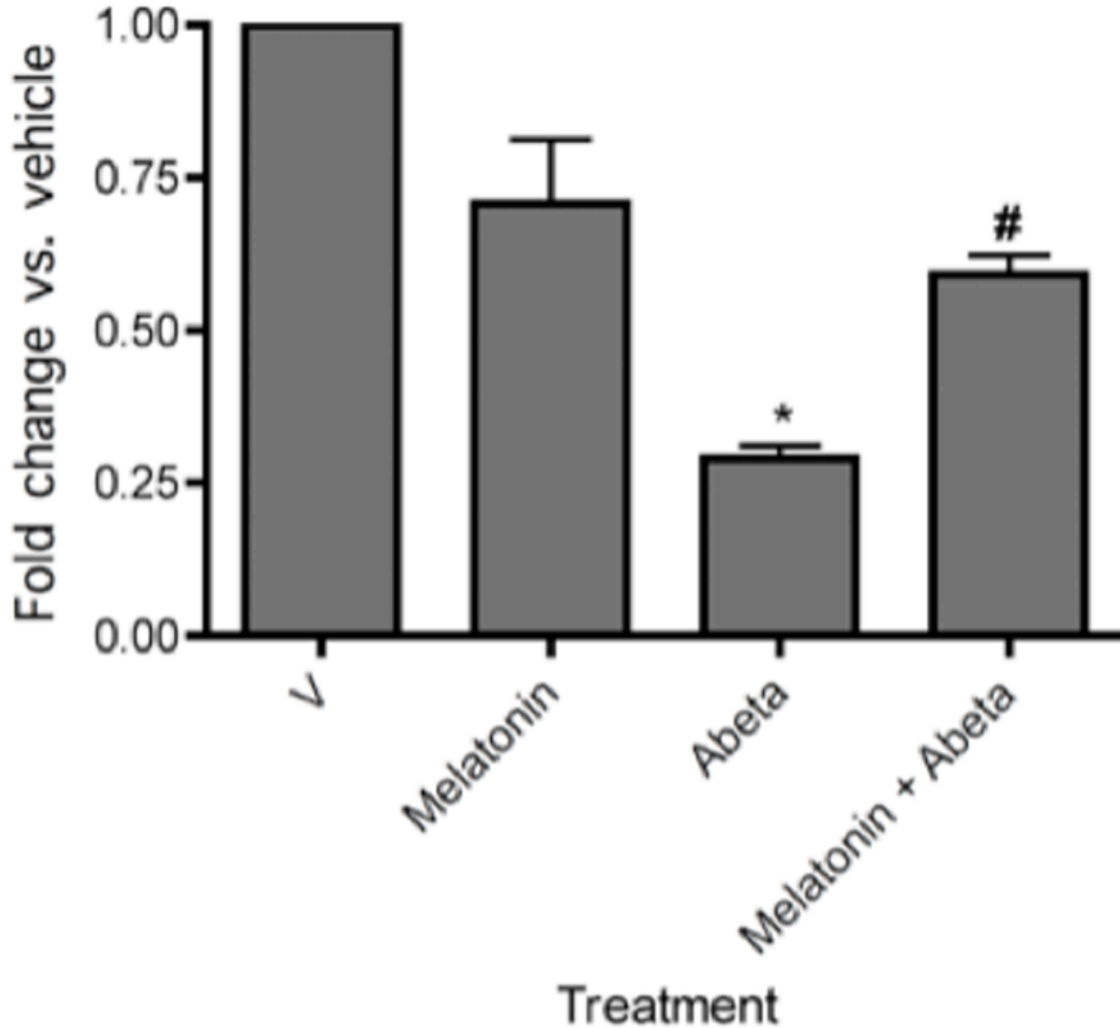


Figure E-2 - Melatonin is neuroprotective against A β in RGC-5 cells. The cells were treated with vehicle (V), 50 μ M melatonin, 2 μ M A β (1-42), or both melatonin and A β . After a 24 hour incubation, the remaining cell # was measured using the MMT assay. Data presented are the mean with the standard error of the mean of 3 independent experiments with each condition repeated in triplicate per experiment. * $p < 0.01$, Abeta vs vehicle, # $p < 0.05$ Abeta vs mealtonin+Abeta, one-way ANOVA, Bonferroni post-test. (Data and figure credit: M. Vasefi)

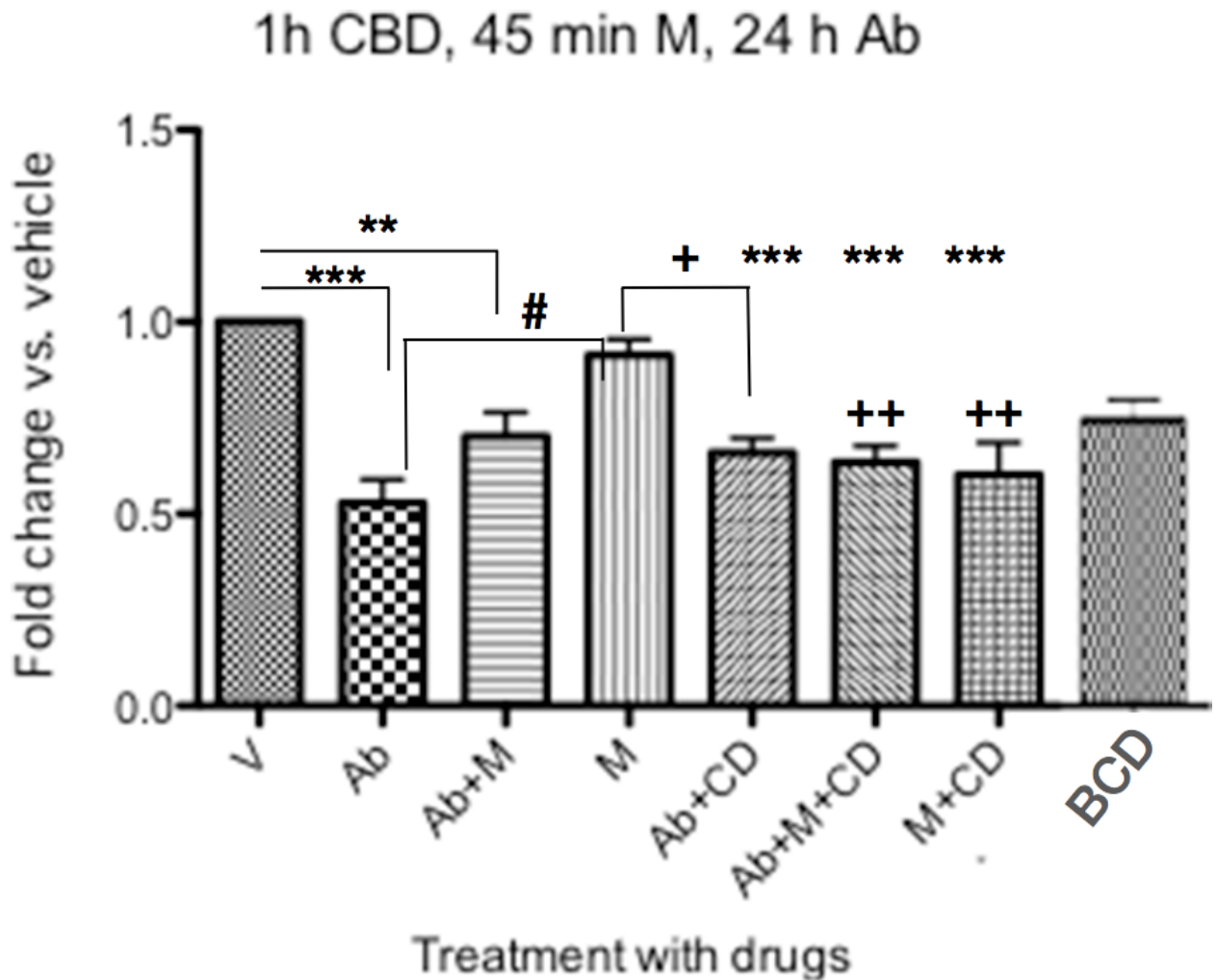


Figure E-3 - Melatonin is neuroprotective against A β in RGC-5 cells. The cells were treated with vehicle (V), 50 μ M melatonin, 2 μ M A β (1-42), or both melatonin and A β . After a 24 hour incubation, the remaining cell # was measured using the MMT assay. Data presented are the mean with the standard error of the mean of 3 independent experiments with each condition repeated in triplicate per experiment. Labeled values p < 0.05. 95 % CI for (V vs Ab) 0.2021 to 0.7422, (V vs Ab+M) 0.06962 to 0.5260, (V vs Ab+CD) 0.1120 to 0.5684, (V vs Ab+M+CD) 0.1368 to 0.5932, (V vs M+CD) 0.1696 to 0.6260, (M vs Ab+CD) 0.02518 to 0.4816, (M vs Ab+CD) 0.04998 to 0.5064, (M vs Ab+CD) 0.08272 to 0.5391, (Ab vs M) -0.6554 to -0.1153. One way ANOVA, Bonferroni post-test. (Data and figure credit: M. Vasefi)